IMPROVING PHASE GRATING AND ABSORPTION GRATING DIFFUSERS

Konstantinos DADIOTIS

School of Computing, Science and Engineering

University of Salford, Salford, UK

Submitted in Partial Fulfilment of the Requirements of the Degree of Doctor of Philosophy, October 2010

Echo (□Ηχώ) in ancient mythology was a mountain nymph well known for her melodic voice and beautiful singing. Myth has it that during a quarrel with Pan (god of shepherds and flocks), he caused confusion in nearby shepherds that led them to kill her and tear her to pieces which they scattered throughout the land. Gaea (Earth) out of mercy collected the scattered pieces which she buried where she found them. However, the pieces kept her godly melodic voice. Thus, she remains scattered throughout the planet trying to make herself heard by repeating what she hears.

TABLE OF CONTENTS

FIGURE CAPTIONS

SYMBOL AND ABBREVIATION INDEX

Symbols

c	speed of sound
d	well depth
d_c	autocorrelation diffusion coefficient
d_n	normalised autocorrelation diffusion coefficient
E	energy
f	frequency
f_0	diffuser design frequency
f_r	resonant frequency
G	Green's function
h	impulse response
H	transfer function
H_0	0^{th} order Hankel's function
I	intensity
j	imaginary unit
k	wavenumber
k_c	characteristic wavenumber
m	mass
mod	function that indicates the least non-negative remainder
M	population of a family of sequences
N	sequence length

p	pressure
P, p	sequence integer number generator
$\vec{r}$	position vector
r_m	losses
R	reflection coefficient
R_{XX}	autocorrelation function
s	sequence
S	surface
T	transfer matrix component
t	Helmholtz Resonator neck depth
t'	Helmholtz Resonator neck depth including the radiation impedance
u	particle velocity
V	volume
w	well width
z_c	characteristic impedance
z_n	normalised surface impedance
z_s	surface impedance
α	absorption coefficient
α_r	approximate absorption coefficient
β	surface admittance
β_n	normalized surface admittance
δ	end correction
δ_c	scattering coefficient

ε open area

θ , ψ angle

λ wavelength

λ_0 diffuser design wavelength

λ_r resonant wavelength

ρ density

τ delay

φ phase

ω angular frequency

n, r, m, ζ, ξ, i counters

Abbreviations

ACF	Autocorrelation Function
AGD	Absorption Grating Diffuser
BEM	Boundary Element Modeling
LSD	Lüke Sequence Diffuser
MLS	Maximum Length Sequence
MLSD	Maximum Length Sequence Diffuser
PRD	Primitive Root Diffuser
PGD	Phase Grating Diffuser
PWRD	Power Residue Diffuser
QRD	Quadratic Residue Diffuser

ACKNOWLEDGEMENTS

I would like to thank my family for their support throughout my studies. My parents Loukas and Petroula for their help and encouragement for success, my brother Dimitris for his advice and his help in my introduction to programming and my fiancée Georgia for the emotional support she provided and the patience she showed during my studies.

I am gratefully to the supervisory team of Prof. Cox and Prof. Angus for their help and guidance for the duration of my PhD studies. I feel I need to thank Prof. Cox in particular for his supervision of the completion of my research and the writing of this thesis.

I feel indebted to all the members of the Acoustics Research Centre of the University of Salford whether students or member of staff for the excellent cooperation and companionship. They made my experience of living and studying among them a memory that I will cherish forever.

I would like to thank in particular my colleague Richard Hughes for the excellent cooperation and the numerous hours of discussion on diffusers that stretched beyond the limits of the University.

Finally, I want to thank Dr. Peter D'Antonio for his advice on diffuser design.

I would also like to acknowledge the support of the Engineering and Physical Sciences Research Council, UK for funding this project through their Doctoral Training Account Studentship.

ABSTRACT

This thesis investigates room acoustic diffusers based on number sequences, exploring their shortcomings and presents improvements.

Standard Phase Grating Diffusers display frequencies where they act like flat plates and fail to diffuse. To overcome this, two new sequences (Lüke and power residue) are introduced. The diffusers based on these sequences display extended frequency range compared to standard ones such as Quadratic Residue and Primitive Root Diffusers. Their performance is studied using Boundary Element Modelling which shows that they can avoid flat plate phenomena in the audible frequency range. Furthermore, it is shown that by taking advantage of their inner symmetries Quadratic Residue and Primitive Root Diffusers can be created from smaller components thus allowing for the flat plat effect to be mitigated.

Next, Absorption Grating Diffusers are investigated. They consist of ideally absorbing and reflecting elements. For their implementation heavily damped Helmholtz Resonators are investigated showing that they give an approximation of the required distribution of admittance on the surface.

Then the performance of ideal Absorption Grating Diffusers is investigated using Boundary Element Modelling. Even with idealised completely absorbing elements, the performance of the diffuser is shown not to achieve substantial diffusion. This arises because edge diffraction from the reflecting elements weakens at high frequencies. At frequencies where smaller elements are creating substantial scattering, larger elements are producing specular reflections. Furthermore, due to the lack of cancellation, the specular reflected lobe is insufficiently attenuated, because it can only be changed through absorption.

Improvements to the original design are suggested. By changing reflective elements to reactive ones, scattering can be extended to higher frequencies. This allows for a range of frequencies were more reflecting elements display substantial dispersion. Also, implementing the absorbing elements using porous material in a shallow well allows some reflection, resulting in cancellation in the specular reflection lobe due to interference.

Measurements of the scattered pressure distribution of absorption grating surfaces are carried out and then compared to Boundary Element Modelling simulations using surface admittance data measured in an impedance tube. The agreement between measurement and simulation is

excellent proving the accuracy of this simulation method for these applications. The results show that the samples tested perform as two level Phase Grating Diffusers, with some energy loss, while their diffusion characteristics are shifted to lower frequencies. This arises because of the lower speed of sound in the porous medium. This implementation is shown to absorb 50% of the incident sound while the rest is scattered uniformly but only over a limited bandwidth.

INTRODUCTION

The acoustical quality of any performance space such as a concert hall, an auditorium, a club or a studio is the key factor in the perception of sound in it. For this reason these spaces are designed specifically for their application as they require different characteristics based on their use[1]. The sound field in a room consists of the interaction of the direct sound with the indirect reflections from its boundaries. The relationship between the amount of absorption on the walls and the sound decay of a room was established by Sabine[2] which launched modern room acoustic design[1].

The density and amplitude of the reflections dictates the acoustic characteristics of the space[3] and relates to its performance. The response of a boundary can be characterized in terms of absorption, reflection or diffusion. While the application of the right amount of absorption can be used to set the required reverberation time of a room[2] it does not necessarily take care of strong reflections from the boundaries of the room that can produce echo problems[4]. Furthermore, in cases that very little absorption is required in a small room there is need for diffusers to deal with the modal response of the space. Diffusers are structures whose main goal is to scatter the incident wave rather than attenuate it[5]. For this reason they can be used to deal with strong reflections from boundaries without removing sound energy from the space.

Diffuser research was ignited by Schroeder who suggested using number sequences to create diffusing surfaces[6]. Based on his concept, a category of diffusers was created known as Phase Grating Diffusers. Using the same mathematical approach Angus later presented the concept of Absorption Grating Diffusers[7] which are structures that combine the use of absorbing and reflecting elements to achieve diffusion.

In this thesis the characteristics of both Phase Grating and Absorption Grating Diffusers are investigated. The thesis is split into three parts:

The first part of the thesis presents the theoretical background to sequence based diffusers. It discusses the measures that are used to assess diffusers, simulation techniques that are used to predict their performance and methods that have been established to measure their scattered field. The limitations and the disadvantages of Phase Grating Diffusers that have been established in the literature are presented and two new Phase Grating Diffusers are presented

that, based on their characteristics, have the potential to perform better than the many in common use. Boundary Element Modelling is used to predict their performance and compare them to commonly used Phase Grating Diffusers.

The second part of the thesis centres on Absorption Grating Diffusers. Their design concept is presented and their requirements are discussed. Porous absorbers and absorbing structures that can be used for their implementation are discussed along with measurement methods and analytical models that are used to assess their absorbing characteristics. The use of densely layered mineral wool behind a perforated structure is investigated as an implementation of highly absorbing elements. Boundary Element Modelling is used to investigate the absorbing and scattering capabilities of ideal Absorption Gratin Diffusers. Finally methods of improving their performance are introduced either by using reactive elements or by using less absorbing elements.

The third part of the thesis summarises the conclusions and contributions of the thesis and presents new areas of research that can stem from its findings.

PART I. PHASE GRATING DIFFUSERS

Phase Grating Diffusers (PGD) were invented in the 1970's by Manfred Schroeder, when he introduced the concept of using maximum length sequences to improve sound diffusion in concert halls and reverberation chambers[6, 8-10]. He suggested that by pseudorandomly arranging wells of a constant depth on a surface (Figure 1-1) sound diffusion can be achieved[6]. This would be the case when the wave reflected out of the wells has opposite phase from the one reflected from the front surface.

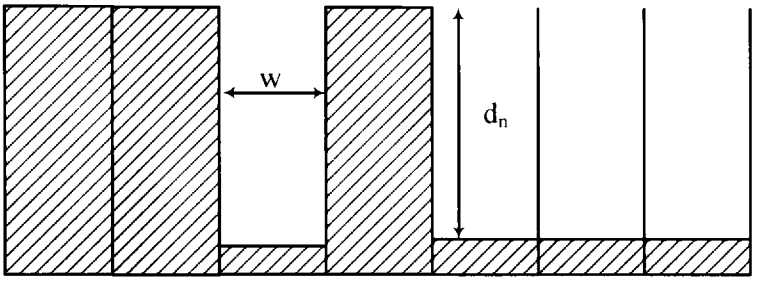

Figure 1-1. One period of a Maximum Length Sequence Diffuser (MLSD) of well width w and depth of the n^{th} well, d_n.

Based on the same concept Schroeder later suggested using wells of varying depth that would be dictated by integer based pseudorandom sequences such as quadratic residue (Figure 1-2) and primitive root sequences[8]. These diffusers were soon to become commonly used by the industry[5, 8, 11-12]. In 1983, the first sequence based PGD product was created by RPG that was presented in 1984 by D'Antonio *et al*[13]. It was a Quadratic Residue Diffuser (QRD) that found application in recording studios at first and later in other architectural spaces[5, 12].

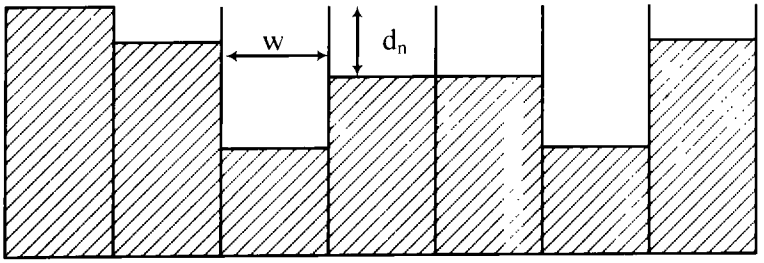

Figure 1-2. One period of a Quadratic Residue Diffuser (QRD) of well width w and depth of the n^{th} well, d_n.

PGDs suffer from limited bandwidth. When the wavelength becomes small in comparison to the width of the wells sound wouldn't propagate as a plane wave in the well causing cancellation in the well. Moreover, when the wavelength becomes double the common factor of the well depths all the wells re-radiate in phase resulting in the diffuser acting like a flat plate.

Hence, concepts to increase the bandwidth have been developed. First, a fractal diffuser was designed. This considered reforming the bases of the wells into smaller diffusers that would disperse sound at higher frequencies when the wavelength would be small compared to the width of the wells[14].

To make products easy to handle, small structures that would be repeated to cover a substantial surface are often used. The problem is that periodic repetition of a structure introduced periodicity lobes in the scattered pressure distribution. The problem of periodicity was first addressed by Angus who introduced the idea of modulation to achieve wide band diffusion in 1995[15-16]. She suggested using a binary pseudorandom sequence to position two different diffusers that resulted in a wider band of application.

Other suggestions abandoned sequence-based diffusers altogether and focused on using optimization algorithms to generate a sequence with a wide band of diffusion[17].

In this part of the thesis Phase Grating Diffusers (PGD) are discussed. Prediction models and measuring methods are examined. Coefficients and characteristics of diffusion quality are debated and the principles of diffusion design are depicted. Later, standard PGDs such as QRD and MLSD are presented and their characteristics and limitations are discussed. Finally, new pseudorandom sequences are introduced and their performance is compared with the industry standards.

Chapter 1. Introduction to diffusers

In this Chapter, some background theory is presented which is used in the thesis. Firstly, the descriptors used to evaluate the performance of diffusers are presented and their merit and quality discussed. An introduction to 1-D pseudorandom sequences is made and the methods of generating 2-D sequences are presented.

1.1. Measures of diffusion

While polar plots of the scattered pressure distribution are useful, there is a need for a coefficient that represents the "quality" of diffusion in a more compact way. When introducing Phase Grating Diffusers (PGD), Schroeder suggested the equality of energy contained in the periodicity lobes[8]. While this concept had some merit at the time, it requires periodic repetition of the diffuser which is not only unnecessary but undesirable as well (see Section 3.3). So another measure of diffuser quality is required. An ideal descriptor as has been suggested by Hargreaves *et al*[18] should:

- *have a solid physical basis;*
- *be clear in definition and concept, and related to the current role of diffusion in room acoustics;*
- *consistently evaluate and rank the performance of diffusers;*
- *apply to all the different surfaces and geometries found in rooms;*
- *be measurable by a simple process;*
- *be bounded;*
- *be easy to predict.*

A number of descriptors have been presented over time that satisfy some of the above characteristics[18]. There are two descriptors, which are globally accepted, that vie for the position of the most representative measure of diffusion; these are the scattering coefficient and the diffusion coefficient.

1.1.1. Scattering coefficient

Mommertz and Vorländer developed the scattering coefficient[19-20]. The total energy E_{total} leaving the element is split into the specular reflected energy E_{spec} and the scattered energy E_{scat} where:

$$E_{total} = E_{spec} + E_{scat} \qquad 1.1$$

where E_{spec} is the energy referring to the angular pressure that is due to the dimensions of the surface and thus is correlated with that reflected from a plate of the same dimensions whilst E_{scatt} is the energy that is scattered due to the surface structure.

The scattering coefficient δ is defined as:

$$\delta = \frac{E_{scat}}{E_{total}} = 1 - \frac{E_{spec}}{E_{total}} \qquad 1.2$$

As is evident from equation 1.2 the scattering coefficient does not take into account how the energy is distributed into different angles of reflection. It only takes into account whether the energy is in the specular direction or not.

Another expression for the scattering coefficient when the pressures at reflection angles θ_i of constant angle difference are known is:

$$\delta_c = 1 - \frac{|\sum_{i=1}^{n} p_1(\theta_i) p_0^*(\theta_i)|^2}{\sum_{i=1}^{n} |p_1(\theta_i)|^2 \cdot \sum_{i=1}^{n} |p_0(\theta_i)|^2} \qquad 1.3$$

where $p_1(\theta)$ is the reflected pressure distribution of the surface under investigation, $p_0(\theta)$ is the reflected pressure distribution of a plane surface of the same size and n is the number of reflection angles.

The expression 1.3 allows for the measurement of the coefficient to be made when the scattered pressure distribution is known. The measurement of the random incidence scattering coefficient has been standardised[21].

1.1.2. Diffusion coefficient

Hargreaves *et al*[18] developed the autocorrelation diffusion coefficient:

$$d_c = \frac{(\sum_{i=1}^{n} |p(\theta_i)|)^2 - \sum_{i=1}^{n} |p(\theta_i)|^2}{(n-1) \sum_{i=1}^{n} |p(\theta_i)|^2} \qquad 1.4$$

where $p(\theta_i)$ is the pressure in the i^{th} angle of reflection θ_i and n is the number of receivers in the polar response.

Autocorrelation gives the similarity of the energy distribution with itself, how invariant it is with the angle of reflection. In order to take the pattern of the diffusion coefficient due to the

dimensions out of the criterion the concept of a normalised diffusion coefficient has been suggested[11]. It is referred to as the normalised diffusion coefficient:

$$d_n = \frac{d_c - d_{ps}}{1 - d_{ps}} \qquad 1.5$$

where d_c is the diffusion coefficient of the sample in question and d_{ps} is that of a rigid plane surface with the same dimensions of the sample.

The measurement of autocorrelation diffusion coefficient has been standardised by the Audio Engineering Society[22] and is in the process of being included in ISO17497-2[23].

1.1.3. Discussion

There is a lot of discussion on the subject of which coefficient most accurately characterises the diffusion characteristics of a surface. Both the scattering and the diffusion coefficient have values that range from 0 (specular reflection) and 1 (perfect diffusion). However, an issue arises when one considers what the perfect scattering refers to. The scattering coefficient does not consider the pattern of the polar reflection of the surface. It only takes into account that there is no energy in the angle of specular reflection. On the other hand the diffusion coefficient requires exactly the same reflection in all angles regardless of the angle of the incident wave.

The scattering coefficient has found application in geometric acoustic models[24]. The diffusion coefficient, on the other hand, gives a better idea of the diffusion characteristics of a surface as its aim is homogenous dispersion of sound in all directions rather than focusing in a specific angle of reflection. For this reason it is usually preferred in diffusion design.

1.2. Sequences

Since this thesis is centred on diffusers that are generated from number sequences it is important to discuss their origin. For good diffusion, the sequences should display a flat power spectrum (see Chapter 3). Consequently, they should have an autocorrelation function that resembles a Kronecker delta[6, 8]. In order for a sequence to have this property it must have a random arrangement of coefficients. Given the small length of the sequences that is required for the design[11], 7 is most common for a QRD[13], it is unlikely to achieve a random arrangement. For this reason, pseudorandom sequences have been designed that display random properties.

1.2.1. 1-D sequences

1-D pseudorandom sequences have been studied and applied by other fields of science[8] resulting in a large number of them being created over the years[25]. The most well known in acoustics is the binary Maximum Length Sequences (MLS)[25] as they are widely used in measurements[11]. The ones used for PGDs are integer based pseudorandom sequences[11]. The most famous of which are the quadratic residue e.g. [0,1,4,2,2,4,1] and primitive root sequence e.g. [1,3,2,6,4,5] based on the prime number p = 7[25].

1.2.2. 2-D sequences

When a 1-D sequence in used a 1-D diffuser is created that scatters sound only in a semi-circle. In order for the sound to be scattered in all directions (hemisphere) a 2-D diffuser is required.

Superimposing a 1-D sequence on 2 dimensions

A simple way of creating such a diffuser is to use one sequence in each direction (Figure 1-1) [26]. If the two sequences s_1 and s_2 to be used are generated by the functions f_1 and f_2 by the equations:

$$s_1(n) = f_1(n) \bmod p_1$$
$$s_2(n) = f_2(n) \bmod p_2 \qquad 1.6$$

where p_1 and p_2 are the generators of the sequences, *mod* is a function giving the minimum positive remainder and n is the position of the coefficient in the sequence.

One of them is used to generate the grating of the rows and the other of the columns. The coefficient of the 2-D sequence that is positions in x^{th} row and y^{th} column is given by the equation:

$$s(x,y) = f(x,y) \bmod p \qquad 1.7$$

where $f(x,y) = f_1(x) + f_2(y)$ and p is the smallest common product of p_1 and p_2.

In Figure 1-1 an example is presented of a 2-D sequence created from a 1-D quadratic residue sequence of prime 7. Since only one sequence is used $p_1 = p_2 = p = 7$ and $f(x,y) = f_1(x) + f_1(y)$. This construction is illustrated in

Figure 1-2.

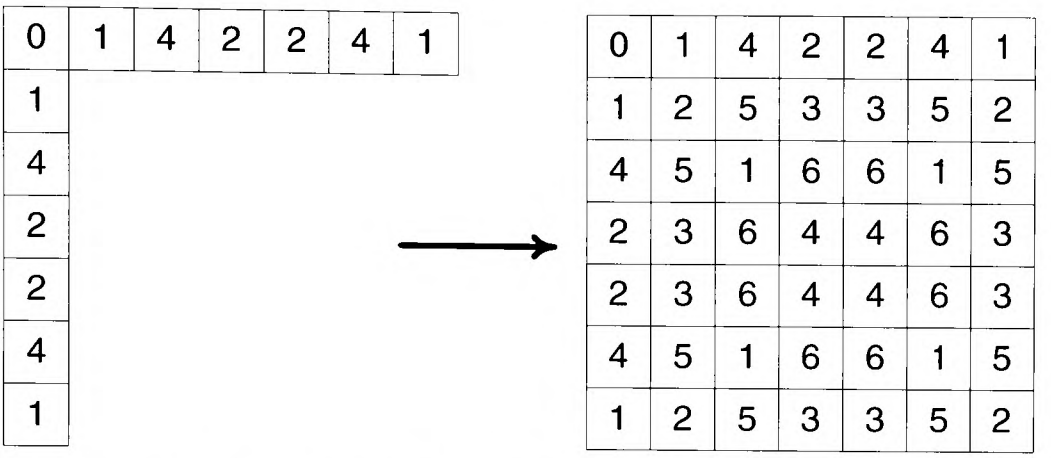

Figure 1-1. Generating a 2-D sequence from a 1-D quadratic residue sequence.

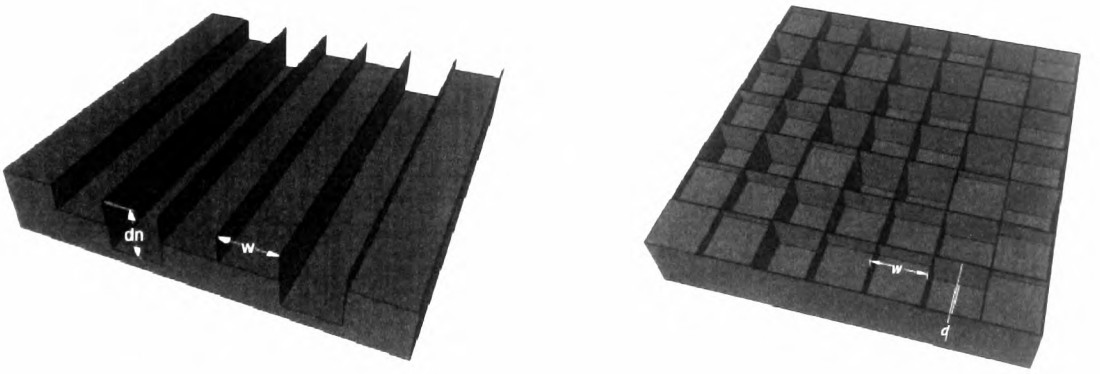

Figure 1-2. From 1-D to 2-D QRD.

Chinese Remainder Theorem

Another way of creating a 2-D sequence is to fold a long 1-D sequence into a 2-D array. A way of doing this is to use a technique known as the Chinese Remainder Theorem[10]. This technique preserves the sequence's autocorrelation characteristics[27]. So by folding a 1-D sequence with 1-D Kronecker delta autocorrelation function using the Chinese Remainder theorem the resulting 2-D sequence will display an autocorrelation function in the form of a 2-D Kronecker delta.

$N_1 = 5$

1	17	13	9	5
6	2	18	14	10
11	7	3	19	15
16	12	8	4	20

$N_2 = 4$

Figure 1-3. The positions of the coefficients of a 20-coefficient long sequence when folded in a 4×5 array using the Chinese Remainder Theorem.

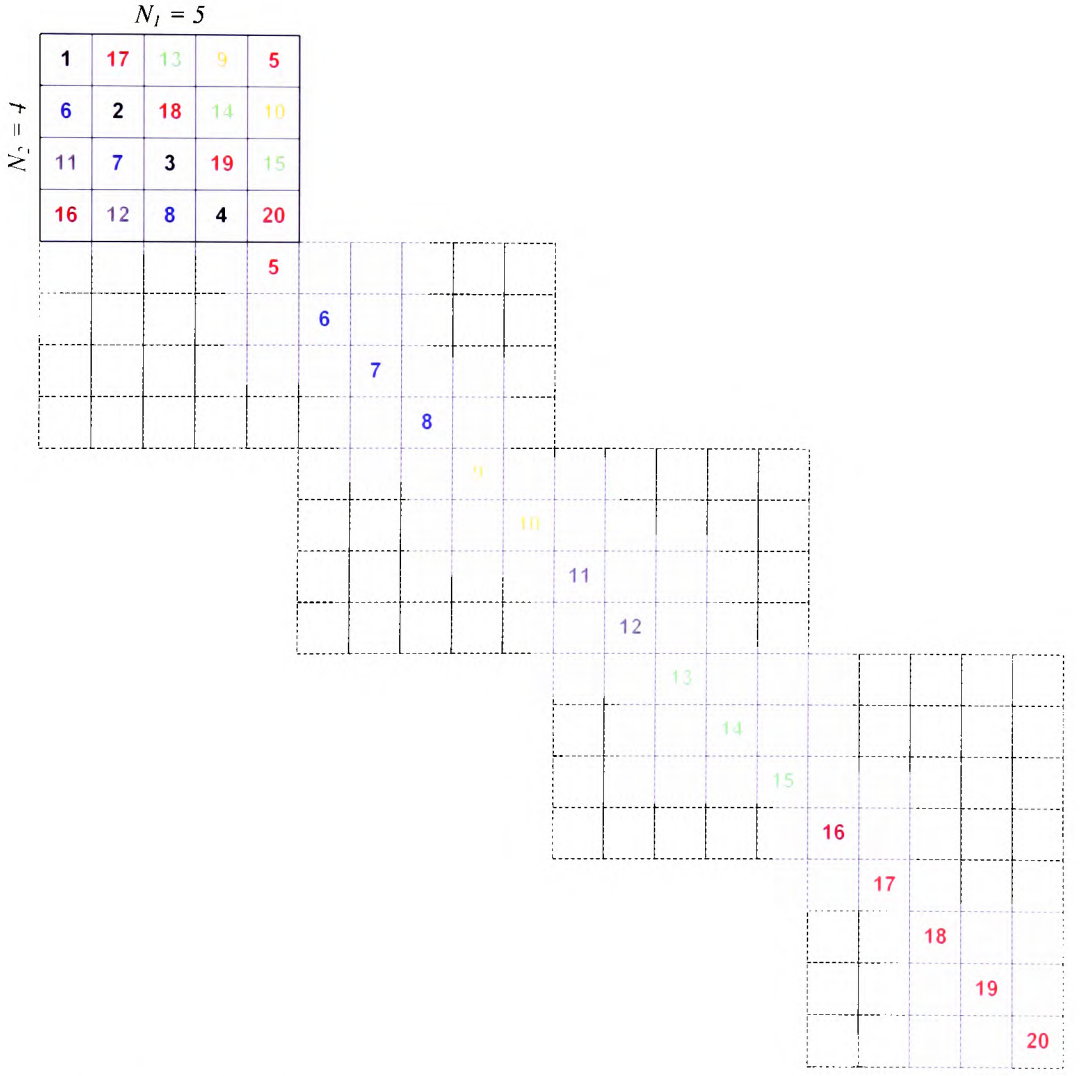

Figure 1-4. Generating the positions of the coefficients of a 20-coefficient long sequence when folded in a 4×5 array using the Chinese Remainder Theorem throught the use of a space of parrallel arrays.

The Chinese Remainder Theorem[28] suggests that if n states the position of a coefficient in a 1-D sequence of length N, while n_1 and n_2 are the coordinates of that coefficient in a 2-D $N_1 \times N_2$ array (where N_1 and N_2 are co-prime) then they are connected by the equation:

$$\begin{aligned} n_1 &= n \bmod N_1 \\ n_2 &= n \bmod N_2 \end{aligned} \qquad 1.8$$

where $N = N_1 \cdot N_2$.

To give an example, a 1-D sequence of length 20 can be folded in a 4×5 2-D array (given the fact that 4 and 5 are co-prime) (Figure 1-3).

Folding in this way coincides with positioning the coefficients diagonally in a space of parallel $N_1 \times N_2$ arrays. The position on the 2-D grid is dictated by its position in its given array (Figure 1-4).

Changing the folding steps in the Chinese Remainder Theorem

The Chinese remainder theorem dictates positioning the coefficients diagonally, moving one step left and one step down. But, the autocorrelation properties can be retained even with different folding steps. In this case the positions of the coefficients are set by the equations:

$$\begin{aligned} n_1 &= \big(n + (n-1) \cdot (step_1 - 1)\big) \bmod N_1 \\ n_2 &= \big(n + (n-1) \cdot (step_2 - 1)\big) \bmod N_2 \end{aligned} \qquad 1.9$$

where $step_1$ and $step_2$ are the folding steps. In order for positions not to coincide the steps must not be divisor of the respective dimension. For instance, if a 20 coefficient long sequence must be folded in a 4×5 array the value of 2 can't be used for $step_2$. If this value is used then equation 1.9 will give $n_2 = (2n) \bmod 4 + 1$. This means that n_2 takes up only odd value which cannot be accepted since the lines 2 and 4 of the array will be empty while the locations of lines1 and 3 will correspond to two coefficients.

An example of folding the sequence using folding $step_1 = 2$ and $step_2 = 3$ is displayed in Figure 1-5. This method allows for a sequence to be folded in any number of different ways resulting in 2-D sequences with the same ideal autocorrelation characteristics. This offers the diffuser designer more options as he can choose the configuration that is more aesthetically

appealing or even take advantage of the diffusers inner symmetries (as will be shown in Section 4.4.2).

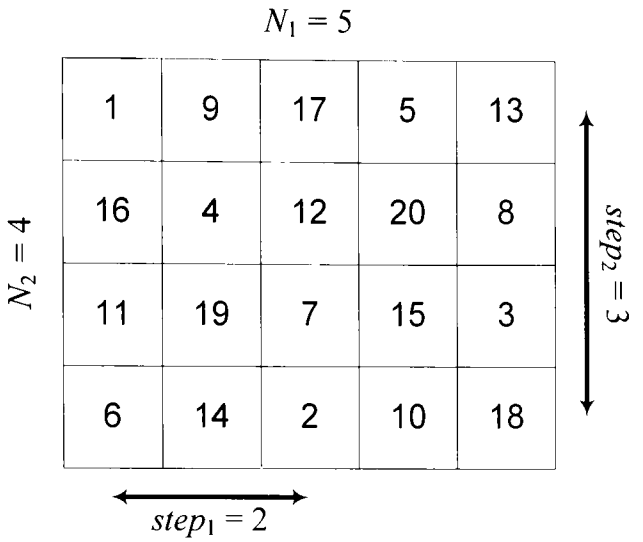

Figure 1-5. The positions of the coefficients of a 20-coefficient long sequence when folded in a 4×5 array with $step_1 = 2$ and $step_2 = 3$.

1.3. Summary

In this Chapter an introduction to some aspects of diffuser design were made. The coefficients that are used by both the scientists and the industry to assess the performance of diffusers have been presented and their characteristics have been discussed. Furthermore, 1-D sequences that can have been used to generate 1-D PGDs have been mentioned. Methods of creating 2-D arrays from 1-D sequences that have been used in the past were presented. Finally, a novel method to produce more than one 2-D array from a given 1-D sequence has been introduced. In the following Chapter simulation techniques and measuring methods of the scattered pressure distribution from a diffuser are going to be presented.

Chapter 2. Assessing a diffuser

In order for the quality of a diffusing structure to be established there is need for the scattered pressure distribution to be attained. In this Chapter numerical methods for the prediction of the scattered pressure of a surface will be discussed, while the measuring method that was used in this thesis will be presented.

2.1. Prediction methods

When Schroeder introduced the concept of using phase grating to achieve sound diffusion he suggested that the far field polar pattern would be given by the Fourier transform of the reflection coefficients of the surface[8]. If a structure that displays variation of its reflection coefficient in one dimension was sampled every w and R_n was the reflection coefficient of each sample then the far field scattered pressure would be:

$$p(\theta) = \sum_{n=0}^{N-1} R_n e^{-jn \cdot kwsin\theta} \qquad 2.1$$

where θ is the angle of reflection, n is the sample number, k the wavenumber and N the number of samples. Note that this is a Discrete Fourier Transform of $kwsin\theta$, and for this reason the prediction method is often referred to as a Fourier model.

Since then a number of methods for the prediction of the scattered pressure distribution from a surface have been developed[11].

2.1.1. Boundary Element Modelling (BEM)

This method uses the Helmholtz-Kirchhoff integral equation to estimate the pressure at a given point by adding the pressure direct from the source with the sum of the pressure reflected from different patches of the surface. The reflected pressure is estimated by the surface integral of the pressure and its derivative over the reflecting surface[29]:

$$\left.\begin{array}{ll} \vec{r} \in E & p(\vec{r}) \\ \vec{r} \in s & \frac{p(\vec{r})}{2} \\ \vec{r} \in D & 0 \end{array}\right\} = p_i(\vec{r}, \vec{r}_0) + \int_s \left(p(\vec{r}_s) \frac{\partial G(\vec{r}, \vec{r}_s)}{\partial n(\vec{r}_s)} - G(\vec{r}, \vec{r}_s) \frac{\partial p(\vec{r}_s)}{\partial n(\vec{r}_s)} \right) ds \qquad 2.2$$

where E, D are the domains outside and inside the surface s (Figure 2-1). $\vec{r}(x, y, z)$, $\vec{r_i}(x_i, y_i, z_i)$ and $\vec{r_0}(x_0, y_0, z_0)$ are the position vectors of the point of interest, a point on the

surface s and the source of the wave respectively. $p(\vec{r})$, $p_i(\vec{r},\vec{r}_0)$ and $p(\vec{r}_s)$ are the pressures at the point of interest, the direct radiated pressure of the source to the receiver and that at a point on the surface. n is the normal to the surface pointing outwards, ds is an infinitely small portion of the surface and $G(\vec{r},\vec{r}_s)$ is the free field Green's function:

$$G(\vec{r},\vec{r}_s) = \frac{e^{-jkr}}{4\pi r}, \qquad \text{where } r = |\vec{r} - \vec{r}_s| \tag{2.3}$$

For a 2-D case Green's function is given by the Hankel function:

$$G(r) = \frac{-j}{4} H_0^{(2)}(kr) \tag{2.4}$$

Where $H_0^{(2)}$ is the Hankel function of the 2nd kind of order 0.

In the case that the surfaces are considered locally-reacting the pressure derivative can be connected with the pressure using the surface admittance:

$$\frac{\partial p(\vec{r}_s)}{\partial n(\vec{r}_s)} = jk\beta(\vec{r}_s)p(\vec{r}_s) \tag{2.5}$$

where β is the surface admittance pointing outwards from the surface. In the case of a reflective surface $\beta \rightarrow 0$ and consequently the pressure derivative can be omitted from equation 2.2.

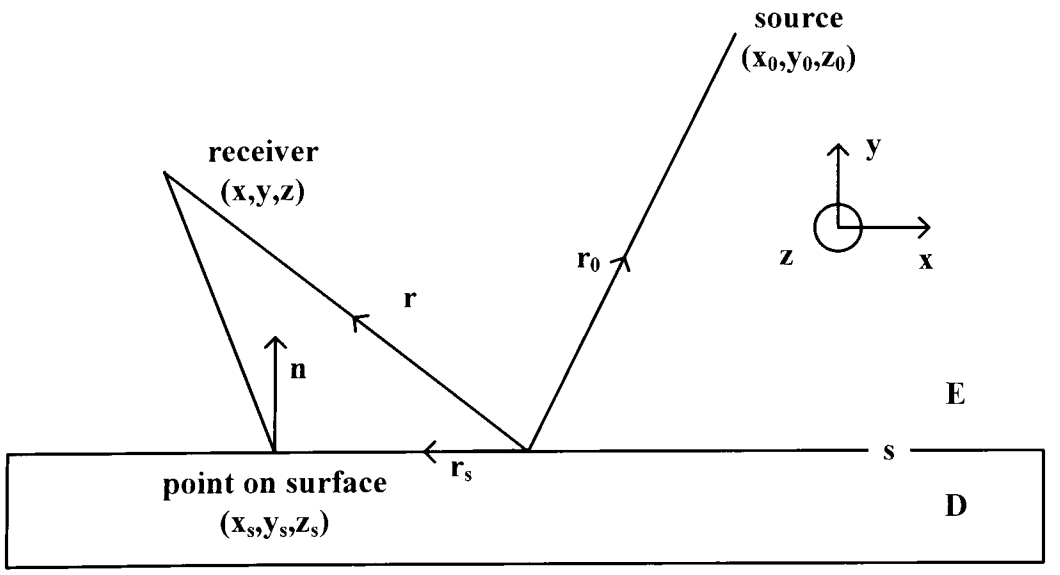

Figure 2-1. The Geometry of the boundary integral equation.

For the numerical calculation the surface must be meshed into N small elements (Figure 2-2). Their size is set usually much smaller than the wavelength so that the pressure and its derivative can be considered constant[12]. In this thesis this limit is set to a tenth of the wavelength ($\lambda/10$). The solution is then carried out in two steps. First the surface pressures on the elements are estimated and after that the pressure at any point in space can be calculated.

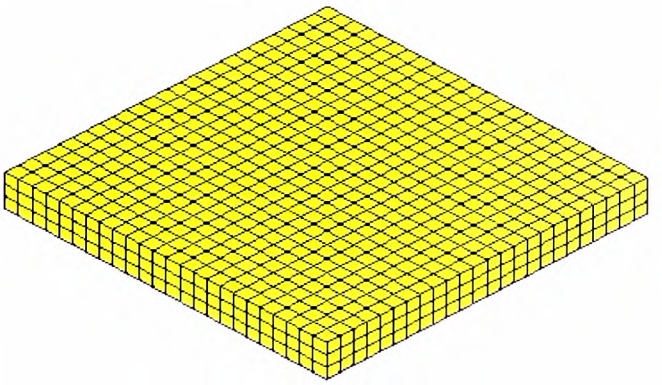

Figure 2-2. A plane surface meshed for a BEM.

In order for the surface pressures to be estimated eq. 2.2 must be solved simultaneously for the N surface elements. The simulation rests on solving the system of N equations that is shown here in the form of a matrix:

$$\left(\frac{1}{2}\mathbf{I}_N + \mathbf{A}\right)\mathbf{P} = \mathbf{P}_i \qquad 2.6$$

where $\mathbf{I}_N$ is the $(N \times N)$ identity matrix, $\mathbf{P}$ and $\mathbf{P}_i$ are $(1 \times N)$ matrices of the surface pressures and the pressure directly from the source to the surface respectively and $\mathbf{A}$ is the $(N \times N)$ matrix which states the contribution from the m^{th} element to the n^{th} and s_m is the surface of the m^{th} element. Its coefficients are formed by introducing eq. 2.5 in the integral of eq. 2.2:

$$A_{mn} = \left(\frac{\partial G(\vec{r_n}, \vec{r_s})}{\partial n_m(\vec{r_s})} - G(\vec{r}, \vec{r_s})jk\beta_m\right)s_m \qquad 2.7$$

The solution of equation 2.6 can be reached by calculating the inverse of the matrix $\left(\frac{1}{2}\mathbf{I}_N + \mathbf{A}\right)$. As a result of that the surface pressures can be estimated:

$$\mathbf{P} = \left(\frac{1}{2}\mathbf{I}_N + \mathbf{A}\right)^{-1} \mathbf{P}_i \qquad 2.8$$

Once the surface pressures are known the integral equation, for $\vec{r} \in E$, gives the pressure at any point in the E domain.

This method offers a direct solution to the Boundary Integral Equation and is used in the Part 2 of the thesis for the prediction of the scattered pressure distribution of Absorption Grating Diffusers[30].

Thin panel Boundary Element Modelling

In order to reduce the computation time of the method other formulation must be used. Terai[31] presented equations that connect the surface of the two sides of an infinitely thin surface which are used to form the thin panel BEM. The pressure difference $p(\vec{r}_{s,1}) - p(\vec{r}_{s,2})$ between the front and back of the plate is given by the equation[31]:

$$0 = \frac{\partial p_i(\vec{r}_0, \vec{r}_{s,1})}{\partial n(\vec{r}_{s,1})} + \int_S \{p(\vec{r}_{s,1}) - p(\vec{r}_{s,2})\} \frac{\partial G^2(\vec{r}, \vec{r}_{s,1})}{\partial n(\vec{r}_1)\partial n(\vec{r}_{s,1})} ds \qquad 2.9$$

With the pressure difference known the pressure at a given external point is given by the equation:

$$p_i(\vec{r}) = p_i(\vec{r}_0, \vec{r}_1) + \int_S \{p(\vec{r}_{s,1}) - p(\vec{r}_{s,2})\} \frac{\partial G(\vec{r}, \vec{r}_{s,1})}{\partial n(\vec{r}_{s,1})} ds \qquad 2.10$$

The use of the thin panel BEM becomes very useful when modelling the scattered pressure distribution from Phase Grating Diffusers (PGD) (Figure 2-3(a)). Their geometry considers the existence of very thin fins that can be easily modelled with this method.

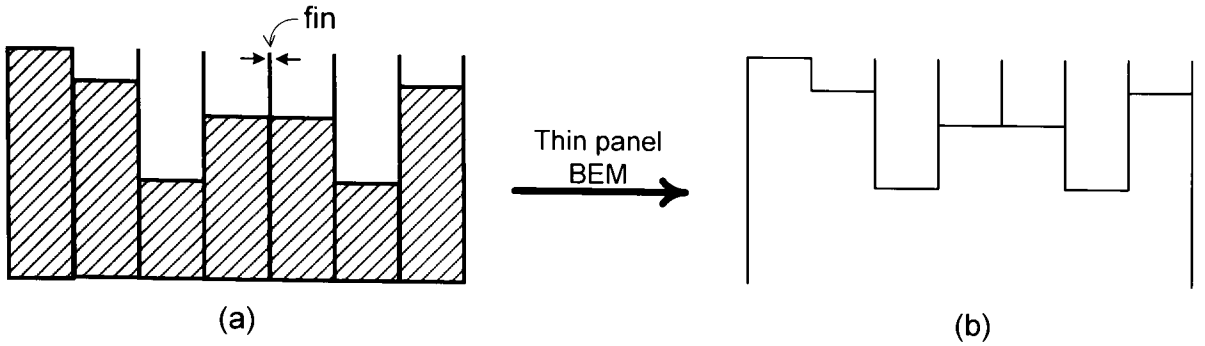

Figure 2-3. Quadratic Residue Diffuser (QRD) geometry in the thin panel BEM.

The diffusers are attached on walls so the area of interest is the space on the front of the structure. This means that the structure can be meshed as is presented in Figure 2-3(b) since the back has very little interference with the scattering at the front of the diffuser in the higher frequency bandwidths where scattering is significant. Leaving the back open has the added advantage that there is no enclosure created that can produce non-unique solutions. This indirect solution to the Boundary Integral Equation is the ideal BEM formulation to simulate the performance of PGDs[32-33] and therefore it is used in Chapters 3 and 4[34].

When a large surface is to be modelled the Boundary Element Method can become very computationally expensive. The process can be sped up by making a number of approximations.

2.1.2. Fraunhofer or Fourier Model

The Fraunhofer Model starts from the same integral equation as the Boundary Element Method (eq. 2.2). The approximations that have been taken suggest that this model should only be considered in the far field. Consider normal incidence sound. The scattered pressure at a point in space is given by[11]:

$$p_s(\vec{r}) = -\frac{jkb}{8\pi^2}\frac{e^{-jk(r_0+r)}}{rr_0} sinc\left(\frac{kb}{r}\right)(cos\theta + 1)\int_{x_s=-\alpha}^{x_s=\alpha} R(x_s)e^{jkx_s sin\theta}dx_s \qquad 2.11$$

In this equation the integration is the Fourier transform of the reflection coefficient in the $kx_s sin\theta$ domain. This is a similar result to the one that Schroeder reached. It is common for the $(cos\theta + 1)$ factor to be neglected and to follow the Fourier approach (eq. 2.1).

This is an elegant method that connects the distribution of reflection characteristics of a surface with the scattered pressure but it refers only to the far field response.

Far-Field

The far field is defined as the distance at which the difference between the minimum and the maximum path length from the panel to the receiver is small compared to the wavelength (Figure 2-4)[11]. This region is located where the distance between the receiver and the surface is large compared to the maximum dimension of the surface:

2.12

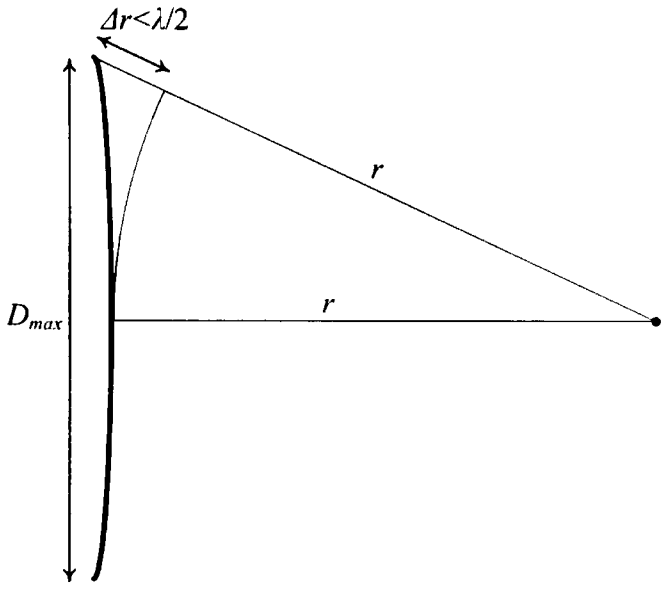

Figure 2-4. Far-field determination.

The first requirement is rarely an issue if the second one is met. When they are met all the point on the surface can be considered to be the same distance from the receiver[35]. The surface is in the far field when[11, 23, 35]:

2.13

The region that falls under the far-field category changes for oblique positions. The furthest case for small surfaces is when the receiver is in the normal of the surface. If the surface is wide, then the receivers must be further away for grazing angles.

Far-field conditions are not always possible in measurements. In these cases other requirements are needed. Such a case is referred to in Section 2.2.

2.2. Scattered pressure distribution measurement methods

The measurement of the scattered pressure distribution is in the process of being internationally standardized ISO:17497-2[23]. The standard is at the moment a committee draft based on the Audio Engineering Society standard AES-4id-2001[22] and it considers measurement in a three or a two dimensional domain under free field conditions.

The simplest way of measuring polar plots is if the diffuser is 1-D. Such diffusers scatter sound in one plane and the polar response of interest is limited to two dimensions. For this measurement a semi-anechoic chamber is used[22]. The reflective floor of the chamber is taken into account by considering the image of the sample (Figure 2-5).

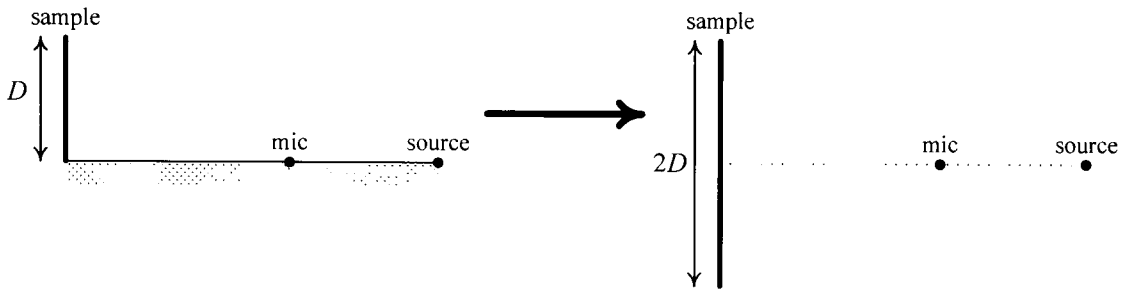

Figure 2-5. Free-field equivalent of the semi-anechoic chamber.

The setup of the measurement is depicted in Figure 2-6 with the speaker being at the bottom of the figure. 37 microphones are set in an arc spaced apart by $\Delta\varphi=5^{\circ}$ with a radius of R = $1.4m$. The radius was dictated by the width of the room which is $3.3m$. The samples that were tested had a maximum width of $70cm$ and a height of $30cm$. If the mirror image of the samples is taken into account then they appear to be $60cm$ tall.

The measurements were carried out in the semi-anechoic chamber of the University of Salford. For the recording a 44 channel NetdB real-time analyzer was used (Pro-121 and Pro-132 combined)[36-37]. The source needed to be as close to the floor of the chamber as possible (see Figure 2-5) so the Visaton SC 4 ND[38] speaker was used which has a flat response from $1kHz$ up to $22kHz$ and is $5cm$ in diameter which resulted in its centre being $2.5cm$ from the floor. Since the microphones are in the path of the loudspeaker they needed to be as small as possible so as not to interfere. So they were made less than $5mm$ in diameter using miniature omni-directional capsules that have flat response in the range of operation of the speaker.

Although far-field measurements are the ideal case for diffusion measurement they are not realistic for high frequencies (eq. 2.13) as they require a very big anechoic chamber unless the sample is really small. So the international standard requirement of 80% of the receivers being outside the specular reflection zone was met. This led the source to be placed at a distance of $3.7m$ for the $70cm$ wide samples and $3.2m$ for the $40cm$ ones. The measurements were carried out only for normal incidence due to geometric restrictions of the room.

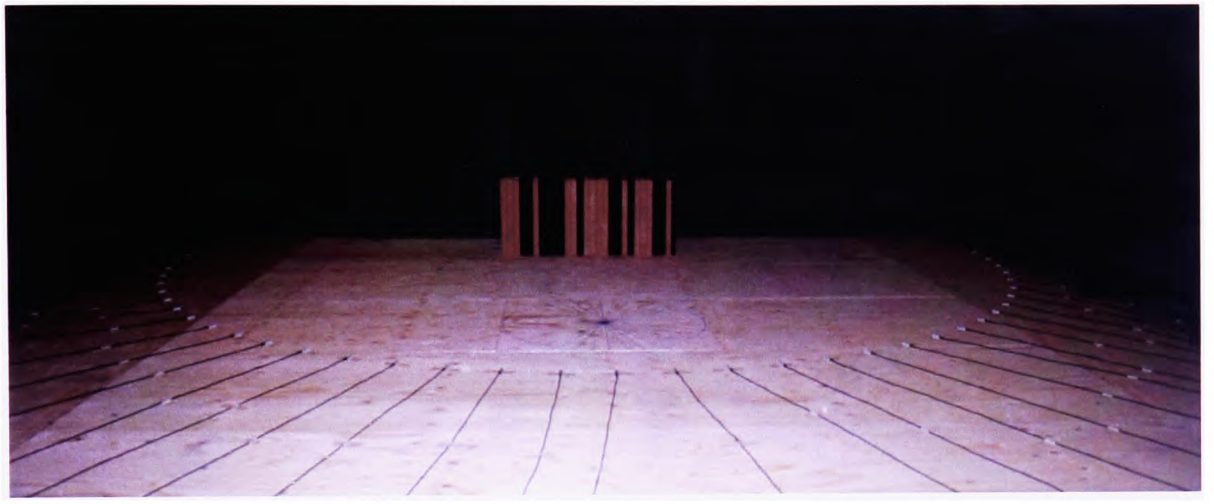

Figure 2-6. Single plane polar response measurement set-up in the semi-anechoic chamber.

In order for the scattered impulse response of the sample to be estimated the impulse response of the sample must be de-convolved with the loudspeaker-microphone response at each scattering angle. Furthermore, the interference of the room needs to be accounted for as well. The de-convolved sample response h is given by the equation[23]:

———————— 2.14

where FT and IFT are the forward and inverse Fourier transforms respectively. h_s and h_b are the impulse response with and without the sample respectively and $h_{l\text{-}m}$ is the loudspeaker-microphone response.

The impulse responses are measured using a Maximum Length Sequence. First the microphone-loudspeaker response $h_{l\text{-}m}$ is measured by positioning the loudspeaker in the place of the sample facing each microphone. Then the loudspeaker is placed facing the sample-area and two measurements are carried out one with h_s and one without the sample h_b (Figure 2-7).

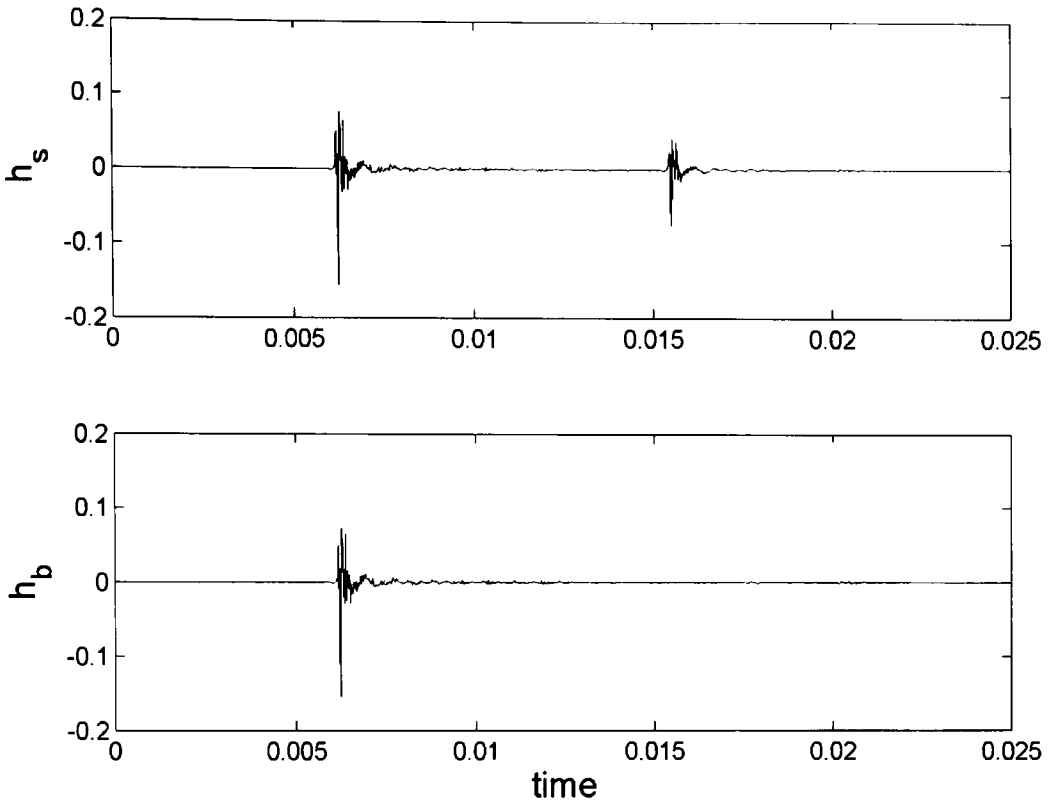

Figure 2-7. Measured impulse responces with and without the sample.

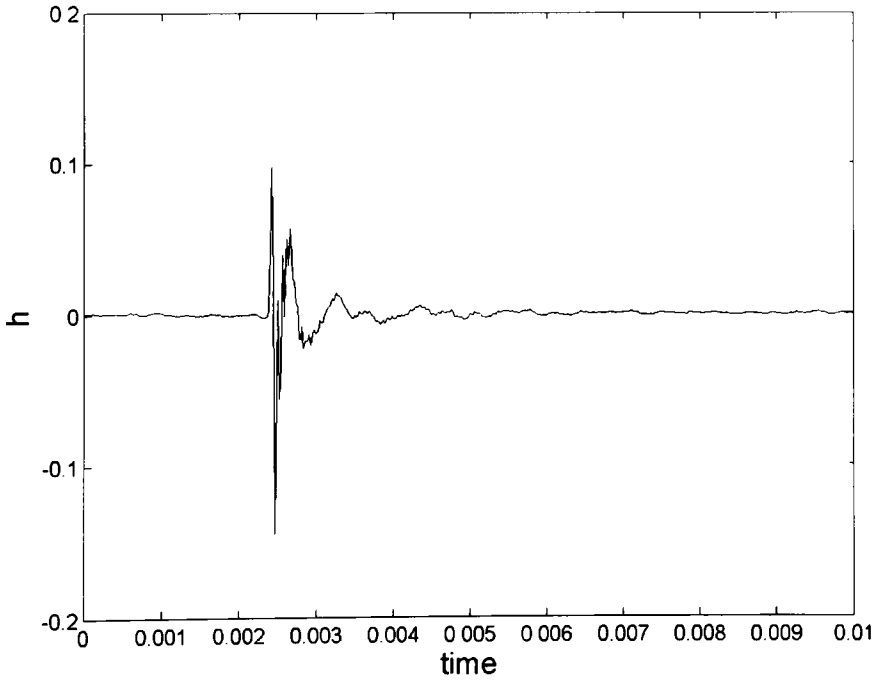

Figure 2-8. Measured scattered impulse response of the sample.

The common peak corresponds to the incident wave that gets recorded by the microphone before it reaches the sample area. The second peak of h_S contains the scattered response from the sample. After the application of equation 2.14 the response is windowed to remove the residue from the incident sound. Thus the scattered impulse response that is used to generate the polar response of the sample is acquired (Figure 2-8). The polar plot for each frequency is obtained by Fourier Transforming the impulse responses of the 37 miniature microphones (Figure 2-9).

Despite the efforts to follow the standard to the letter the requirement for signal to noise ratio was not met. The standard suggests a value of at least $40dB$ for a reference flat plate. In the measurements carried out for this thesis the signal to noise ratio did not exceed $25dB$ due to the low sensitivity of the microphones used. Despite this deviation the measured scattered pressure distribution displayed the expected behaviour.

Since the sample is a flat reflective surface the scattered pressure distribution is expected to be symmetric. As can be seen in Figure 2-9 there is a notable difference for instance at $\pm 5\pi/8$. The reason for this is the fact that the plot suffers from errors in the positioning of the microphones in the arc. Due to the existence of sharp variations in the plot even a 0.1° error in the position of the microphone can result in a substantial error in measurement.

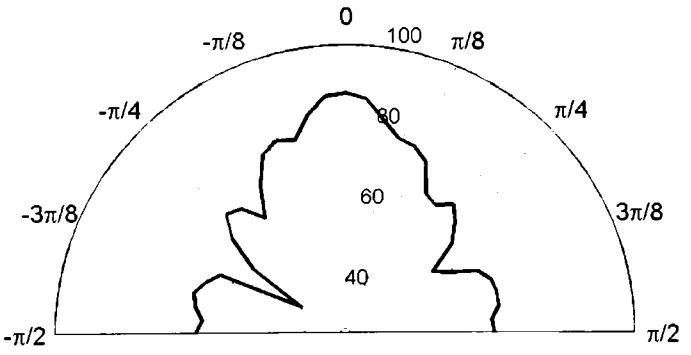

Figure 2-9. Measured normal incidence scattered pressure distribution of a rigid surface $70cm$ wide at $1.8kHz$.

2.3. Measurements Vs Simulations

Measurements are tedious to conduct and time consuming, so simulations are used in this thesis for the estimation of the performance of diffusers. In order to establish the validity of the prediction models comparison with measurements need to be carried out.

The measured sample is a flat rigid plate of 70*cm* width, 10*cm* depth and 30*cm* height. Since the system discussed in the previous Section measures the scattered field in one plane 2-D simulation is going to be used for the investigation. The simulation will consider an infinitely tall surface but the measured sample is tall enough for that not to be a factor given that the area of interest is that close to the floor of the chamber.

2.3.1. Boundary Element Modelling

The geometry of the measurement is introduced in 2-D BEM and Figure 2-10 displays the polar plots of the scattered field at a number of distinct frequencies. Although the patterns are not dissimilar the reflected pressure predicted by BEM diminishes as the frequency increases. This is due the fact that the 2-D BEM considers cylindrical wave propagation which is given by a 0^{th} order Hankel function (eq 2.4) that attenuates the sound wave with distance r as a function of $\left({}^{1}/_{rf}\right)$.

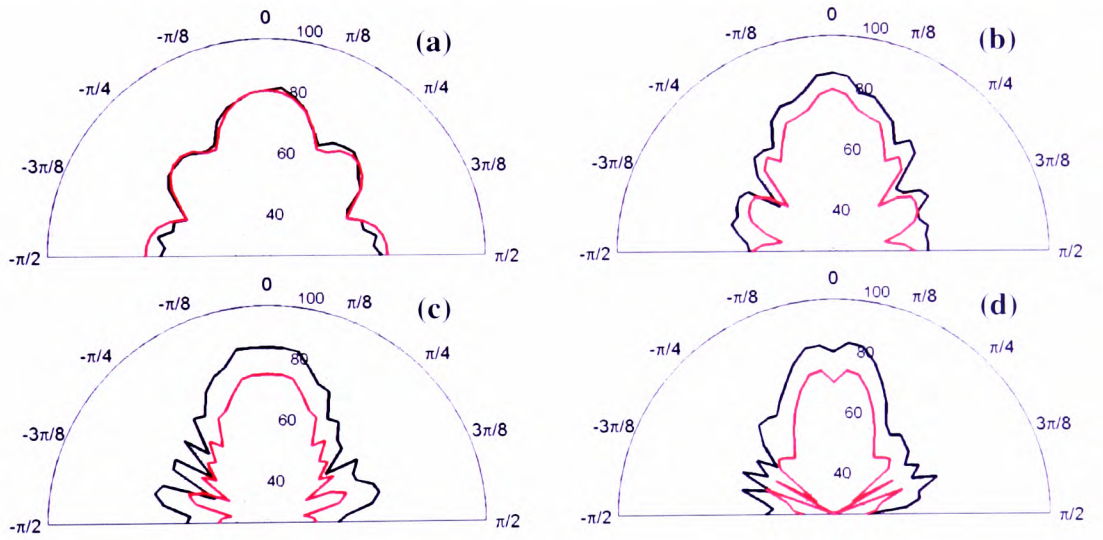

Figure 2-10. Normal incidence scattered pressure distribution (dB) measurement Vs BEM prediction from a rigid surface. (a) 1*kHz*, (b) 2*kHz*, (c) 4*kHz* and (d) 6*kHz*. ——— Measured, ——— Predicted.

In order to compensate for this effect, the reflected pressures must be normalised to a reference pressure. In order for the reference pressure to be representative of the distance the sound wave travels the reference point can be the scattered pressure at the 0^{o} receiver. In this way reflected energy will be lost so the normalisation will be done to the same overall reflected energy per frequency. This allows for the patterns of the scattered pressure distribution to be compared. The results are displayed in Figure 2-11.

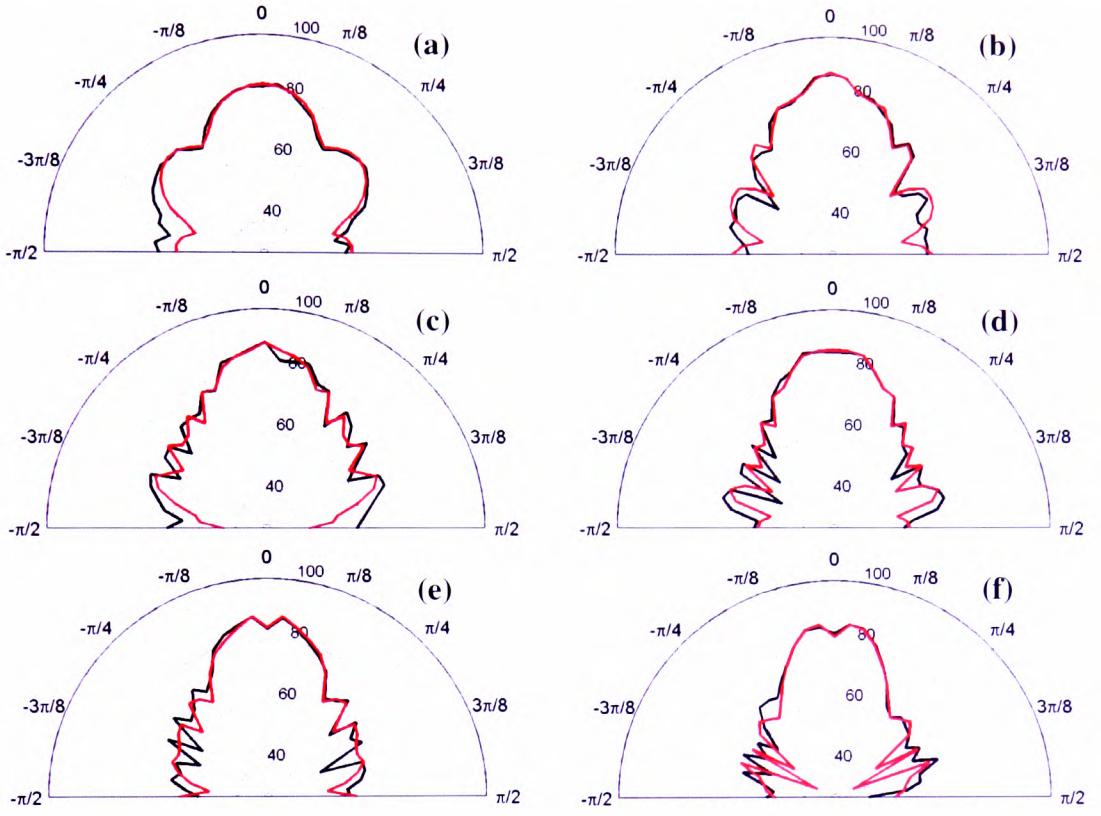

Figure 2-11. Normal incidence scattered pressure distribution (dB) measurement Vs BEM prediction from a rigid surface normalized to the same sum of the reflected pressure. (a) $1kHz$, (b) $2kHz$, (c) $3kHz$, (d) $4kHz$, (e) $5kHz$ and (f) $6kHz$. ——— Measured, ——— Predicted.

BEM simulation manages to predict quite accurately the distribution at small angles of reflection ($< \pm\pi/4$) while seemingly failing only at oblique angles of reflection at high frequencies. The reason for this difference is the existence of a large number of narrow periodicity lodes at high frequencies that occur so close together that they fall within the error of placing the microphones in their arc as discussed in Section 2.2.

Comparison of measurements and simulations from partly absorbing surfaces will be conducted in Section 9.2.1 where the performance of Absorption Grating Diffusers is going to be investigated.

2.3.2. Fourier Model

While 2-D BEM considers the geometry of the source and sample; the Fourier Model considers plane wave incidence and only models the front surface of the sample. Instead of a point source plane wave propagation is considered and the receivers are considered to be located in the far field so only the angle of reflection is taken into account.

Figure 2-12 displays the polar plots of the scattered field at a number of distinct frequencies as predicted by the Fourier Model compared to measurement. Given the fact that the model does not consider wave attenuation the graphs have been normalised to the same sum of reflected pressure. At $1kHz$ the prediction is in agreement to the measurement with the exception of the oblique angles of reflection, at $2kHz$ the agreement occurs only in the locations and width of the lobes while at higher frequencies there is no agreement.

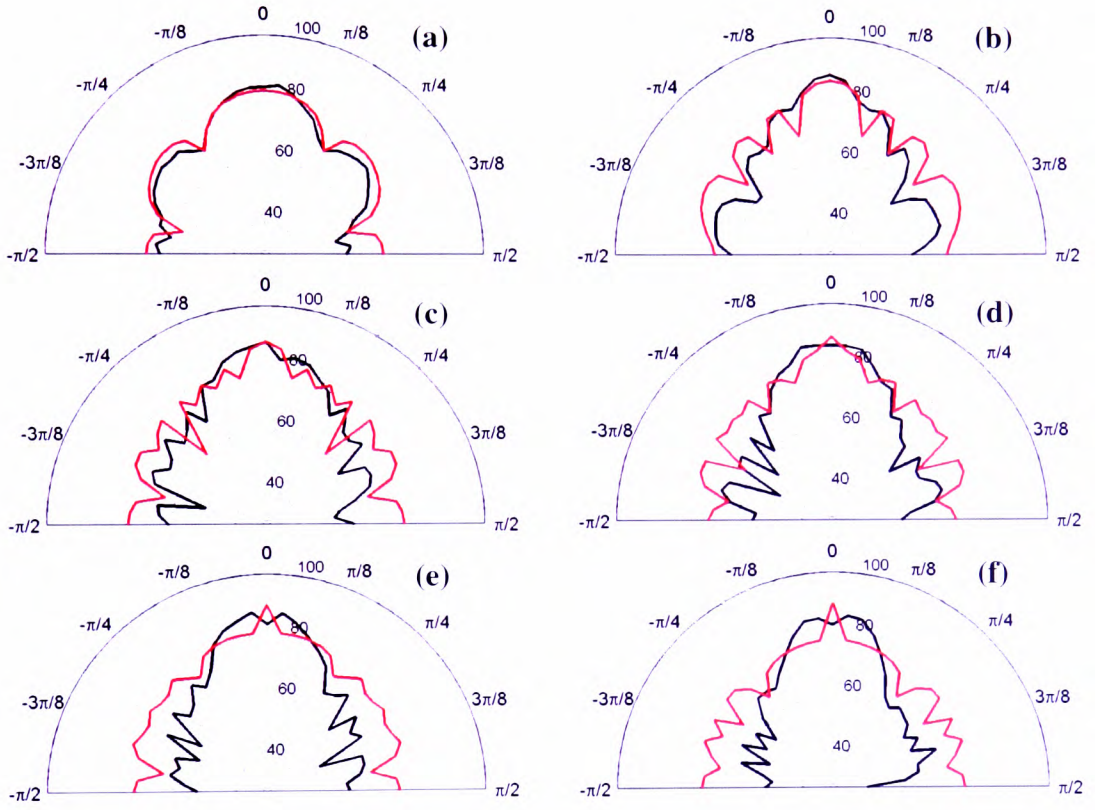

Figure 2-12. Normal incidence scattered pressure distribution (dB) measurement Vs the Fourier Model prediction from a rigid surface normalized to the same sum of the reflected pressure. (a) $1kHz$, (b) $2kHz$, (c) $3kHz$, (d) $4kHz$, (e) $5kHz$ and (f) $6kHz$. ——— Measured, ——— Predicted.

The Fourier Model considers that a plane surface consists of a series of point omni-directional sources which results in overestimation of pressure in the non specular reflection lobe which is evident in Figure 2-12(b). The limitations of the Fourier Model are coupled with the fact that the comparison is done between far field prediction and near field measurement to result in the disagreement at higher frequencies. At Figure 2-12(c-f) the measured specular reflection lobe has widened containing more receivers (see Section 2.2) while the Fourier Model considers only a single receiver in that lobe. To the Fourier Model

can show only the potential of a structure to diffuse and not be used to access its performance.

2.3.3. Discussion

There is a trade-off between accuracy of prediction and computational speed with the different models. The Fourier Model is very fast but it is an idealization of the problem. It does not correctly model evanescent waves close to the surface, it considers incident plane waves and is only applicable in the far field. However, it is an elegant model that connects the distribution of the reflection coefficient on the surface with the scattered response. That is why it finds application in diffuser design.

The Boundary Element Method is more accurate and has been shown to give accurate predictions for Phase Grating Diffusers[31] but is computationally expensive. There are methods that allow for the number of elements to be reduced such as the thin-panel Boundary Element Method[31] or exploitation of the symmetries of the surface[11] but even then it remains time consuming.

The angular resolution of the polar plots in this chapter have been dictated by the measurement procedure were the receivers were placed with an increment of 5^{o}. At later stages of this thesis angular resolution of 1^{o} will be used when predicting the performance of diffusers. This will give a better representation of the performance of diffusers.

2.4. Summary

This Chapter contained the various methods that have been use in the past to attain the scattered pressure distribution from a diffuser. Boundary Element Modelling has been shown as the most exact but at the same time more computationally expensive simulation technique. The Fourier Model on the other hand has been shown to give a very elegant connection between the distribution of reflection coefficients on a surface and the scattered pressure distribution from it. Finally, the method to measure the scattered field that was used in this thesis has been presented and compared with both 2-D BEM and Fourier Model. In the two following Chapters PGDs are going to be discussed. In Chapter 3 the reasoning behind standard PGDs is going to be presented and issues surrounding diffuser design such as periodicity and modulation are going to be addressed. Later, in Chapter 4 new PGDs are going to be introduced.

Chapter 3. Standard Phase Grating Diffusers

The most common category of diffusers is Phase Grating Diffusers (PGD). In this Chapter these structures are going to be presented. Their inherent limitations are going to be discussed and the issue of periodicity is going to be addressed. Modulation techniques are going to be used to be deal with the problem of periodicity.

3.1. The diffusers

The introduction to this thesis presented sequences for PGDs, here the diffuser design is examined in more detail.

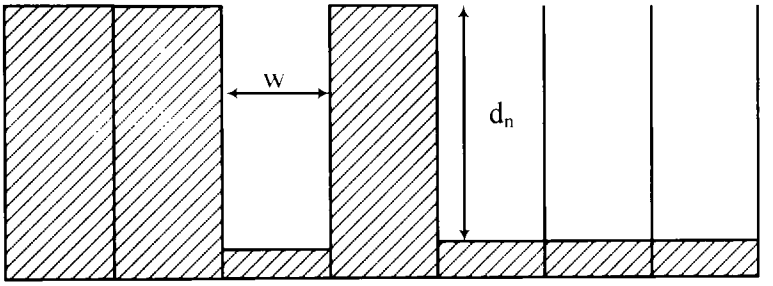

Figure 3-1. One period of a Maximum Length Sequence Diffuser (MLSD) of well width w and depth of the n^{th} well, d_n.

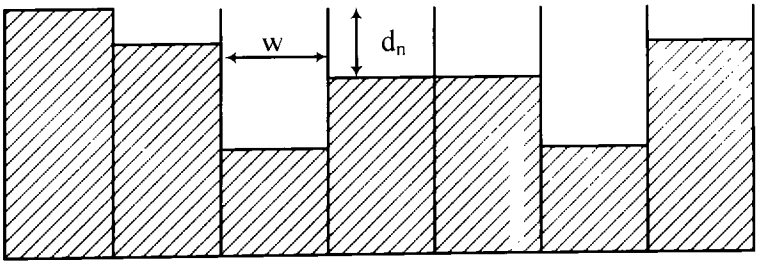

Figure 3-2. One period of a Quadratic Residue Diffuser (QRD) of well width w and depth of the n^{th} well, d_n.

The depth of the n^{th} well d_n in the diffuser is set using a pseudorandom sequence[8]:

$$d_n = \frac{s_n \lambda_0}{2P} \qquad 3.1$$

where s_n is the n^{th} term of the pseudorandom sequence, λ_0 is the design wavelength, and P is the integer the sequence has been generated using, e.g., a prime p for QRDs.

The distribution of the phase φ_n and the reflection coefficient R_n is given by[8]:

$$\varphi_n(f) = 2\pi \frac{s_n}{P} \cdot \frac{f}{f_0} \tag{3.2}$$

$$R_n(f) = exp\left(j2\pi \frac{s_n}{P} \cdot \frac{f}{f_0}\right) \tag{3.3}$$

where f is the frequency of the incident wave and f_0 is the design frequency of the diffuser.

The pseudorandom sequences are chosen based on the Fourier Method. So a structure that has reflection coefficients whose Fourier Transform has a uniform magnitude should diffuse well. The Wiener-Khinchin theorem states that the square of the magnitude of the sequence's Fourier Transform is equal to the Fourier transform of its autocovariance (or autocorrelation) function. As a result a sequence of reflection coefficients whose autocorrelation function is a Kronecker delta function, will display good diffusion properties. Such sequences include the quadratic residue sequences (Figure 3-3).

The quadratic residue sequences are generated for any prime number P by the equation[25]:

$$s_n = n^2 \ mod \ P \tag{3.4}$$

where $n \in [1, P]$ and *mod* is a function giving the minimum positive remainder.

For this type of pseudorandom sequences the integer number generator P is prime and it is equal to the length of the sequence ($N = P$). The autocorrelation function R_{XX} of the sequence is[25]:

$$R_{XX} = \begin{cases} P & \tau = 0 \\ 0 & -\dfrac{P-1}{2} \le \tau \le \dfrac{P-1}{2}, \ (\tau \neq 0) \end{cases} \tag{3.5}$$

where τ denotes the autocorrelation delay.

The distribution of reflection coefficients displays these autocorrelation properties for frequencies f_a that the phase distribution is:

$$\varphi_n(f_a) = 2\pi \frac{s_n}{P} \tag{3.6}$$

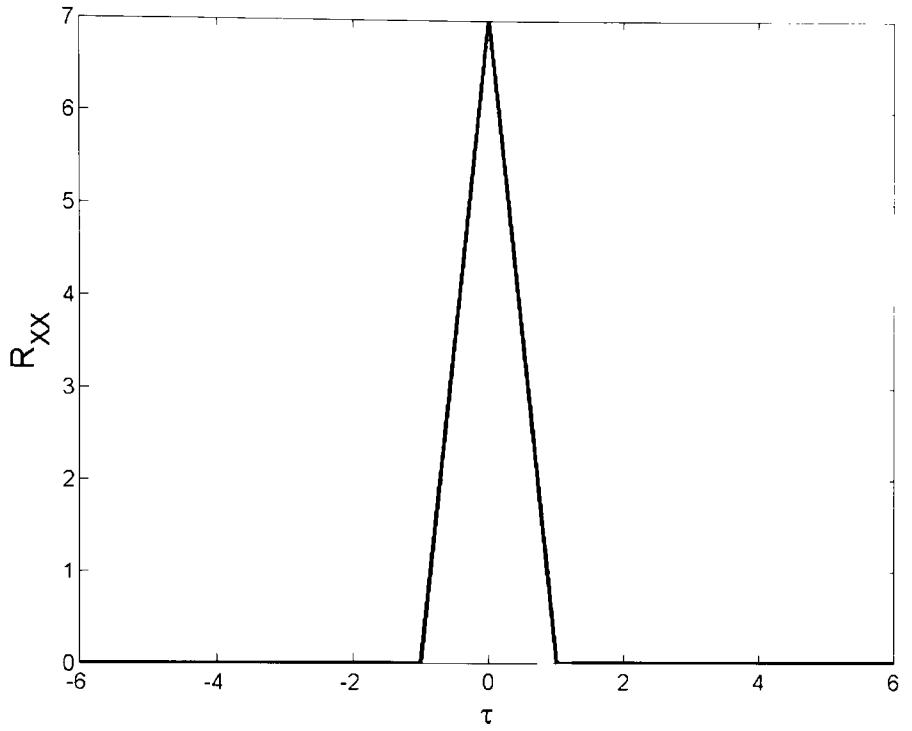

Figure 3-3. Magnitude of autocorrelation function of a quadratic residue sequence (P=7).

Due to phase's modular nature the distribution on the surface is the same for most integer multiples of the design frequency:

$$f_a = af_0 \tag{3.7}$$

where α is an integer that is not a multiple of P.

At these frequencies the reflection coefficients retain the same phase differences (Figure 3-4):

$$\varphi_n(\alpha f_0) = 2\pi \frac{s_n}{P} \cdot \frac{\alpha f_0}{f_0} = 2\pi \frac{\alpha s_n}{P} = \pm 2\pi \frac{s_n}{P} \tag{3.8}$$

This suggests that the diffuser performs best at these frequencies. When α becomes equal to P then the diffuser perform like a plane surface (see Section 3.2.1).

There are sequences that although their autocorrelation functions do not go to 0 when it is out of phase ($\tau \neq 0$) they still display a steady level. Other sequences that have found application in diffuser design are the primitive root sequences, the maximum length sequences *etc.*

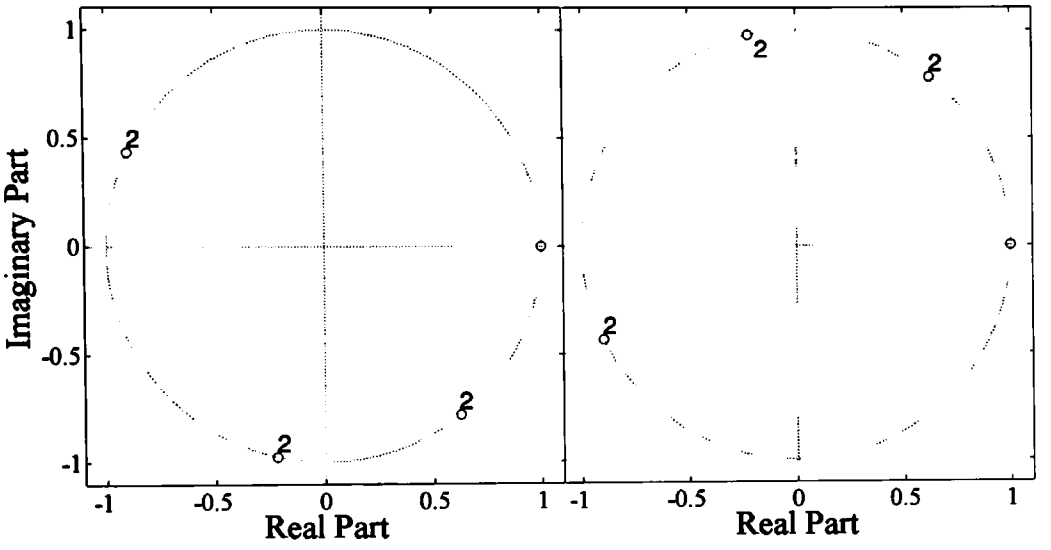

Figure 3-4. Reflection coefficients of a 1-D QRD (N = 7) at 1, 2 and 4 (left) 3, 5, 6 (right) times the design frequency.

3.2. Disadvantages

PGDs display notable limitations. Some are inherent problems of their design while others steam from the inaccuracy of the Fourier Model that is used to choose the sequence that generated them.

3.2.1. Flat plate frequencies

When α is a multiple of the integer generator the phases of all the reflection coefficient will become multiples of 2π, and so all the reflection coefficients will be 1[16]. This will result in the structure acting like a flat reflective surface. These flat plate frequencies, as shown in Figure 3-5, are given by:

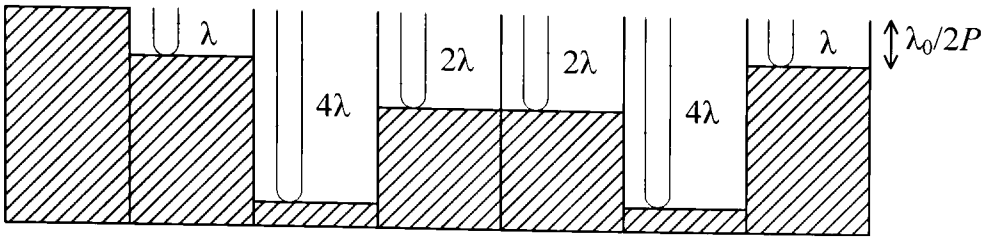

Figure 3-5. The flat plate effect of a QRD (P=7).

While in theory every such structure displays an infinite number of flat plate frequencies, in reality it is rare for there to be more than one of these frequencies in the bandwidth of concern. When that is the case, it is common to refer to the first of them as 'the' flat plate frequency.

3.2.2. Well cut-off frequencies limitations

Due to the fact that plane wave propagation in the wells is assumed, there is an upper frequency limit to the design. When half the wavelength becomes smaller than the well width then the waves will no longer propagate as plane wave within the wells. This will cause the reflection coefficients to deviate from the ones required. The upper frequency limit is:

$$\lambda_{min} = 2w \qquad \text{or} \qquad f_{max} = {}^{c}/_{2w} \tag{3.10}$$

where c is the speed of sound and w is the smallest dimension of the wells cross-section.

3.3. Periodicity

Probably the most controversial issue surrounding diffuser design is periodicity. Since their introduction PGDs have been considered as structures with regularly spaced patches of different reflection coefficient generating an inherent regularity to the structure. Later the choice of sequences with good autocorrelation properties steered towards periodic repetition of the diffusers[8]. Even the standard for the measurement of the scattered pressure distribution from a surface requires a structure of several periods to be tested if the diffuser is to be used periodically[23].

Any type of repetition causes periodicity lobes to be introduced in the autocorrelation function of the reflection coefficient. This results in the introduction of periodicity lobes in the pattern of the scattered pressure distribution above a low frequency limit.

A typical case of periodicity comes from the regular distribution of the reflection coefficient on a surface. In order to portray this problem a 1-D diffuser will be considered. It will be considered that its reflection coefficient is constant for patches of width w throughout its surface:

$$R(x) = R(nw) = R_n \ , \quad \text{for } n = 0, 1, 2, \dots, N-1 \tag{3.11}$$

where N is the number of patches.

The scattered intensity distribution I_s can be estimated using the Fourier Method (see Section 2.1.2):

$$I_s(\theta) = \left| we^{-jk'Nw/2} \cdot sinc\left(k'w/2\right) \right|^2 \cdot \left| \sum_{n=0}^{N-1} R_n e^{jk'(n+1)w} \right|^2 \tag{3.12}$$

where θ is the angle of reflection, $k'=ksin\theta$ and N is the number of patches of the diffuser.

The $sinc^2(x)$ function that has been introduced in equation 3.12 causes lobbing to be introduces in the distribution of scattered intensity. The pattern it introduces can be seen in Figure 3-6 for w/λ = 0.5. This lobe causes the distribution to be less uniform and therefore degrades the performance of the diffuser.

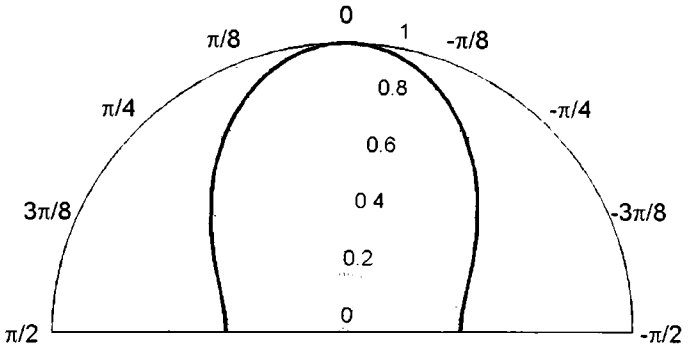

Figure 3-6. Lobing introduced by the constant patches of reflection coefficient when the width of the patches is equal to half of the wavelength (w/λ = 1/2).

To cover large surface areas more than one period of a diffuser structure is commonly used. The repetition of the sequences causes harmonics to be created in the autocorrelation function. This creates sharper grating lobes and as a result a less uniform scattering distribution. The scattered intensity distribution in the case of Q diffusers is given by the interference pattern of Q identical source:

$$I_{tot}(\theta) = I_s(\theta)\frac{sin^2\left(Qk'W/2\right)}{sin^2\left(k'W/2\right)} \qquad 3.13$$

where $I_s(\theta)$ is the scattered intensity distribution of a single period of diffuser, Q is the number of periods, k' is equal to $ksin\theta$ and W is the width of one period of the diffuser.

The interference pattern degrades the performance of the diffuser as it causes for more lobing to be introduced to the scattered intensity distribution. In Figure 3-7 the lobing effect is displayed for $Q = 3$, $W/\lambda = 2$.

The superposition of the two types of periodicity is displayed in Figure 3-8. This is an effect that will become more evident in absorption grating diffusers, as will be shown in Chapter 5.

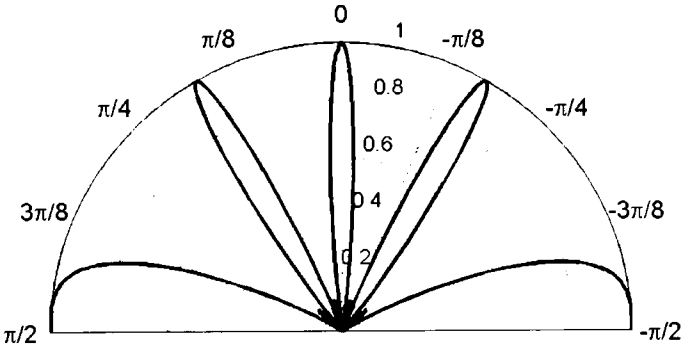

Figure 3-7. Lobing introduced by 3 periodic repetition of the diffusers when the width of a single diffuser is equal to two times the wavelength ($W/\lambda = 2$).

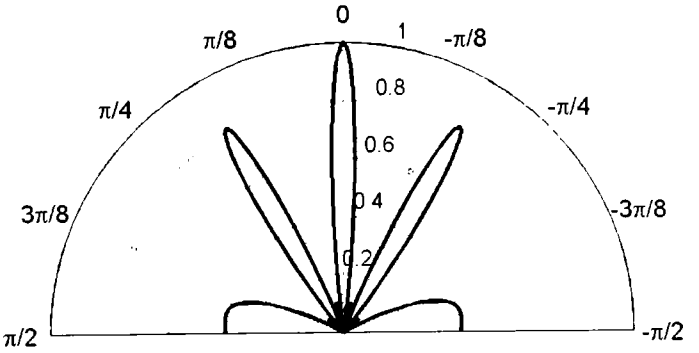

Figure 3-8. Lobing introduced by the combination of constant patches of reflection coefficient and periodic repetition of the diffuser ($Q = 3$, $N = 4$, $w/\lambda = 1/2$).

3.4. Modulation

Ways of dealing with periodicity have been devised as regular arrangement of the reflection coefficients is ill-advised. While in cases that more than one period is required it is necessary to modulate the base sequence with another [15-16, 39-41]. In order to modulate two sequences a binary pseudorandom sequence is required. The binary sequence defines the order in which the sequences will be placed with 1 corresponding to the first sequence and 0 to the second (Figure 3-9).

Modulation will be used extensively in Chapter 4 to deal with the degrading effect that periodicity has on the performance of PGDs. It will also be used to improve the beam steering effect of Lüke Diffusers (Section 4.2.2).

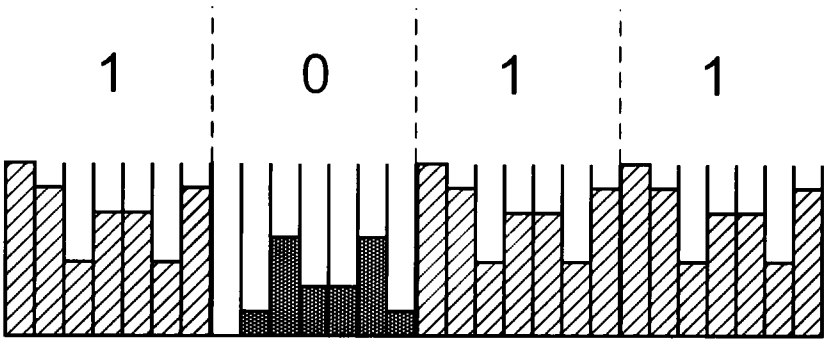

Figure 3-9. Modulation of two PGDs using the binary sequence [1,0,1,1].

There are three major ways of choosing the second sequence to be used in the modulation. The simplest way of presenting them is by considering PGDs (Section 3.1).

3.4.1. Using the inverse of the base sequence:

An inverse sequence is created by subtracting the original sequence from the integer that it was generated from. So, for example, the sequence that will generate the inverse diffuser of the quadratic residue sequence with P = 7 [0,1,4,2,2,4,1] is calculated by subtracting this sequence's coefficients from its integer number generator, 7 in this case, to give [7,6,3,5,5,3,6] as the inverse (Figure 3-10).

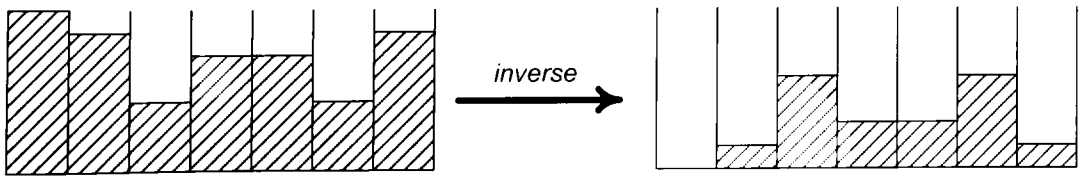

Figure 3-10. The inverse of a QRD (P=7).

The inverse diffuser reflects the opposite phases from the original. Since the arrangement is done using a pseudorandom sequence the resulting structure will display the phase grating behaviour of a larger PGD with two levels. This technique is widely used[41] and, as will be further used in Chapter 4.

3.4.2. Using the base sequence in reverse order:

Another technique for modulation is to use the same sequence but in reverse order. In practice this is easily achieved by rotating the diffuser in its plane such that its left becomes its right. The modulation is essentially a diffuser and its mirror image. For example, for primitive root sequence with P = 7 [1,3,2,6,4,5] the mirror diffuser is simply [5,4,6,2,3,1]. This method has the added advantage of the overall structure having the same depth as the base diffuser; in addition it only requires one base diffuser. However, it only works if there is a degree of asymmetry in the base diffuser (Figure 3-11), as shall be shown for the new Luke diffusers later. For instance the QRD of P = 7 is [0,1,4,2,2,4,1] and is mirror [1,4,2,2,4,1,0] which display the only variation of the 0 which is moved from the beginning to the end of the sequence.

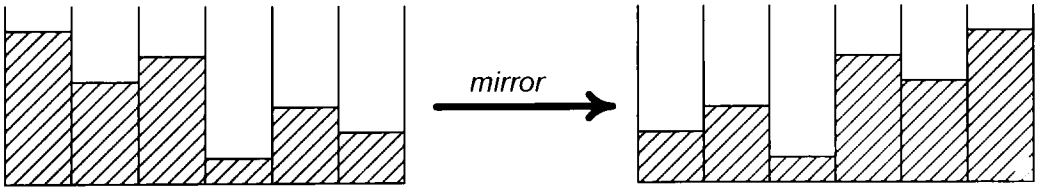

Figure 3-11. The mirror of a PRD (P=7)

3.4.3. Using a different sequence to that of the base diffuser:

In principle any alternate sequence may be used, but it is usual to use one that is performing better than the base sequence at the frequencies where it is performing badly. For example, two sequences with different flat plate frequencies. Angus, for instance, used a combination of P = 5 and P = 7 QRDs[39] while Cox *et al* used a combination of P = 7 and P = 11 PRDs[42]. Since they used the same design frequency for the diffusers their flat plate frequencies occurred at different points. It can also be used in cases of families of sequences such as the Power Residue and the Lüke Diffusers that will be examined in Chapter 4.

3.5. Diffusion

The diffusion coefficient for a standard PGD can be seen in Figure 3-12. In this plot the normalised diffusion coefficient of 5 periods of QRD of prime generator p=7 is displayed. The design frequency is set to $1kHz$ (Figure 3-13a) and the well width to $5.1cm$. The overall width of the structure is $1.8m$. The key frequencies to be noted are the peaks of diffusion at approximately the multiples of the design frequency. At these multiples the phase changes generated by the wells is the same with that at the design frequency (eq 3.8) resulting in good diffusion (Figure 3-13b). The exceptions lie in the 7^{th} multiple that is the first flat plate frequency (Figure 3-13c) of the diffuser (eq 3.9).

It is noteworthy to point out that the diffuser performs like a plane surface, when the normalised diffusion coefficient is equal to 0. Apart from the flat plat frequencies this happens consistently for frequencies below $860Hz$. This frequency coincides with that when λ becomes comparable to the width of the period of diffuser W. This is a low frequency limit of the diffuser:

$$\lambda_{max} = W \qquad \text{or} \qquad f_{min} = {}^{c}/_{W} \qquad 3.14$$

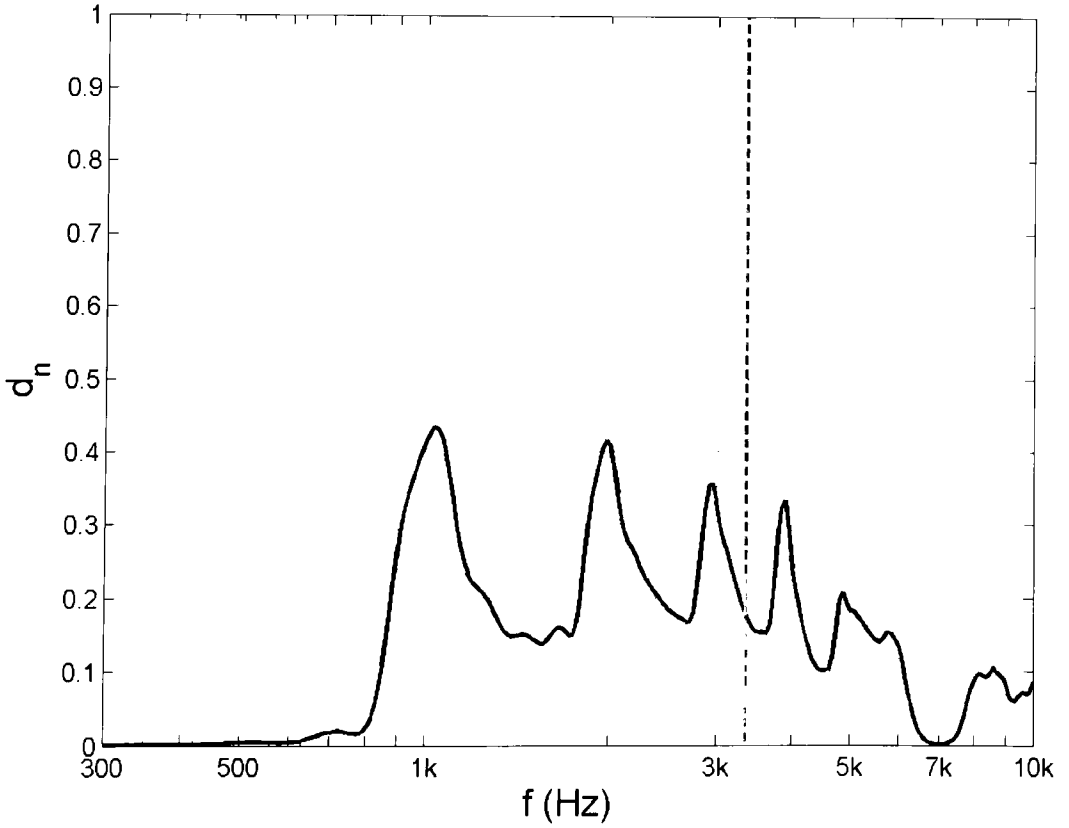

Figure 3-12. Normalised diffusion coefficient Fourier Model prediction of 5 periods of QRD (p=7) with the design frequency set at 1 kHz (▪▪▪▪ upper frequency limit).

The frequency of 3.36 *kHz* is the high frequency limit associated with the wave propagation in the well as discussed in Section 3.2.2. The prediction for frequencies higher than this limit will deviate from the performance of the diffuser. They are included in the graph as they present the diffusion trend.

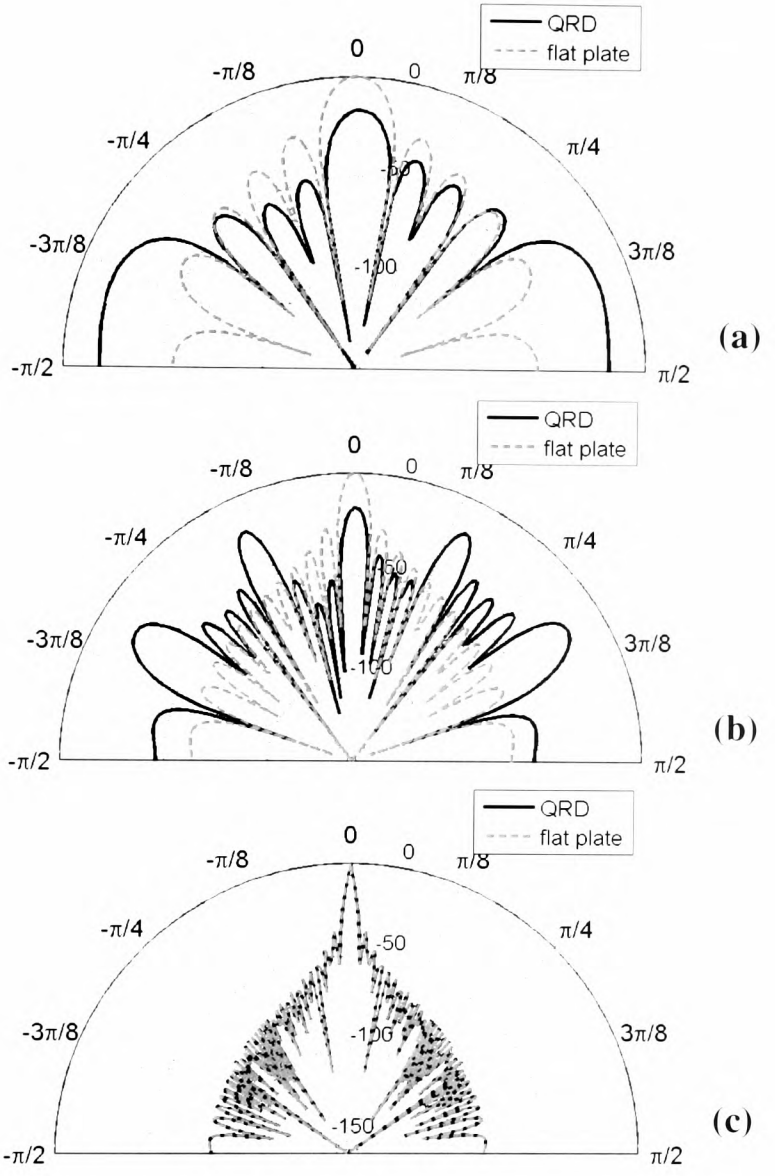

Figure 3-13. Normal incidence scattered pressure distribution Fourier Model prediction of 5 periods of QRD (p=7) at the design frequency at $f = f_0 = 1kHz$ (a), $f = 2f_0 = 2kHz$ (b) and the flat plate frequency $f = 7f_0 = 7kHz$ (c).

A very important factor in the location of the peaks of the diffusion coefficient has to do with the periodicity of the structure. The scattered field contains the pattern of 5 point sources

positioned at the centre of each diffuser (Figure 3-14). These sources would be spaced a diffuser width W apart. If the diffusers were wider the interference pattern of these sources would change. This change would alter the peaks of the diffusion coefficient.

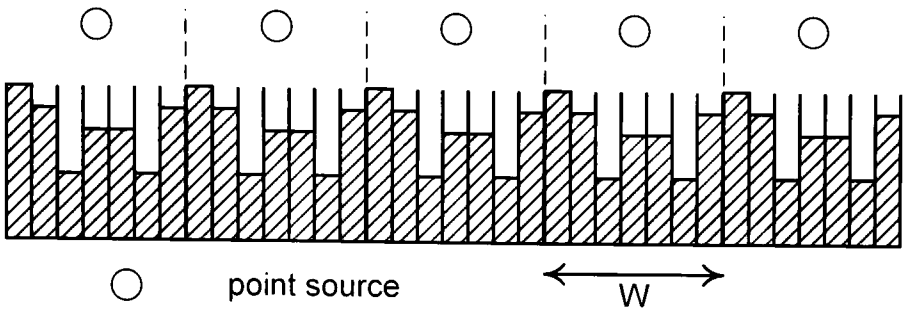

Figure 3-14. The periodicity equivalent of 5 periods of a QRD.

It is important to remember the limitations of the Fourier Model that was used for the simulations here. The model considers plane wave propagation in the wells without taking into account the cut off frequency of the well (eq 3.10). For the given well-width the high frequency limit is at $^{c}/_{2W} \cong 3.3kHz$. This suggests that the behaviour for most of the bandwidth of this graph will only be approximately correct. For more accurate predictions Boundary Element Modelling must be used.

3.6. Summary

With the conclusion of this Chapter the foundation of PGDs is completed. How they are generated from pseudorandom sequences has been presented and their frequency limitations have been outlined. The modulation techniques that can be used to address the problem of periodicity that arises from the periodic repetition of a single diffuser have been explained. Finally, the Fourier Method was used to investigate the characteristics of a standard Quadratic Residue Diffuser. In the following Chapter new PGDs are going to be introduced.

Chapter 4. New sequences for Phase Grating Diffusers

The research question being examined in this Chapter is whether it is possible to design diffusers with higher flat plate frequencies by applying new number sequences based on larger integer generators.

Standard Phase Grating Diffusers (PGD) like Quadratic Residue Diffusers (QRD) and Primitive Root Diffusers (PRD) have a limited frequency range due to the flat plate effect that occurs when all the wells radiate in phase. The frequencies at which this occurs are directly linked with the integer P that generates the pseudorandom sequence. For both QRD and PRD the flat plate frequency is P times the diffuser's design frequency. In order for the phenomenon to take place outside the audible range a large number generator is needed which will result in a long sequence as their length is similar to the generator ($N_{QRD} = P$, $N_{PRD} = P$-1). As a small diffuser is easier to construct and handle, the length of the pseudorandom sequence is usually small limiting its integer generator as well. In this Chapter an alternative approach using number sequences is presented that, although short in length, are based on large integers. Two pseudorandom sequences, Power Residue and Type-II Lüke, have this desired characteristic. The performance of Power Residue Sequence Diffusers (PWRD) and Lüke Sequence Diffusers (LSD) is investigated using numerical simulations. Of the two PWRDs are shown to move the flat plate effect to much higher frequencies as expected, while LSDs are shown to require modulation in order to achieve substantial diffusion.

4.1. Power Residue Sequence Diffusers (PWRD)

Power residue sequences are generating by under-sampling primitive root sequences (Figure 4-1). The relationship between the generator and the length of the sequence changes dramatically. For every PRD a number of PWRDs can be created that preserve the prime generator but reduce the width of the structure by a fraction equal to the sampling step. By changing the sampling starting point a family of PWRDs can be formed.

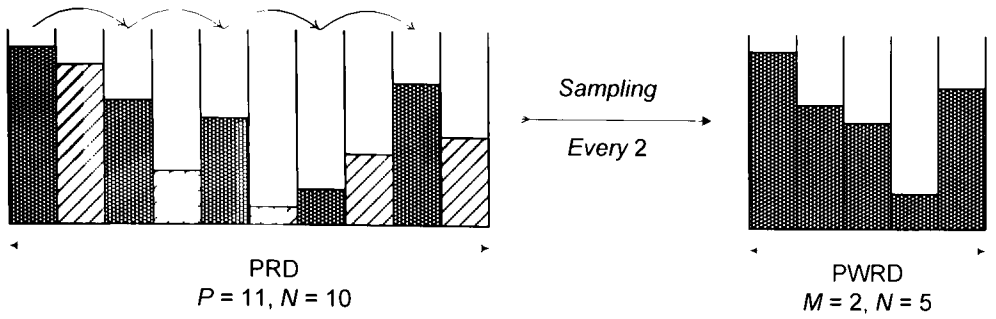

Figure 4-1. PWRD (P = 11, M = 2, r = 0) generated from a PRD (P = 11).

4.1.1. The sequence

Power residue sequences are based on any prime number P that can be expressed in the form:

$$P = M \cdot N + 1 \qquad 4.1$$

where M and N are integers. M power residue sequences of period N can be generated using the equation[25]:

$$s_n^{(r)} = \alpha^{r+Mn} \bmod P \qquad 4.2$$

where $0 \leq r < M$, $0 \leq n < N$, α is a primitive root of P and *mod* indicates the least non-negative remainder. A primitive root of P is any number α with the property that any co-prime to P is congruent to a power of $a \bmod P$[25].

In the case that a set of M integers $D = [s_{n,1}, s_{n,2}, \ldots, s_{n,M}]$ are modulo an integer P they are said to form an integer difference set if every integer $m \neq 0$ can be expressed in exactly χ ways in the form:

$$s_{n,\zeta} - s_{n,\xi} = m \bmod p \quad , \; where\, \zeta \neq \xi \in [1{:}M] \qquad 4.3$$

The properties of the difference set are usually represented using the nomenclature (P,M,χ)[25]. If, and only if, the power residue sequence forms a cyclic difference set (P,M,χ), then the reflection coefficients that it generates displays two level autocorrelation magnitudes[25]:

$$|R_{XX}(\tau)| = \begin{cases} N & \tau = 0 \\ \sqrt{N - \frac{N}{M} + \frac{1}{M}} & -\frac{N-1}{2} \leq \tau \leq \frac{N-1}{2}, \ (\tau \neq 0) \end{cases} \quad 4.4$$

where R_{XX} is the ACF and τ is the delay variable. Figure 4-2 shows the magnitude of the ACF for a number of power residue sequences of the same length that have been created from different generators. As is obvious from this figure, their out-of-phase magnitude is always greater than 0 and becomes greater as M increases. This means that they display worse ACF properties than QRD that displays out-of-phase magnitudes equal to 0 (Figure 3-3).

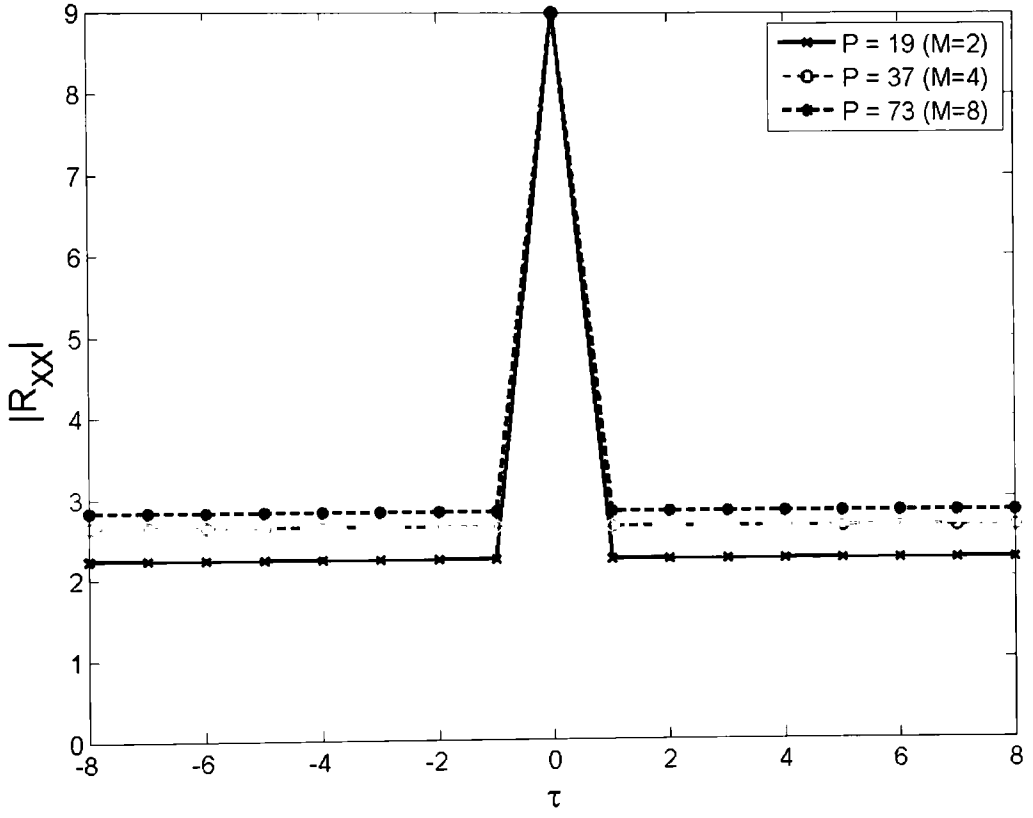

Figure 4-2. Magnitude of autocorrelation function of all power residue sequences of period N = 9 that can be generated from different prime numbers.

The out of phase non-zero value of the ACF is not uncommon as other pseudorandom sequences display such a characteristic. When the out-of-phase is real, it translates to a DC component in the Fourier Transform of the reflection coefficient which dictates an added feature in the angle of specular reflection. For primitive root and maximum length sequences that have out-of-phase ACF[25] equal to -1 this manifests as a null in the angle of specular reflection, a characteristic that has been exploited in diffuser design[42-43].

In the case of power residue sequences the ACF is not constant out-of-phase. While the magnitude is constant the phase is not so (Figure 4-3). This effect deviates from the requirement of a Kronecker-delta like behavior and undoubtedly will degrade the evenness of the spectrum.

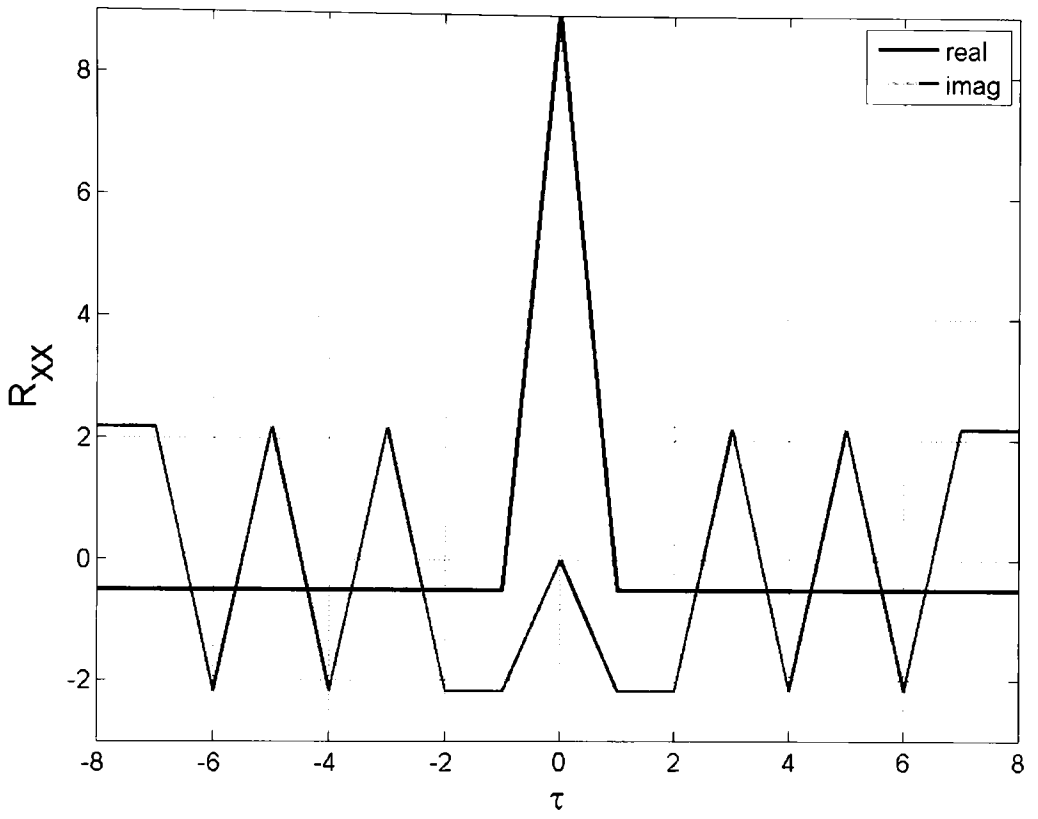

Figure 4-3. Autocorrelation function of a power residue sequences of period N=9 and generegator P=19.

As already mentioned, power residue sequences are under-sampled primitive root sequences, with a sample taken every M^{th} coefficient, with a different starting point (dictated by r), as shown in Figure 4-1.

In the case of primitive root sequence of $P = 11$, the primitive root is 2, and the sequence is $[1, 2, 4, 8, 5, 10, 9, 7, 3, 6]$. For $M = 2$, and $r = 0$ every other coefficient is taken to form the power residue sequence starting from the first $s_n^{(0)} = [1, 4, 5, 9, 3]$ while for $r = 1$ the starting point is the second term of the original primitive root sequence $s_n^{(1)} = [2, 8, 10, 7, 6]$. Note that the one sequence is the inverse of the other: if the coefficients of $s_n^{(1)}$ are cyclically

shifted left 2 positions, it becomes $[10, 7, 6, 2, 8]$. So in this case, the two power residue sequences are connected via the equation:

$$s_n^{(0)} = P - s_{n-2}^{(1)} \tag{4.5}$$

This connection between the two sequences results in pairs of diffusers in a family that perform similarly, because pairs have reflection coefficients with opposite phases. For families of power residue sequences with more than 2 sequences this phenomenon takes place for those that are spaced $M/2$ sequences away with the required shift left being $\left(\frac{N}{2} - 1\right)$.

$$s_n^{(r)} = P - s_{n-(N/2-1)}^{(M/2-r)} \tag{4.6}$$

There are three cases that form cyclic difference sets that can be applied in the creation of power residue sequences[25]:

$$M = 2 \text{ and } N \text{ is odd}$$

$$M = 4 \text{ and } N = \zeta^2 \text{ where } \zeta \text{ is odd} \tag{4.7}$$

$$M = 8 \text{ and } p = 8 \cdot \zeta^2 + 1 = 62 \cdot m^2 + 9 \text{ where } \zeta \text{ and } m \text{ are odd}$$

Since the goal is to push the flat plate effect to higher frequencies, the most promising cases follow the last rule as it combines higher primes P with short sequences. The first case that falls under this category is:

$$M = 8, n = 3, m = 1 \Rightarrow p = 73 \tag{4.8}$$

This generates a short sequence typical of the length used in practical Schroeder diffusers (period $N = 9$) but with a prime number generator of 73. One such sequence is $s_n^{(1)} = [1, 2, 4, 8, 16, 32, 64, 55, 37]$, which is the first of the family ($r = 0$). The higher prime number gives a first flat plate frequency of 73 times the design frequency. This fact becomes more impressive if one considers that a QRD with the same characteristic frequencies would consist of 73 wells (Figure 4-4).

A primitive root sequence with period $N = 10$ being generated from the prime $P = 11$ will have a flat plate frequency at 11 times the design frequency, less than 6 times lower. It will actually display 6 flat plate frequencies before the power residue diffuser displays its first.

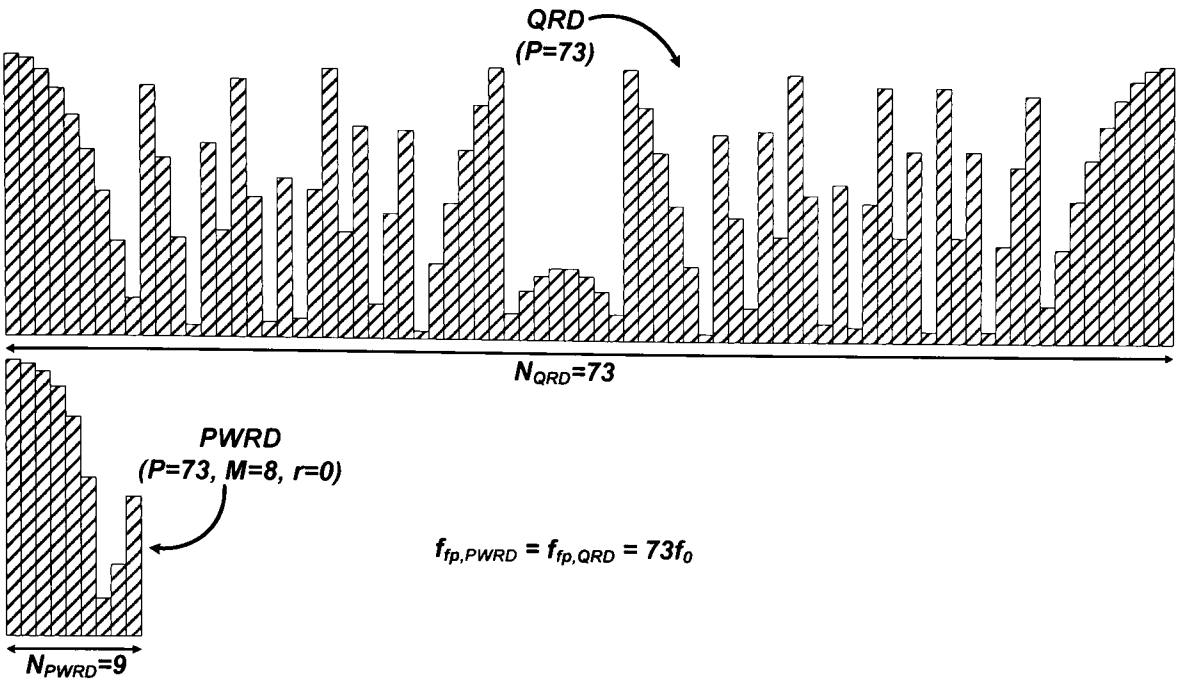

Figure 4-4. A QRD and a PWRD with the same design and flat plate frequency.

4.1.2. The diffusers

The cases of PWRD of period $N = 9$ are taken into consideration. They have a length which is similar to many commercial devices while they can be generated using all the cases of cyclic difference sets that have been suggested in 4.7. This allows the performance of sequences with the same length but of different autocorrelation properties and different prime number generator to be examined.

Given that the choice of sequence is based on the Fourier Model the performance of the diffusers will be examined using the same technique. The structures to be tested will consist of 5 periods of $40cm$ wide PWRDs. The resulting structure is $2m$ wide resulting in a low frequency limit of $857.5Hz$ (eq. 3.14). The well width is $4.4cm$ which results in the upper frequency limit of the diffuser being $3.9kHz$. The design frequency is set to $1kHz$.

The first case is created when a PRD of length 18 (P=19) is sampled every other well. Then 2 PWRDs ($M = 2$) of length $N = 9$ can be formed:

$$s_n^{(0)} = [1, 4, 16, 7, 9, 17, 11, 6, 5]$$
$$s_n^{(1)} = [2, 8, 13, 14, 18, 15, 3, 12, 10] \qquad 4.9$$

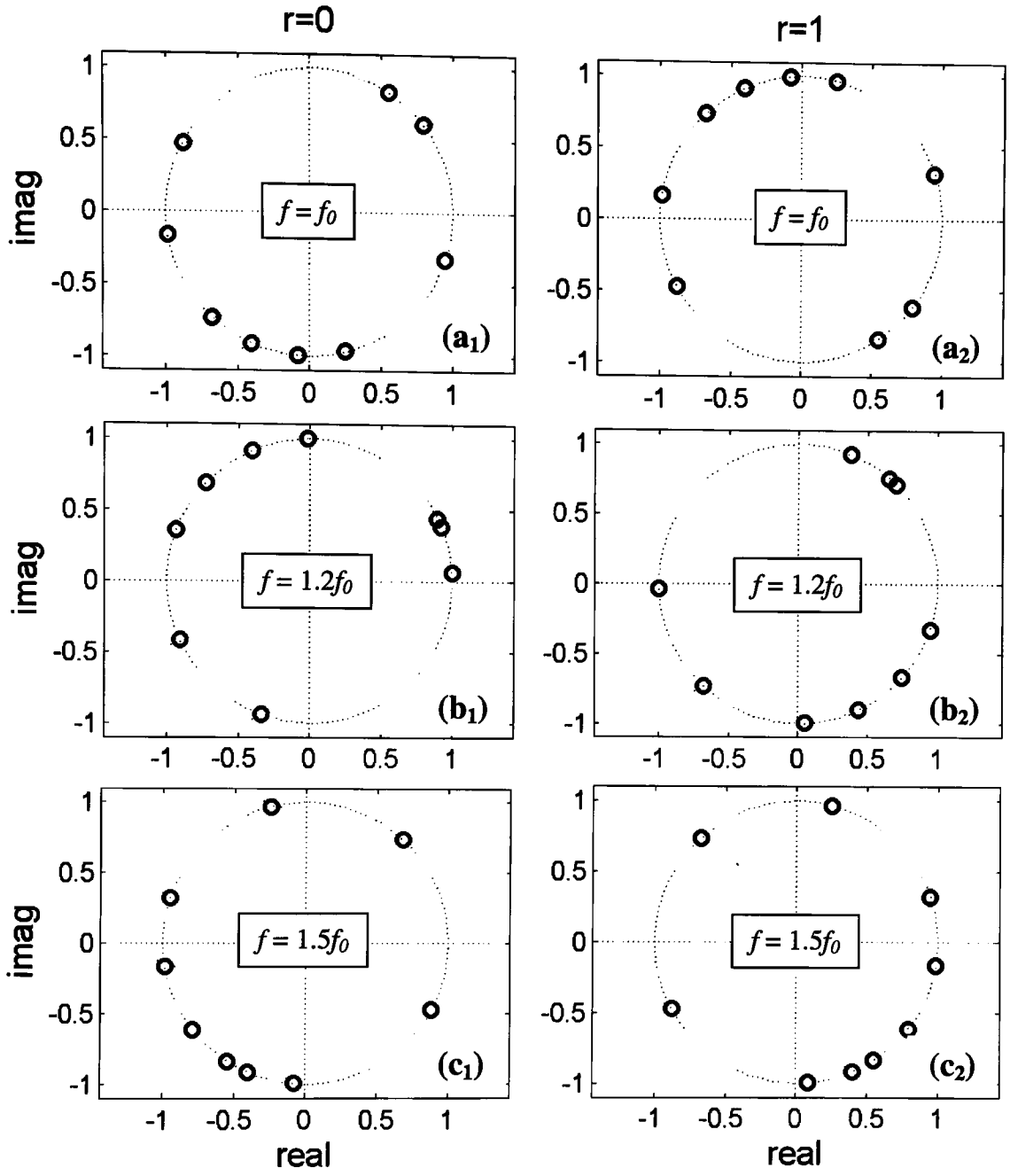

Figure 4-5. Argand diagrams of the reflection coefficients of the PWRDs (P = 19) for the different frequencies.

The two sequences are the inverse of one another (see Section 4.1.1) which results in reflection coefficients, at multiples of the design frequency, to display opposite phases, as can seen in the Argand diagrams of Figure 4-5(a). The different sign in the phases will result in the same scattered pressure distribution from the two diffusers with an inversion of the angles of reflection (Figure 4-6(a and c)). This relationship is not the same for other frequencies. At

these frequencies the distribution of the phases is the same for both diffusers but the values of the phases are not opposite as before (Figure 4-5(b and c)). This factor manifests itself in the polar responses of the diffusers (Figure 4-6b) which no longer display the symmetry that was evident at the multiples of the design frequency.

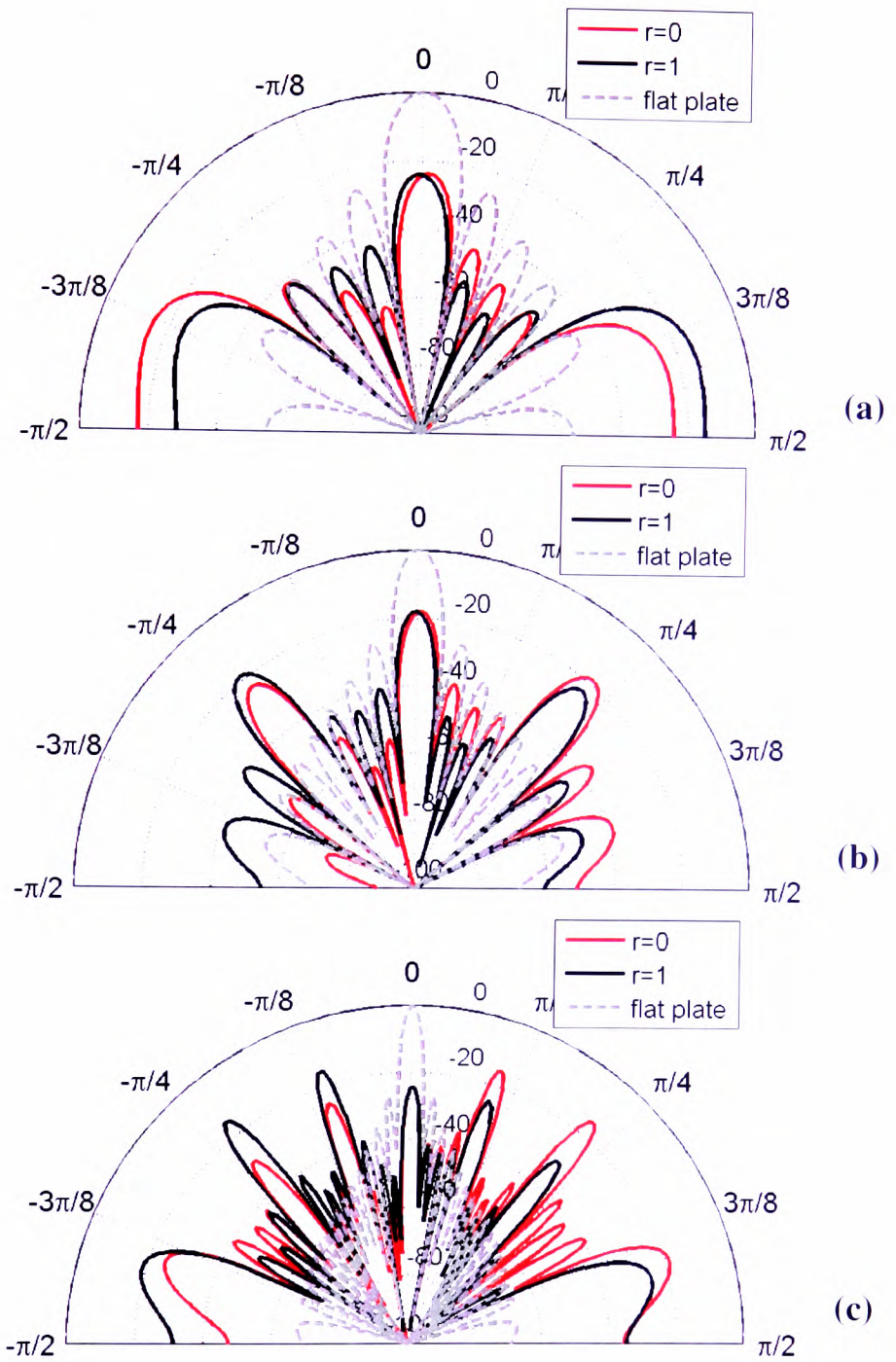

Figure 4-6. Fourier Model prediction of the normal incidence scattered level distribution of the two PWRDs (P=19, M=2) at the design frequency f_0 (a), at $f = 1.5f_0$ (b) and $f = 2f_0$ (c).

The normalised diffusion coefficients of these PWRDs are presented in Figure 4-7. They display their flat plate frequency at $19 \cdot f_0 = 19kHz$ as expected. The two diffusers display similar diffusion characteristics throughout this frequency range. The coefficient takes the same value for both cases at the multiples of the design frequency and displays only small variations at other frequencies. Variations that are due to the different position of their phase distribution in the Argand diagram.

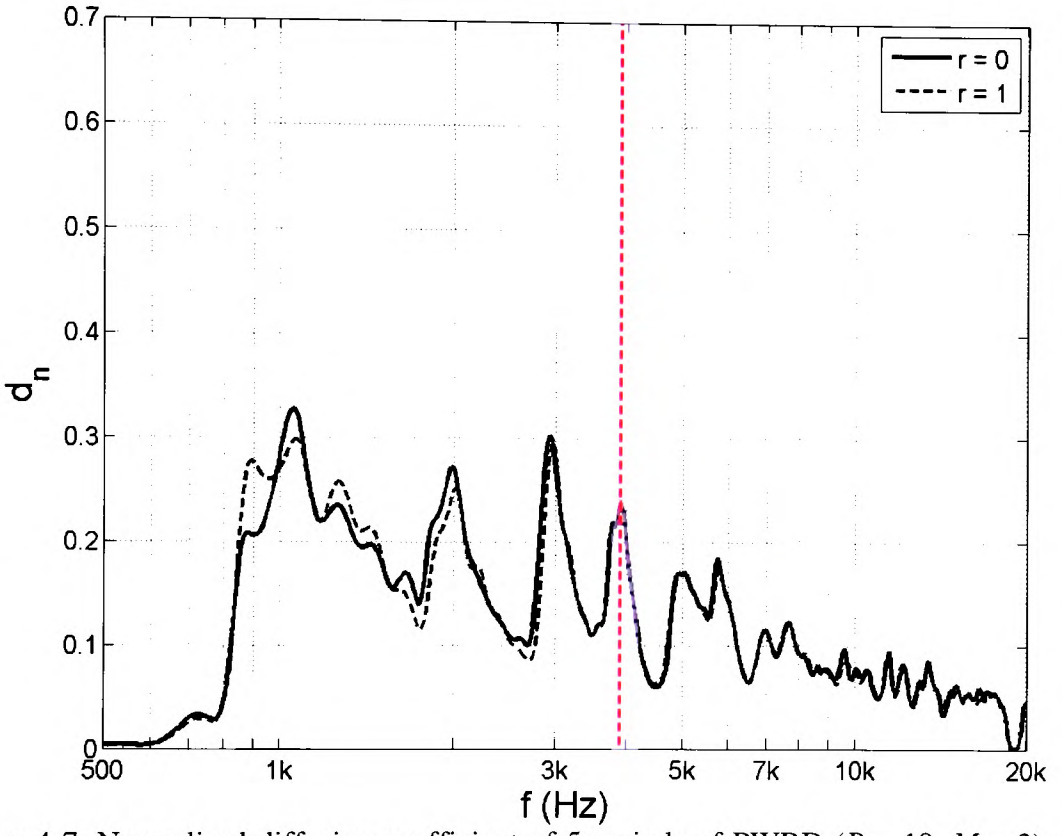

Figure 4-7. Normalised diffusion coefficient of 5 periods of PWRD (P = 19, M = 2) with a design frequency f_0 = $1kHz$, the width of the wells was set to $4.4cm$, estimated using the Fourier Model (---- upper frequency limit).

The PWRDs (P=19, M=2) did not allow diffusers with the same periodic autocorrelation characteristics but different reflection coefficient's distribution to be compared.

Such a comparison is possible for the following example. The PWRDs are taken from a PRD of length 36 (P=37) when samples every 4 wells (M=4). The result is 4 distinct diffusers of length N=9:

$$s_n^{(0)} = [1, 16, 34, 26, 9, 33, 10, 12, 7]$$

$$s_n^{(1)} = [2, 32, 31, 15, 18, 29, 20, 24, 14] \qquad 4.10$$

$$s_n^{(2)} = [4, 27, 25, 30, 36, 21, 3, 11, 28]$$

$$s_n^{(3)} = [8, 17, 13, 23, 35, 5, 6, 22, 19]$$

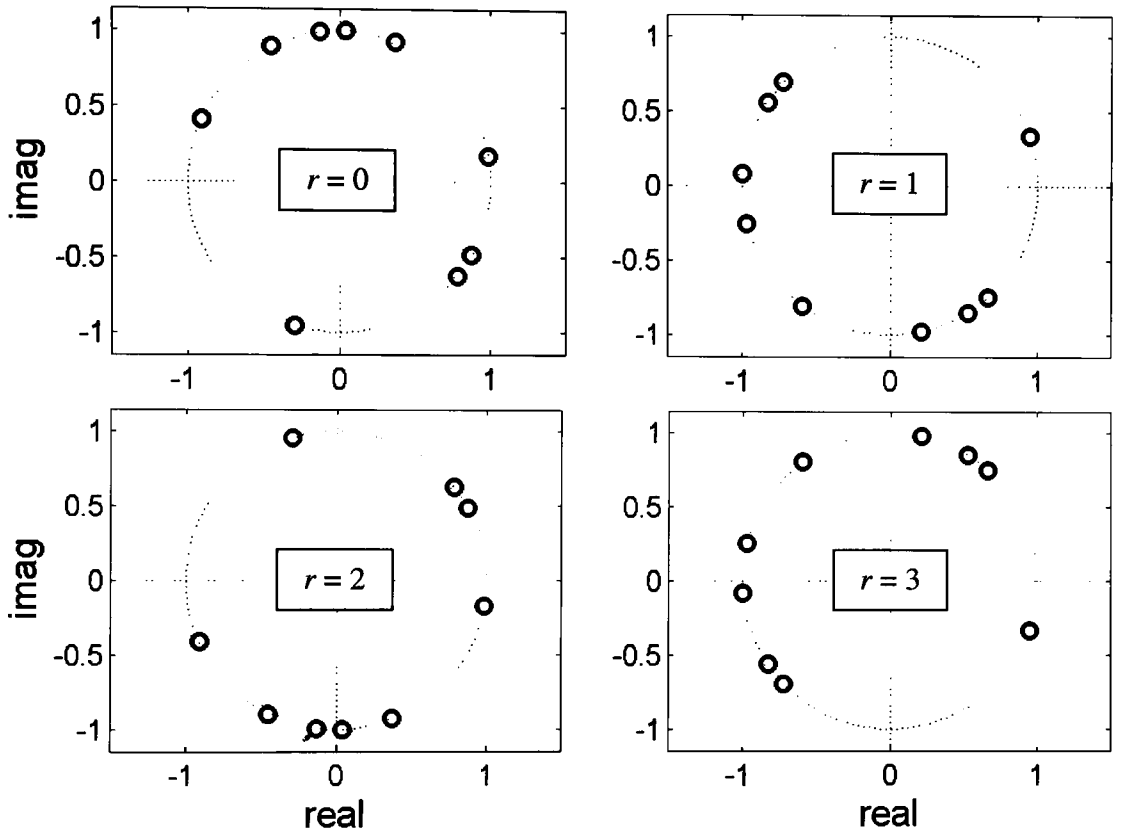

Figure 4-8. Argand diagrams of the reflection coefficients of all PWRDs (P=37, M=4) at the design frequency f_0.

These diffusers can be paired again with their inverse as can be seen in Figure 4-8. For this reason the diffusion coefficient of the first two is presented in Figure 4-9, since that of the other two will be similar. The coefficient displays similar trend for both PWRDs but it is obvious that it is not the same. While outside the frequency range of the plot the flat plate effect occurs at $37 \cdot f_0 = 37kHz$ as expected, which is outside the audible frequency range.

Even though the two diffusers display identical periodic autocorrelation properties at the multiples of the design frequency they do not have the same polar responses (Figure 4-10). This raises a new limitation of the design procedure. The desirable autocorrelation properties are only an indication of which surface phase grating can achieve uniform dispersion, as it refers only to the design frequency of the diffuser and does not contain information of its performance at other frequencies.

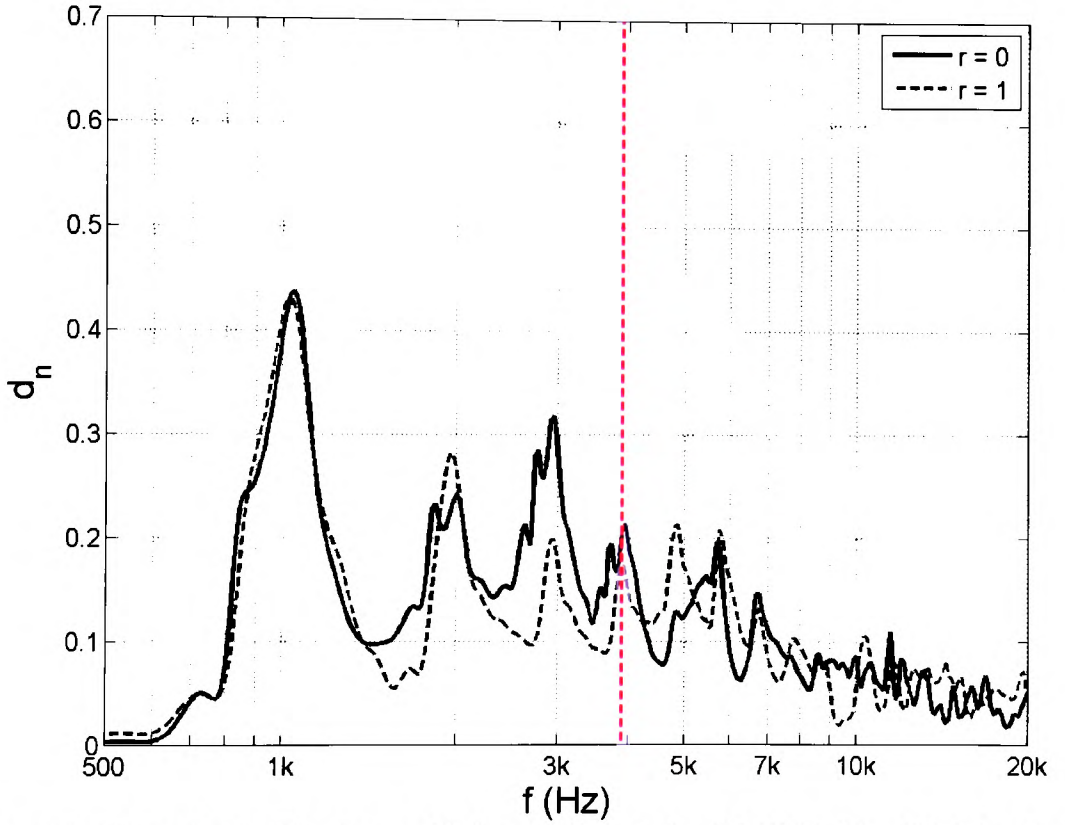

Figure 4-9. Normalised diffusion coefficient of 5 periods of PWRD (P = 37, M = 4) with a design frequency f_0 = $1kHz$, the width of the wells was set to $4.4cm$, estimated using the Fourier Model (---- upper frequency limit).

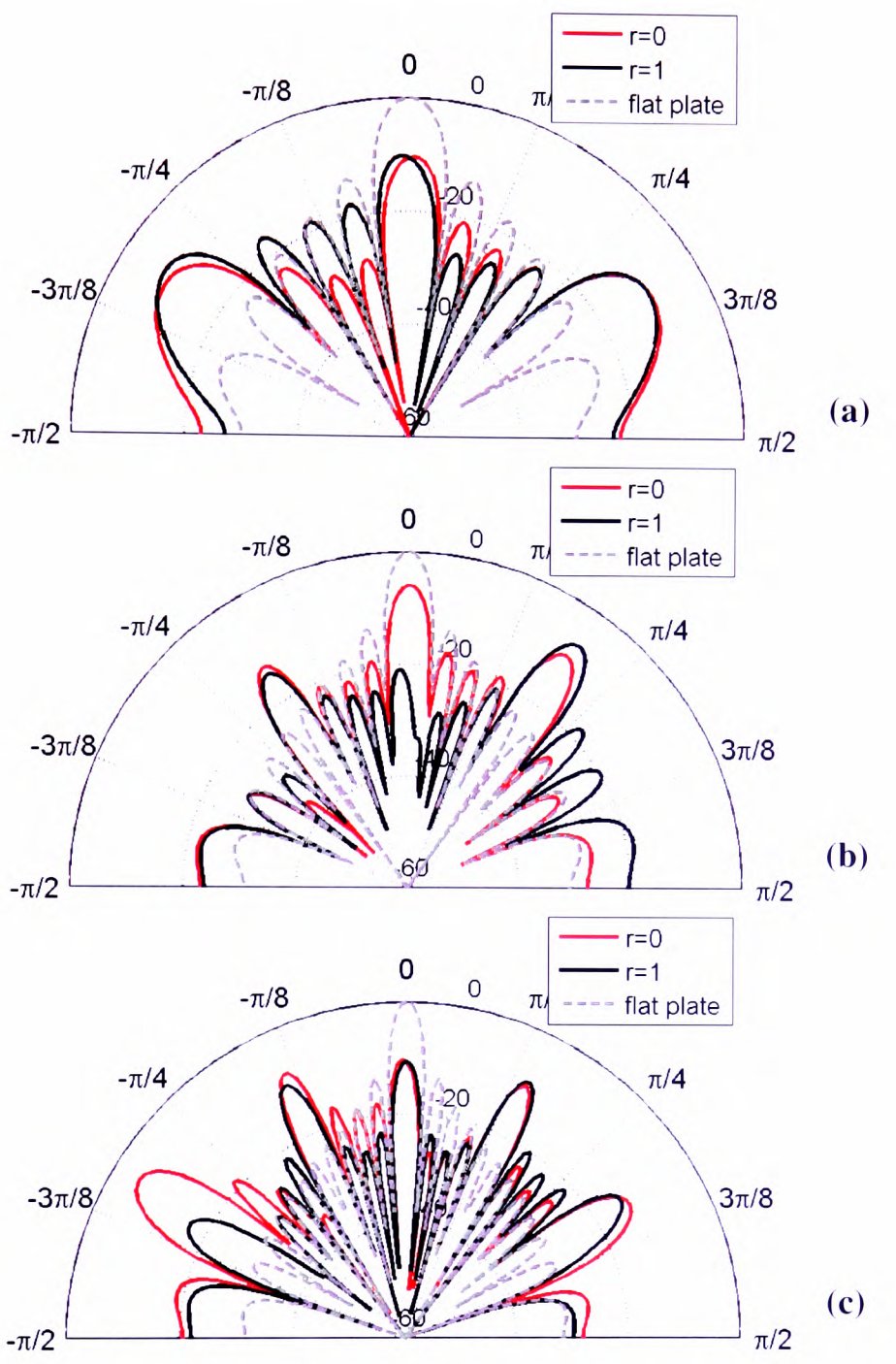

Figure 4-10. Fourier Model prediction of the normal incidence scattered level distribution of the two PWRDs (P=37, M=4) at the design frequency f_0 (a), at f=1.5f_0 (b) and f=2f_0 (c).

The last family of PWRDs that is going to be considered is the one that corresponds to the largest sampling step (eq 4.7) possible. When sampling every 8th well (M=8) the PRD generated by P = 73 a family of 8 PWRDs, of length N = 9, is formed:

$$s_n^{(0)} = [1, 2, 4, 8, 16, 32, 64, 55, 37]$$

$$s_n^{(1)} = [5, 10, 20, 40, 7, 14, 28, 56, 39]$$

$$s_n^{(2)} = [25, 50, 27, 54, 35, 70, 67, 61, 49]$$

$$s_n^{(3)} = [52, 31, 62, 51, 29, 58, 43, 13, 26]$$

$$s_n^{(4)} = [41, 9, 18, 36, 72, 71, 69, 65, 57] \qquad 4.11$$

$$s_n^{(5)} = [59, 45, 17, 34, 68, 63, 53, 33, 66]$$

$$s_n^{(6)} = [3, 6, 12, 24, 48, 23, 46, 19, 38]$$

$$s_n^{(7)} = [15, 30, 60, 47, 21, 42, 11, 22, 44]$$

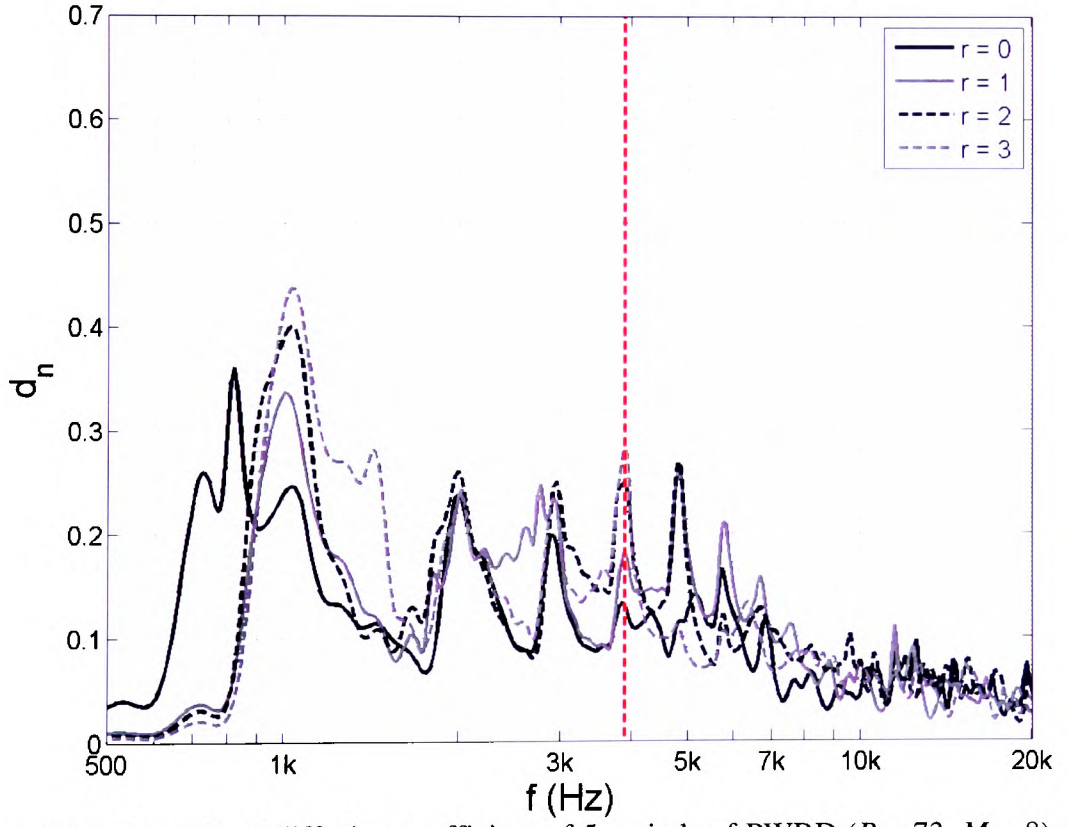

Figure 4-11. Normalised diffusion coefficient of 5 periods of PWRD (P = 73, M = 8) with a design frequency f_0 = 1kHz, the width of the wells was set to 4.4cm, estimated using the Fourier Model (---- upper frequency limit).

In Figure 4-11 the normalised diffusion coefficient of the first 4 of PWRDs of this family. In this case the flat plate frequency is 73·f_0 = 73kHz which is far outside the audible frequency

range. An interesting phenomenon that is evident from this graph is that the first of the PWRDs of the family start diffusing at a lower frequency than the rest. This is another example of the autocorrelation properties of a sequence not "telling the full story"

As has been stated earlier, the lower frequency limit of the diffuser geometries being tested here is when the wavelength fits into one period of the diffuser. This suggests that the PWRD (r=0) in question appears to have the behaviour of a larger structure when applied periodically. If one looks to the form of this PWRD a difference from that of the other diffusers becomes evident. Its wells are arranged in groups of similar depths, which suggests that at lower frequencies the wells do not act individually but as averages of these groups (Figure 4-12).

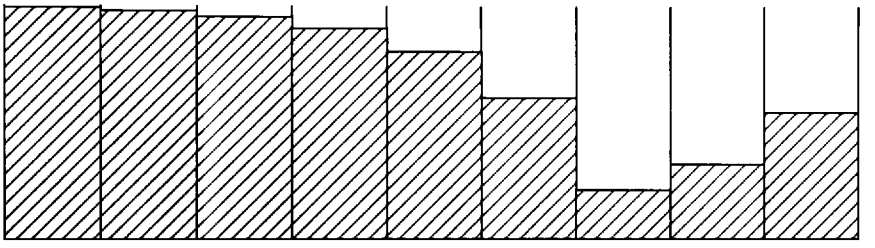

Figure 4-12. PWRD (P=73, r=0).

The predictions presented for PWRDs have been made using the Fourier Model which is the one that was used in the choice of the pseudorandom sequences. As has been discussed before (Section 3.2.2) this simulation technique does not account for the high frequency limit of the diffusers (eq. 3.10). For a 4.4cm well width of the PWRDs this frequency is approximately 3.9kHz. This means that the predictions above this frequency will be inaccurate unless the wells are themselves partitioned into sub-wells.

The more accurate BEM[44] is going to be used now in the comparison with more standard PGDs. Since the Fourier Model considers only a surface of a given distribution of reflection coefficients the structures have been regarded as 1-D. So the diffusers were compared with a rigid plate. BEM on the other hand models the whole structure in 2-D. The comparison is going to be made with a reflection structure of the same outer dimension that is going to be referred to as "plane surface".

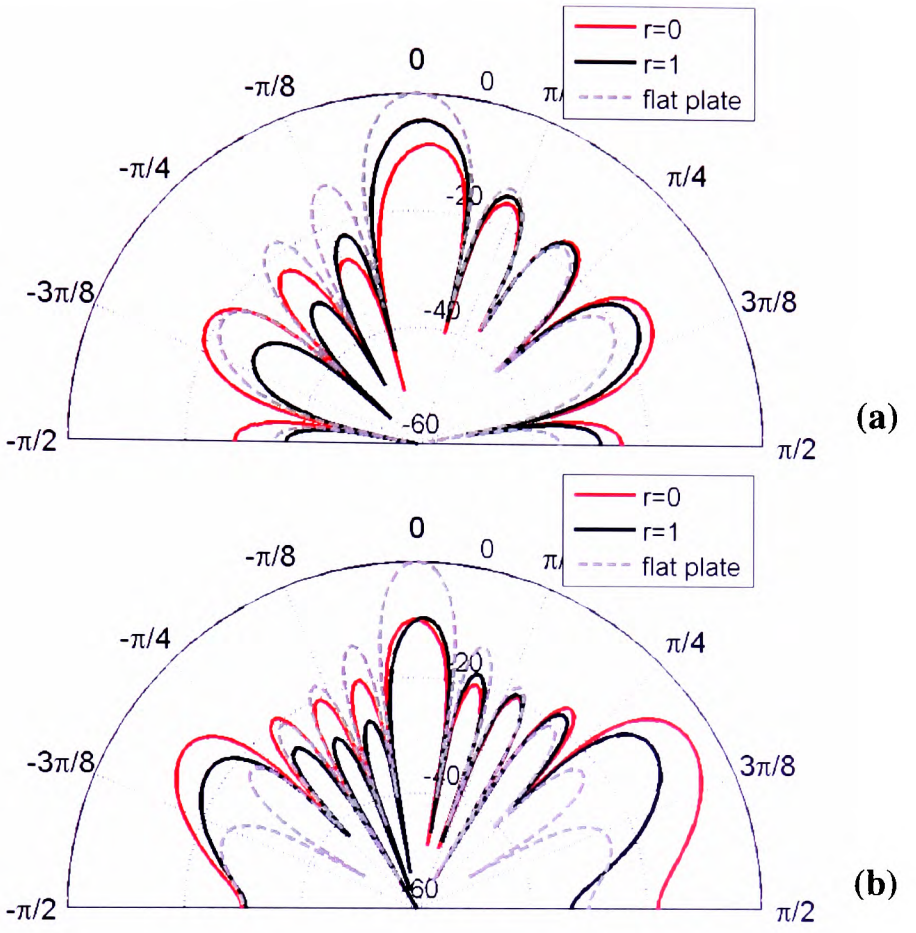

Figure 4-13. Fourier Model prediction of the normal incidence scattered level distribution of the two PWRDs ($P = 37$, $M = 4$) at $f = 0.8f_0$ (a) and the design frequency f_0 (b).

The following configuration is considered. Overall structures of $2m$ wide and the same design frequency are examined. Given that the main point of interest is the flat plate frequency the design frequency will be set to $500Hz$ in order for the flat plate effect to occur within the frequency range of examination.

The PWRDs are arranged in 5 periods with their well widths set to $4.4cm$. Given their design frequency and their prime number generator their flat plate frequencies are expected to be 8.5, 18.5 and 37.5 kHz respectively which will be outside the frequency range of examination. For comparison 8 periods of PRD ($P = 7$) and 6 periods of QRD ($P = 7$) are used. As can be seen in Figure 4-14 they both diffuse like a plane surface at 3.5 and $7kHz$. Noteworthy is the second flat plate frequency which although higher than the application bandwidth of the diffuser it is still evident.

The reason behind the peak that appears for the case of the PRD at 350Hz is that it displays a similar structural behaviour with the one described for the latest PWRD(P = 73,r = 0) (Figure 4-12) since its coefficients are $[1, 3, 2, 6, 4, 5]$. The difference in the pattern of the diffusion coefficient is related more than anything with the different number of periods that were used in the two cases, as periodicity is the dominant factor in these cases.

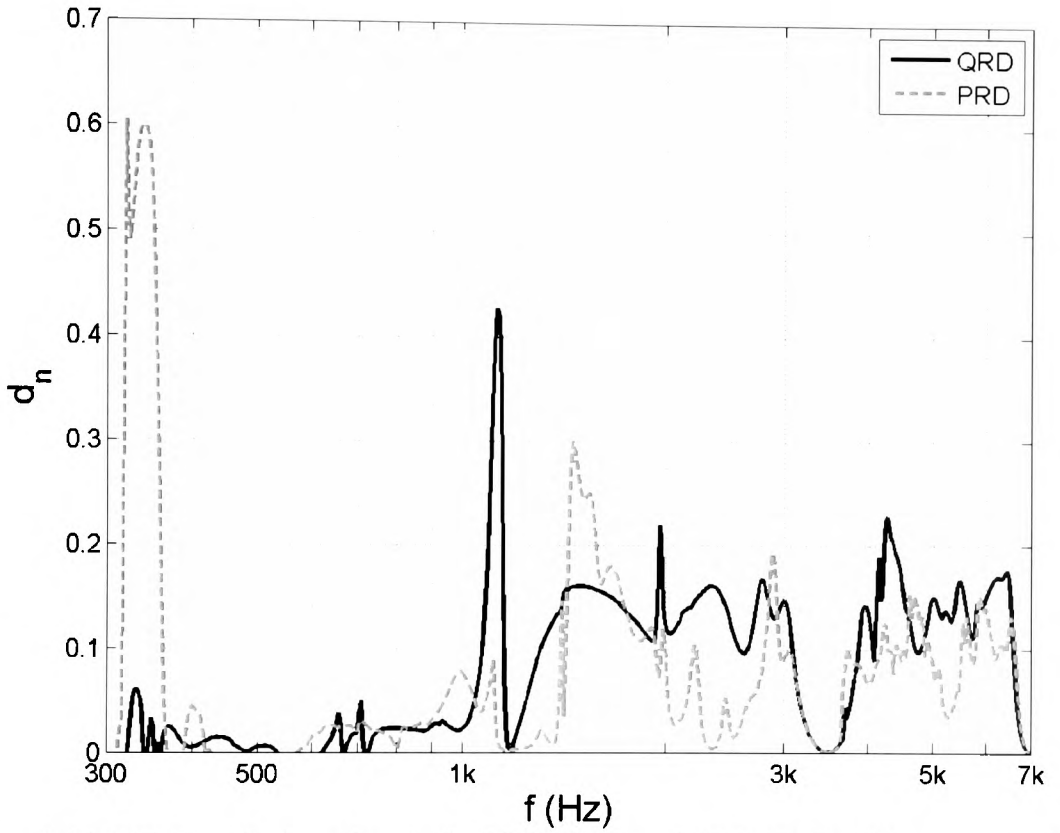

Figure 4-14. BEM prediction of periodic QRD (P=7) and PRD (P=7) of the same total width ($2m$) and design frequency (f_0=500Hz).

When the overall performance is regarded, it is easier to compare diffusion coefficients in 1/3rd octave band averages. While it is good for the comparison between diffusers it fails to display the flat plate frequencies as it averages them out.

One case from each family of PWRDs is presented in Figure 4-15. These 3 diffusers where chosen over others of their family because they performed better. Both PWRD (P = 19) performed identically on their own, as one is the inverse of the other. The other two PWRDs were chosen because they appeared to perform better than, or at least as well as, the rest of the diffusers in their family. Overall, the most promising are the diffusers of larger integer number (P = 37 and P = 73) as they display more uniform diffusion over the bandwidth. Furthermore, the fact that there are more than 2 diffusers in these families, allows more

design options. The shallowest diffuser from the PWRD is the one based on the prime $P = 73$ which displays a maximum depth of $26.4cm$. The other 2 cases have maximum depths around $30cm$. While shallowest of the diffusers in this graph is the QRD (maximum depth around $20cm$) it does have two flat plate frequencies in the graphs bandwidth.

The PWRDs have no problematic frequencies within this bandwidth. From this comparison in particular, $P = 73$ has better diffusion than all the other ones. While it is not obvious in Figure 4-15 it displays more stable diffusion than the other PWRDs when it is not averaged over 1/3rd octave bands.

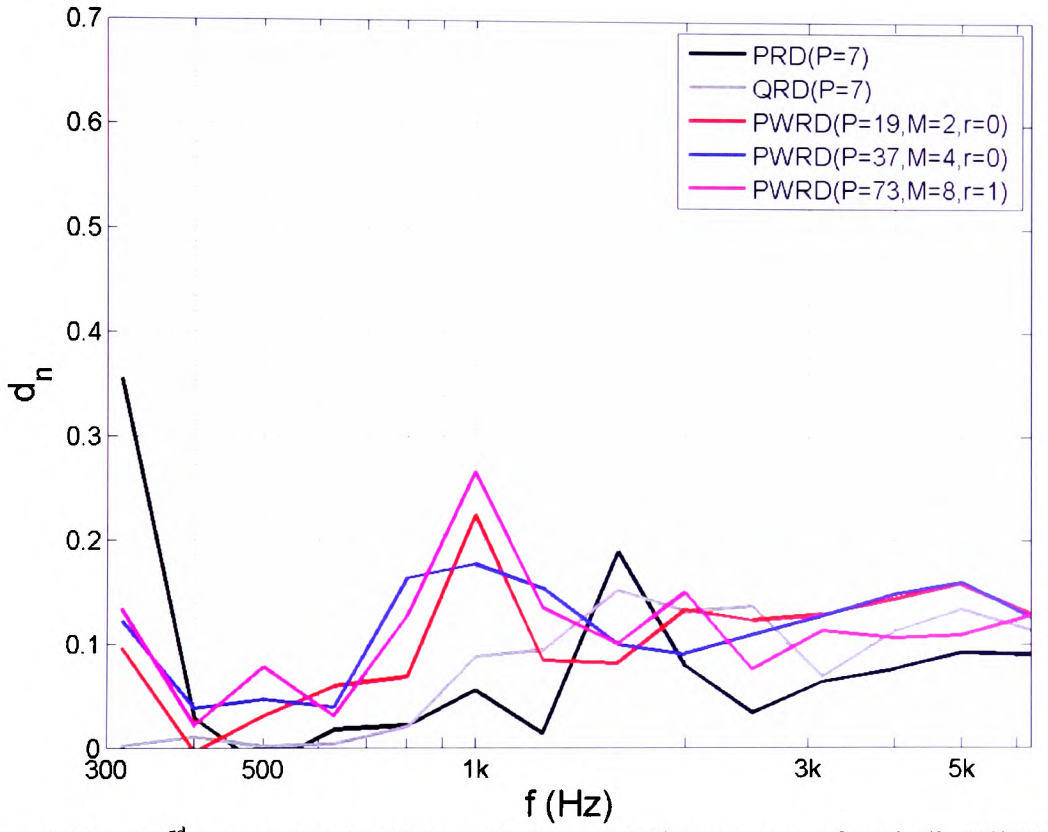

Figure 4-15. 1/3rd octave band BEM prediction of different types of periodic PWRD, PRD and QRD of the same total width.(Note: Both PRD and QRD have plate plate frequency at $3.5kHz$ which is averaged out)

Their performance can be further improved if modulation is used to minimize the problem of periodical repetition of the same diffuser. Since PWRDs do not present any notable problems until their flat plate frequency, the problem of periodicity is the only one that needs addressing. The widely used modulation with the diffuser's inverse can be applied in this case. The modulations with the mirror diffuser and another diffuser of the same family can be used as well. Usually a pseudorandom binary sequence is used for the modulation. In this

case since there is a requirement for comparison with other diffusers finding pseudorandom sequences of the appropriate length is not possible. For this reason non-periodic sequences with the best possible autocorrelation properties were used. The binary sequence [1 , 0 , 1 , 1 , 0] has been used to modulate the PWRD.

Figure 4-16 shows the normalised diffusion coefficient of a PWRD of period N = 9, prime number generator P = 73 and r = 1. All modulations diffuse much better than the periodic case; in addition modulation with the inverse diffuser performs more uniformly compared to the others.

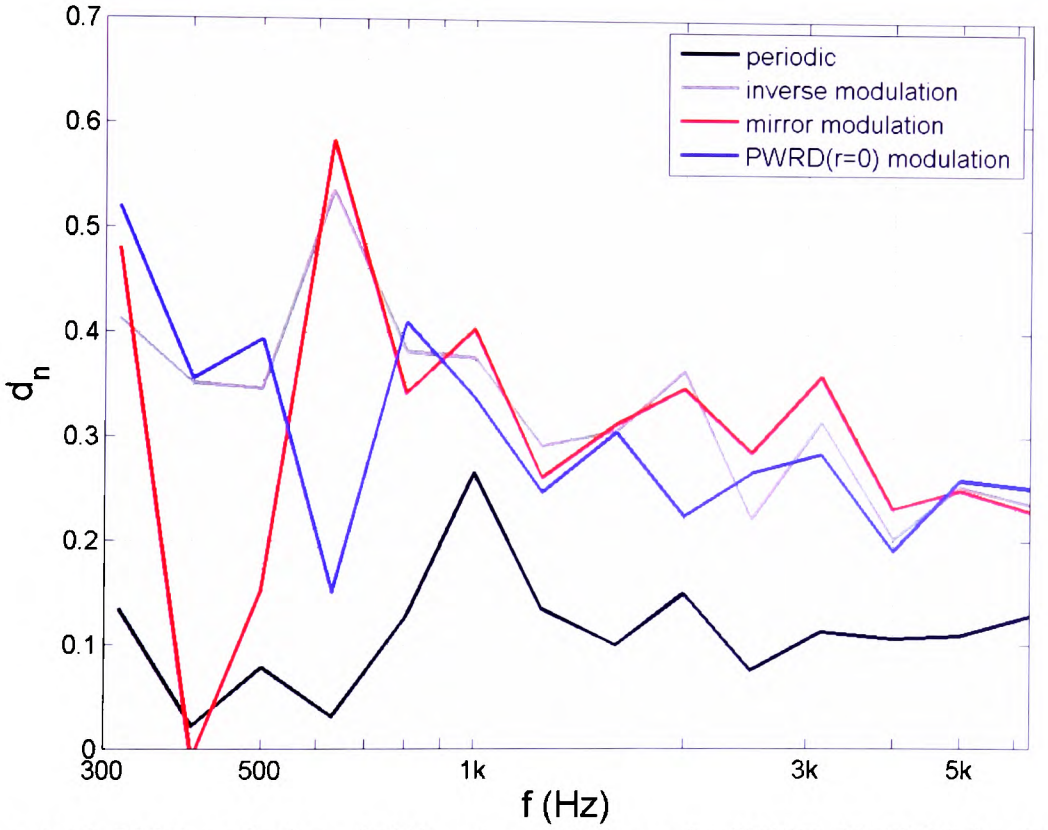

Figure 4-16. BEM prediction of different modulations of a PWRD (P=73,M=8,r=1) of the same total width.

4.2. Lüke Sequence Diffusers (LSD)

Type-II Lüke sequences are generated by superimposing steady step sequences to primitive root sequences. Due to the primitive root sequences' length being different from their integer generator the resulting type-II Lüke sequences will have an integer generator will be the product of the two. For any PRD of length N and generator P, N different Lüke sequence

diffusers (LSDs) are created for different step-sizes, with $N{\cdot}P$ generator. A schematic of the creation of a LSD (P=42, r=1) in shown in Figure 4-17.

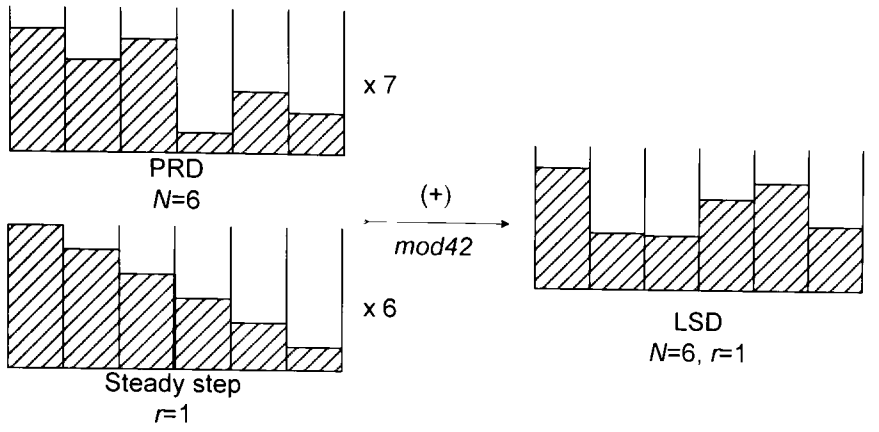

Figure 4-17. LSD (P=42, r=1) generation from the PRD (P=7).

In this case, a steady step sequence is imposed on a PRD increasing the generator while preserving the PRDs size.

4.2.1. The sequences

Type-II Lüke sequences are generated for any given prime p. They are formed in families of p-1 sequences which are given, for different values of r, by the equation [25, 45]:

$$s_n^{(r)} = \alpha^n(p-1) + rnp \bmod p(p-1) \qquad 4.12$$

where α is the primitive root of p.

The sequences are generated via the integer $P = p(p-1)$ and have a period length of $N = p - 1$. A necessary condition is $0 \leq n, r \leq p-2$.

The reflection coefficients of type-II Lüke sequences have the following, two valued, autocorrelation magnitudes[25]:

$$|R_{XX}(\tau)| = \begin{cases} p-1 & \tau = 0 \\ 1 & -\frac{p-1}{2} \leq \tau \leq \frac{p-1}{2}, \ (\tau \neq 0) \end{cases} \qquad 4.13$$

where R_{XX} is the autocorrelation and τ is the autocorrelation delay variable. This autocorrelation function magnitude is the same as that of a primitive root sequence of the same period. Figure 4-18 shows the properties for an example family of sequences based on p = 7. It is important to note while primitive root sequences have purely real periodic autocorrelation function type-II Lüke sequences have complex.

Essentially the type-II Lüke sequences are formed by superposing the primitive root sequence q of prime p:

$$q_n = \alpha^n \bmod p \qquad 4.14$$

and a steady step sequence t of the same period:

$$t_n = rn \bmod (p-1) \qquad 4.15$$

with r giving the step size, as shown in Figure 4-17.

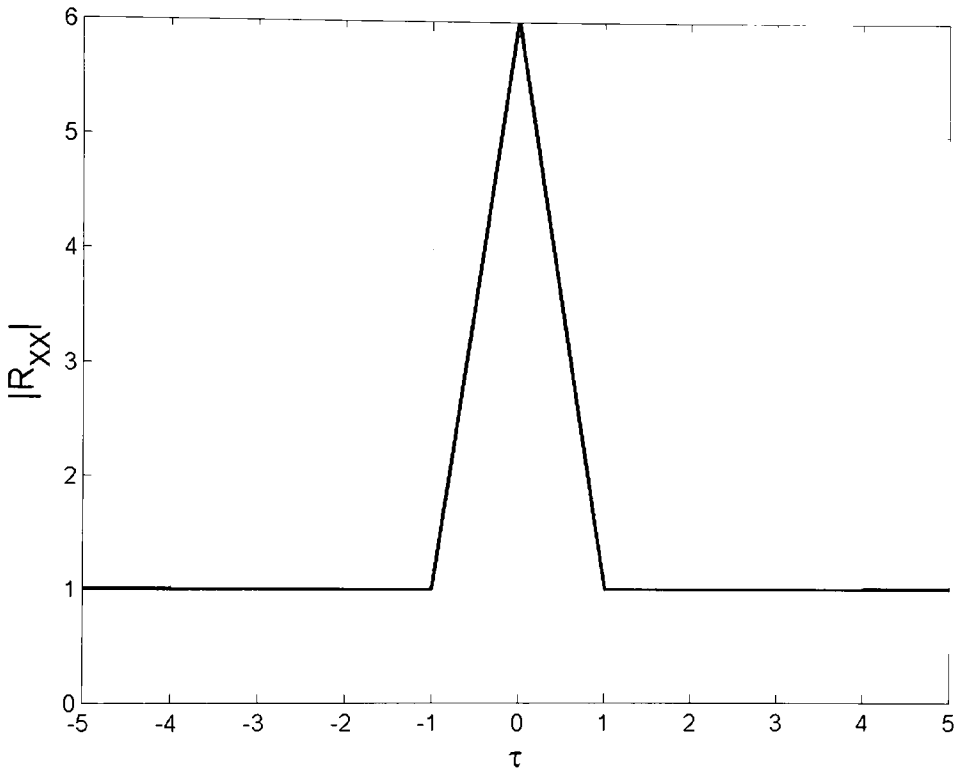

Figure 4-18. Magnitude of the autocorrelation function of the family of Type-II Lüke sequences (p = 7, P = 42).

For the above reason, every primitive root sequence can be considered to be the first sequence (r = 0) of each type-II Lüke sequence family. On the other hand it can be considered that from any primitive root sequence a set of p-2 new type-II Lüke sequences can be generated, each one with a different step size. This is possible because a linear ramp can be added to any number sequence, provided the period is correct, without changing the autocorrelation properties. This theorem is known as the shift theorem.

To give an example for P = 7 the primitive root sequence is $q_n = [1, 3, 2, 6, 4, 5]$. In order for all the coefficients to become equal the sequence has to be multiplied with 7 which is the

generator of the sequence. The first type-II Lüke sequence (P=42, r=1) is created by superimposing the steady step sequence $t_n = [1,2,3,4,5,6]$ resulting in $s_n = [6, 25, 26, 15, 10, 23]$. In order for thes coefficient to do the same they need to be multiplied with 42. Therefore, by using type-II Lüke sequences it is possible to increase the frequency at which all the wells radiate in phase by a factor of 6.

4.2.2. The diffusers

Type-II Lüke sequences are formed by the addition of a step sequence to a Primitive Root sequence. Consequently, diffusers that are generated with steady step sequences of opposing inclinations can be paired as they perform similarly. This leaves one sequence that cannot be paired, the middle one which is generated for $r = N/2$.

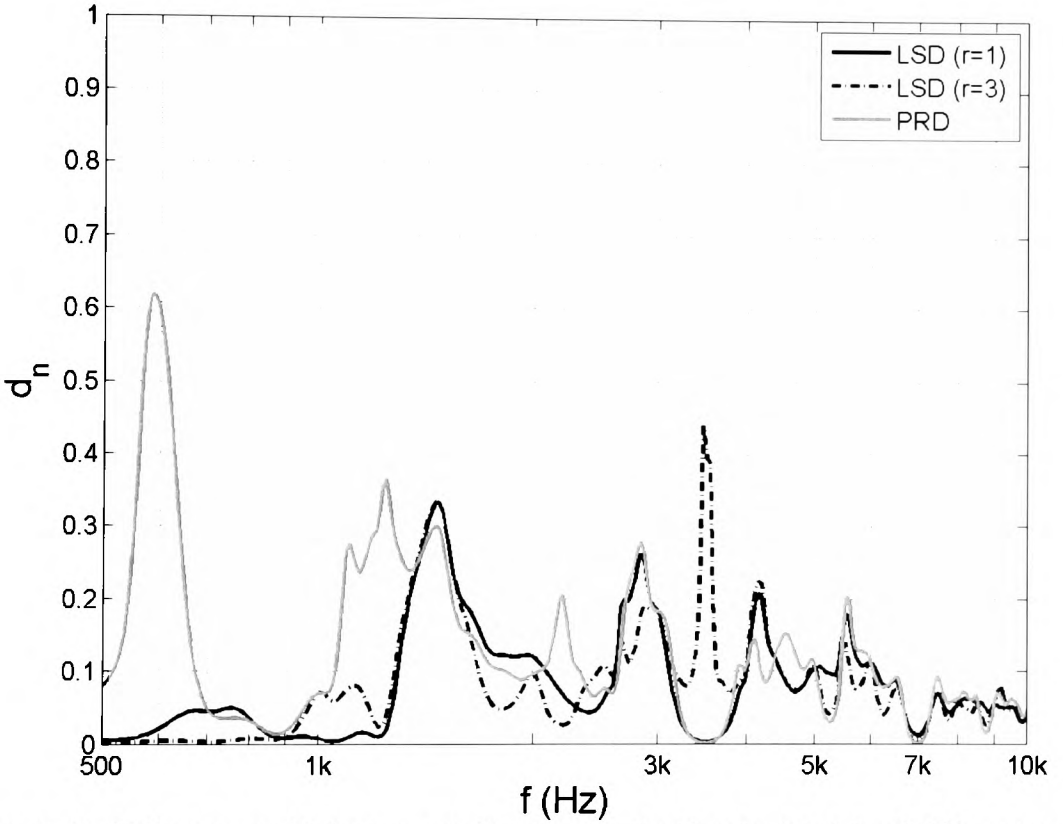

Figure 4-19. Diffusion coefficient, as predicted using the Fourier Model, of different types of periodic PRD (P=42) and PRD (P=7) of the same total width.

The case of Lüke Sequence Diffusers (LSD) generated by the integer P = 42 is considered. These are diffusers of period N = 6 and well width approximately 4.2cm. Their design frequency is f_0 = 500Hz. 8 periods of the diffuser are used. This gives a structure with an overall width of 2m. Given their equal size they are going to be compared with their equivalent PRD.

Figure 4-19 displays the diffusion coefficients of some diffusers of this family of LSDs along with the equivalent PRD. The PRD as expected displays a flat plate effect at $7 \cdot f_0 = 3.5kHz$. Surprisingly though, while LSDs are expected to display their first flat plate effect at $42 \cdot f_0 = 21kHz$, the one with r=1 displays a dip in the diffusion coefficient similar to the PRD's flat plate effect at 3.5kHz. On the other hand there is sharp peak in the case of r=3 at that frequency.

This is because the LSD with $r = 1$ causes redirection rather than diffusion at this frequency. The reflection coefficients at $3.5kHz$ have phases of 0, $\pi/3$, $2\pi/3$, π, $4\pi/3$, $5\pi/3$ which have equal phase shift increment of $\pi/3$ from one well to the next. This constant phase increment of the reflection coefficients is why the main reflected lobe is redirected into another direction; it is identical to the phase shifts used to beam steer loudspeaker arrays. This behaviour is inherent in LSDs because they are formed by adding a PRD to a linear stepped ramp. At the frequency in question, all the reflection coefficients of the base PRD are equal to 1 with a phase shift of 0, leaving only the linear stepped ramp. Essentially the PRD disappears and the diffuser acts like a tilted flat plate. This can be seen in Figure 4-20 where the scattered intensity distribution from two periods of this LSD ($r = 1$) is compared to that from a plane surface of the same size and shows that the diffuser is redirecting instead of scattering the incident wave.

This is a very interesting example of why the scattering coefficient has not been chosen. The scattering coefficient for the tilted flat plate frequency of the LSDs would be high as the energy is scattered out of the zone of specular reflection; and this phenomenon would go unnoticed.

All the LSDs of the family display this behaviour with the exception of the middle one (in this case $r = 3$) (Figure 4-19) which appears to be dispersing the incident wave uniformly. However, a closer inspection reveals that the reflection coefficients at this frequency are simply +1 and -1 one after the other (representing a steady phase shift of π). Based on the Fourier Model, cancellation in the specular reflection direction occurs (Figure 4-21a). In reallity, mutual interactions between adjacent wells will tend to 'smooth out' the surface pressure distribution and reduce the cancellation in real surfaces. At the same time the periodicity of the reflection coefficient will result in sharp periodicity lobes to be introduced in the scattered polar response. This can be seen in Figure 4-21b where the same configuration is examined using the more exact BEM.

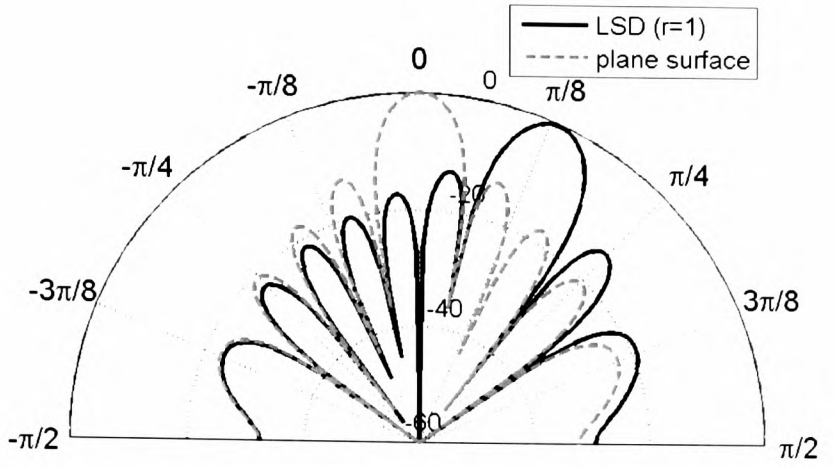

Figure 4-20. Normal incidence scattered level distribution (dB) at the tilted flat plate frequency of 2 periods of LSD ($P = 42$, $r = 1$) predicted using the Fourier Model.

All sequences of the same family perform almost identically when considered in a $1/3^{rd}$ octave band. They vary in their performance at specific frequencies and in the overall variation of their diffusion coefficient with frequency. The diffusers that have $r = 2$ and $r = 4$ display more variation of diffusion with frequency and have many dips in the diffusion coefficient. For this reason they are considered to perform worse than $r = 1$, 3 and 5. On the other hand the diffuser with r=3 displays a flat plate effect just like PRD it was generated from.

Another aspect worth taking into consideration is the maximum depth of the diffusers because of the space it removes from the room. For this family of LSDs $r = 1$ displays the smallest maximum depth of 21.3*cm* which is considerably smaller than that of the equivalent PRD which is 29.5*cm*, for the given design frequency. However, although LSD ($r = 1$) appears to be the most promising it does not perform any better than the equivalent PRD.

The dips that are evident in the diffusion coefficients of all three structures around 1.2 and 2.4*kHz* are due to the periodicity caused by the repetition of the base diffuser 8 times. Because of this, the structures can be considered as 8 point sources spaced 25*cm* apart which will generate additional minima due to the grating lobes generated by that periodicity.

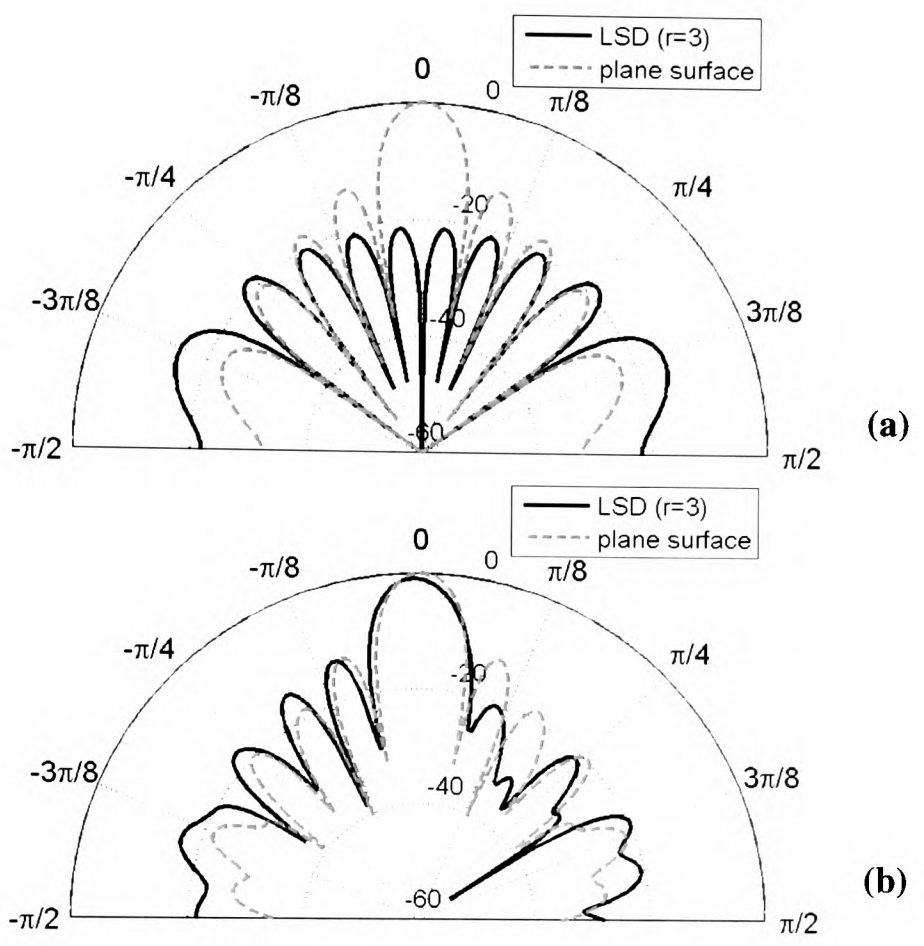

Figure 4-21. Normal incidence scattered level distribution (dB) at the tilted flat plate frequency of 2 periods of LSD (P = 42, r = 3) predicted using the Fourier Model (a) and BEM (b).

Using Boundary Element Modelling the performance of LSDs can be more accurately compared with that of the equivalent PRD (Figure 4-22). The initial prediction of the behaviour of the other LSD (r = 1) is shown to be quite accurate. It also becomes evident that it does not perform any better than the PRD with the exception of the area around 500Hz.

As shown above, at some frequencies the LSDs simply redirect the sound because they act like beam steerers. In general, diffusers should be dispersing sound and not simply redirecting it. An effective solution is to modulate the diffuser with another that, at the problematic frequencies, redirects sounds into another angle. Such a diffuser could be the inverse or the mirror image of the first diffuser or an LSD from the same family constructed from a step sequence of opposing inclination. Figure 4-23 displays the scattered distribution from such composite structures at this frequency. The main lobe of the periodic diffuser has been substituted by two wider lobes of less energy. Thus the incident wave is scattered more uniformly in comparison to the periodic diffuser.

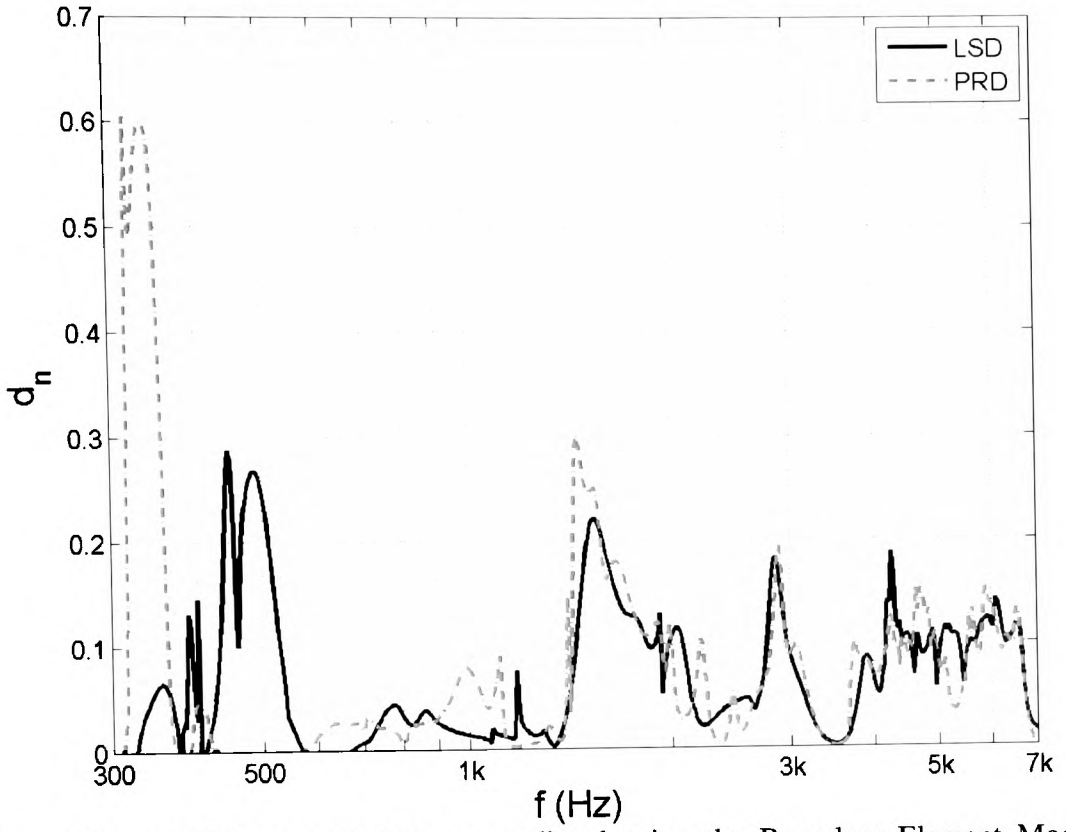

Figure 4-22. Diffusion coefficient, as predicted using the Boundary Element Model, of different types of periodic Lüke and Primitive Root diffusers of the same total width.

The binary sequence [1, 0, 0, 1, 1, 0, 1, 0] was used to modulate the base diffuser, LSD (P=42, r=1), in the three different ways discussed in Section 3.4. Modulation improves the overall performance of the diffuser, as shown in Figure 4-24, because the diffusion coefficient is higher for all frequencies compared to the periodic case.

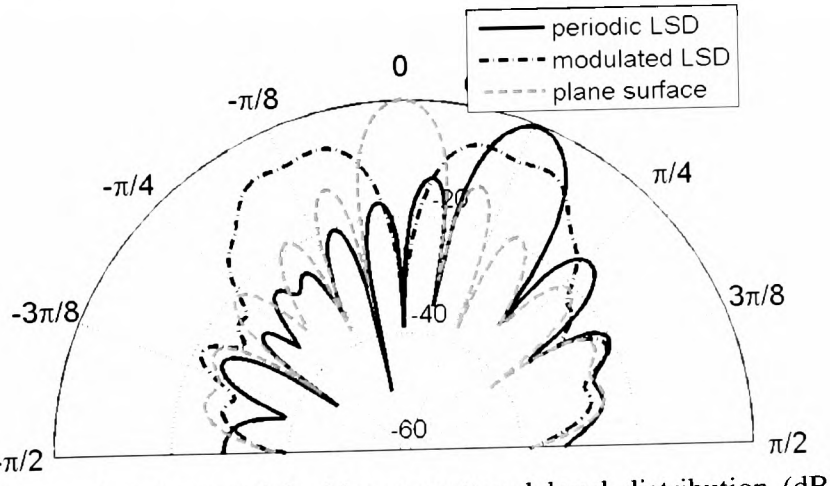

Figure 4-23. BEM predicted normal incidence scattered level distribution (dB) at the flat plate frequency for 2 periods of LSD (p = 7, r = 1) periodic and modulated with its inverse in comparison with a plane surface of the same width.

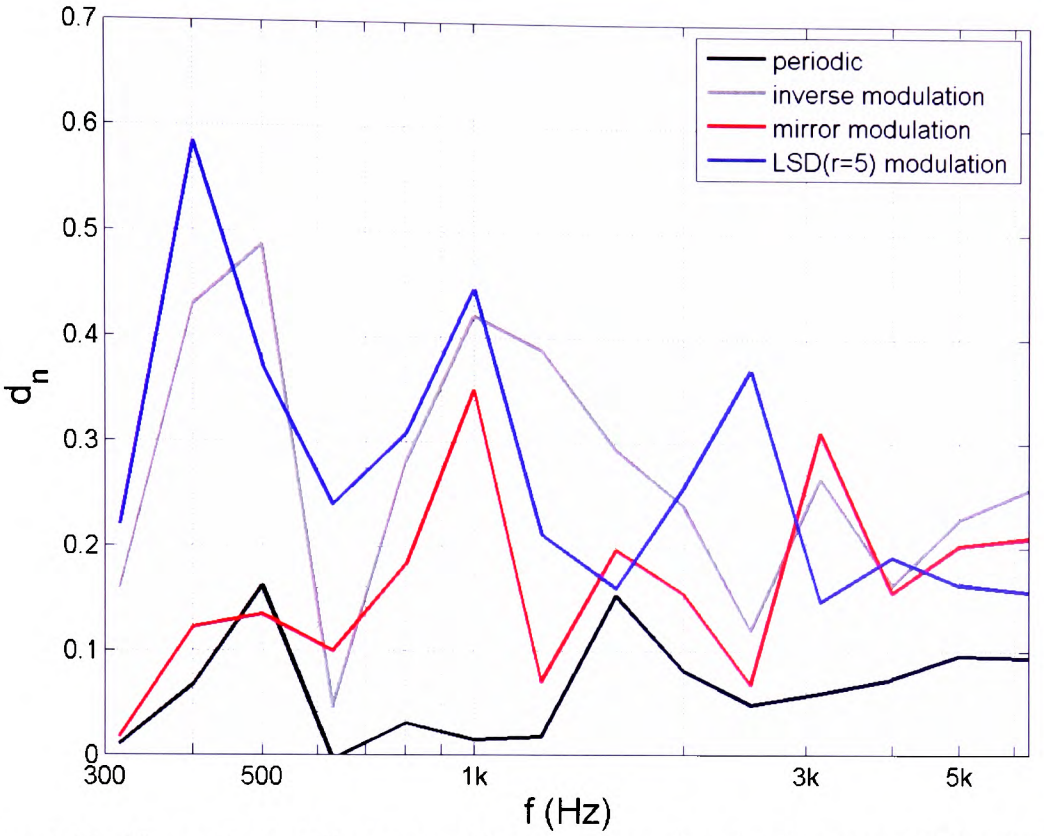

Figure 4-24. Normalised diffusion coefficient, as predicted using the BEM, of different modulations of LSD ($P = 42$, $r = 1$) of the same total width.

It is important to note that for the periodic case and the modulation with the mirror diffuser the maximum depth is 21.3*cm* while for the inverse it is 29.5*cm* and for the LSD of opposing inclination ($r = 5$) it is 32.7*cm*. From these three modulations the one with the inverse diffuser and the other with the LSD ($r = 5$) seem to disperse best. However, if the maximum depth is taken into account, the fact that the modulated with the mirror diffuser will take up less space from the volume of the room could make it more desirable for some applications.

The phenomenon of periodicity could be used to treat the problem of beam steering occurring with the LSD. Consider a structure that is composed of periodic repetition of LSDs. If the maximum reflection lobe could be set on the angle that a minimum of the periodicity pattern occurs, it could be cancelled out. Unfortunately in order for that to be accomplished a large number of periods must be considered while the wells must be thinned down to unrealistic values.

4.3. Discussion

Two new types of diffusers have been presented and their performance has been investigated in comparison to a standard PRD. But which is the best sequence, Type-II Lüke or Power Residue?

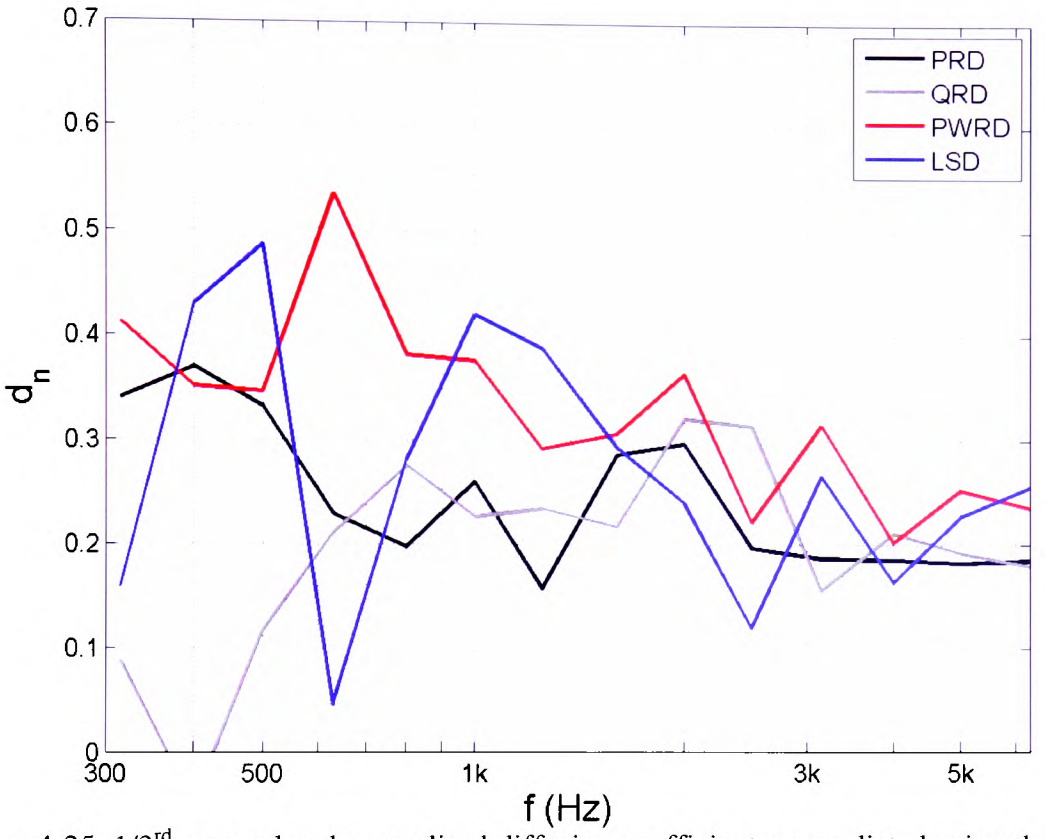

Figure 4-25. 1/3rd octave band normalised diffusion coefficient, as predicted using the BEM, of different types of modulated diffusers, with their inverse, of the same total width.

Figure 4-25 indicates that the PWRDs seem to be better. It shows that the PWRD modulated with the inverse has better diffusion coefficients than the other surfaces. They have no problematic frequencies, where they are unable to scatter the incident wave, and they have a more uniform diffusion coefficient over this bandwidth.

The LSD ($P = 42$, $r = 1$), shown in the above figure, is more ambiguous. It is evident that they do not diffuse as well as the QRD and the PRD. It must be noted that these two diffusers display a flat plate effect at $3.5kHz$ even when modulated with their inverse; the 1/3rd octave band spectra hide this effect. The periodic version of the LSDs have a tilted flat plate at that frequency, but when modulated manages to avoid the problem. Modulated the LSD is preferred to a PRD or QRD because it is well behaved until the flat plate frequency at $21kHz$.

4.4. Further Suggestions

It is possible to use the inner symmetries of the sequences to ones advantage. Such cases are discussed here. In the first Sections methods to make the industry standards QRDs and PRDs through the use of smaller components is presented while in the second Section a new 2-D PRG with interesting characteristics is introduced that should be further investigated.

4.4.1. Using half a QRD or PRD instead of the full one

The use of small sequences is dictated by the need for a period of the diffuser to be small. This makes it easy to move and apply. For standard PGDs this results in a small integer generator and low flat plate frequency. PWRDs and LSDs have been presented as options of sequences that have generators substantially greater than their size.

QRDs and PRDs display symmetries that can be exploited to achieve a similar effect. Quadratic residue sequences are symmetric around the centre of the device. For $P = 7$ the sequence is $s_n = [0, 1, 4, 2, 2, 4, 1]$, which could be rearranged in the form $[2, 4, 1, 0, 1, 4, 2]$. The diffuser can be split in half (Figure 4-26) and only one half of it to be constructed. The other half is the same as the first but put in a different orientation.

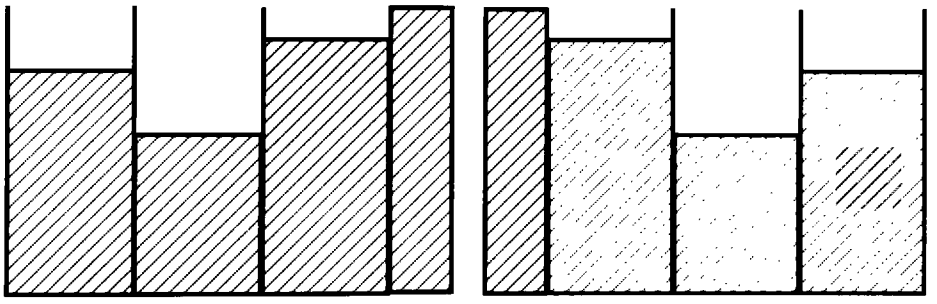

Figure 4-26. Half a QRD used to form a full diffuser.

So instead of using a QRD of length $N = 7$ and generator $P = 7$ half a QRD of length N=13 can be used. The structure to be moved and positioned would be the same approximate length but the generator and with that the flat plate frequency would be double.

In the case of primitive root sequences the second half is the inverse of the first half. Take for example the primitive root sequence of prime $P = 7$ which is $s_n = [1, 3, 2, 6, 4, 5]$. The sequence $s'_n = [6, 4, 5]$ is the inverse of the sequence $s''_n = [1, 3, 2]$:

$$s_n = [s'_n, s''_n] \quad , \quad s'_n = p - s''_n \qquad 4.16$$

The coefficients of a primitive root sequence are connected via the equation:

$$s_n = p - s_n\left(n + \frac{p-1}{2}\right) \quad , \quad n = 1, 2, \ldots, \frac{p-1}{2} \qquad 4.17$$

This symmetry can allow for only half of a primitive root sequence to be constructed if the structure is has thin well terminations (Figure 4-27). In a similar scenario with the one suggested for QRDs the ratio of generator-to-width can be doubled.

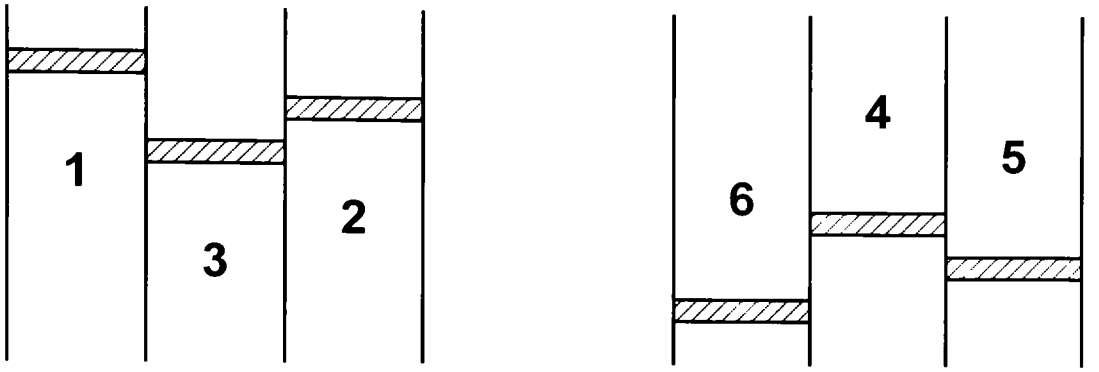

Figure 4-27. PRD (p=7) split into two half that are inverse of one another.

$N = 5$

1	17	13	9	5
6	2	18	14	10
11	7	3	19	15
16	12	8	4	20

$M = 4$

Figure 4-28. The positions of the coefficients of a 20-coefficient long sequence when folded in a 4×5 array with the Chinese Remainder Theorem.

4.4.2. Folding PRD forming parallel PWRDs

When folding a 1-D sequence using the Chinese Remainder Theorem (see Section 1.2.2) into a $M \times N$ 2-D sequence one effectively samples it every M coefficients with a different starting point and arranges it, in inverse order, into the rows dictated by that starting point. As can be seen in Figure 1-3 the 1-D sequence (length 20) is folded into a 4×5 sequence. The first row of the 2-D sequence consists of the coefficients $[1, 5, 9, 13, 17]$ inverse order

which can be obtained from sampling the 1-D sequence every $M = 4$ coefficients. The second row displays a similar pattern ($[2, 6, 10, 14, 18]$) but with a starting point the 2nd coefficient.

As discussed in Section 4.1 power residue sequences are generated by sampling primitive root sequences. This suggests that by folding a primitive root sequence in the appropriate dimensions it can be arranged in pattern where its rows are power residue sequences. These sequences will be in reverse order than expected though. In order for that to happen though the folding dimensions have to be consecutive numbers otherwise the coefficients of each row will not be in the required order.

Based on the cases that have been presented (Eq. 4.7) the dimensions possible are 2×3 and 8×9. The first case corresponds to a very small sequence but the second one looks ideal. The folded 2-D sequence will be:

$$s_{mn} = \begin{bmatrix} 1 & 37 & 55 & 64 & 32 & 16 & 8 & 4 & 2 \\ 10 & 5 & 39 & 56 & 28 & 14 & 7 & 40 & 20 \\ 27 & 50 & 25 & 49 & 61 & 67 & 70 & 35 & 54 \\ 51 & 62 & 31 & 52 & 26 & 13 & 43 & 58 & 29 \\ 72 & 36 & 18 & 9 & 41 & 57 & 65 & 69 & 71 \\ 63 & 68 & 34 & 17 & 45 & 59 & 66 & 33 & 53 \\ 46 & 23 & 48 & 24 & 12 & 6 & 3 & 38 & 19 \\ 22 & 11 & 42 & 21 & 47 & 60 & 30 & 15 & 44 \end{bmatrix} \tag{4.18}$$

The rows as expected consist of mirrored power residue sequences.

As discussed in Section 1.2.2 a 2-D sequence with the same autocorrelation properties can be achieved with different folding steps. If the folding step is set to the same as the number of columns, 8 in this case, the power residue sequences will be in order.

$$s_{mn} = \begin{bmatrix} 1 & 2 & 4 & 8 & 16 & 32 & 64 & 55 & 37 \\ 10 & 20 & 40 & 7 & 14 & 28 & 56 & 39 & 5 \\ 27 & 54 & 35 & 70 & 67 & 61 & 49 & 25 & 50 \\ 51 & 29 & 58 & 43 & 13 & 26 & 52 & 31 & 62 \\ 72 & 71 & 69 & 65 & 57 & 41 & 9 & 18 & 36 \\ 63 & 53 & 33 & 66 & 59 & 45 & 17 & 34 & 68 \\ 46 & 19 & 38 & 3 & 6 & 12 & 24 & 48 & 23 \\ 22 & 44 & 15 & 30 & 60 & 47 & 21 & 42 & 11 \end{bmatrix} = \begin{bmatrix} s_n^{(0)} \\ s_{n+1}^{(1)} \\ s_{n+2}^{(2)} \\ s_{n+3}^{(3)} \\ s_{n+4}^{(4)} \\ s_{n+5}^{(5)} \\ s_{n+6}^{(6)} \\ s_{n+7}^{(7)} \end{bmatrix} \tag{4.19}$$

When comparing the folded primitive root sequence with the power residue sequences in equation 4.11 it is seen that the only difference is a shift of one coefficient per row.

A PGD based on this 2-D sequence should display very good diffusion properties in the horizontal dimension. The performance of this diffuser needs to be tested in the future.

4.5. Summary

In this Chapter the problem of the flat plate frequency of Phase Grating Diffusers (PGD) has been discussed. Two new pseudorandom sequences have been presented which have much larger integer generators than their length. From them Power Residue Diffusers (PWRD) are shown to move the flat plate frequency outside the audible frequency range while Lüke Sequence Diffusers (LSD) redirect rather than disperse the incident wave at the flat plate frequency. While the performance of LSDs is corrected at the critical frequency with modulation they are shown not to perform better than the industries standards. On the other hand a PWRD was proven to perform better and more uniformly than industries standards without displaying any frequencies were they acted like a flat plate.

In the concluding Section of this Chapter some practical suggestions were introduced as to how the inner symmetry of QRDs and PRDs could be used to mitigate the flat plate frequency problem. Furthermore, a 2-D diffuser that consists of parallel PWRDs has been presented that displays good potential and should be further examined.

This Chapter concludes the first Part of the thesis that investigates ways to improve Phase Grating Diffusers. The second Part of the thesis investigates Absorption Grating Diffusers.

PART II. ABSORPTION GRATING DIFFUSERS

In 1995, the theoretical concept of a new class of sequence-based diffusers was presented by Angus, Absorption Grating Diffusers (AGD)[7, 27, 46]. Instead of wells of different depths they consisted of absorbing and reflecting patches that were positioned in a grid based on a binary unipolar sequence. Not being subject to the requirement of sound propagating in wells, as was the case with PGDs, they have a much smaller profile. Cox took the idea even further and introduced phase gratings in ADGs forming ternary and quadriphase sequence diffusers[47].

There has never been a comprehensive study on the effectiveness of AGDs. The published work on the subject is based on approximate prediction models that while an indication of the behaviour of these devices cannot conclusively prove their performance. Furthermore, there hasn't been any discussion of how these surfaces are going to be implemented in reality given that their requirement of ideally absorbing element at all frequencies is unattainable especially at low frequencies. The only suggestion was made by D'Antonio who used a pseudorandomly perforated mask in front of a layer of absorbing material[48] without investigating though if its behaves as an AGD.

In this part of the thesis Absorption Grating Diffusers (AGD) are being discussed. First, their theoretical concept is presented and a review of the related literature is made. Then methods of assessing the absorbing properties through analytical models and measurements are presented. The types of absorbing elements that can be used to implement these surfaces are presented and their characteristics and limitations are discussed. Later a realistic way to implement a surface that consists of nearly perfectly absorbing elements is presented. Then the performance of ideal Absorption Grating Diffusers is investigated using Boundary Element Modelling and their diffusion capabilities are explained. Finally, improvements to the performance of these devices are presented by either introducing reactive elements or using less absorbing element.

Chapter 5. Introduction to Absorption Grating Diffusers

In this Chapter the theory behind Absorption Grating Diffusers (AGD) is presented. Their requirements are discussed and their advantages and disadvantages presented. Existing devices are mentioned and their deviation from the original concept is pointed out.

While phase grating diffusers achieve different reflection coefficients by acting on the sound wave's phase, binary amplitude diffusers act on the wave's magnitude by either absorbing or reflecting the incident wave.

5.1. Introduction

The concept was presented by Angus[7] in 1995 who used the same foundation of the number theory that Schroeder used for the Phase Grating Diffusers[8] presented in Section 3.1. She suggested that if the grating the magnitude of the reflection coefficient of a surface rather than its phase[7]. So instead of a structure consisting of wells that produce the required phases of the reflection coefficient the structure would be flat and consist of areas of ideal absorption and ideal reflection resulting in reflection coefficients of 0 and 1 respectively.

The grating of reflection coefficients still needs to display two-level autocorrelation function in compliance to the Fourier Theorem (Section 2.1.2) thus a binary unipolar pseudorandom sequence is needed. Most binary pseudorandom sequences are designed bipolar so they contain coefficients of -1 and 1 but they can be converted to unipolar by switching the -1s to 0s. While the bipolar sequences display ideal autocorrelation properties, this characteristic is compromised when transformed into unipolar ones as is displayed in Figure 5-1 for the case of a Maximum Length Sequence (MLS).

There are a number of binary sequences that consist of approximately 50% absorbing and reflective elements that can be used for this application such as Maximum Length Sequence (MLS), Legendre, Golden, twin prime, Hall sequences and others[25, 49]. Given the requirements of pseudorandom sequences[25] and their limited number of coefficient values, the short binary pseudorandom sequences are the same regardless of their type. If a sequence with smaller weight is required Angus[27] suggested another category of binary sequences with good autocorrelation function known as optical sequences. They consist of a small

percentage of 1s (around 25% for long sequences) which results in the surface being too absorbing or too reflecting based on whether the 1s will state the reflective or the absorptive patches. The number of 1s can be increased by combining sequences of the same family but that will deteriorate the autocorrelation properties of the final sequence[50].

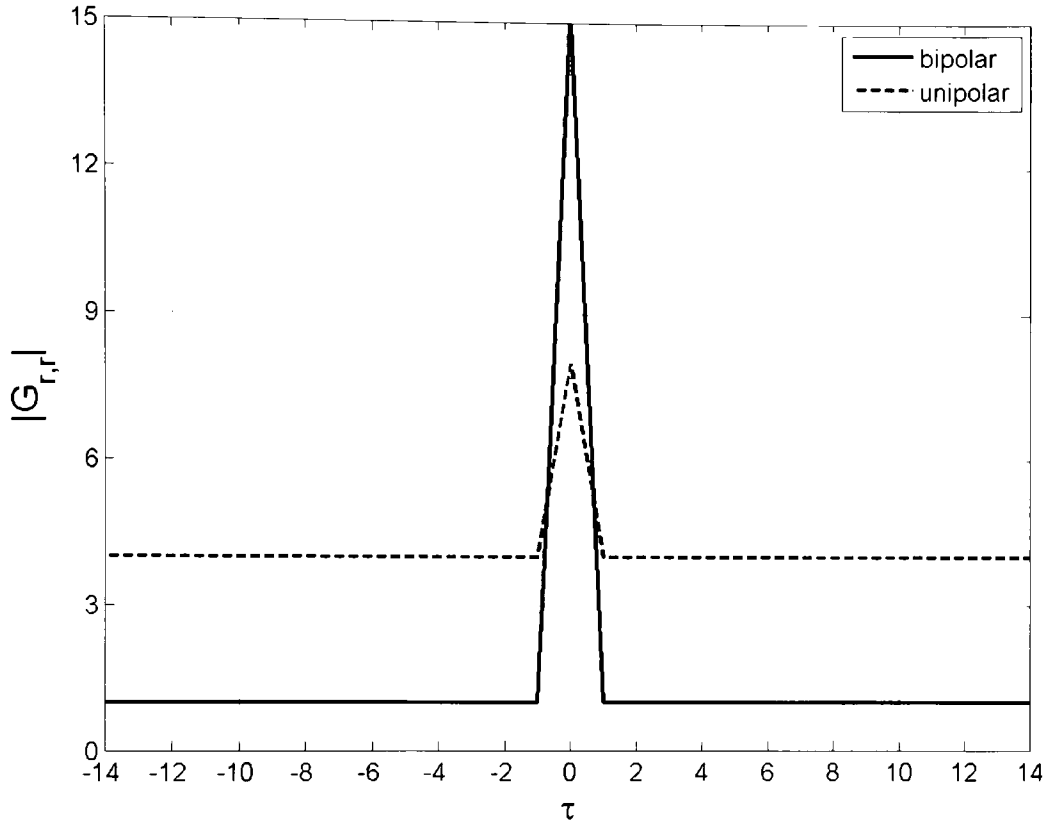

Figure 5-1. Autocorrelation function for a bipolar and a unipolar MLS(k=4) of period N = 15.

In this thesis MLSs are going to be used as they have good autocorrelation properties and they display approximately the same number of 0s and 1s. The percentage of 1s in the sequence gives its weight which in the case of unipolar MLSs is close to 50%. This suggests that at high frequencies we can expect the diffuser to absorb half the incident energy. Given that this thesis considers short pseudorandom sequences the MLSs used may also be another type of binary sequences. Even when that is the case they will be referred to as MLS in tribute to Schroeder who used them in their bipolar form for the introduction of PGD[6].

The case of a 1-D AGD created from the MLS (k = 3) of length N = 7 is presented in Figure 5-2.

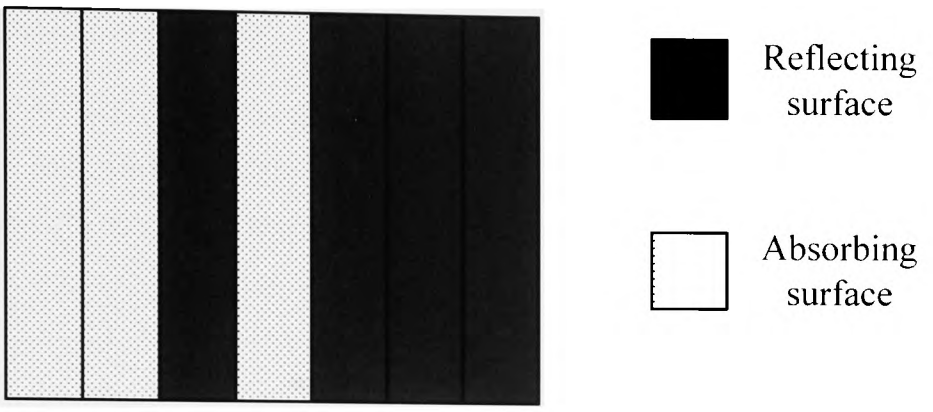

Figure 5-2. 1-D Absorption Grating Diffuser constructed using a MLS (k = 3), s_n = [0, 0, 1, 0, 1, 1, 1]

5.2. Advantages and Disadvantages

AGDs do not require well propagation. This means that they do not have the frequency limit of PGDs that are associated with well propagation which require half the wavelength to be larger than width of the well (Section 3.2.2). Furthermore, while PGDs have a design frequency that is associated with the profile of the structure this is not the case for Absorption Grating Diffusers. They do not have in principle a design frequency. So an Absorption Grating Diffuser could be implemented in theory with a small profile as long as the absorbing elements meet the requirement for ideal absorption. Another advantage that they have is that they are flat, a desirable characteristic that makes them more appealing to architects and decorators.

On the other hand a notable disadvantage in AGDs as presented comes from the fact that the reflection coefficient can take only two values. On the surface with a regular spaced grid of such a 2-value reflection coefficient the periodicity induced by the constant width of the elements will be a problem to be reckoned with. Payne-Johnson *et al*[46] have presented the concept of varying the dimensions of absorbing patches in order to tackle this problem. Another improvement has been suggested by Cox *et al*[47] who introduced ternary and quadriphase diffusers that contain wells in the grating achieving added diffusion through cancellation.

5.3. Reasons for Doubt

No thorough study has been carried out to identify the diffusion and absorption qualities of AGDs. Most of the discussion around them has used the approximate Fourier Model to predict their performance.

The idea of AGDs has been based on the Fourier Model which, as discussed Section 2.3.3 for PGDs, is an approximation of the performance of a structure. In the case of AGDs this model considers that the surface performs like an array of omni-directional sources positioned in the place of the reflecting elements. This means that in order for the Fourier Model to apply the reflecting elements must scatter energy uniformly (Figure 5-3).

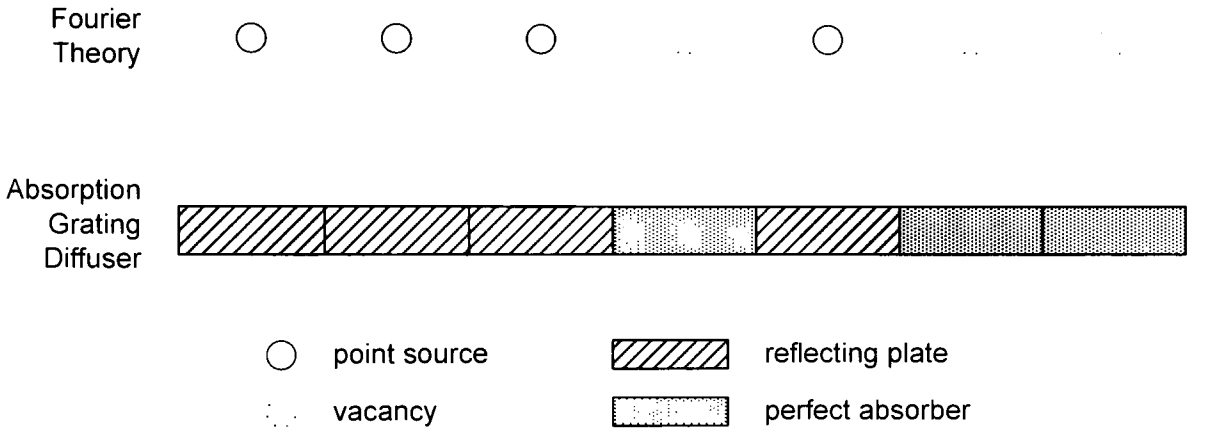

Figure 5-3. Fourier theory equivalent of a AGD.

So the questions that arise are:

"Can the reflective elements scatter energy uniformly as required by the Fourier Model?"

In the case that they can:

"Is the scattered energy substantial to achieve diffusion?"

Another issue with their design concept is its requirement for elements of ideal absorption steady with frequency. This is difficult to achieve in reality especially at low frequencies. So another question is:

"How can an ideal or near ideal absorbing element be implemented in reality?"

An AGD has been constructed by RPG and bears the name BAD™ panel[48]. It consists of a mask with pseudorandomly arranged perforations positioned in front of a layer of porous material (Figure 5-4). The holes are considered to perform as Helmholtz Resonators and act as the absorbing elements of diffuser while the rigid areas of the mask act as the reflectors. The mask is covered by an acoustically transparent fabric for aesthetic reasons. This implementation of an AGD is easy to construct and light in comparison to PGDs which makes it cheaper to make and easier to mount on a wall.

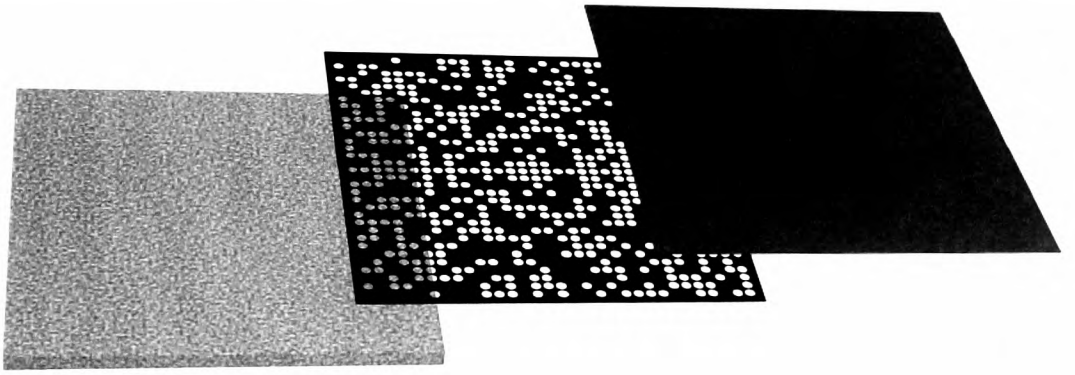

Figure 5-4. BAD™ panel manufactured by RPG.

The perforated mask in front of a porous material is a configuration that is used to form absorber as will be discussed in Section 6.4.2. The holes are arranged periodically in that setup and the whole surface acts as an absorber consisting of Helmholtz Resonator with identical absorption which is enforced by the regular arrangement of the holes. There is no evidence to support that by making the mask pseudorandom the holes will behave independently with the same absorption characteristics. On the contrary the behaviour of a perforation is dependent on its spacing with neighbouring ones. So the question is:

"Is it possible to construct an Absorption Grating Diffuser using a perforated mask in front of a layer of porous material?"

In this part of the thesis the answer to the above questions will be investigated. In Chapter 7 impedance tube measurements are used to investigate the performance of perforated masks in front of porous materials and to establish whether they can meet the requirement of the theory of AGD for ideally absorbing and reflective elements. Then in Chapter 8 the prediction of the performance of AGD is conducted using Boundary Element Modelling. Their characteristics

are investigated and their diffusion and absorption capabilities are discussed. Finally, in Chapter 9 improvements to the original design are suggested.

In order to set the theoretical background of study presented in Chapters 7 and 8, an introduction to the coefficients, prediction models and measurement techniques that are used in this part are presented in the following Chapter.

Chapter 6. Absorbers

Before investigating the scattered pressure distribution from partially absorbing surfaces a surface must be characterised. In this Chapter absorbers are discussed. Measures used to describe their performance are presented along with different types of absorbing elements. In addition, measuring methods are outlined.

6.1. Measures

The term absorber is used for materials or structures that absorb significant acoustical energy. Absorbers have been studied meticulously for over a century, and there are accepted measures that can be used to access their performance.

The design concept of the sequence generated diffusers is based on the Fourier Model (see Section 2.1.2) which requires knowledge of the distribution of the reflection coefficient. It is defined as the fraction of the reflected pressure p_{ref} and the incident pressure on the surface p_{inc} over the from the surface:

$$R = \frac{p_{ref}}{p_{inc}} \qquad 6.1$$

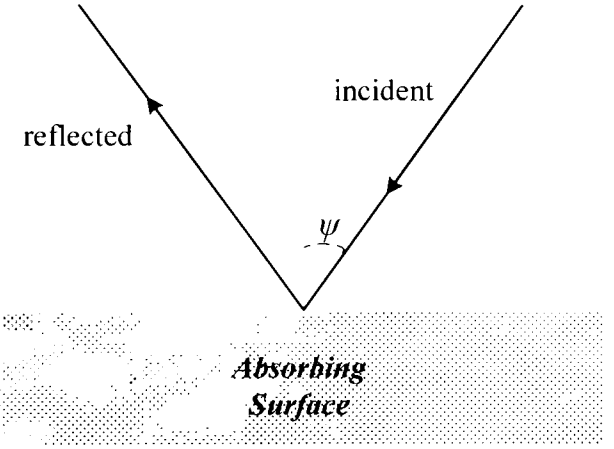

Figure 6-1. Sound reflection from through a surface.

Its magnitude gives the amount of pressure reflected of the surface while its phase is the phase change between the incident and the reflected wave. All the information required to characterise a surface as far as its reflecting and absorbing properties are contained in the

reflection coefficient for a given surface but it is angle dependent. There is another coefficient that is not dependent of the angle, the surface impedance[51]:

$$z_s = \frac{\rho_0 c_0}{cos(\psi)} \cdot \frac{1+R}{1-R} \qquad 6.2$$

where ρ_0 and c_0 are the density and the speed of sound in air and ψ is the angle of incidence (see Figure 6-1). The real part of the surface impedance is known as the resistance and it gives a measure of the energy loss while the imaginary is known as the reactance and it gives the phase change.

As mentioned in Section 2.1.1 Boundary Element Modelling (BEM) requires the surface admittance as an input. The surface admittance is the inverse of the surface impedance:

$$\beta = \frac{1}{z_s} = \frac{cos(\psi)}{\rho_0 c_0} \cdot \frac{1-R}{1+R} \qquad 6.3$$

In most practical application, the real valued absorption coefficient based purely on energy is most commonly used to characterise the absorbing capabilities of a surface:

$$a = 1 - |R|^2 \qquad 6.4$$

In this thesis all impedance and admittance coefficients are going to be normalised to the characteristic impedance of air ($z_0 = \rho_0 c_0$):

$$z_n = \frac{z_s}{\rho_0 c_0} = \frac{1}{cos(\psi)} \cdot \frac{1+R}{1-R}$$

$$\beta_n = \frac{1}{z_n} = \frac{\rho_0 c_0}{z_s} \qquad 6.5$$

The aforementioned coefficients all refer to the characteristics of a surface. There are others that refer to the characteristics of the material. Such coefficients that are going to be used in this thesis are the characteristic impedance z_c and the characteristic wavenumber k_c which are used to estimate the surface characteristics of different layers of absorbing materials as is discussed in the following Section.

6.2. Prediction models

The use of analytical models has been studied in acoustics to allow for the prediction of the surface characteristics of a layer of porous absorbing material. The main interest of this thesis

is centred on the surface characteristics, as this knowledge is required from all scattering simulation techniques used (BEM and Fourier Model).

Transfer Matrix Model

Allard[52] describes a model for predicting the surface impedance $z_{s_{i+1}}$ of a multi-layered absorbing surface if the characteristic impedance z_i, the characteristic wavenumber k_i and the depth d_i of each layer are known. In the case that the wave is propagating normal to the surface (Figure 6-2) the problem has only one dimension.

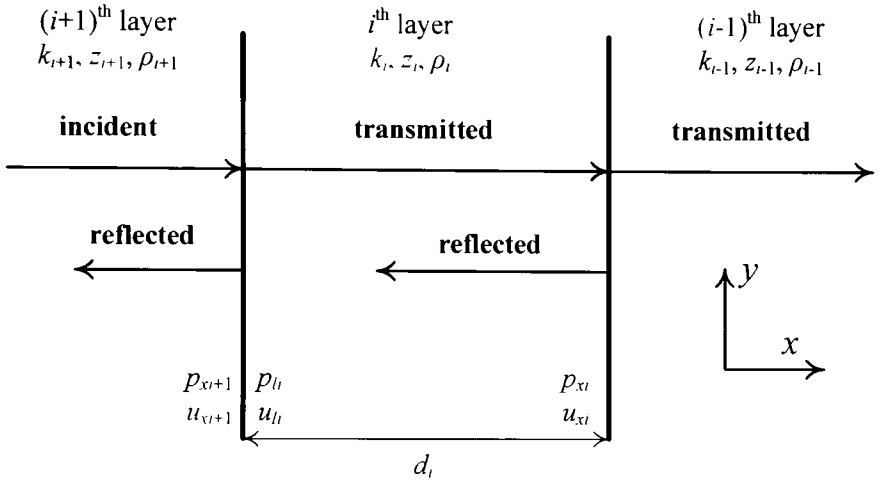

Figure 6-2. Geometry of the propagation of sound through a multi-layer medium.

By taking into account the continuity of the pressure and the velocity at the boundaries, the surface pressure and velocity on the boundaries of the layer can be connected if the characteristics of the layer are known:

$$\begin{bmatrix} p_{l_i} \\ u_{l_i} \end{bmatrix} = \begin{bmatrix} p_{x_{i+1}} \\ u_{x_{i+1}} \end{bmatrix} = \begin{bmatrix} cot(k_i d_i) & j\frac{\omega\rho_i}{k_i} sin(k_i d_i) \\ j\frac{k_i}{\omega\rho_i} sin(k_i d_i) & cot(k_i d_i) \end{bmatrix} \cdot \begin{bmatrix} p_{x_i} \\ u_{x_i} \end{bmatrix} \qquad 6.6$$

where the subscripts l_i and x_i refer to the values at the top and the bottom of the i^{th} layer respectively and the subscript i refer to the characteristics of the i^{th} layer, while ρ is the density, d is the width of the layer and ω is the angular frequency.

From equation 6.6 the surface impedance of the i^{th} layer $z_{s_{i+1}}$ can be estimated if the surface impedance of the $(i\text{-}1)^{th}$ layer z_{s_i} and the characteristics of the i^{th} layer are known:

$$z_{s_{i+1}} = \frac{p_{x_{i+1}}}{u_{x_{i+1}}} = \frac{-jz_{s_i} z_i \cot(k_i d_i) + z_i^2}{z_{s_i} - jz_i \cot(k_i d_i)} \qquad 6.7$$

In the case of only one layer of absorptive material in front of a rigid backing (Figure 6-3) the surface impedance $(i\text{-}1)^{th}$ layer is infinite. Equation 6.7 is simplified to:

$$z_{s_{i+1}} = \frac{-jz_{s_i} z_i \cot(k_i d_i) + z_i^2}{z_{s_i} - jz_i \cot(k_i d_i)} \cong -jz_i \cot(k_i d_i) \qquad 6.8$$

Equation 6.8 allow for the characteristics of any surface to be calculated from the characteristic impedance and wavenumber of the layer behind it.

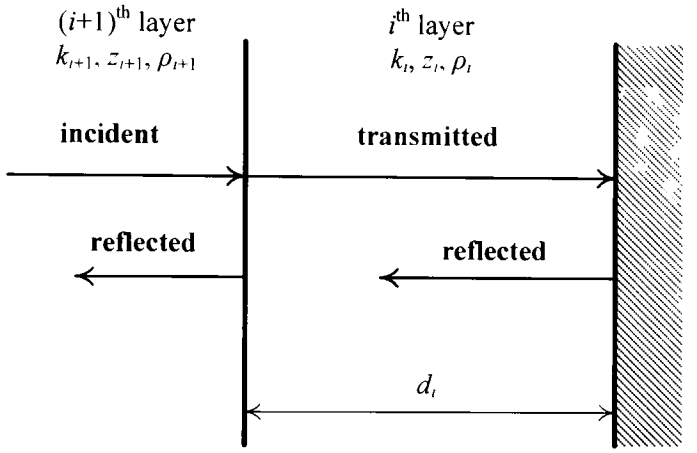

Figure 6-3. Geometry of the propagation of sound through a single layer medium in front of a rigid backing.

Prediction models of the characteristic properties of a porous material

There are a number of prediction models that estimate the characteristic impedance and characteristic wavenumber of a porous material[52]. These are empirical or theoretical models that focus on the characteristics of an infinite layer of a known acoustic medium. For their application a number of characteristics of the medium are needed, for example the flow resistivity in required for the Delany and Bazley model[53]. Furthermore, they have limitations in their bandwidth of application.

In this thesis the characteristic impedance and wavenumber of the porous materials investigated are going to be obtained by measurements in an impedance tube as will be presented in Section 6.3.2. This method has the advantage that it does not require previous knowledge of the characteristics of the material and it is limited in bandwidth only by the limitations of the tube. Furthermore, they will allow for better comparison of scattering

between measurements and simulations for the performance of Absorption Grating Diffusers (AGD) as the characteristics used in the simulations will correspond to the actual material used in the measurement rather that their estimation from its properties.

6.3. Impedance tube measurements

To develop AGDs requires knowledge of the absorption properties of porous materials and Helmholtz Resonators. In order to attain this information impedance tube measurements were carried out. In this Section the measurement methods to acquire either the surface impedance or the characteristic impedance and wavenumber used in this thesis are going to be discussed.

6.3.1. Surface impedance measurement

The surface impedance of a structure can be measured in an impedance tube. The measurement is carried out under the plane wave conditions enforced by the tube. The method used during this thesis was the transfer function method[54] the setup of which can be seen in Figure 6-4.

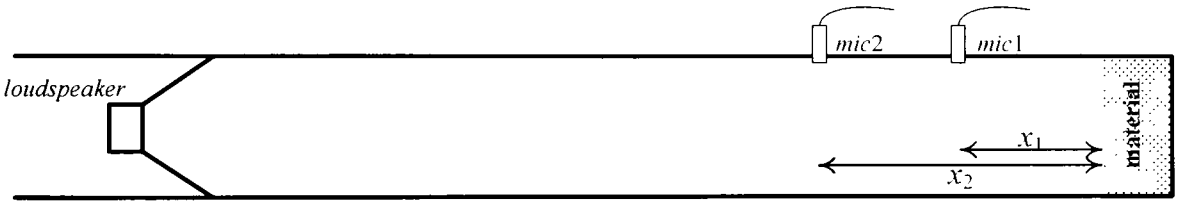

Figure 6-4. Impedance tube setup for measuring surface impedance.

By measuring the pressure at two positions (x_1, x_2) the transfer function between the two positions is found:

$$H = \frac{p_2}{p_1} = \frac{e^{jkx_2} + R \cdot e^{-jkx_2}}{e^{jkx_1} + R \cdot e^{-jkx_1}} \qquad 6.9$$

The reflection coefficient is found by re-arranging 6.9:

$$R = \frac{H \cdot e^{jkx_1} - e^{jkx_2}}{e^{-jkx_2} - H \cdot e^{-jkx_1}} \qquad 6.10$$

Once the reflection coefficient is known then the surface impedance z_s and the absorption coefficient α can be found via equations 6.2-6.4.

In order for this method to work the pressure at the two points must be different. So the spacing between them must not be too small compared to the wavelength while being smaller than it. This translates to the transfer functions frequency limits:

$$f_u < \frac{0.45c}{|x_1 - x_2|}$$
$$f_l > \frac{c}{20 \cdot |x_1 - x_2|} \qquad 6.11$$

where x_1 and x_2 are the distances of the two microphones from the sample (see Figure 6-4).

The frequency range can be extended by using more than two microphone positions. That would create more pairs of measurements and as a result a wider applicable bandwidth.

This solution applies only for plane wave propagation. Such conditions can be reached in an impedance tube (Figure 6-4) up to the cut-off frequency:

$$f_u > \frac{c}{2d} \qquad 6.12$$

where c is the speed of sound of the medium (air in this case) and d is the maximum width of the tube. In the case that the tube has a circular cross-section, d is the diameter while if the cross-section is rectangular it is the diagonal. The system of equations 6.11 and 6.12 gives the overall frequency limits of this measuring system.

This method used to measure the surface impedance of Helmholtz Resonators is going to be discussed in the following Chapter. The square impedance tube of Figure 6-5 is used. It has a cross-section of $5.4 \times 5.4 cm^2$ and ½ inch microphones are positioned at $x_1 = 9.93cm$ and $x_2 = 15.03cm$ from the end of the tube. So the frequency limits of the tube are $300Hz$ and $3kHz$ and the Brüel & Kjær Pulse 3560 was used for the data acquisition and analyses[55]. Swept-sine signal[56] that was generated from the analyser was used for the measurement.

In order for Helmholtz Resonators to be tested in front of a volume of air or a layer of porous material an extension of varying depth is used (Figure 6-6). In this way perforated plates can be securely fixed between the tube and the extension. The termination and parts of the sides of this extension are wooden so it is not perfectly rigid. When tested the extension gave an absorption coefficient of 0.05.

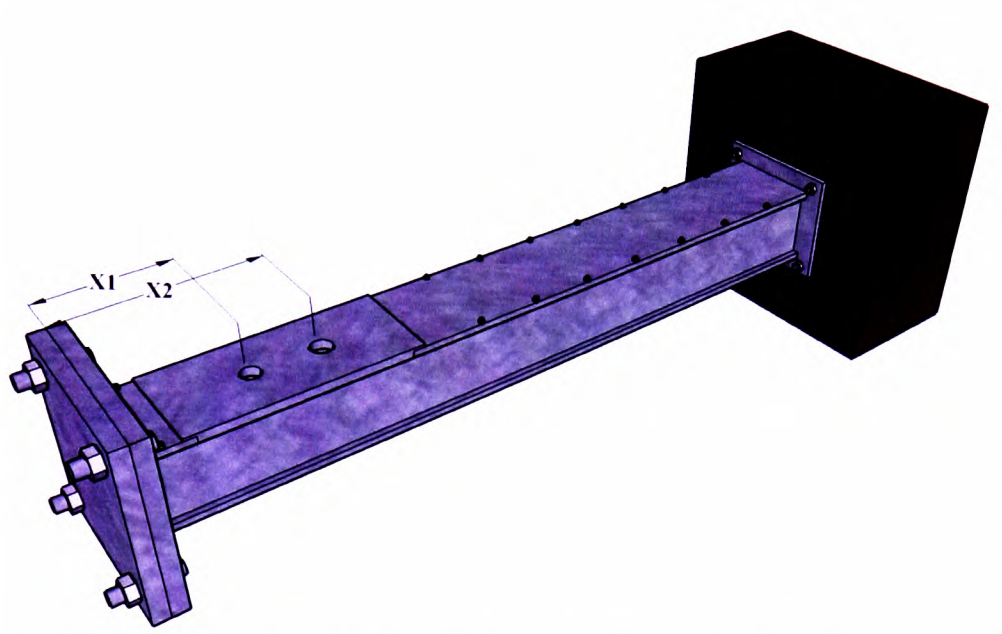

Figure 6-5. Square impedance tube with cross-section $5.4\times5.4cm^2$, ½ inch microphones positioned at $x_1 = 9.93cm$ and $x_2 = 15.03cm$ (frequency range $300Hz < f < 3kHz$).

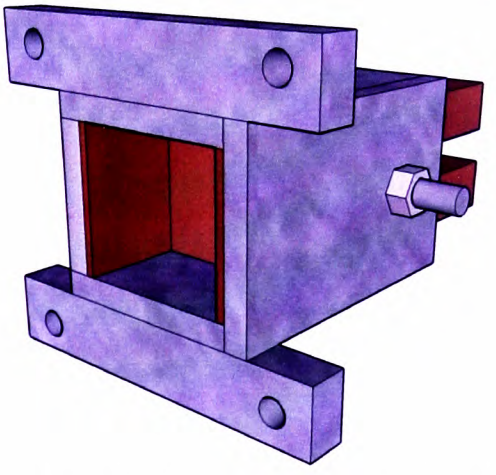

Figure 6-6. Impedance tube extension of adjustable depth with wooden termination.

The plates that are used for the measurement are substantially larger than the cross-section of the tube (Figure 6-7) as they need to be big enough to be screwed on. By creating a hole on the plate a Helmholtz Resonator is formed. Measurements using this technique will be presented in Section 6.4.2.

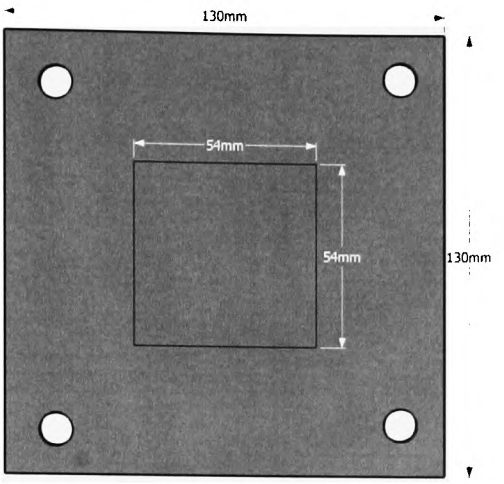

Figure 6-7. Plate geometry.

6.3.2. Measurement of characteristic properties

The knowledge of the surface impedance characterises a specific layer of an absorbing material, but it does not contain any information about the behaviour of a layer of different depth. In order to obtain that information, the characteristic impedance and characteristic wavenumber are needed which though eq. 6.8 can give the surface characteristics of any layer of a given material. These properties can be acquired through impedance tube measurements.

The measurement can be done through the measurement of the surface impedance of two different thicknesses of a material[57] but in this thesis the estimation was from transmission loss measurements[58]. The reason the two thickness method is not used is because it requires measurement of the surface impedance two samples of exactly the same properties that are cut in two different thicknesses. The existence of two different samples introduces possible errors in the measurement method that are not present in the transmission loss method that uses a single sample.

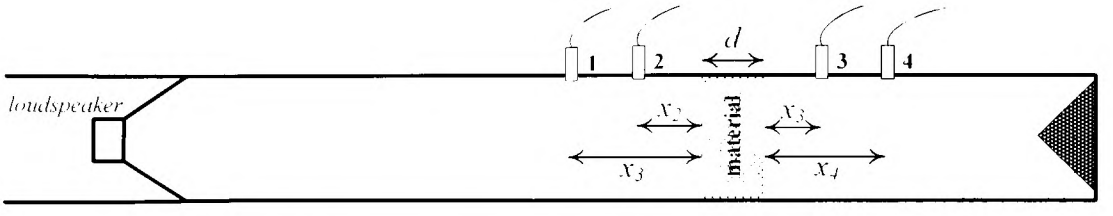

Figure 6-8. Impedance tube setup for measuring characteristic impedance and characteristic wavenumber.

The material characteristics can be measured using an impedance tube in the setup displayed in Figure 6-8. The characteristics of a medium are contained in the four transfer matrix components T_{11}, T_{12}, T_{21} and T_{22} that connect the pressure p and particle velocity u of the sound wave at the two surfaces of the material[58].

$$\begin{bmatrix} p \\ u \end{bmatrix}_{left} = \begin{bmatrix} T_{11} & T_{12} \\ T_{21} & T_{22} \end{bmatrix} = \begin{bmatrix} p \\ u \end{bmatrix}_{right} \tag{6.13}$$

This is a system of two equations with the four transfer matrix components unknown. By testing the same sample under two different impedance tube terminations a solvable system of four equations is created:

$$\begin{bmatrix} p^r & p^o \\ u^r & u^o \end{bmatrix}_{left} = \begin{bmatrix} T_{11} & T_{12} \\ T_{21} & T_{22} \end{bmatrix} = \begin{bmatrix} p^r & p^o \\ u^r & u^o \end{bmatrix}_{right} \tag{6.14}$$

where the superscripts indicate the two different impedance tube terminations, *r* for rigid and *o* for open-tube.

The pressure and particle velocity at each side of the sample can be expressed as[58]:

$$\begin{aligned} p_{left} &= Ae^{jkx} + Be^{-jkx}, \quad u_{left} = \frac{1}{\rho c}\left(Ae^{jkx} - Be^{-jkx}\right) \\ p_{right} &= Ce^{jkx} + De^{-jkx}, \quad u_{right} = \frac{1}{\rho c}\left(Ce^{jkx} - De^{-jkx}\right) \end{aligned} \tag{6.15}$$

By measuring the pressure at two points on either side of the sample the coefficient *A*, *B*, *C* and *D* are estimated:

$$\begin{aligned} A &= \frac{p(x_1)e^{-jkx_2} - p(x_2)e^{-jkx_1}}{2jsin\left(k(x_1 - x_2)\right)}, \qquad B = \frac{p(x_1)e^{-jkx_1} - p(x_1)e^{-jkx_2}}{2jsin\left(k(x_1 - x_2)\right)} \\ C &= \frac{p(x_3)e^{-jkx_4} - p(x_4)e^{-jkx_3}}{2jsin\left(k(x_1 - x_2)\right)}, \qquad D = \frac{p(x_4)e^{-jkx_3} - p(x_3)e^{-jkx_4}}{2jsin\left(k(x_1 - x_2)\right)} \end{aligned} \tag{6.16}$$

Substituting eq. 6.15 in 6.14 one gets:

$$\begin{bmatrix} A^r \\ B^r \end{bmatrix} = \begin{bmatrix} \left(T_{11} + \frac{T_{12}}{\rho c} + pcT_{21} + T_{22}\right)\frac{e^{-jkd}}{2} & \left(T_{11} - \frac{T_{12}}{\rho c} + pcT_{21} - T_{22}\right)\frac{e^{jkd}}{2} \\ \left(T_{11} + \frac{T_{12}}{\rho c} - pcT_{21} - T_{22}\right)\frac{e^{-jkd}}{2} & \left(T_{11} - \frac{T_{12}}{\rho c} - pcT_{21} + T_{22}\right)\frac{e^{jkd}}{2} \end{bmatrix} \begin{bmatrix} C^r \\ D^r \end{bmatrix}$$

$$\begin{bmatrix} A^o \\ B^o \end{bmatrix} = \begin{bmatrix} \left(T_{11} + \frac{T_{12}}{\rho c} + pcT_{21} + T_{22}\right)\frac{e^{-jkd}}{2} & \left(T_{11} - \frac{T_{12}}{\rho c} + pcT_{21} - T_{22}\right)\frac{e^{jkd}}{2} \\ \left(T_{11} + \frac{T_{12}}{\rho c} - pcT_{21} - T_{22}\right)\frac{e^{-jkd}}{2} & \left(T_{11} - \frac{T_{12}}{\rho c} - pcT_{21} + T_{22}\right)\frac{e^{jkd}}{2} \end{bmatrix} \begin{bmatrix} C^o \\ D^o \end{bmatrix} \quad 6.17$$

The system of equations 6.16 and 6.17 can be solved to produce the transfer matrix components T_{11}, T_{12}, T_{21} and T_{22} from the pressure measurements.

Once these components are known, the characteristic impedance and wavenumber of the material can be calculated[58]:

$$k_c = \frac{1}{d}\sin^{-1}\left(\sqrt{-T_{12}\cdot T_{21}}\right) \quad 6.18$$

$$z_c = \sqrt{\frac{T_{12}}{T_{21}}} \quad 6.19$$

where d is the depth of the material tested.

The system used for the measurement was the Brüel & Kjær 4206-T impedance tube kit[59] displayed in Figure 6-9. It consists of two tube components of different diameter that can be attached to the speaker (left end of the tube) and four ¼ inch microphones. The wider tube component is supplied with three microphone positions on each side of the sample allowing for the frequency ranges of eq. 6.11 to be extended. The wide one (diameter of $10cm$) (Figure 6-9a) has frequency range from $500Hz$ to $6.4kHz$ and the smaller one (diameter of $2.9cm$) (Figure 6-9b) has $50Hz$ to $1.6kHz$ resulting in the kit having a combined frequency range from $50Hz$ to $6.4kHz$. The signal that was used for the measurement was a swept-sine[56] generated from the Brüel & Kjær Pulse 3560[55] analyser.

The characteristic impedance and wavenumber of black open cell was measured with this method and they are presented in Figure 6-10 and Figure 6-11. These measurements will be used in Section 9.2 where the scattered pressure distribution from a surface that partly consists of this material is going to be simulated in BEM.

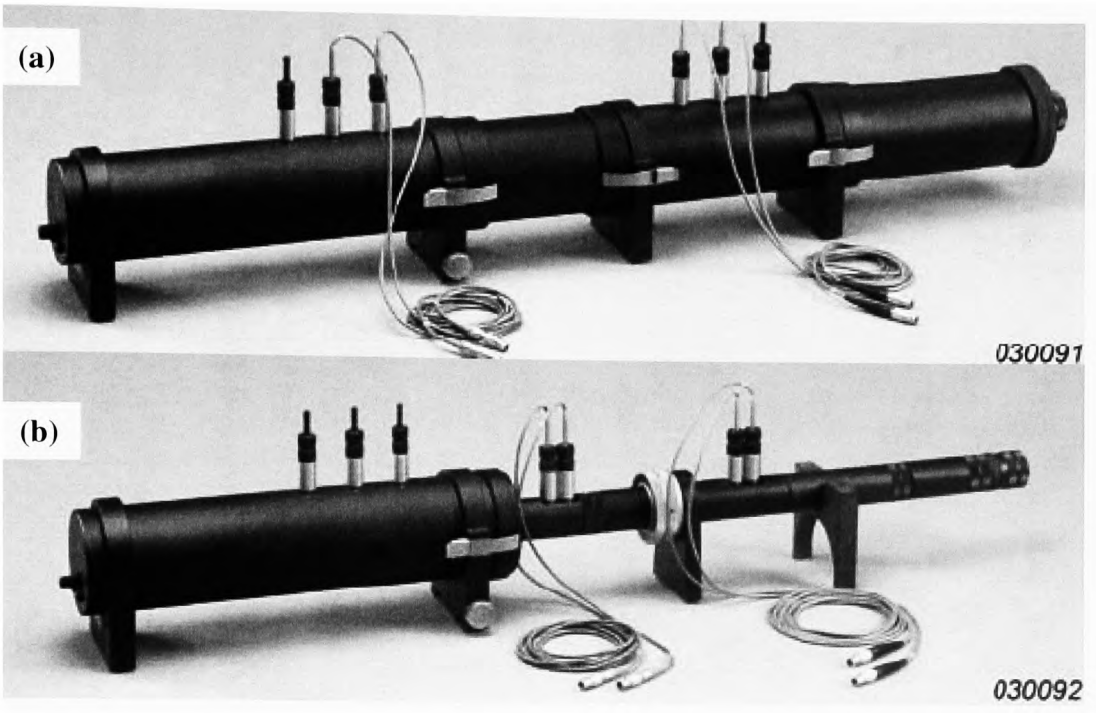

Figure 6-9. Brüel & Kjær 4206-T impedance tube kit for measuring characteristic impedance and characteristic wavenumber.

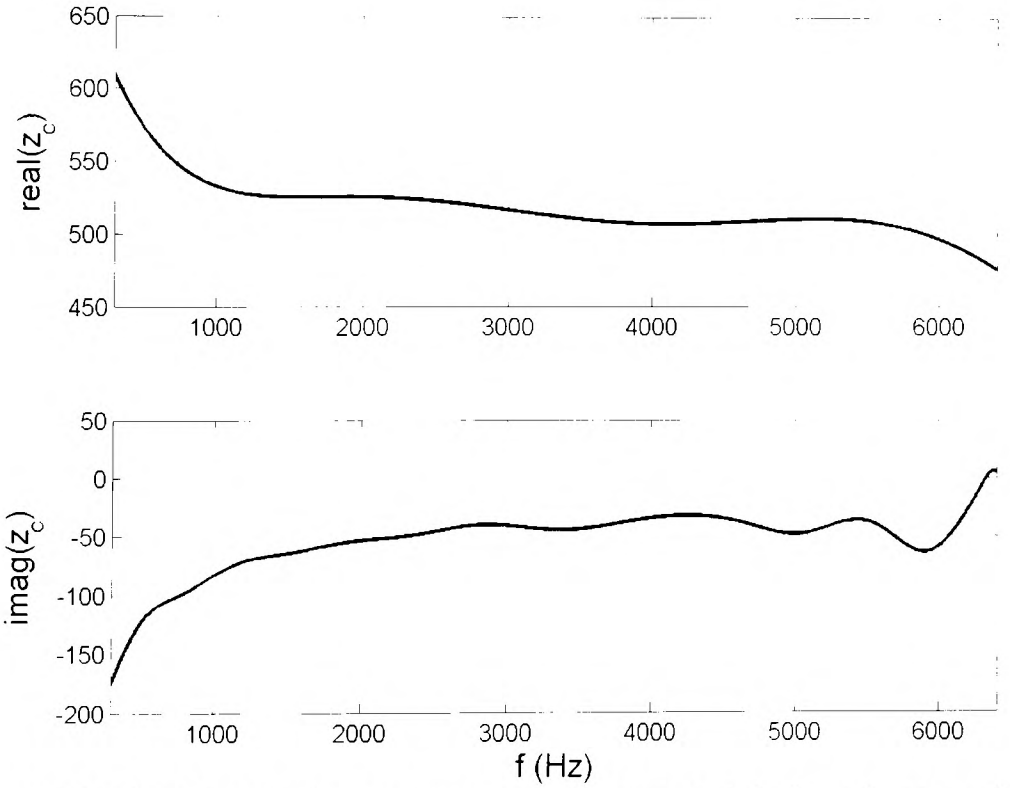

Figure 6-10. Impedance tube measurment of the characteristic impedance z_c of black open cell foam.

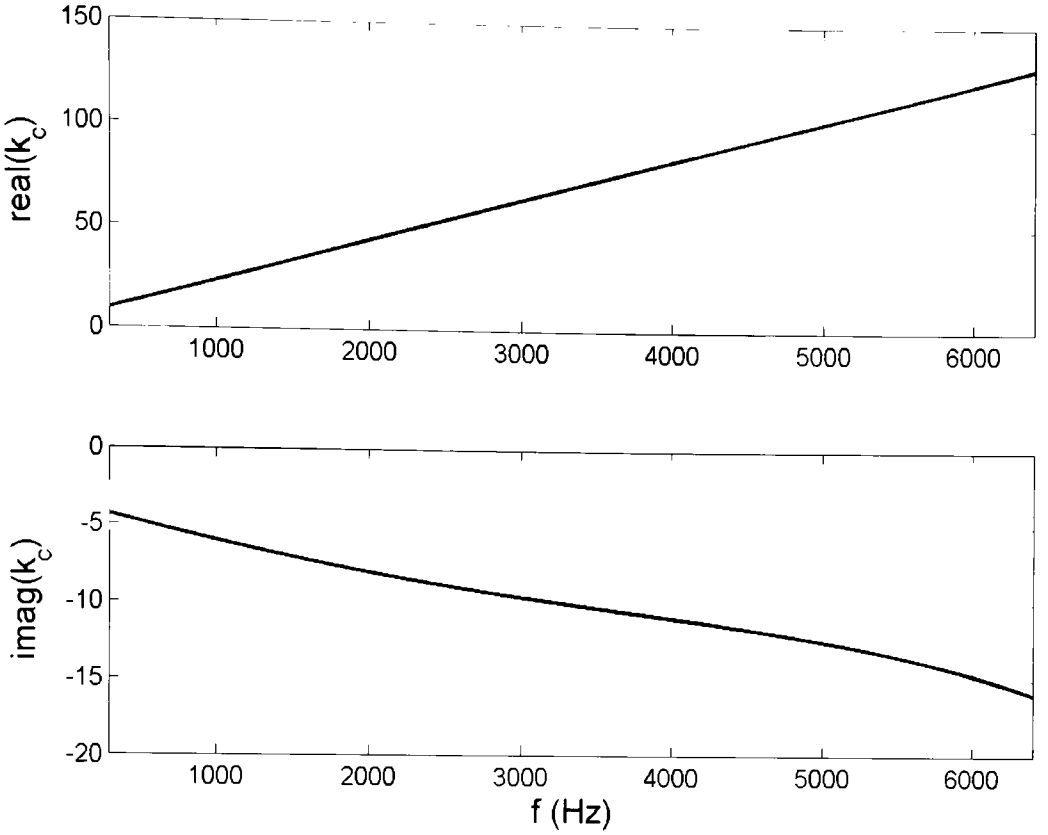

Figure 6-11. Impedance tube measurement of the characteristic wavenumber k_c of black open cell foam.

6.4. Types of absorbers

Since there is a requirement of absorbing elements in the design of absorption grating diffusers it is important to point out methods for their implementation.

6.4.1. Layer of porous materials

The most common absorbing materials are porous. Their absorbing characteristics are due to viscous losses as the sound penetrates through the pores. The surface impedance of a layer of porous material can be either measured directly in an impedance tube (see Section 6.3.1) or can be estimated from the characteristic impedance z_c and characteristic wavenumber k_c of porous material using the Transfer Matrix Model (eq. 6.8). When the surface impedance is known the other surface coefficients of the material can be calculated as discussed in Section 6.1.

The trend of the absorption coefficient of $5cm$ of foam estimated from the characteristic impedance and wavenumber, measured in the previous Section, can be seen in Figure 6-12. The disadvantage of implementing the absorbing element, of an Absorption Grating Diffuser,

in this fashion is the requirement of a substantial depth of the absorbing material to achieve absorption close to 1 at low frequencies. This becomes evident in this graph where the first peak of substantial absorption is achieved when a quarter of the wavelength fits into the depth of the material ($f = 1.7kHz$).

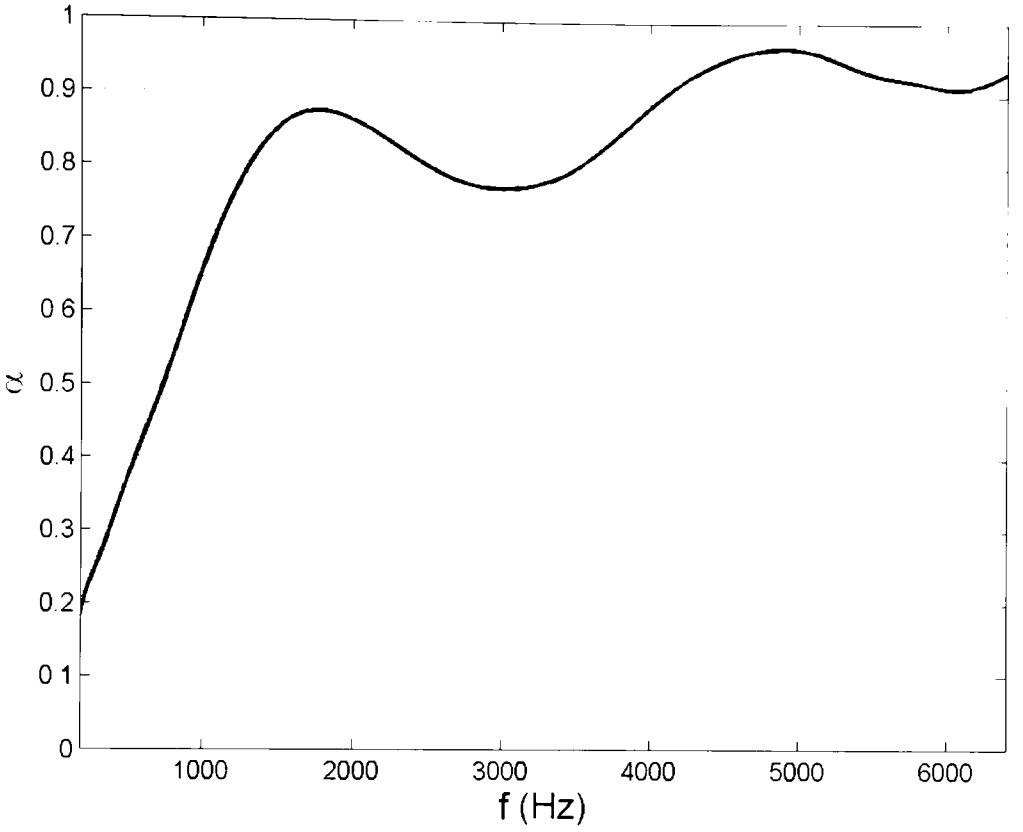

Figure 6-12. Absorption coefficient of $5cm$ deep open cell estimated from its characteristic impedance and wavenumber.

6.4.2. Helmholtz Resonators

A simple device that can achieve low frequency absorption without requiring too much space is the Helmholtz Resonator (Figure 6-13). They are devices that absorb acoustic energy and re-radiate it when the acoustic pressure drops. They are named after Hermann Von Helmholtz who first wrote about them in 1863[60]. He suggested them as tuners since they can be set-up very accurately to reinforce a specific frequency. Baron Rayleigh presented a more extended theoretical analysis of the function of such resonators in 1896[61]. Although these are the first scientific references on Helmholtz Resonators their history and applications go a long way back. They have been used in ancient Greek and Roman open theatres to increase the reverberation times and reinforce the performer's voice as well as in many early churches to provide absorption by resonance[62].

A Helmholtz Resonator is the acoustical equivalent of mass on a spring and consists of an empty cavity with a neck (Figure 6-13). So its function can be split into two components the mass of air in the hole and that in the cavity. The volume of air in the cavity acts as a spring and the air in the neck as the mass that oscillates. When the device is exposed to the resonant frequency the air in the neck will oscillate and energy will be lost due to friction with the sides of the neck and also dispersed from the sides of the cavity. For frequencies away from resonance the absorption is minimal unless the hole is sub-millimetre in size[63].

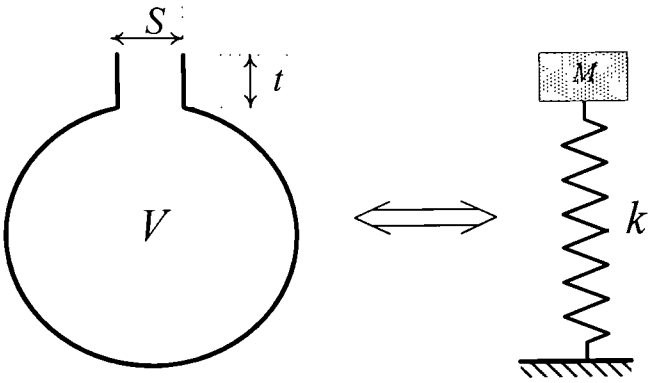

Figure 6-13. A Helmholtz Resonator and its mechanical equivalent.

Similar to its mechanical equivalent the resonant frequency of the Helmholtz Resonator is[64]:

$$f_r = \frac{c}{2\pi}\sqrt{\frac{S}{t' \cdot V}} \qquad 6.20$$

where c is the speed of sound, S is the area of the opening, V is the volume of the cavity and t' the length of the neck including the end correction:

$$t' = t + 2\delta\alpha \qquad 6.21$$

where α is a characteristic size of the opening (ex. the radius for a circular perforation) and δ is the end correction.

The end correction is considered to approximate the fact that it is not only the mass of air in the neck that oscillates but air close to the opening as well due to the radiation impedance. This effect has its roots in the flow of air through a structure with varying cross-section. The flow lines narrow in the smaller cross-section and cause the particle velocity to increase. The opposite effect occurs when the air moves from the smaller cross-section to the bigger one.

There is a transition state between the two cross-sections where the flow lines narrow and widen. In the case of Helmholtz Resonators this transition state of the flow lines results in more than just the air in the neck to participate in the oscillation. For a baffled circular neck opening where a is the radius of the opening the end correction is $\delta = 0.85$.

By altering the stiffness of the spring or changing the mass of the mechanical oscillator, the resonant frequency can be varied. By changing the size of the cavity or the neck of the resonator, the resonant frequency of the Helmholtz resonator can be tuned.

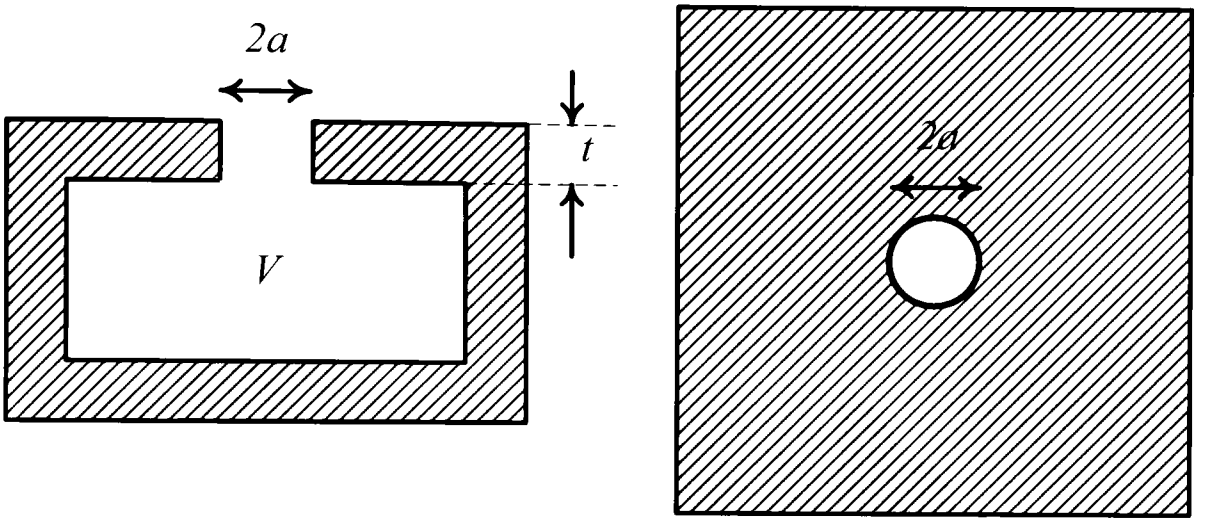

Figure 6-14. Helmholtz Resonator with cavity volume V, hole-depth d and hole-radius a, morphed into a surface.

A Helmholtz Resonator can be morphed into a flat surface as is depicted in Figure 6-14. The neck in this case is the hole-area of a perforated plate. The absorption coefficient of this structure can be measured in an impedance tube (see Section 6.3.1). The performance of a Helmholtz Resonator with design frequency $f_r = 900Hz$ (cavity volume $V = 38cm^3$, hole-area $S = 2cm^2$ and hole-depth $t = 1.5mm$) is displayed in Figure 6-15. It achieves maximum absorption at resonance while at other frequencies the absorption is minimal with the exception of the area around $1.9kHz$. This second resonance is due to the vibrating plate of thickness t that forms the top of the device. If the plate was solid it would be expected to display resonance at $2.4kHz$. Here due to the hole it has less mass and therefore it has shifted to lower frequencies. By altering the stiffness of the plate this peak will shift and can be pushed out of the frequency range of interest.

The Q factor of the absorption coefficient is relatively large and the bandwidth of absorption is small, as losses are relatively small. Given that the absorbing elements need to display ideal absorption for a substantial bandwidth the use of Helmholtz Resonators in this form does not meet the requirements for absorption grating diffusers. In order to achieve absorption for a wider frequency range absorbing material must be included in the volume. The Helmholtz Resonator when the cavity is occupied with absorbing materials is referred to as "loaded"

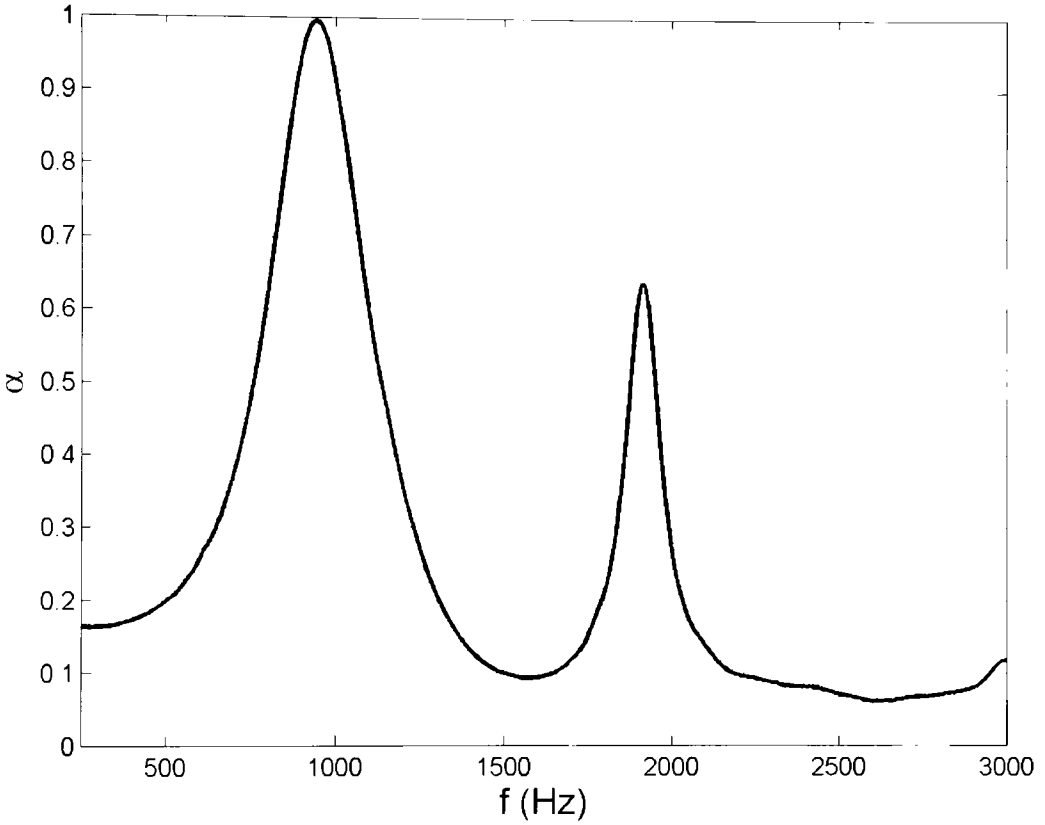

Figure 6-15. Measured absorption coefficient in an impedance tube of a Helmholtz Resonator morphed into a surface with resonant frequency $f_r = 900Hz$ (cavity volume $V = 38cm^3$, hole-area $S = 2cm^2$ and hole-depth $t = 1.5mm$).

Loaded Helmholtz Resonators

The existence of absorbing material usually moves the resonance to higher frequencies and reduces the peak of absorption, while the Q factor will decrease as the hole-diameter augments. The shift in the resonant frequency and the increase in the bandwidth of absorption are results of the added damping in the cavity.

Periodically repeated loaded Helmholtz Resonators on an infinite surface have been studied[65]. They can be implemented by considering a perforated surface a distance from a

rigid backing. Above a certain frequency, they can be approximated by considering only one period of the surface. Each period due to the symmetry of the surface can be considered as an independent Helmholtz Resonator. The volume of the resonator will be the one contained in a period as is portrayed in Figure 6-16.

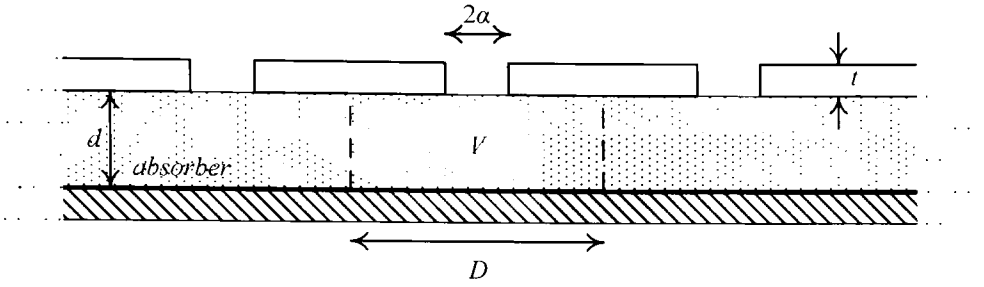

Figure 6-16. Periodically perforated surface backed by absorbing material in front of a rigid backing.

The resonant frequency of a perforated surface in front of a rigid backing can be found by adapting equation 6.20:

$$f = \frac{c}{2\pi}\sqrt{\frac{\varepsilon}{t' \cdot d}} \qquad 6.22$$

where c is the speed of sound in air d the distance between the perforated plate and the backing, t' is the plate thickness t including the end correction and ε is the open area of the plate which is given by the equation:

$$\varepsilon = \frac{\pi\alpha^2}{D^2} \qquad 6.23$$

where α is the radius of the hole and D is the period of the surface.

The vibrating mass of air in the volume is:

$$m = \frac{\rho}{\varepsilon}(t + 2\delta\alpha) \qquad 6.24$$

where ρ is the density of air and δ is the end correction.

The end corrections have been estimated by Ingard[66] for circular (where α is the radius of the hole) and square apertures (where 2α is the side of the hole) and small open areas ($\varepsilon < 0.16$). But Cremer and Müller[64] have presented an estimation of the end correction for open areas up to the limited case of $\varepsilon = 1$:

$$\delta_c = 0.8\left(1 - 1.47 \cdot \varepsilon^{1}/2 + 0.47 \cdot \varepsilon^{3}/2\right) \quad 6.25$$

Even though the knowledge of how to estimate the resonant frequency is an important first step in understanding the behaviour of these devices, it is not enough to allow for accurate prediction of their behaviour. Another, important information is losses within the device. The losses when the cavity of the resonator is empty stem from the friction in the neck which is negligible if the holes are not sub-millimetre.

That is the reason why in order to achieve some absorption, away from the resonant frequency, absorbing material must be included in the volume. If the volume is filled with absorptive material as Figure 6-16 shows, the hole can be considered to be filled with the material as well due to radiation impedance. The air that flows through the hole will come up against the resistivity of the material. Due to radiation impedance the losses will be from the portion of absorber that is behind the cross-section of the hole:

$$r_m = \frac{\sigma d}{\varepsilon} \quad 6.26$$

The transfer matrix prediction model which was analysed in Section 6.2 can give a complete solution of the performance of a periodically perforated surface if the characteristic impedance z_c and wavenumber k_c, of the absorbing material, are known. The surface impedance of the absorber behind the perforation z_{s1} will be:

$$z_{s1} = -jz_c \cot(k_c d) \quad 6.27$$

If the mass effect of the perforation is added to surface impedance of the absorbing material the surface impedance of the perforated surface can be estimated:

$$z_{s2} = \frac{t'}{\varepsilon} j\omega\rho + z_{s1} \quad 6.28$$

In Chapter 5 where the concept of Absorption Grating Diffusers was presented they were described as surfaces with pseudorandomly arranged absorbing and reflecting elements. If loaded Helmholtz Resonators are going to be used for their implementation then the performance of non-periodic arrangements of resonators needs to be investigated. Such structures have not been meticulously investigated and the only reference to their performance is that they absorb like a periodic arrangement of Helmholtz Resonators with the

same open area, provided that the distances between the holes are large in comparison to their diameter[64].

6.5. Summary

In this Chapter acted as a literature review on absorbing structures. The basis for assessing the qualities of such elements was presented. The methods for the prediction and measurement, in an impedance tube, of their surface and characteristic coefficients that are used in this thesis were illustrated. Absorbing structures that will be used as elements of the Absorption Grating Diffusers were presented and their performance characteristics were discussed.

In the following Chapter whether an Absorption Grating Diffuser which can be implemented by incorporating loaded Helmholtz Resonators in a surface is going to be investigated. In order to do so a wider band of absorption from these devices will be attempted while the discussion on the behaviour of non-periodic arrangements of Helmholtz Resonators is going to be extended.

Chapter 7. Implementation of the absorbing elements with perforations on a mask

One way of implementing the Absorption Grating Diffusers (AGD) considers a layer of absorbing material behind a randomly perforated surface (Figure 5-4). It considers the holes to act as loaded Helmholtz Resonators (absorbers) and the rigid areas as reflectors. Such structures can achieve absorption in the hole-areas close to the ideal requirement of AGDs for a small bandwidth. Before work can be carried out in sequence design and optimization methods, a better understanding of how perforated surfaces act must be reached. Also a number of implementation issues need to be addressed. There is a need to make the absorbing parts performing the same regardless of how close the neighbouring absorbing parts are located. Finally, the absorbing patches must be made to display stable absorption coefficient equal to 1 for a considerably large bandwidth.

There is no analytical theory that can predict the surface admittance distribution on the surface of such a structure. Investigation of their behaviour is going to be conducted with impedance tube measurements while the applicability of using the measured surface admittance in Boundary Element Modelling (BEM) simulations is going to be studied.

7.1. Holes on a mask

The issues with using a perforated surface in front of layer of porous material is that the holes behave like Helmholtz Resonators resulting in very absorbing surfaces. Furthermore, away from resonance the absorption achieved is poor. So the resulting surface acts similarly to a periodic surface of the same open-area, as suggested in the previous Chapter. The holes interact both inside and outside the cavity resulting in the performance averaging out across the surface. In order for such a device to be used as an AGD it has to consist of purely absorbing and reflective elements.

Some insight to the behaviour of perforated surfaces can be found through surface impedance measurements in an impedance tube with a square cross-section (Figure 6-5). This setup allows for the prediction of the surface characteristics of periodic surfaces to be measured. By measuring a single period of such a surface it can be considered to be identical to an infinitely

wide periodic surface by considering its mirror images in respect to the sides of the tube[67]. Two simple examples are portrayed in Figure 7-1.

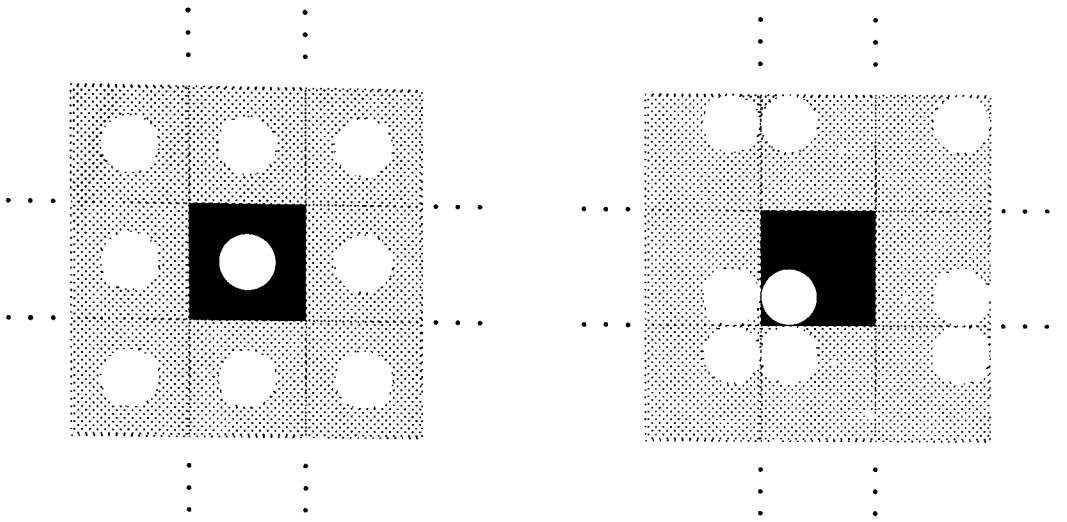

Figure 7-1. The cross-section that is tested in the square impedance tube can be considered to be a single period of an infinitely wide surface.

7.2. Helmholtz Resonator impedance tube measurements

For the measurements the square tube presented in Section 6.3.1 is used using the adjustable extension (Figure 6-6) so that the perforated plates can be fixed in front of a volume of air or a layer of porous material. Some of the patterns of sample plates that were tested are portrayed in and Figure 7-2.

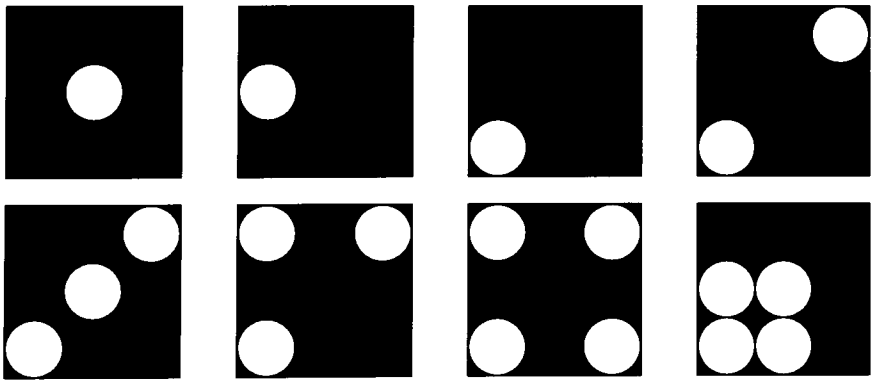

Figure 7-2. Sample plates out of 1.5*mm* aluminium sheets.

Helmholtz Resonators with empty cavity were tested with the hole located in the centre of the sample area. In Figure 7-3 the absorption coefficient of cases, with 29*mm* cavity depth and 1.5*mm* plate thickness, for different hole-diameters are presented. Unfortunately, the

resonances of the perforated plates around $1.6kHz$ limit the measurement bandwidth. As a result of this, the resonant frequency of large open area plates cannot be seen. In order to minimise the resonance of the plate either damping of the vibration of the plate must be imposed or a thicker plate must be used for the measurement. Another solution would be to use plates of a different material that would be stiffer than the aluminium used.

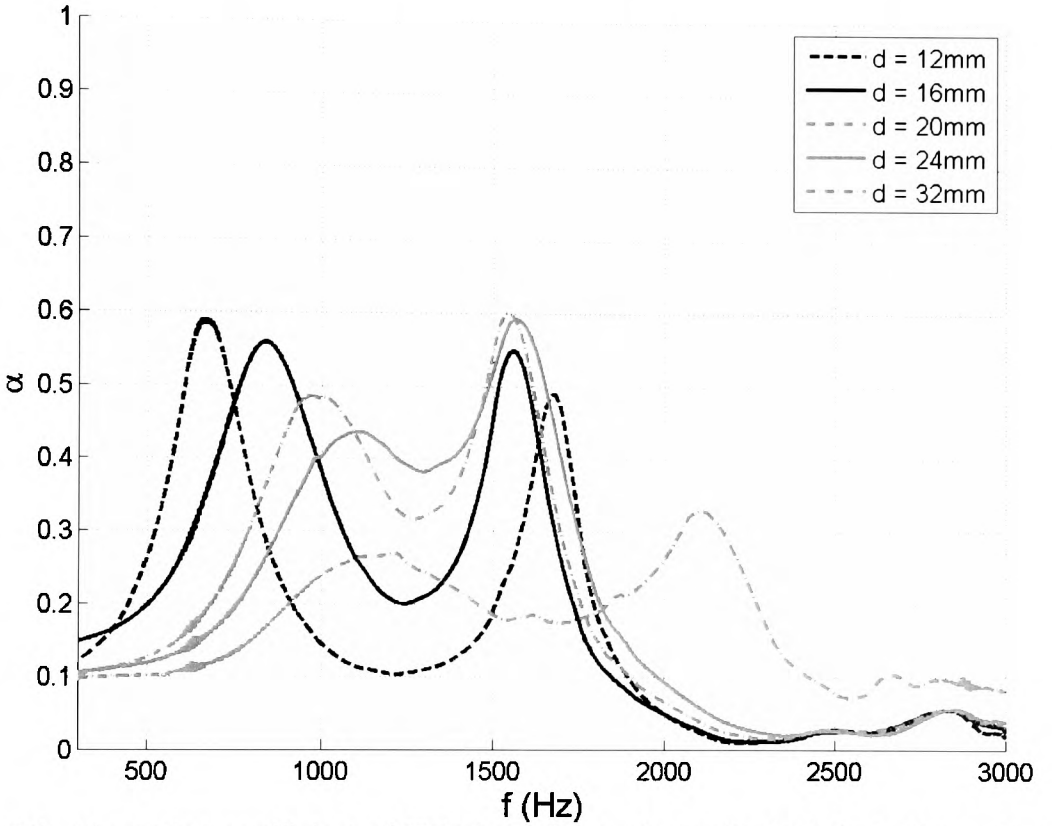

Figure 7-3. Absorption coefficient of Helmholtz Resonators with the hole in the center of the sample of varying hole-diameters (d) for the same cavity volume ($2.9\text{x}5.4^2 cm^3$) and plate thickness ($1.5mm$).

The absorption achieved with the empty cavity does not achieve stable absorption for a substantial bandwidth. In order to achieve a broader bandwidth of application the cavity of the resonator must be filled with absorbing material. If the cavity is filled with highly resistive material then the resonance can be damped. This would result in a lower but wider absorption peak. To illustrate this effect layered mineral wool is used in the cavity. This material consists of layers of mineral wool densely packed and compressed resulting in a highly resistive material. The normalised surface impedance for a layer of $29mm$ in relation to air can be seen in Figure 7-4. The resistivity of the material which is given by the real part suggests that the surface displays twice the resistivity of air.

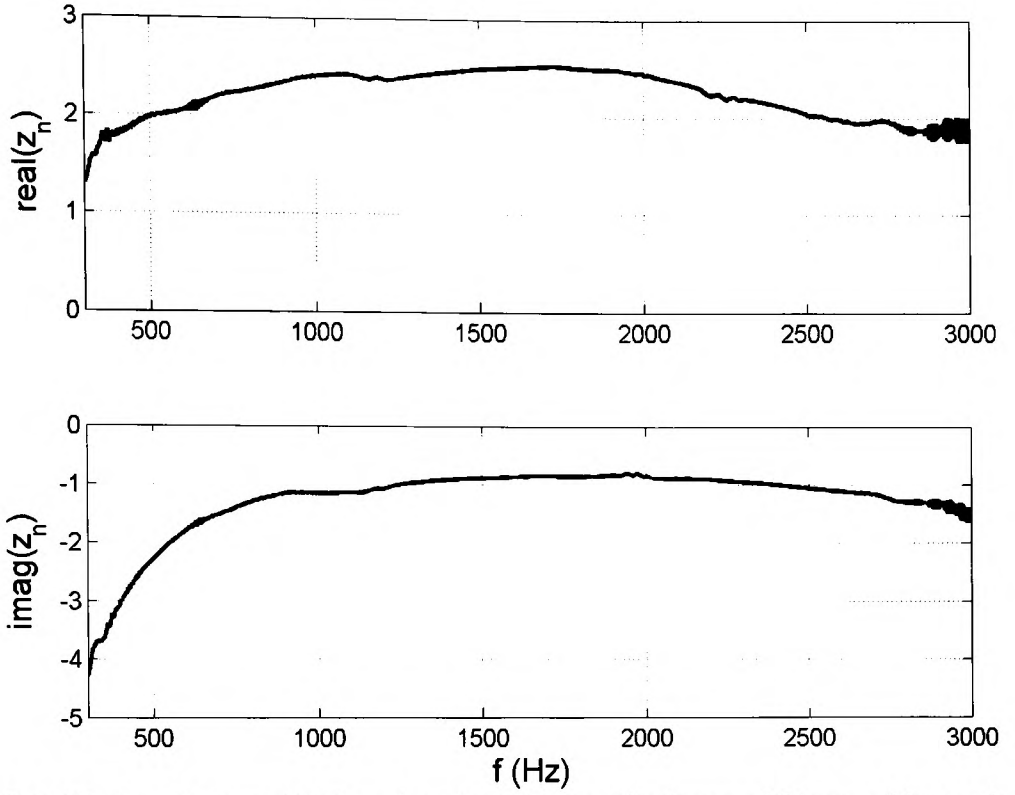

Figure 7-4. Measured normalised surface impedance of a layer of 29*mm* of layered mineral wool.

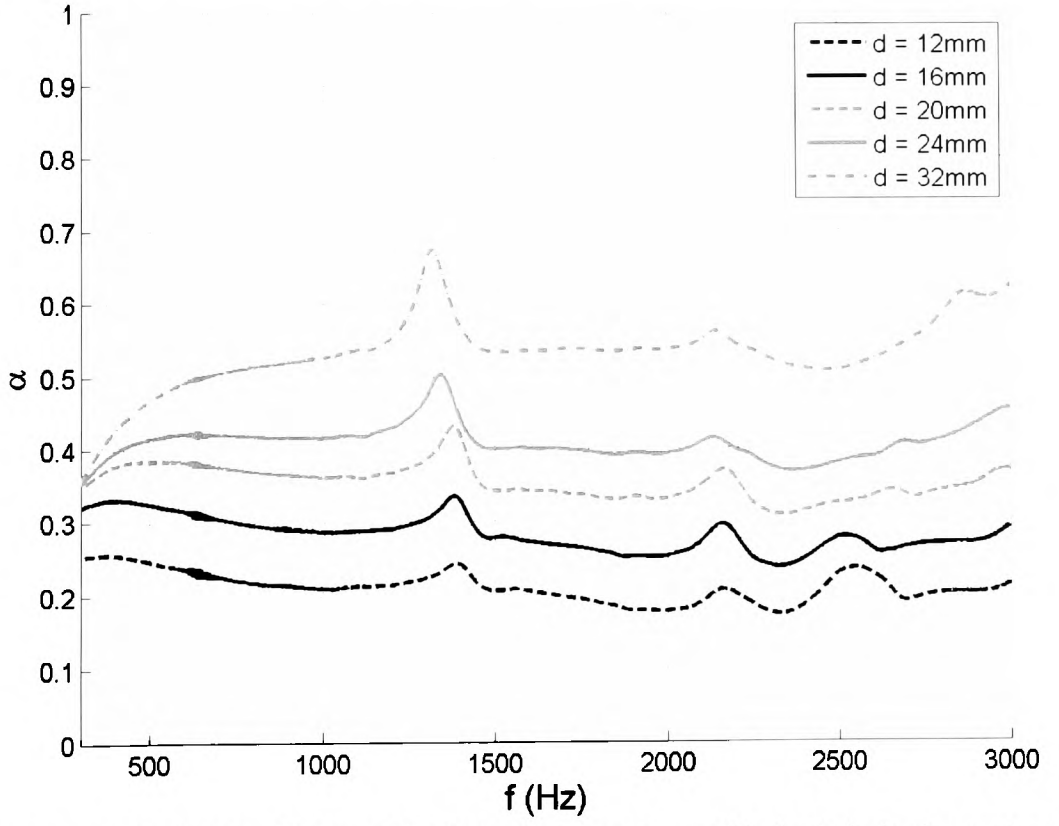

Figure 7-5. Absorption coefficient of Helmholtz Resonators with the hole in the center of the sample of varying hole-diameters (*d*) for the same cavity volume ($2.9\times5.4^2 cm^3$) and plate thickness (1.5*mm*) loaded with layered mineral wool.

Some measurements of the loaded Helmholtz Resonators with this mineral wool occupying its cavity are displayed in Figure 7-5. The depth of the cavity was set to 29*mm* and the same plate samples were tested as before. These results are very encouraging for AGD design. Their steady absorption with frequency can be adapted in the concept of the design; however the absorption coefficient is less than unity.

As can be noticed the plate resonances that were evident in the case of the empty cavity in Figure 7-3 have gone. The mineral wool is in contact with the plate providing damping to the plate. The small peaks of plate resonance that can still be seen in the figure would be reduced even further if the mounting conditions are changed; so it is something that isn't an issue for this discussion.

7.3. Helmholtz Resonator BEM simulation

Since BEM will be used in the prediction of the performance of AGDs a useful idea is to see if the same results can be produced through simulation. The input data that are going to be used are from measurement in the impedance tube. So the level of agreement between simulation and measurement will correspond to whether BEM can accurately reproduce its input.

For this reason the geometry of the measurement is introduced in a direct 3-D BEM[68] with all the surfaces being considered perfectly reflecting with the exception of the sample area. Instead of the speaker, a point source is considered close to the side were the speaker is located. This replacement should go unnoticed as inside the tube plane wave propagation will be forced. BEM can estimate the pressure at the positions were the microphones are located in the measurement. Once these pressures are known, the transfer matrix method can be used to estimate the surface impedance and absorption coefficient using eq. 6.9 and eq. 6.10.

Since the performance of this over-damped Helmholtz Resonator cannot be calculated from any model, the measured data will be used for the simulation. The sample area of the tube is considered to be uniformly absorbing with the surface admittance characteristics previously measured. Figure 7-6 presents the BEM estimation in comparison to the measured input. The agreement is within ±0.03 while it is even better in the low and mid frequencies.

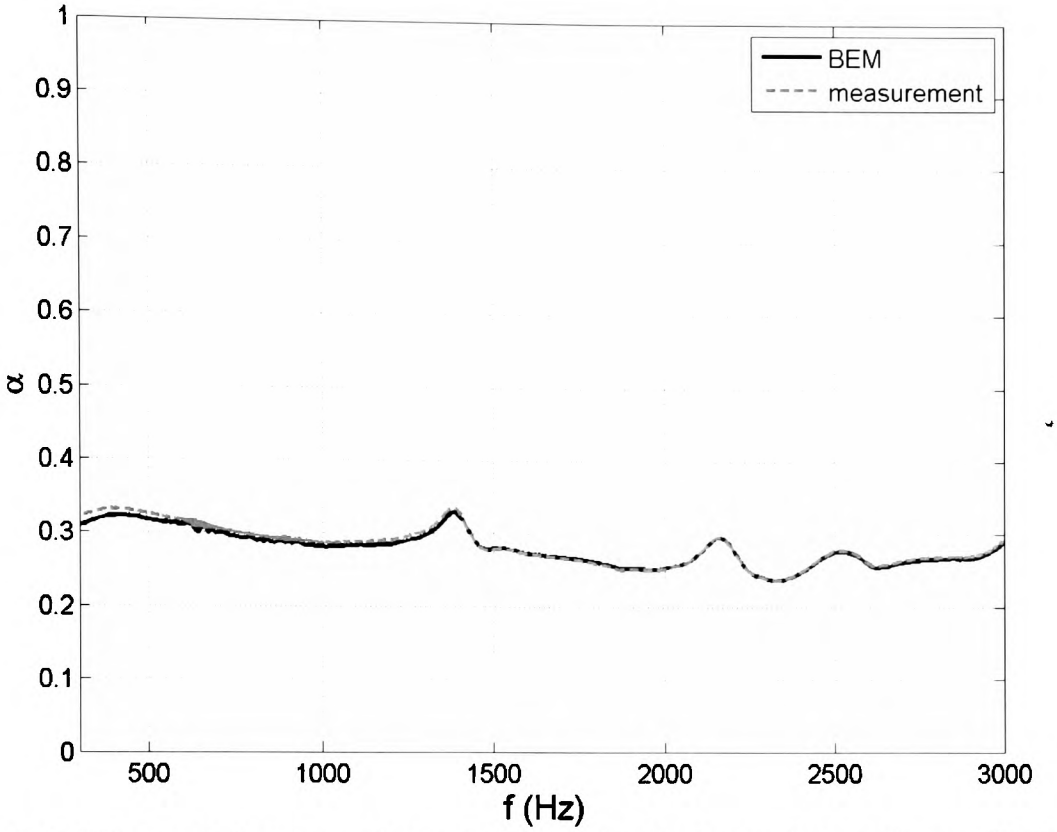

Figure 7-6. BEM prediction for uniform admittance distribution in the sample area. The input was the measured surface admittance of a Helmholtz Resonator with the hole in the center of the sample.

Given the acquired agreement over the bandwidth measured, a perforated surface can be considered to consist of $5.4\times5.4cm^2$ patches with uniform admittance. For the absorbing ones the measured admittance of a Helmholtz Resonator can be used, while for the reflecting an admittance of 0 can be used.

Another way of considering the distribution is for the admittance to be concentrated in the hole-area; while the rest of the surface is considered to be totally reflective. In order for the adequate surface impedance to be estimated the surface impedance of the Helmholtz Resonator has to be multiplied with the open area of the perforated surface. The reason for this is the radiation impedance that occurs as sound propagates through the holes:

$$u_{inc}S_{surf} = u_{holes}S_{holes} \Rightarrow u_{inc} = \frac{S_{holes}}{S_{surf}}u_{holes} \Rightarrow \frac{p}{u_{holes}} = \varepsilon\frac{p}{u_{inc}} \Rightarrow$$

7.1

$$\Rightarrow z_{holes} = \varepsilon \cdot z_{Helm}$$

where u_{inc} is the particle velocity above the perforated surface u_{holes} is the particle velocity in the holes and S_{surf} and S_{holes} are the surface of the plate and the holes respectively. The pressure p right outside and just inside the perforation is considered to be the same due to the radiation impedance of the perforation.

If the case of the measurement of a single perforation with a diameter of $16mm$ is considered then the absorption coefficient of the hole-area based on eq. 7.1 is displayed in Figure 7-7. The absorption coefficient is close to one throughout the investigated bandwidth which complies with the concept of perfectly absorbing and perfectly reflecting parts.

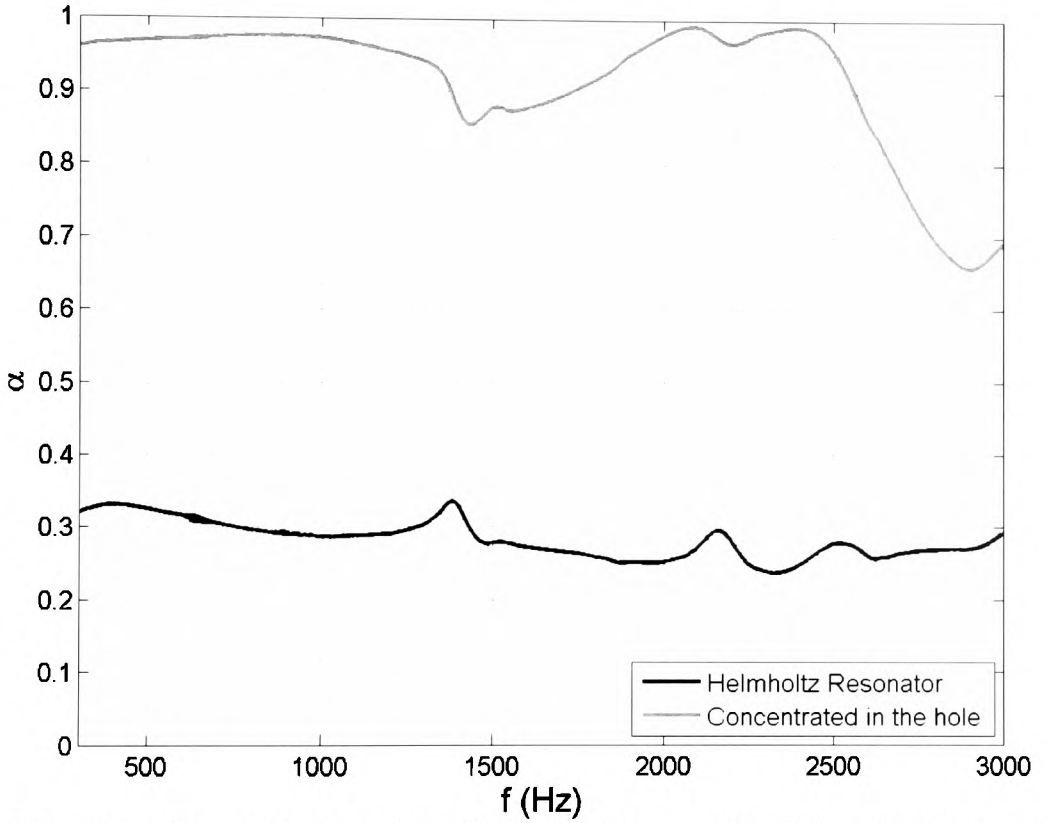

Figure 7-7. Absorption coefficient when all the admittance of the Helmholtz Resonator (d = $16mm$) is concentrated in the hole-area.

A way of seeing if this correspondence can be used is to see if the same results can be achieved using BEM. In this case the absorption is considered located only in the hole-area while the rest of the surface is considered perfectly reflecting.

For this reason the sample area has been meshed in the manner shown in Figure 7-8. The light grey area is the reflecting area while the dark grey is the absorbing. The BEM code used does not allow for curved elements to be modelled so the circle was approximated by a

16side regular polygon. A rectangle with a large number of equal sides inscribed in a circle has almost the same surface with the circle. Such an approximation does not alter the simulation as the elements are much smaller than the wavelength.

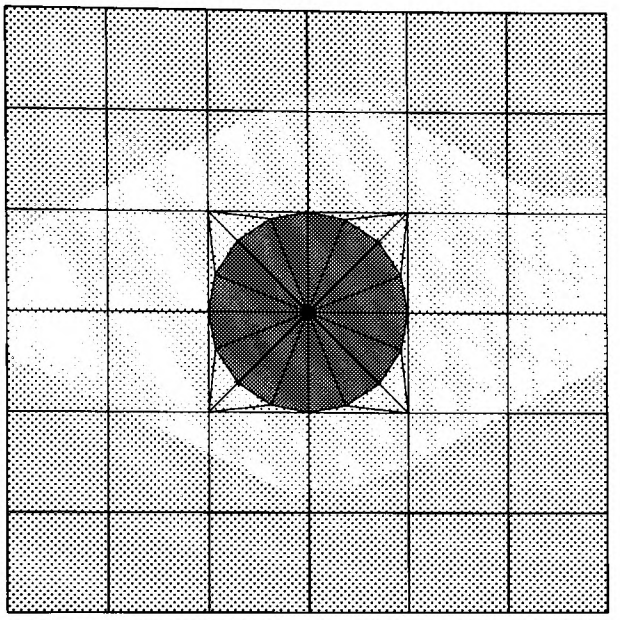

Figure 7-8. Boundary Element modelling sample meshing (light – reflecting, dark - absorbing).

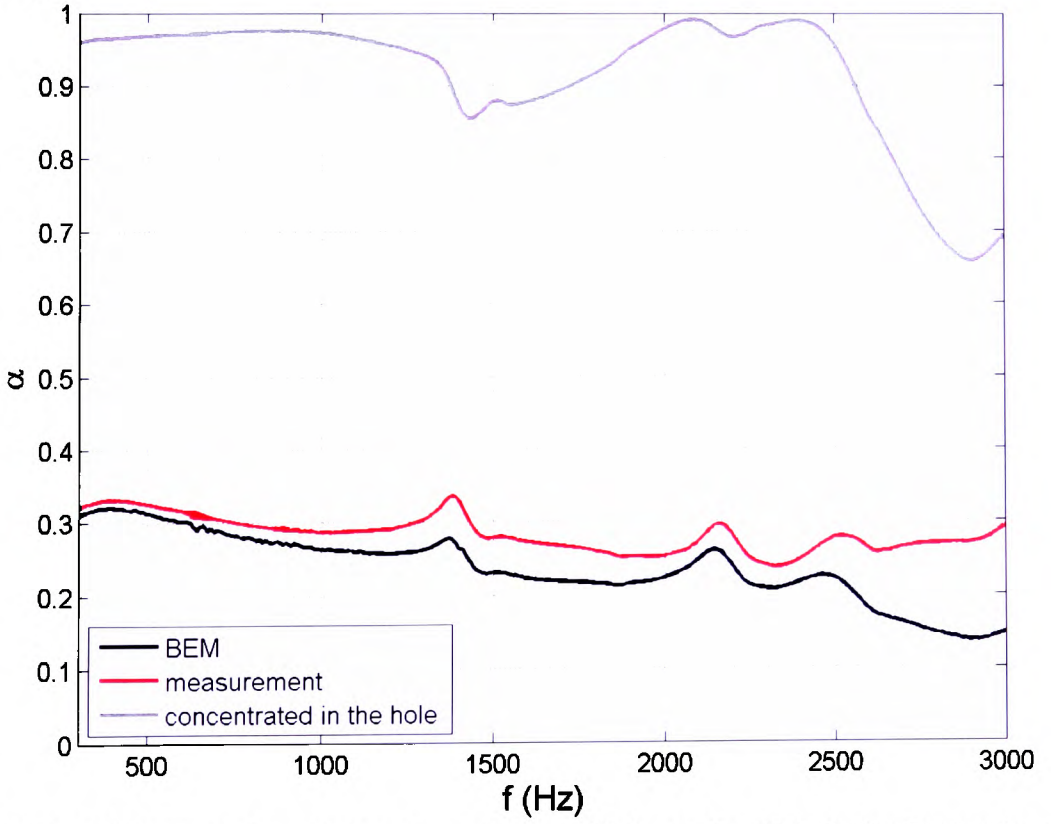

Figure 7-9. BEM prediction of the absorption coefficient of a Helmholtz Resonator when only the hole-area in absorbing. The input is the measured surface admittance of a Helmholtz Resonator divided by the open area.

The BEM result in Figure 7-9 shows similar pattern with the measured absorption coefficient. It under predicts the graph by 0.01 at low frequencies a difference that keeps increasing with frequency resulting in a substantial error (>0.1) at high frequencies. The error is due to the imaginary part of surface impedance (Figure 7-10) that corresponds to the reactive behaviour of the sample. The reason for this increasing error in prediction is due to the fact that when estimating the surface impedance in the hole-area the contribution of the plate was included.

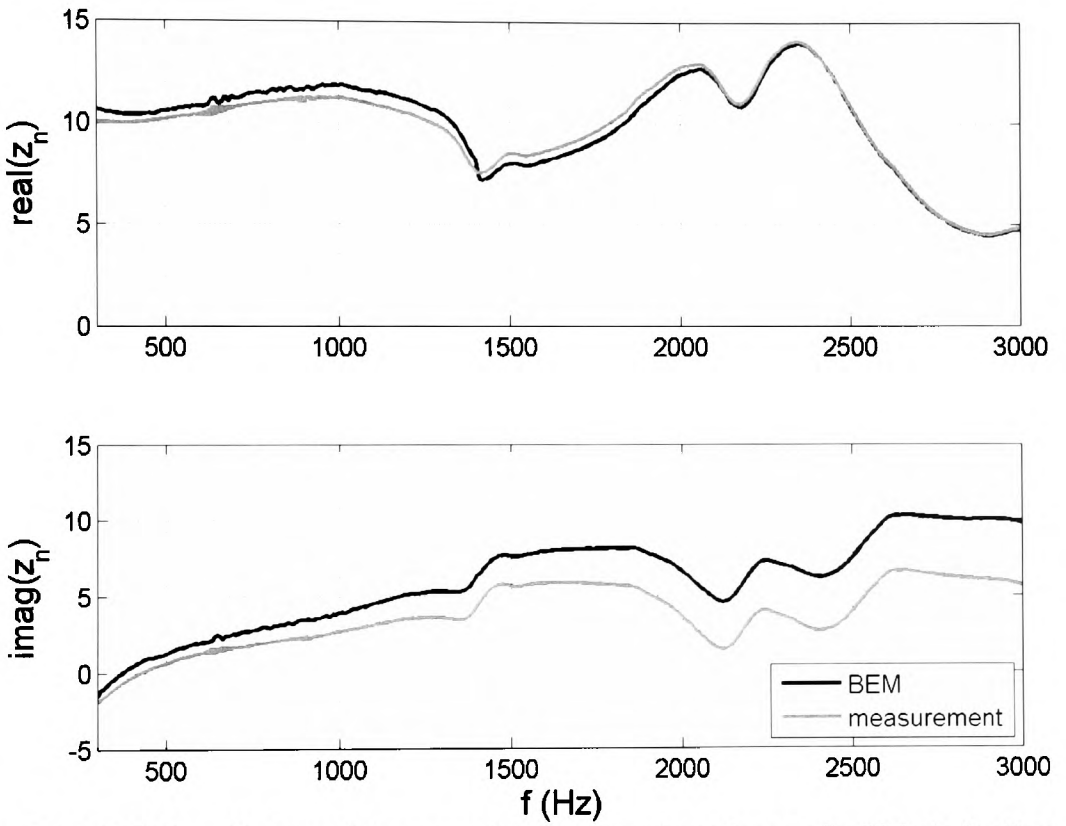

Figure 7-10. BEM prediction of the normalised surface impedance of a Helmholtz Resonator when only the hole-area in absorbing. The input is the measured surface admittance of a Helmholtz Resonator divide d with the open area.

This suggests that perforated surface could be approximated with absorption occurring only in the hole-area. The case tested above refers to a periodic surface. In the case of non-periodic perforations, the impedance corresponding to each hole-area would be different as shown in the next Section.

7.4. Different perforation patterns

In order to see how the performance changes for different patterns of perforations several measurements have been carried out and are presented in Figure 7-11. In all the cases the absorption coefficient is constant across frequency (Figure 7-7). If the admittance is considered to be concentrated only in the hole-area the resulting absorption coefficient of the hole would be close to 1 for all the perforation patterns as was seen for the case of a single perforation of 16*mm* in diameter (Figure 7-12).

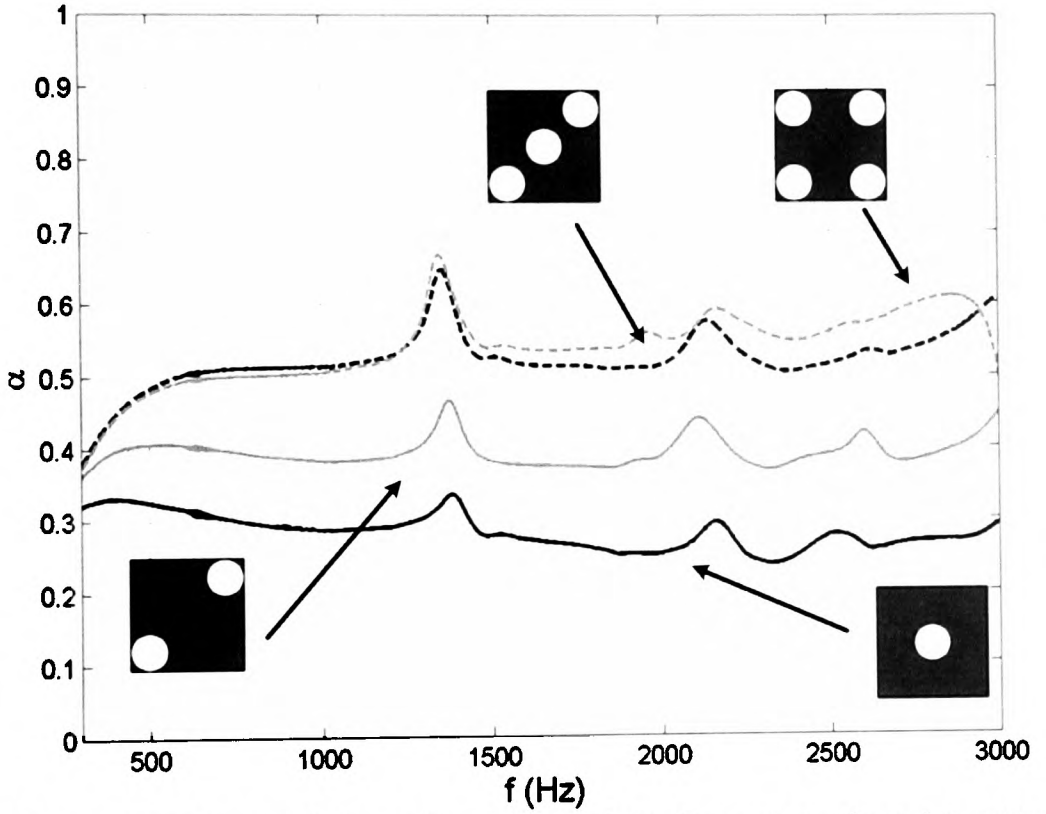

Figure 7-11. Absorption coefficient of loaded Helmholtz Resonators of varying patterns of perforation for the same hole-diameters (16*mm*), cavity volume (2.9x5.4^2*cm*^{3}) and plate thickness (1.5*mm*).

The existence of the layered mineral wool results in the reactance of the device being very low. For the cases presented above the normalised surface admittance can be seen in Figure 7-13. The imaginary part of the surface admittance is close to zero for the cases that consist of more than one perforation.

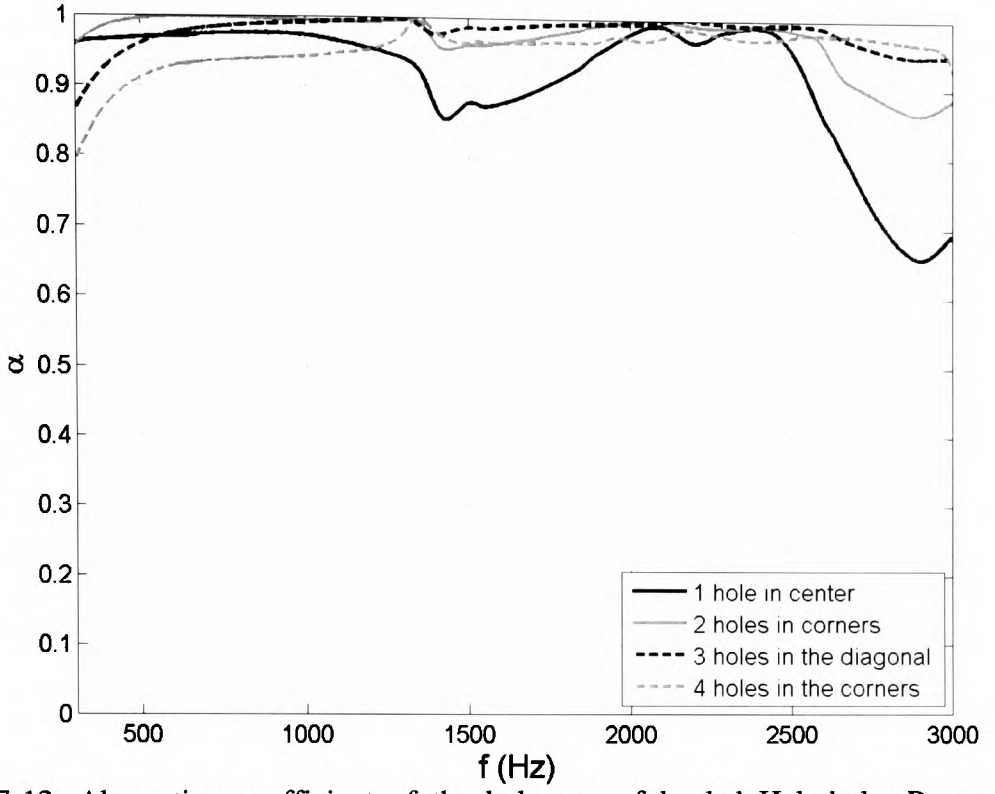

Figure 7-12. Absorption coefficient of the hole-area of loaded Helmholtz Resonators of varying patterns of perforation for the same hole-diameters (16*mm*), cavity volume ($2.9x5.4^2 cm^3$) and plate thickness (1.5*mm*).

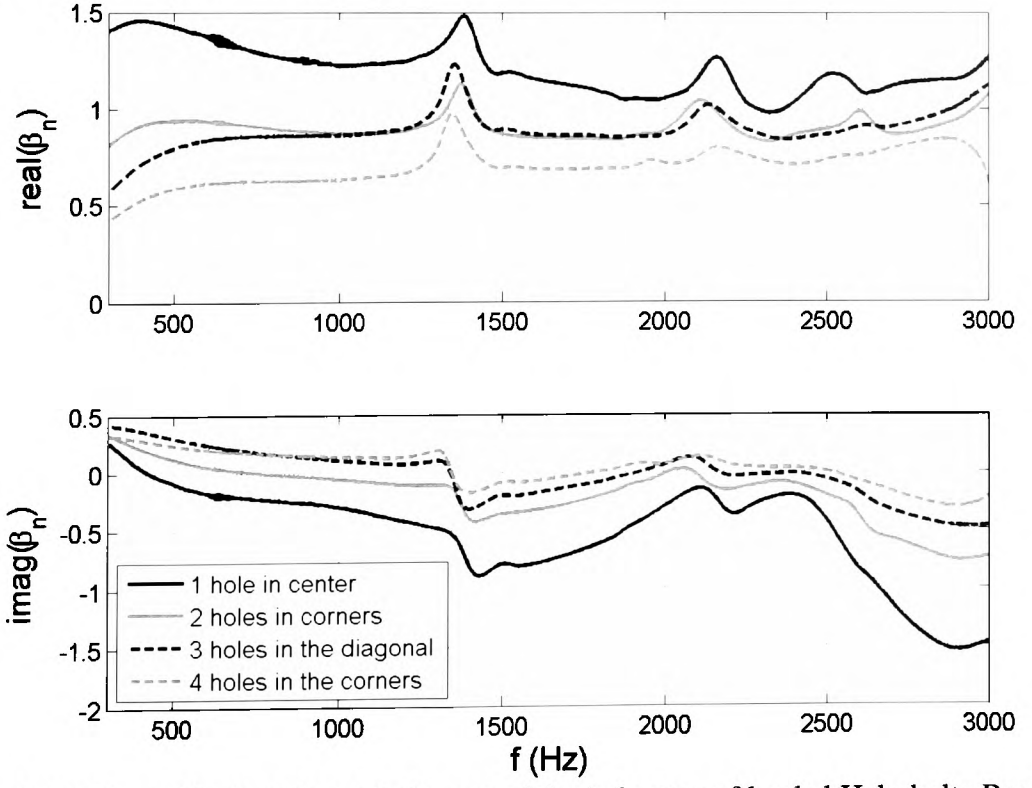

Figure 7-13. Normalised surface admittance of the hole-area of loaded Helmholtz Resonators of varying patterns of perforation for the same hole-diameters (16*mm*), cavity volume ($2.9x5.4^2 cm^3$) and plate thickness (1.5*mm*).

Based on the pattern of the perforations, different performance is achieved. As can evidently be seen in Figure 7-14 devices with the same open area can perform differently based on how the holes are distributed. The top three graphs have an open area of 28% while the bottoms two have 7% open area.

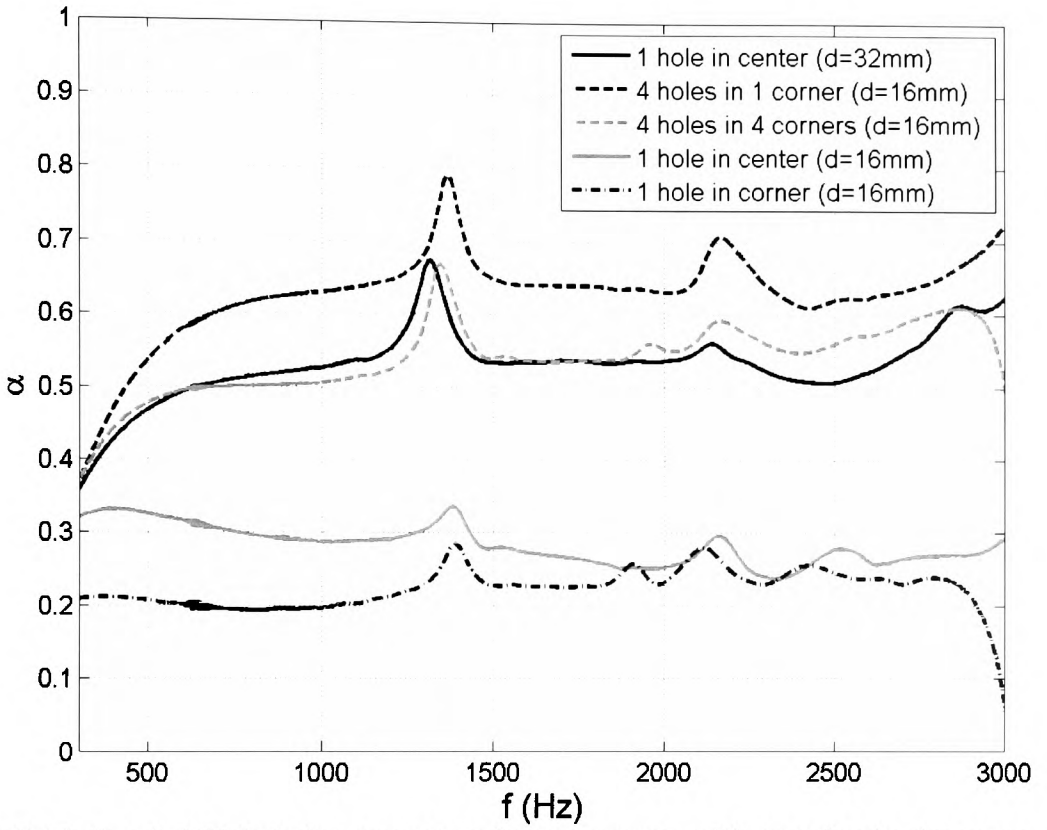

Figure 7-14. Loaded Helmholtz resonators in two groups with samples in the same group having identical open area (top 3 lines - 28%, bottom 2 lines - 7%).

As can be seen the perforation pattern plays a significant role in performance of the surface. Surfaces with the same number of holes provide different absorption based on the spacing of the perforations due to different end correction. This is obvious in the case of the absorption coefficient of a single 16*mm* hole. The absorption coefficient is higher for the perforation located in the middle of the sample area compared to the corner (bottom two lines of Figure 7-14). These two cases, while having the same open-area, represent different perforation patterns and thus display different end corrections. The perforation in the corner performs like a larger hole in a wider pattern (Figure 7-1). This is evident from the fact that a single perforation of 32*mm* in diameter positioned in the centre and 4 perforations of 16*mm* positioned in the 4 corners display the same absorption coefficient (±0.05) (Figure 7-14). This is due to the fact that a hole in the corner combined with its three mirror images from the

sides of the tube will result in a group of closely spaced perforations which will appear as one larger one (Figure 7-15). Two patterns with the same open-area that are different end up displaying the same end correction.

The drop in the absorption coefficient of patterns with perforation in the corners of the sample at high frequencies is due to the wavelength becoming similar to the width of the tube. This suggests that half a wavelength fits into the diagonal of the tube resulting in low pressure at the corners of the tube hence low absorption in the corners.

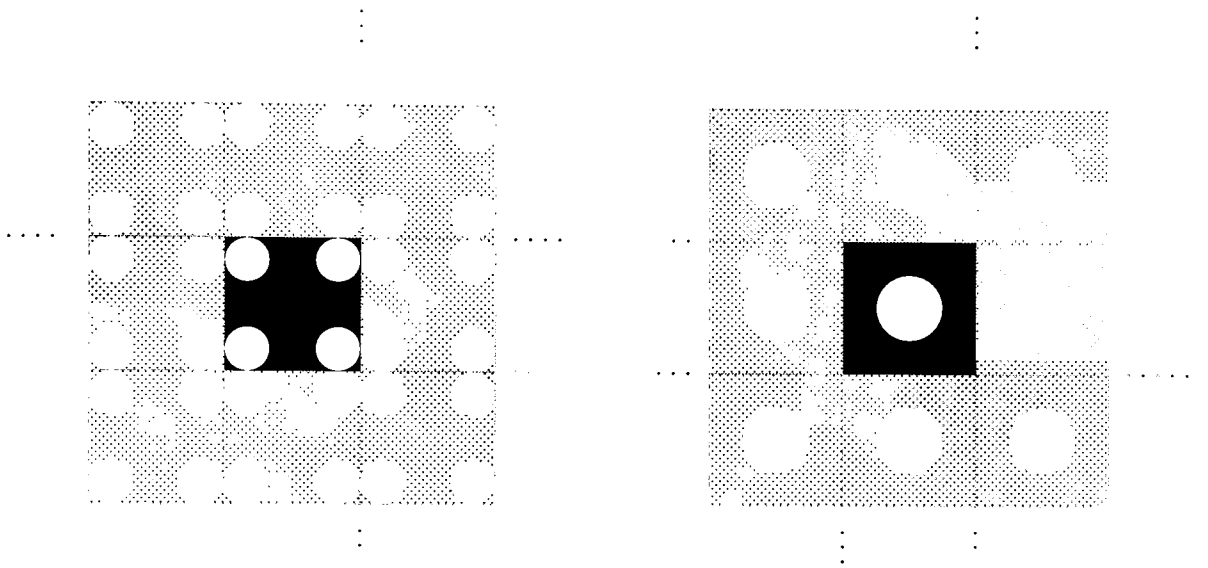

Figure 7-15. Same pattern emerging from different hole configurations.

This suggests that the pattern of the perforations plays a key role in the absorption characteristics of such surface. To the extent that a number of holes will appear as one larger one if placed close together compared to the wavelength. Be that as it may, if the absorption is considered to be concentrated in the hole-area it will be close to 1 regardless of the pattern and average achieved absorption of the surfaces.

So using dense layered mineral wool behind the perforated mask one can achieve the basic requirements for the implementation of AGDs. The high resistivity of the material dampens the resonant behaviour of the holes and results in stable absorption in the bandwidth investigated resulting in a surface that is not highly absorbing. The absorption coefficient of the perforations has been shown to be close to 1 regardless of their spacing. This agrees with the requirement of ideally absorbing and reflecting elements stated by the concept of AGDs.

7.5. Summary

Using dense layered mineral wool some of the issues in the performance of perforated surfaces have been dealt with. The resonant behaviour of the perforations is damped resulting in a structure that does not behave like a Helmholtz Resonator but acts almost purely resistively in the frequency range investigated. This resolved the issue of varying absorption with frequency while achieving a level of absorption of the surface that is not too high. Furthermore, since the rigid area of the plate does not absorb substantial energy the absorbing elements of the surface are the holes. In this configuration the absorption coefficient that corresponds to the hole-area is close to 1 regardless of the spacing of the perforations. This resolves the issue of the varying performance of the absorbing elements. This implementation of AGDs paves the way for these devices to be created in reality.

Furthermore, BEM has been found to predict the absorbing performance of such surfaces. This in turn allows for the performance of the diffusion from these surfaces to be predicted by using BEM on an array of holes. Having shown that AGDs can be created, a more detailed investigation of their performance in carried out. In the following Chapter the performance of ideal 2-D AGDs is discussed.

Chapter 8. Scattered pressure distribution from Absorption Grating Diffusers

In the previous Chapter a realistic approach to the implementation of surfaces consisting of ideally absorbing and reflecting elements has been discussed. In this Chapter the performance of the Absorption Grating Diffusers (AGD), as suggested by Angus are investigated. First, the characteristics of the different components of such a device will be looked into and comparison with the ideal ones will be made. Then, the scattered pressure distribution of AGDs will be tested.

The investigation is carried out in a 2-D domain using Boundary Element Modelling (BEM). The 2-D simulation allows for computational speed without being inferior to 3-D. Isolating the scattering from one dimension of the surface allows for the contribution of that dimension to be investigated while any results can be later expanded to 3-D.

8.1. Reflecting elements

In an AGD the reflecting elements based on the Fourier Theorem are the equivalent of omni-directional sources. So they should scatter pressure equally in all directions which corresponds to a diffusion coefficient of 1. The performance of a thin plate is examined in BEM to find out the extent to which it agrees with the requirement.

The plate is $w = 50cm$ wide and $d = 1mm$ deep. The source is positioned $10m$ away from the sample while 181 receivers with 1° increment are placed in a semicircle with a $5m$ radius. The distance of the source and receivers from the surface are substantial for it to be in the far field. So the specular reflection zone corresponds only to the receiver normal to the surface (0°) while all the other receivers are in the non-specular zone.

In Figure 8-1 the diffusion coefficient of a flat plate is presented as a function of the wavelength of the incident wave. As is evident from this graph the plate does not perform to the standards required as it fails to even approach the value of 1.

The trend of the reflected energy from the sample can be seen in Figure 8-2 where the mean reflected intensity is plotted along with the intensity reflected into and outside the specular reflection zone. All the intensities have been normalised to the incident pressure at the receiver that is normal to the surface.

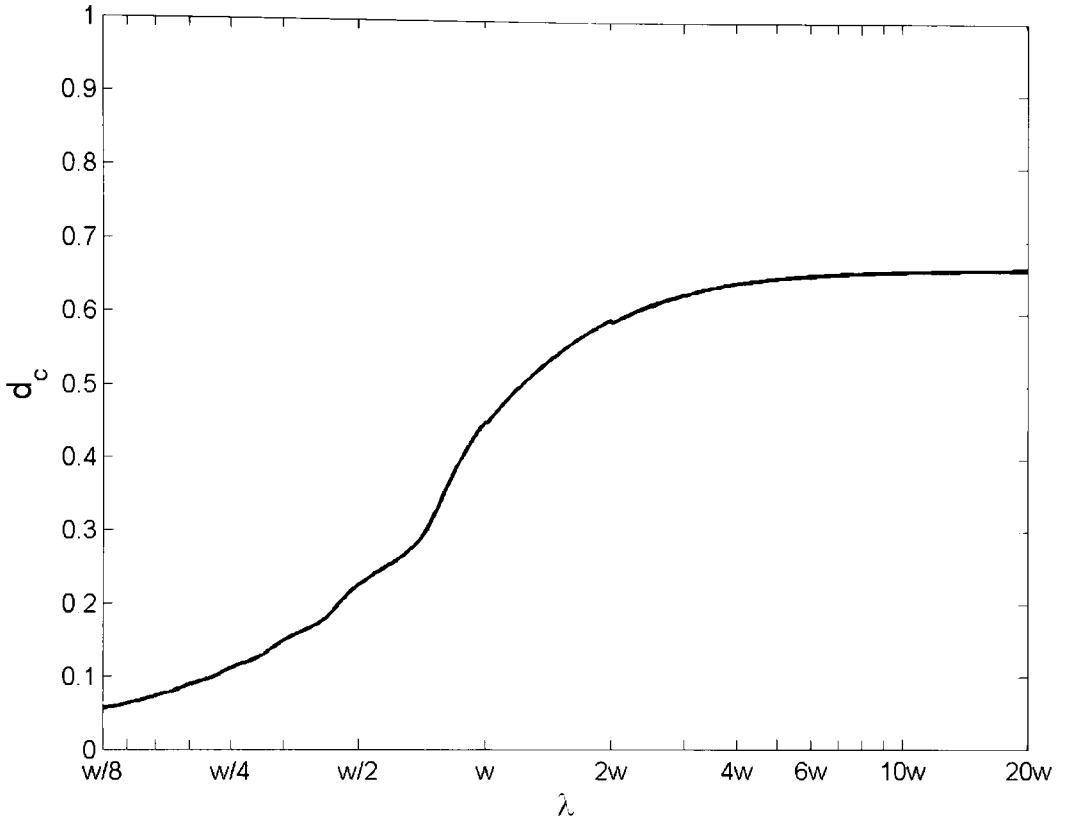

Figure 8-1. BEM predicted diffusion coefficient of a flat plate of width w.

When the sample is small compared to the wavelength it does not reflect substantial energy as it does not pose an obstacle for the sound wave. As the wavelength becomes smaller the sample reflects more energy reaching -20dB when its width becomes comparable to the wavelength ($\lambda = 3w$). For smaller wavelengths than that the sample is large enough to be a substantial obstacle for the sound wave. The maximum reflected energy is displayed when half a wavelength is equal to the width of the plate ($\lambda = 2w$). For $\lambda < w$ the scattered energy stabilises at -20dB.

The scattered energy from the sample can be split into the specular and non-specular reflection zones which correspond to the areas inside and outside of the area of geometric reflection. The scattered energy in the non-specular zone is purely due to the diffraction from the edges of the surface. The edge diffraction is created by the interference between the

waves that are reflected from different parts of the surface. The interference is dictated by the path difference from each point on the surface to the receivers.

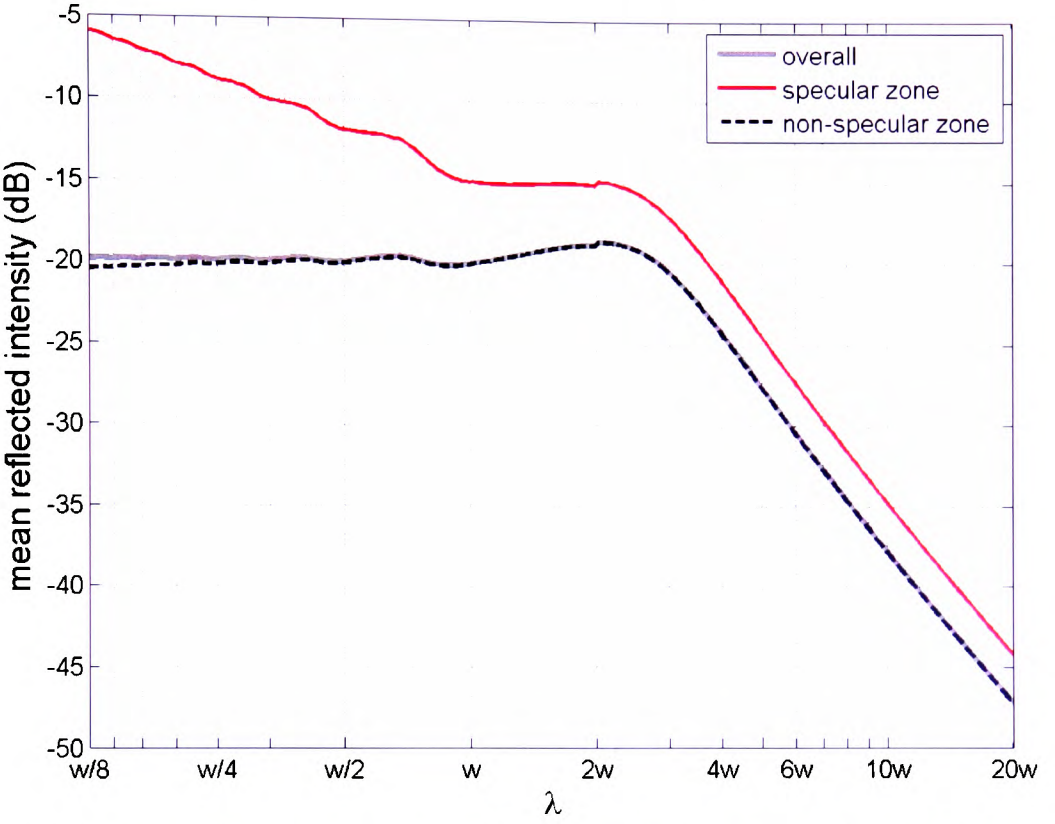

Figure 8-2. BEM predicted mean reflected intensity (dB) in all the angles of reflection, in the specular and non-specular reflection zone from a flat plate of width w normalised to the incident pressure at the receiver that is normal to the surface.

The maximum effect of the edge diffraction is displayed when half a wavelength fits on the width of the sample ($\lambda/2 = w$) (Figure 8-3b). This is the wavelength where the most positive interference is achieved as the largest path difference $\lambda/4$ is achieved at oblique angles between the wave reflected from the centre and the edge of the sample.

As the wavelength becomes smaller the edge diffraction diminishes resulting in the first case of negative interference occurring when $\lambda = w$ at oblique angles of reflection. For small wavelengths ($\lambda < w$) the edge effect weakens as the interference pattern presents more points of negative interaction resulting in the scattered pressure distribution to become less uniform and the specular energy to increase (Figure 8-3a).

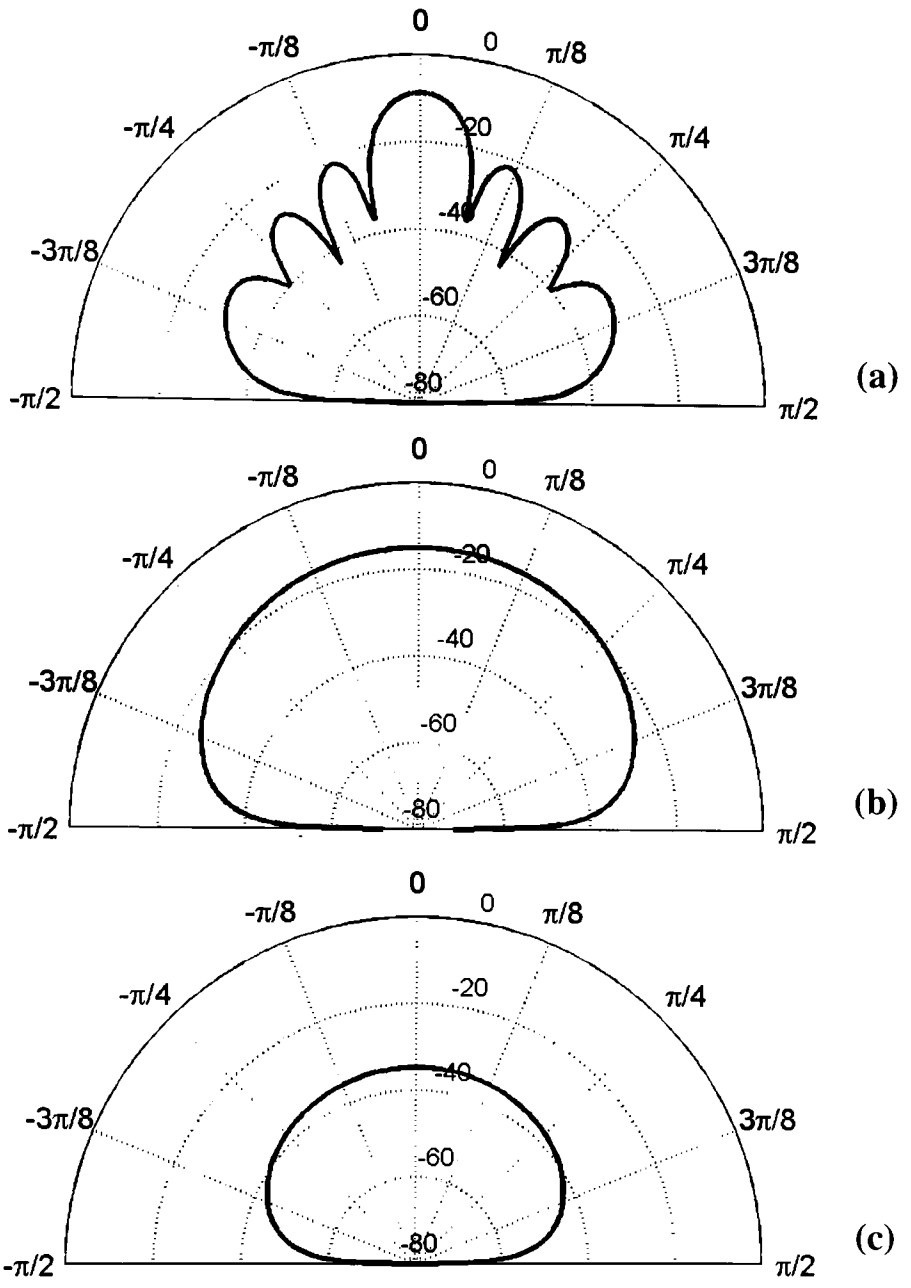

Figure 8-3. BEM prediction of the normal incidence scattered level distribution (dB) from a flat plate of width w at $\lambda = w/4$ (a), $\lambda = 2w$ (b) and $\lambda = 10w$ (c).

The ratio of the sound reflected in the zones of interest depicts the deterioration of the performance of the plate (see Figure 8-4). It shows that while for large wavelengths the difference between the scattered intensity in non-specular and the specular zone is -3dB it deteriorates when the sample becomes comparable to the width of the surface ($\lambda < 4w$).

In order to use the rigid surface in an AGD a bandwidth where it performs similarly to an omni-directional source has to be established. The low wavelength limit would be in the region where $\lambda = w$ as that is the edge diffraction weakens. The value of $\lambda_{min} = 0.83w$ can be used as it is the wavelength the ratio of the non-specular over specular reflected energy drops by 3dB compared to the maximum value (Figure 8-5). The high wavelength limit is stated by the reflected energy. The value of $\lambda_{max} = 3w$ is used as it is the wavelength that the overall reflected energy reaches the value of the energy reflected from the surface at high frequencies.

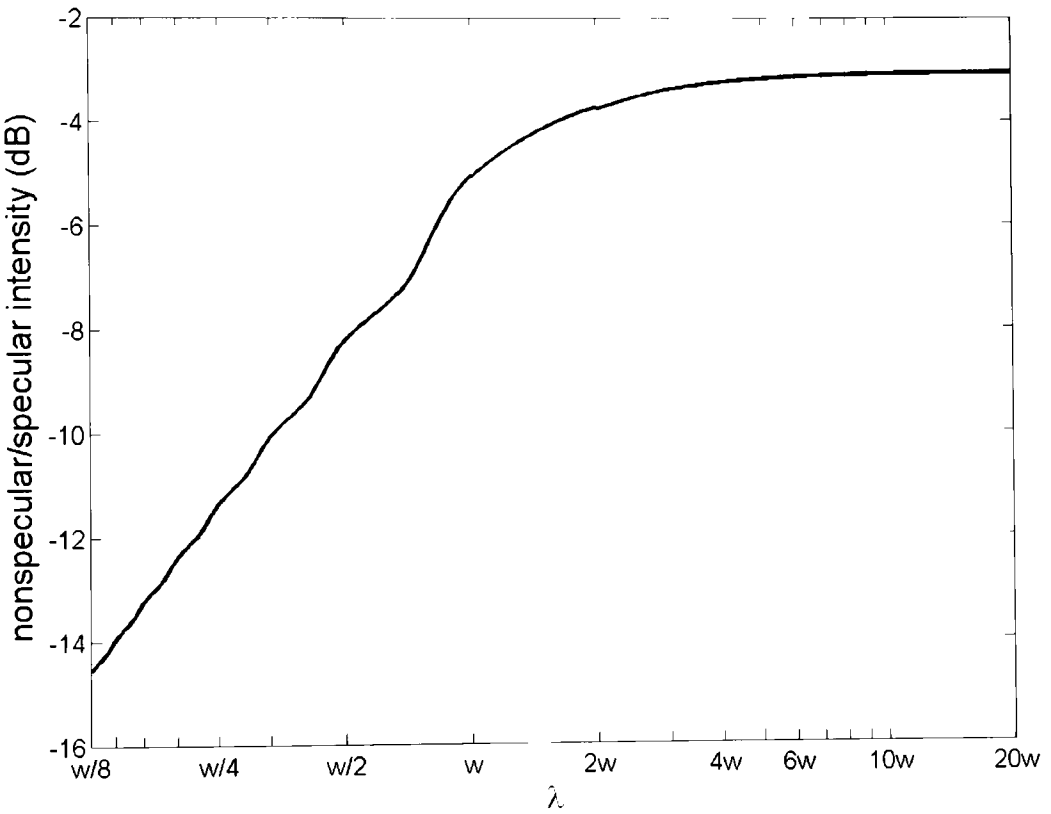

Figure 8-4. BEM predicted ratio of the mean reflected intensity in the non-specular over the specular zone of a plate of width w.

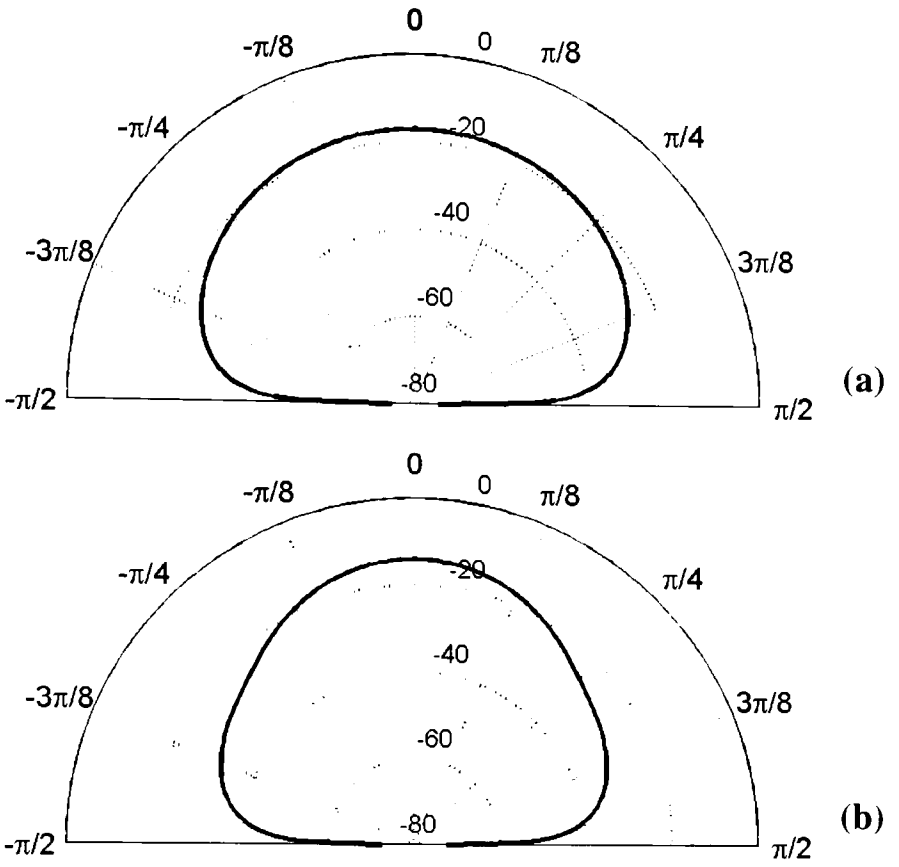

Figure 8-5. BEM prediction of the normal incidence scattered level distribution (dB) from a flat plate of width w at the wavelength limits of applicability for AGDs $\lambda_{max} = 3w$ (a) and $\lambda_{min} = 0.83w$ (b).

8.2. Ideally Absorbing elements

In a AGD the absorbing elements of the diffuser need to display perfect absorption ($\beta_n = 1$) at all frequencies. Their performance cannot be simulated for a single absorbing element in the way that was done in the previous Section for the reflective one. If a perfectly absorbing surface was realised with non-absorbing sides (Figure 8-6) the BEM wouldn't give realistic prediction of how it would perform when incorporated in a surface. The rigid sides and back would result in more energy being reflected from the sample especially at low frequencies.

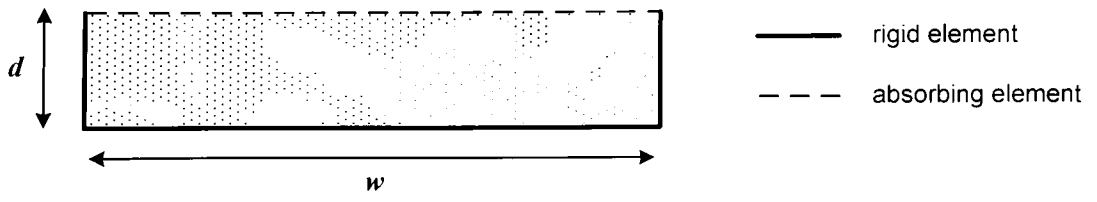

Figure 8-6. BEM realisation of an absorbing surface of width w, normalised surface admittance of $\beta_n = 1$ and rigid sides.

Despite the inability to investigate their performance the absorbing elements are going to be considered to display normalised surface admittance of 1 at normal incidence for all frequencies. This of course is unattainable for any type of absorber but investigation in this idealised form allows for the performance of AGDs to be conducted as a function of the ratio of the wavelength with the dimensions of the elements of the surface.

8.3. Distribution of admittance on a surface

Having examined the building blocks that compose AGDs the scattered response from surfaces with distributed absorbing and reflected elements is examined. Since the absorbing elements are considered ideally absorbing, their normalised surface admittance will be $\beta_n = 1$ for all frequencies.

8.3.1. Pseudorandomly arranged

The pseudorandomly arranged surface of Figure 8-7 is discussed first. It is generated using a single period of MLS ($k = 5$) of length $N = 31$. Each 1 and 0 in the binary sequence correspond to a reflecting and an absorbing element respectively of width w. As a result the sample is $31w$ wide and consists of reflecting element ranging from w to $5w$ wide. The reflecting elements make up 51.6% of the surface.

The simulation was carried out for element widths $w = 25mm$, with the source and receivers placed $20m$ and $10m$ respectively away from the sample. The scattering estimated from this geometry refers to the far-field response of the sample.

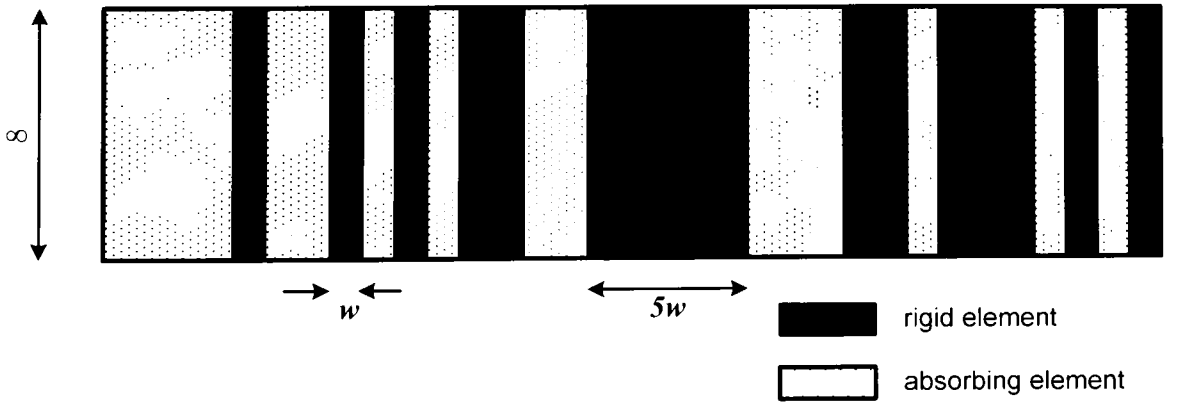

Figure 8-7. Surface with reflecting elements arranged pseudorandomly using a MLS ($k = 5$).

The scattered intensity distribution from this sample can be seen in Figure 8-8 along with that scattered from a rigid surface of the same size. The intensity has been normalised to the

specular reflection lobe of the rigid surface. At low frequencies the wavelength is much larger than any of the reflecting elements and the behaviour of the sample is that of an imperfect absorber (Figure 8-8a) as it is dictated by the evanescent waves on the surface that cause for an equalisation of pressure across front face of device. At higher frequencies when the wavelength is comparable to the largest element the surface fails to provide substantial diffusion (Figure 8-8b). The side lobe energy is increased by up to 15dB and displays some uniformity but it is still rather low to be important. The specular lobe, although attenuated by 6dB due to the absorption of the surface, still dominates the scattered pressure distribution as it is more than 20dB higher than the side lobes. When the wavelength becomes comparable to the smallest elements the performance does not improve (Figure 8-8c).

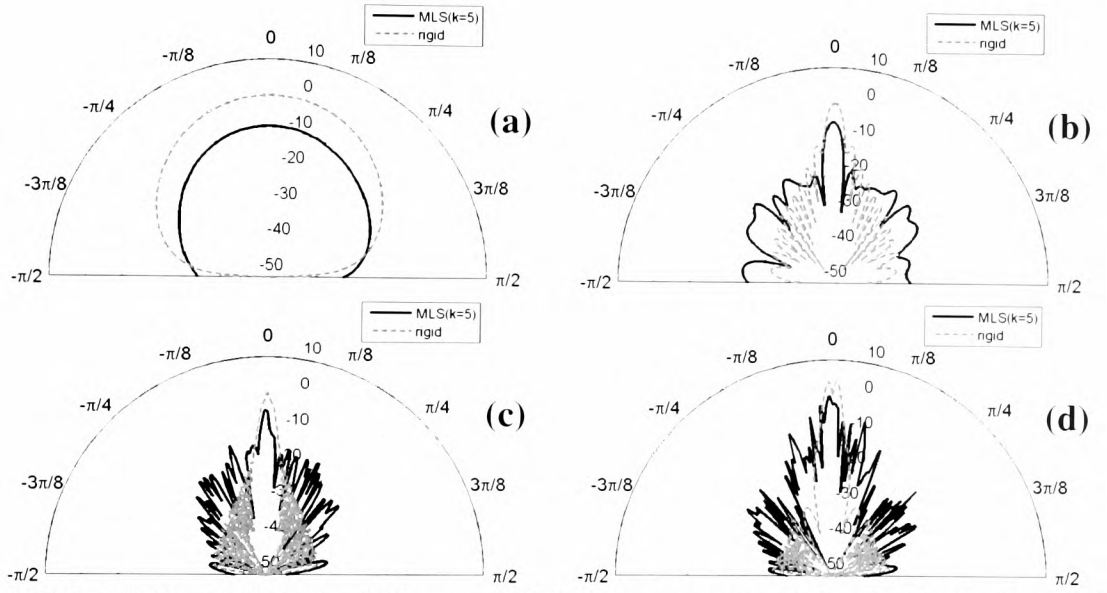

Figure 8-8. BEM prediction of the normal incidence scattered level distribution (dB), normalised to the specular lobe of a rigid surface, of a surface with reflecting elements arranged pseudorandomly with MLS ($k = 5$) at $\lambda = 31w$ (a), $\lambda = 3w$ (b), $\lambda = w$ (c) and $\lambda = w/2$ (d).

The overall behaviour of the surface as predicted using BEM is displayed in Figure 8-9 in terms of the normalised diffusion coefficient of the surface d_n. In the same figure an approximate absorption coefficient a_r is presented which is calculated from the fraction of reflected energy from the AGD E_{AGD} and a rigid surface E_{rs} of the same size:

$$a_r = 1 - \frac{E_{AGD}}{E_{rs}} \qquad 8.1$$

The diffusion coefficient that is achieved for this sequence is not substantial as it fails to exceed even 0.15. There appears to be a jump in diffusion when the wavelength fits onto the whole surface ($\lambda \cong 31w$) but even that is very low.

From the reflected energy point of view, at high wavelengths ($\lambda > 40w$) the diffuser acts as an average absorber since the reflecting elements appear too small. The absorption decreases as the wavelength becomes smaller and becomes 50% when half a wavelength becomes comparable to the width of the smaller reflecting element ($\lambda \cong 2w$). That is the frequency that the smallest reflecting element reaches its maximum reflected energy (see Figure 8-2). At this frequency all the elements act individually due to reduced mutual interaction.

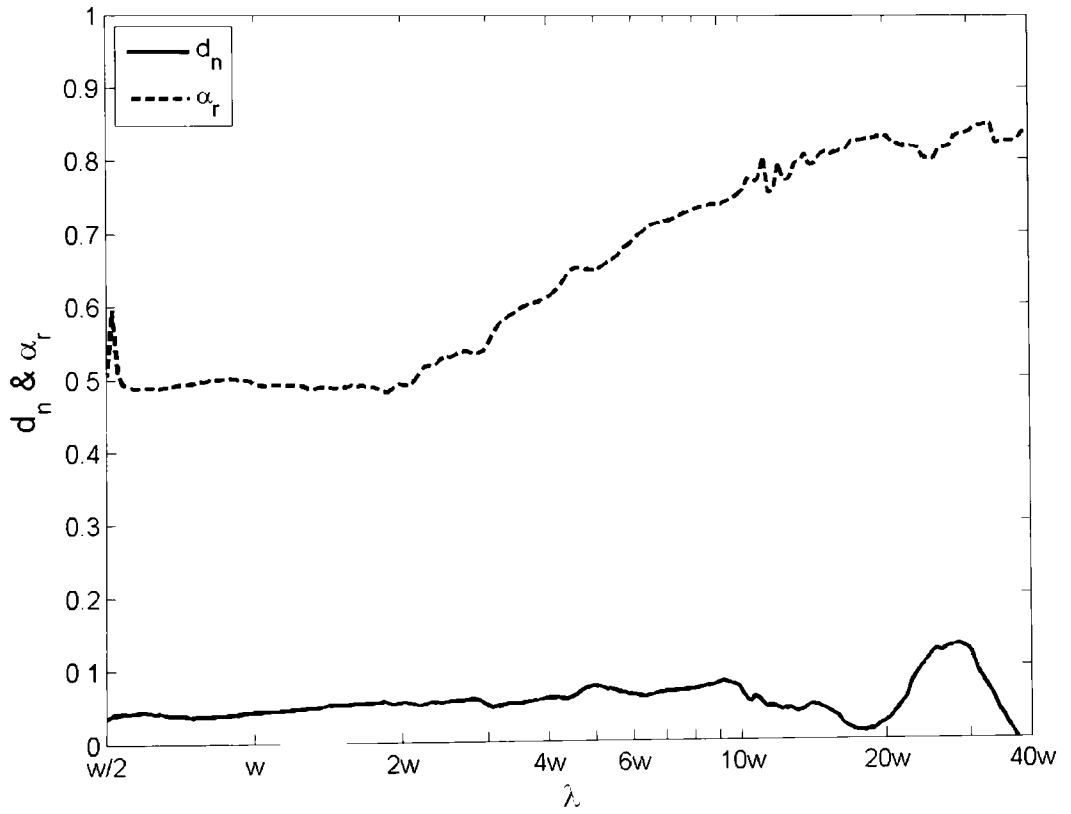

Figure 8-9. BEM prediction of the normalised diffusion coefficient (d_n) and absorption coefficient (a_r) from a suface with reflecting elements arranged pseudorandomly using MLS ($k = 5$).

When the wavelength is comparable with the smallest reflecting elements of the surface, it is very small compared with the largest one ($\lambda = 2w_{min} = 0.4w_{max}$). This wavelength is smaller than the low wavelength limit of omni-directionality of the largest element which is $0.83w_{max}$ that was discussed in the previous Section.

The difference of performance between the reflecting elements of different sizes poses a significant defect of the AGDs. In order to achieve substantial reflected energy the width of the smaller element must be comparable to the wavelength which results in the largest element reflecting specularly.

This suggests that a sequence that would consists of a small number of single 1s and not long series of 1s could be a better candidate. Such a sequence is the lower order MLS ($k = 3$) [1, 1, 1, 0, 0, 1] which contains a single 1 and the largest series of 1s is 3. In order to have a surface of similar width 4 periods of the sequence are considered (see Figure 8-10).

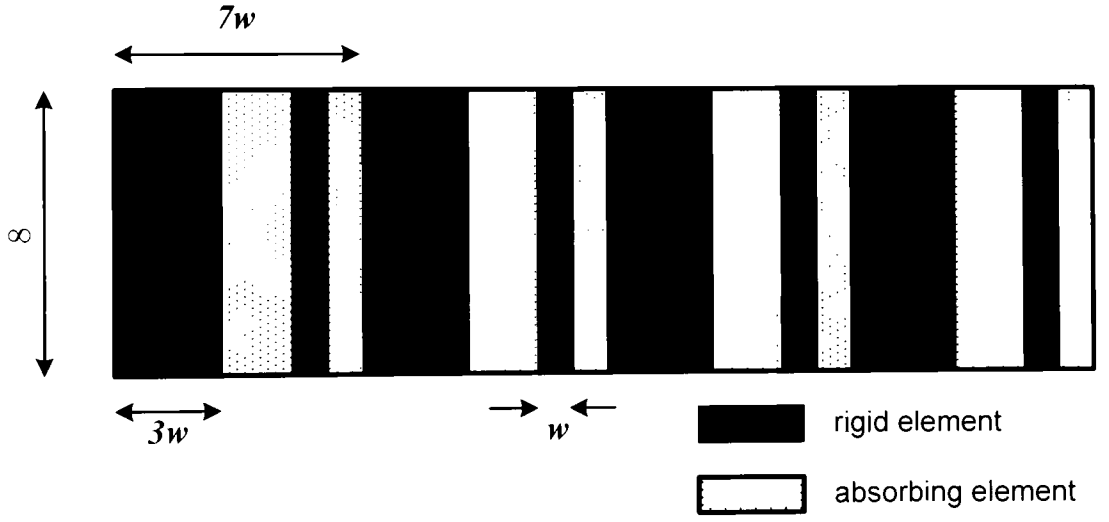

Figure 8-10. Surface with reflecting elements arranged pseudorandomly using 4 periods of MLS ($k = 3$).

The periodic repetition results in periodicity lobes appearing in scattered level distribution. The periodicity lobes appear at oblique angles when the wavelength becomes similar to the width of a single period of the diffuser ($\lambda \cong 7w$). Figure 8-11a displays the scattered response for $\lambda = 7w$ and the periodicity lobes appear at $\pm {}^{3\pi}/_{8}$. As the frequency increases the number of periodicity lobes increase and become more narrow and closer together. In Figure 8-11b all the sharp side lobes are periodicity lobes ($\lambda = 2w$).

This phenomenon at first glance seems to compromise the uniformity of the scattered pressure distribution as has been discussed in Section 3.3. In the case of absorption grating surface though, that fail to scatter energy outside of the specular reflection zone, periodicity lobes are not necessarily a disadvantage. The periodicity lobes that are introduced are of the same height due to the use of the MLS[6] (except the lobe at the specular reflection direction). The existence of these lobes translates to sound scattered away from the specular zone. At $\lambda = 3w$ of instance, the side lobes reach levels of -6dB compared to the specular lobe in comparison to the MLS ($k = 5$) that that didn't exceed -15dB at that frequency.

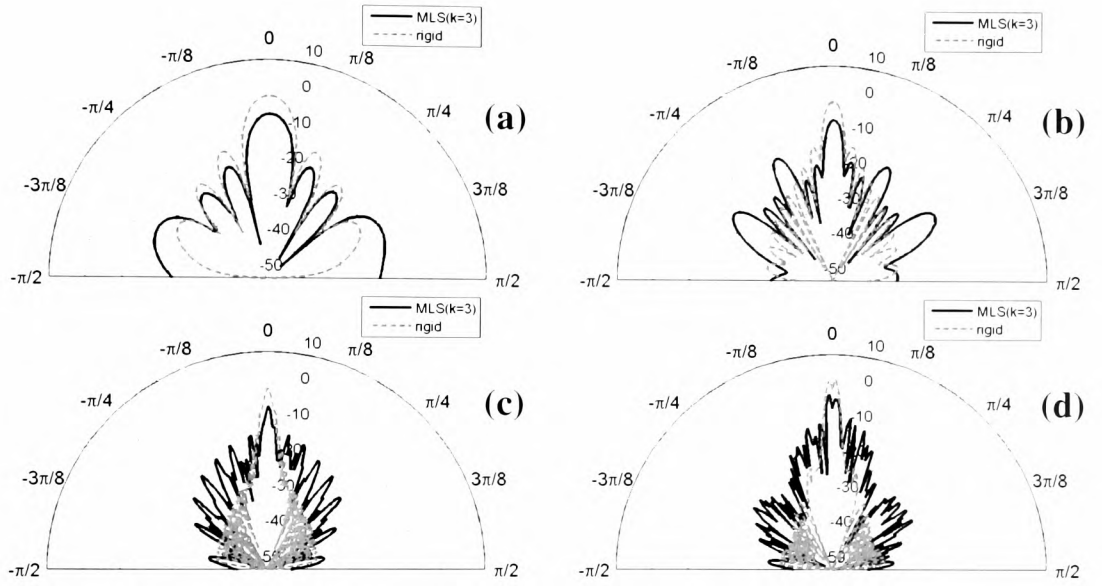

Figure 8-11. BEM prediction of the normal incidence scattered level distribution (dB), normalised to the specular lobe of a rigid surface, of a surface with reflecting elements arranged pseudorandomly using 4 periods of MLS ($k = 3$) at $\lambda = 7w$ (a), $\lambda = 3w$ (b), $\lambda = w$ (c) and $\lambda = w/2$ (d).

Its diffusion coefficient displayed in Figure 8-12 is not substantial though. An interesting characteristic is that d_n is stable for wavelengths smaller that a period of the structure ($\lambda < 7w$) and 0 for wavelength larger than that, a behaviour similar to the one observed in Phase Grating Diffusers (see Section 3.5). Also the absorption a_r shows a rapid decline at the same critical wavelength. It is the introduction of the first periodicity lobe that is the critical factor in this case (Figure 8-11a).

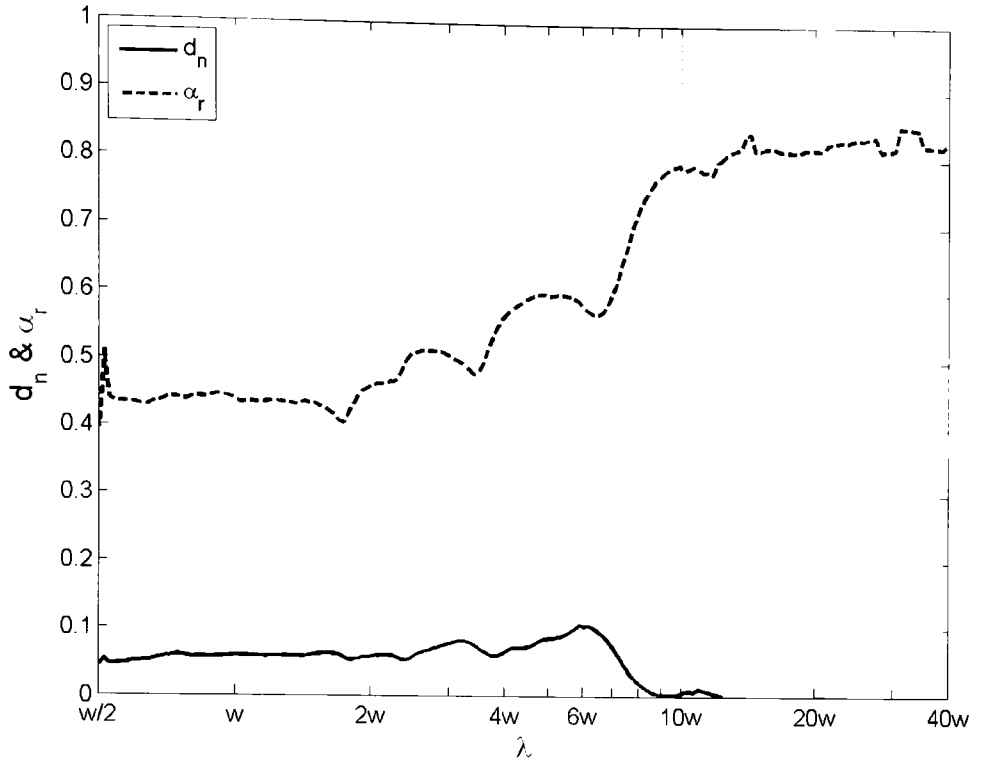

Figure 8-12. BEM prediction of the normalised diffusion coefficient (d_n) and absorption coefficient (a_r) from a suface with reflecting elements arranged pseudorandomly using 4 periods of MLS ($k = 3$).

8.3.2. Periodic

Given that periodicity improved certain aspects, this raises the question whether a purely periodic structure would perform better. For this reason the structure of Figure 8-13 is tested. It consists of reflecting elements of a fixed width $W = 4w$. The diffusion characteristics of the surface are centred again on the characteristic wavelength $\lambda = 8w = 2W$ which is equal

The diffusion coefficient from the periodic structure can be seen in Figure 8-14. The diffusion coefficient reaches its maximum value while the absorption reaches its minimum value in the region of $\lambda = 7w$. In this region two effects coincide, periodicity lobes appear for oblique angles of reflection while the edge diffraction of the reflective elements reaches it maximum point as their width is equal to half a wavelength.

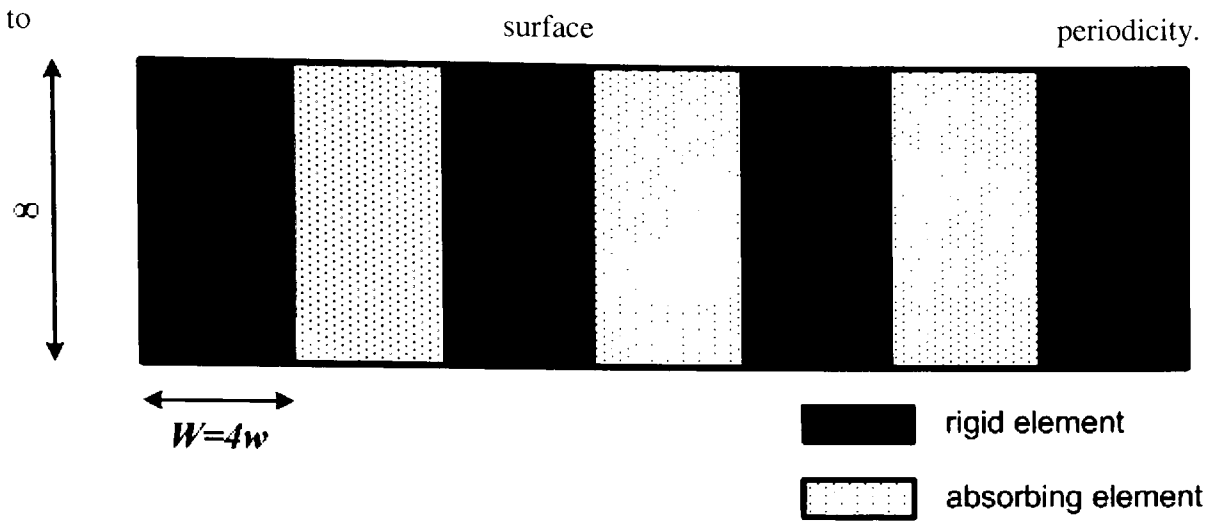

Figure 8-13. Suface with periodicly positioned reglective elements (of width W) positioned every $2W$.

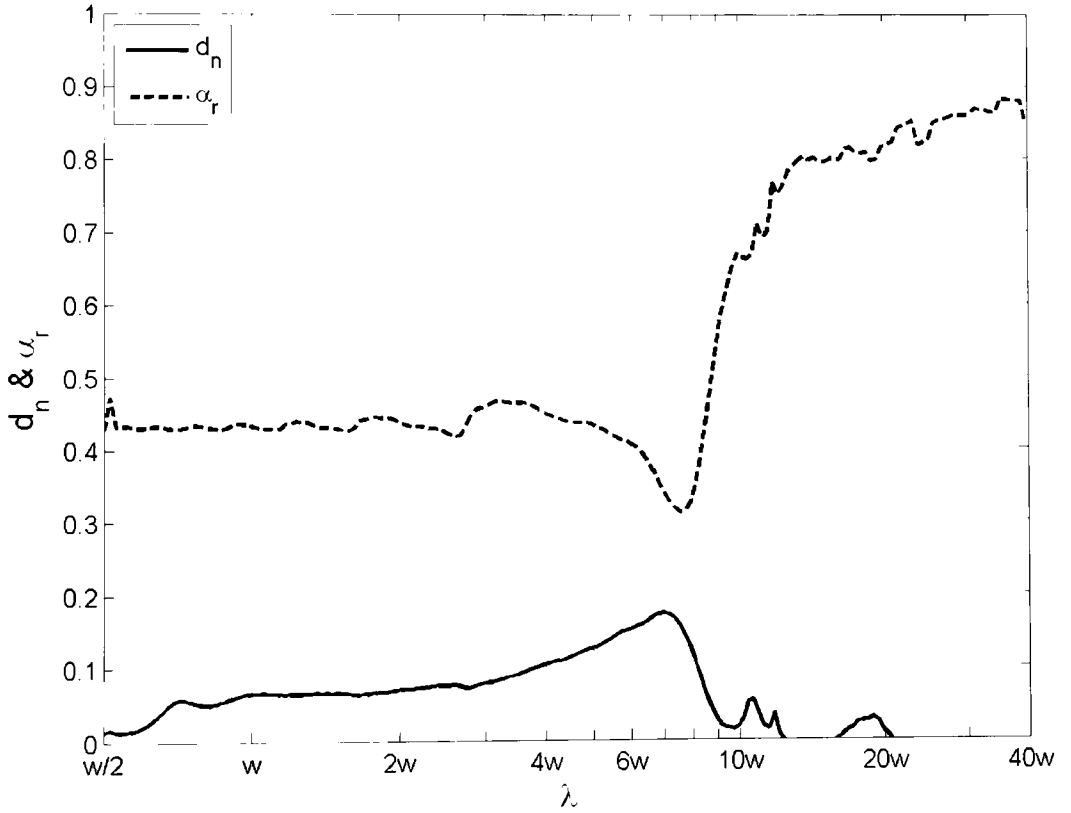

Figure 8-14. BEM prediction of the normalised diffusion coefficient (d_n) and absorption coefficient (a_r) from a suface with periodically positioned reflective elements (width $W = 4w$) positioned every $2W$.

As can be seen in Figure 8-15 in this wavelength the wide periodicity lobes introduced at $\pm\pi/8$ are displaying level just 6dB lower than the specular lobe which translates to increased diffusion with minimum absorption.

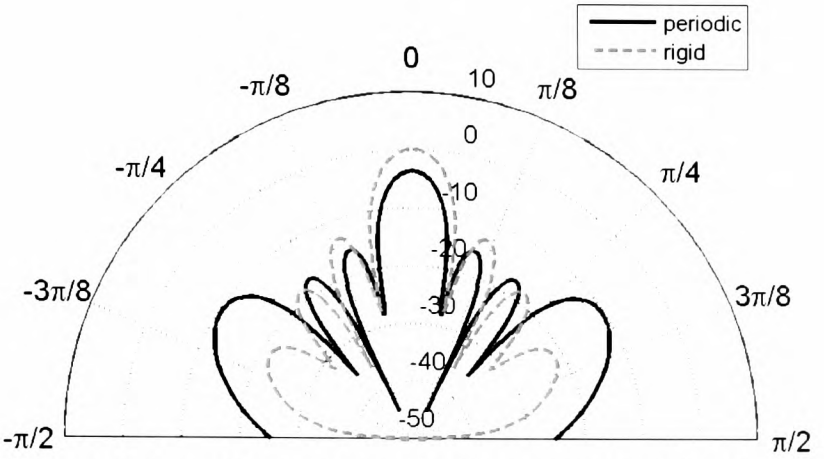

Figure 8-15. BEM prediction of the normal incidence scattered level distribution (dB), normalised to the specular lobe of a rigid surface, of a surface with periodically positioned reflective elements (width $W = 4w$) positioned every $2W$ at $\lambda = 7w$.

The performance, although improved in a small bandwidth around 7w, is still low. Furthermore, it deteriorates at higher frequencies due to the inherent polar response generated by the periodic repetition of the reflecting elements. This is depicted in Figure 8-16 were the pattern of the scattered pressure distribution from the periodic surface is compared to that from one of its reflecting elements. The pattern of each element results in uneven periodicity lobes.

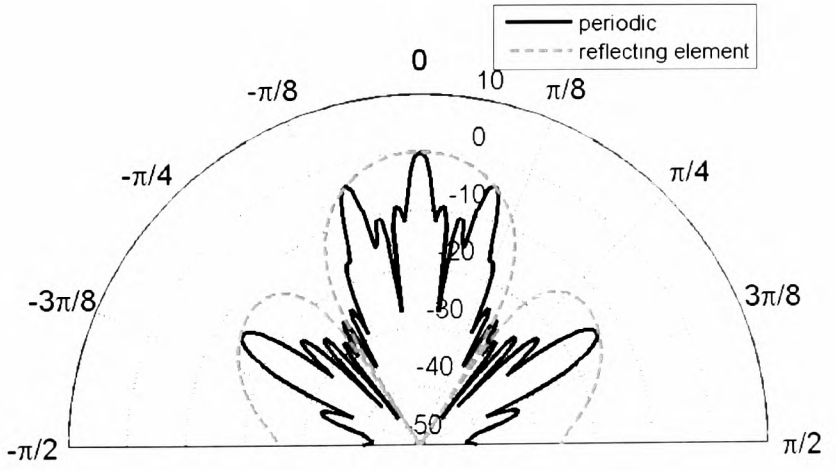

Figure 8-16. BEM prediction of the pattern of the normal incidence scattered level distribution (dB) of a suface with periodically positioned reflective elements (width $W = 4w$) positioned every $2W$ at $\lambda = 2w$ in comparison with a single reflective element.

8.4. Discussion

A number of different arrangements of AGDs have been presented in this Chapter. An outline of the behaviour of each is presented in the Tables below.

The periodic pattern has achieved some diffusion around $\lambda \cong 2W$ in a bandwidth smaller than one octave-band due to the coexistence of periodicity induced lobes and maximum edge diffraction in that frequency. The surface in this bandwidth is not very absorbing (less than 50%) which is desirable. Even at the peak of diffusion, the scattering produced is weak. Consequently, the periodic device has limited scattering performance in terms of both the bandwidth and diffusion produced.

The MLS (k = 5) arrangement produced very weak diffusion for frequencies were the wavelength was smaller than the width of the surface ($\lambda < 31w$) and it remained very absorbing for wavelength larger than twice the width of the smaller reflecting element ($\lambda > 2w$). The structure did not manage to achieve substantial diffusion as the reflective elements displayed a larger variation of widths resulting in them displaying different bandwidths of strong edge diffraction that resulted in the surface performing as an average absorber.

Finally, a surface generated from 4 periods of MLS (k = 3) was tested. It displayed a peak in diffusion when the first periodicity lobes appears ($\lambda = 7w$) which is close to the frequency of maximum edge diffraction from the larger reflective elements. The fact that most of the rigid area of the surface is included in the larger elements resulted in the absorbing properties of this configuration not being too high resulting in less than 60% absorption for wavelengths smaller that the width of a period of MLS (k = 3) ($\lambda < 7w$).

In all the cases discussed peaks of diffusion are achieved at the frequencies where grating lobe were introduced to the scattered pressure distribution. The absorption coefficient at any given frequency is dictated by the percentage of the reflective elements whose width is smaller than half the wavelength. Furthermore, the peaks of the diffusion coefficient don't reach substantial values as the side lobes achieved have much lower energy compared to the specular reflection lobe. The specular lobe is attenuated only by absorption so its level can only drop by 3dB for a 50% absorbing surface.

8.5. Summary

In this Chapter ideal AGDs were investigated. The behaviour of the elements they consist of was presented and their diffusion and absorption properties were discussed. Their reflecting

elements were found to deviate from the require behaviour of omni-directional scatterers as the produced edge diffraction is weak and limited only to an octave. A variety of different structures was tested and their performance was explained. Their most dominant characteristic is that they fail to produce side lobes with comparable energy to the specular lobe.

It should be re-stated that the devices discussed in this Chapter are idealised. They are considered to contain perfectly absorbing elements at all frequencies, than cannot be achieved in reality. So although they represent perfectly the theoretical concept of AGDs, presented in the previous Chapter, they fail to justify the term "diffuser".

From the research presented in this Chapter it can be unequivocally concluded that the theoretical concept of AGD is flawed. In the following Chapter improvements to the performance of these devices is going to be attempted by deviating from the ideal building components to realisable ones with reactive characteristics.

Wavelength	**Behaviour** (periodic)
$\lambda >> W$ **low frequency**	• Little power reflective from solid elements because they are too small compared to wavelength • Evanescent waves result in equalisation of pressure across front face of device. • The device behaves as though it is a homogeneous device with an admittance given by the average admittance across the whole device ($a_r = 93\%$ for average admittance $\beta_{av} = 0.57$)
$\lambda/2 = W$	• Strongest edge diffraction and consequently reflection from the reflective elements resulting in scattering into grazing angles • First grating lobe appears because of periodicity at grazing angles • Maximum diffusion due to the two wide grating lobes at grazing angles • Minimum absorption due to periodicity lobes and strong edge diffraction
$\lambda << W$ **high frequency**	• Elements spacing large compared to wavelength, reflecting and absorbing elements act independently • Weak edge diffraction and consequently specular reflection from the reflective elements resulting in little energy in the side lobes • Absorption stabilises to a minimum value given by the percentage of absorbing elements ($a_r = 43\%$ for average admittance $\beta_{av} = 0.57$) • Multiple grating lobes occur but oblique lobes have low power because edge diffraction is weak and so energy is concentrated in specular reflection direction

Table 1. Behaviour of a suface with periodically positioned reflective elements (width $W = 4w$) positioned every $2W$.

Wavelength	**Behaviour** (4 periods of MLS (k=3))
$\lambda >> 28w$ **low frequency**	• Little power reflective from rigid elements because they are too small compared to wavelength • Evanescent waves result in equalisation of pressure across front face of device. • The device behaves as though it is a homogeneous device with an admittance given by the average admittance across the whole device (a_r = 93% for average admittance β_{av} = 0.57)
$\lambda = 7w$	• Strong edge diffraction from the largest reflecting elements of the surface (maximum edge diffraction at $\lambda = 8w$) • The small rigid elements are too small to reflect substantial energy • First grating lobes at grazing angles as the wavelength fits on one period of the diffuser resulting in maximum diffusion • Drop in absorption due to periodicity lobes and strong edge diffraction from the large elements
$\lambda = 2w$	• Maximum edge diffraction from the small elements but specular reflection from the large ones results in weak diffusion • 6 narrow grating lobes of 10dB lower than the specular • Absorption given by the percentage of absorbing elements (a_r = 43% for average admittance β_{av} = 0.57)
$\lambda << w$ **high frequency**	• Elements spacing large compared to wavelength, reflecting and absorbing elements act independently • Multiple grating lobes seen but oblique lobes have low power because edge diffraction is weak and so energy is concentrated in specular reflection direction • Absorption stabilises to a minimum value given by the percentage of absorbing elements (a_r = 43% for average admittance β_{av} = 0.57)

Table II. Behaviour of a surface with reflecting elements of width w arranged pseudorandomly using 4 periods of MLS (k = 3).

Wavelength	Behaviour (MLS (k=5))
$\lambda >> 31w$ **low frequency**	• Little power reflective from rigid elements because they are too small compared to wavelength • Evanescent waves result in equalisation of pressure across front face of device. • The device behaves as though it is a homogeneous device with an admittance given by the average admittance across the whole device (a_r = 90% for average admittance β_{av} = 0.52)
$\lambda = 31w$	• Peak in diffusion as the wavelength becomes comparable to the width of the sample • Little power reflective from rigid elements as they are still too small compared to wavelength
$\lambda = 10w$	• Strong edge diffraction from the largest reflecting element of the surface (maximum edge diffraction at λ = 10w) resulting in slight rise in diffusion • The small ones are too small to reflect substantial energy • Absorption is high as only the large element reflects substantial energy
$\lambda = 2w$	• Maximum edge diffraction from the smallest elements but specular reflection from the largest one results in weak diffusion • Uniform increased side lobe energy compared to the reference plate (up to 15dB) but 25dB lower than the specular lobe • Absorption given by the percentage of absorbing elements (a_r = 48% for average admittance β_{av} = 0.52)
$\lambda << w$ **high frequency**	• Elements spacing large compared to wavelength, reflecting and absorbing elements act independently • Multiple grating lobes seen but oblique lobes have low power because edge diffraction is weak and so energy is concentrated in specular reflection direction • Absorption stabilises to the minimum value given by the percentage of absorbing elements (a_r = 43%)

Table III. Behaviour of a surface with reflecting elements of width w arranged pseudorandomly using the MLS (k = 5).

Chapter 9. Improvements to Absorption Grating Diffusers

The previous Chapter established that Absorption Grating Diffusers (AGDs) in their original form fail to achieve substantial diffusion. In this Chapter, ways to improve their performance are presented. First, reactive elements are used to increase the non-specular reflected energy from the reflecting elements. Then imperfect absorbing elements are used to allow for cancellation of the specular reflection to occur.

9.1. Reactive elements in the place of the reflective

The scattered field from a reflective element displays low energy in the non-specular zone when the wavelength becomes smaller than its width (see Section 8.1). In this Section an attempt to improve the performance at smaller wavelengths is attempted.

9.1.1. Helmholtz Resonators

A type of structure that scatters the incident sound is Helmholtz Resonators[69]. For this purpose the existence of a Helmholtz Resonator is going to be considered in the place of a reflector. The reasoning for introducing them in the AGDs is that ideal resonators will perform like a reflective structure away from resonance and as a scatterer at frequencies around their resonant frequency.

The resonator is considered ideal with no losses of energy occurring anywhere but the neck of the structure. As discussed in Section 6.4.2 such a structure would display negligible losses. The investigation is going to be conducted once more in a 2-D BEM as the geometry of a 3-D one would become computationally expensive.

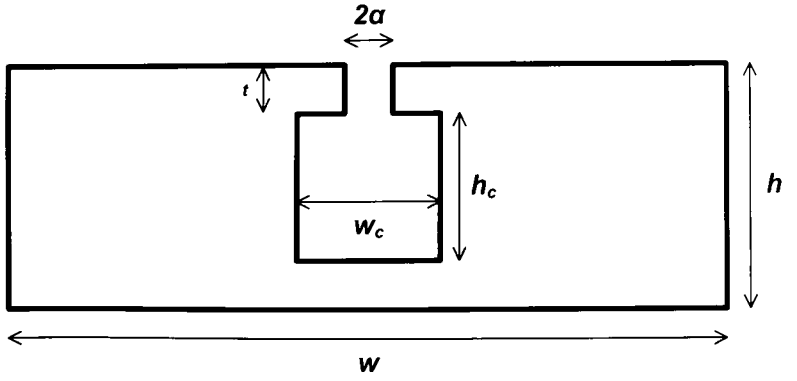

Figure 9-1. A Helmholtz Resonator formed in a 2-D surface.

The structure of Figure 9-1 is considered where the third dimension is considered infinite. The resonant frequency of the 2-D Helmholtz Resonator is:

$$f_r = \frac{c}{2\pi}\sqrt{\frac{a}{t' \cdot S_c}} \qquad 9.1$$

where c is the speed of sound in air and t' is the length of the neck including the end correction.

Since the width of the element can be considered as the low wavelength limit of the non-specular behaviour of a reflective element ($f < c/w$), the resonance should occur at a wavelength lower than the limit ($f_r < c/w$).

The sample tested by the Boundary Element Modelling (BEM) can be seen in Figure 9-2. The outer geometry of the structure is not a rectangle as presented in Figure 9-1 in order to avoid errors in the numerical simulation. BEM only models surfaces and consequently solid parts of the diffuser can appear like cavities which resonate and lead to problems of non-unique solutions. Changing the geometry alters the pressure distribution in the domain behind the sample but does not affect the scattered response in front of the diffuser which is what is important for this study.

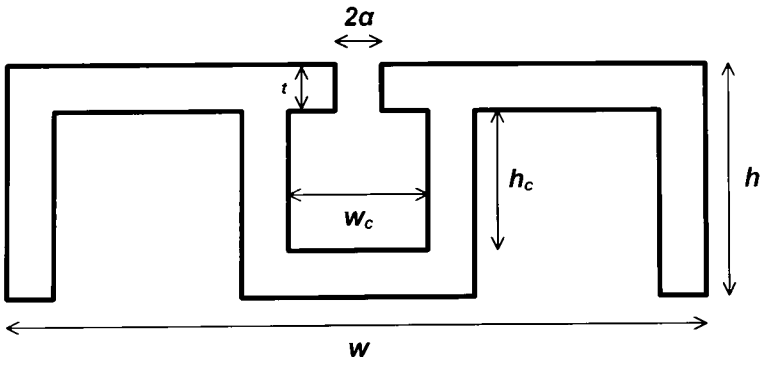

Figure 9-2. 2-D Helmholtz Resonators geometry used in BEM.

The sample tested is $w = 40cm$ wide and $h = 5cm$ deep. The Helmholtz Resonator is placed in the middle of the surface and it has hole-diameter $2a = 1cm$ and hole-depth $t = 1cm$ while the cavity is $S_c = w_c \times h_c = 2\times 3cm^2 = 6cm^2$. Using the end correction of eq. 6.25 the resonant

frequency is expected at $1.27kHz$. In terms of wavelength this corresponds to approximately $2w/3$ which is slightly lower than the width of the sample.

The source is positioned $20m$ from the sample facing the surface normally while the receivers are placed in a $5m$ in radius arch with 1° increment. So the only receiver that is in the specular reflection zone is the receiver normal to surface.

The ratio of non-specular over specular reflected level from this sample can be seen in Figure 9-3 along with that from a plane surface of the same dimensions. Since the point of this investigation is to establish whether these structures can be used as reflective elements the wavelength is presented as a function of the width of the sample w. The Helmholtz Resonator performs like a plane surface at wavelengths away from the resonance while it displays a peak in the level reflected in non-specular angles around the resonant wavelength which is as expected at $2w/3$.

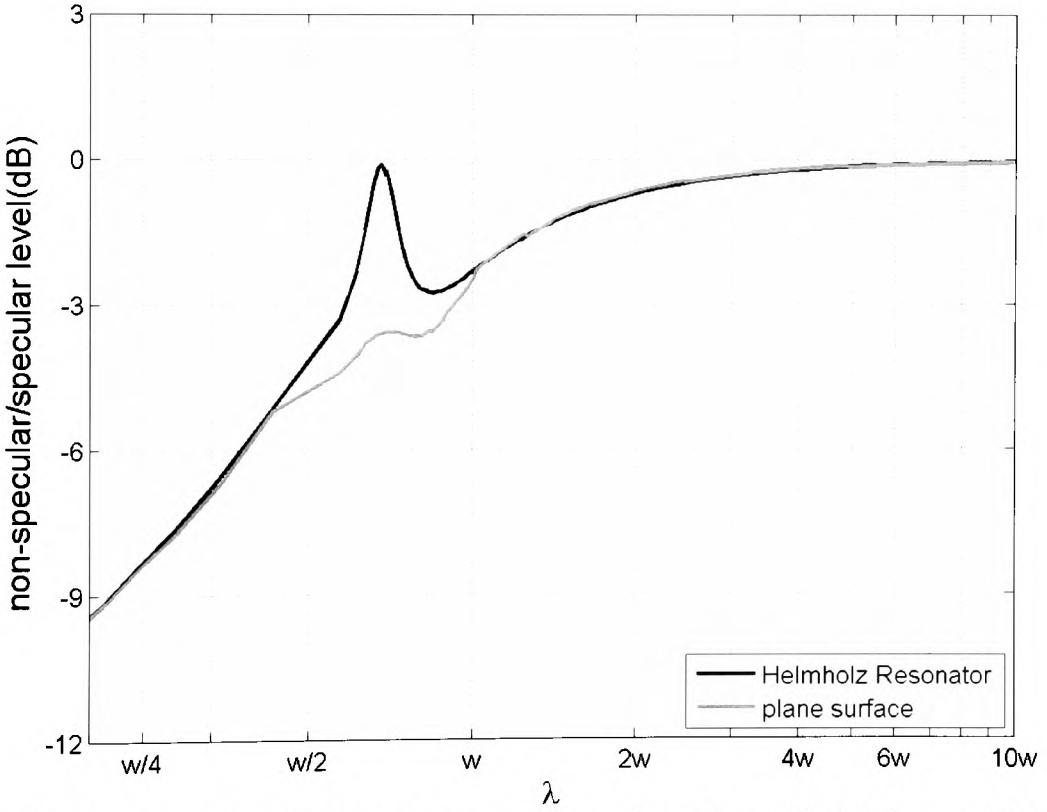

Figure 9-3. BEM predicted non-specular over specular reflected level from a Helmholtz Resonator with a resonant frequecy at $\lambda_r = 2w/3$ compared to a plane surface of the same width w.

By arranging the resonance to occur at a slightly lower wavelength from the width of the surface the bandwidth of non-specular response is extended. If the -3dB level of the non-

specular over specular energy is used as the limit then it has extended from $0.83w$ as discussed in Section 8.1 to $0.58w$. The scattered pressure distribution at characteristic wavelengths is plotted in Figure 9-4. The most noteworthy is Figure 9-4(b) which shows the resonance where the distribution is much more uniform for the Helmholtz Resonator compared to the plane surface.

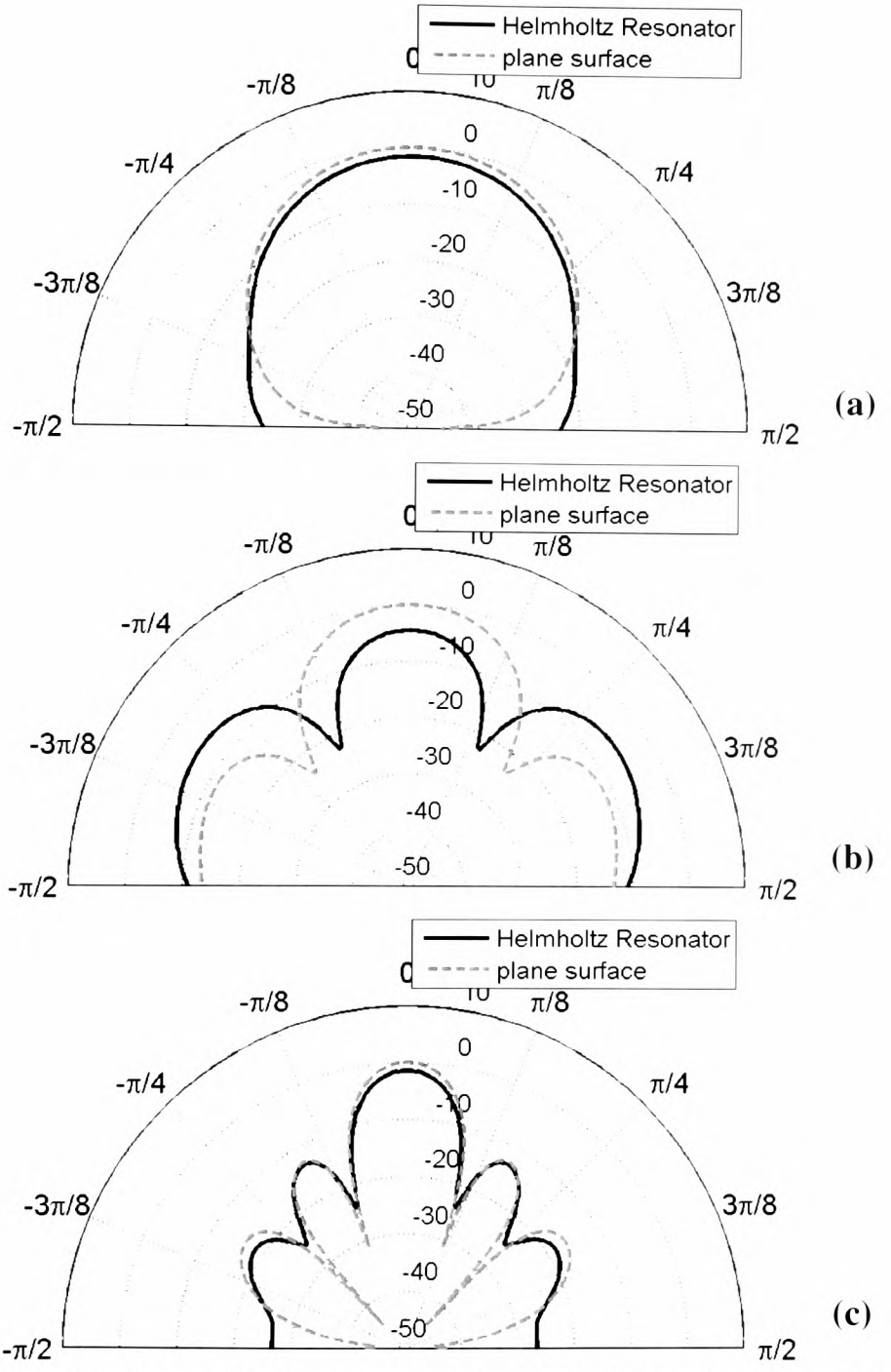

Figure 9-4. BEM predicted normal incidence scattered pressure distribution from a Helmholtz Resonators with resonant wavelength $2w/3$ compared to a plane surface of the same width w at $\lambda = w/3$ (a), $\lambda = 2w/3$ (b) and $\lambda = w$ (c).

The behaviour of a Helmholtz Resonator is not just of dispersion of energy it also causes change in phase. At resonance the reflection coefficient of a non-absorbing Helmholtz Resonator is -1 resulting in a phase change of π to the reflected wave compared to that from a plane surface. This suggests that using reactive elements on AGDs will add cancelation to their performance.

9.1.2. Discussion

In the case discussed in the previous Chapter of an AGD created using the pseudorandom sequence MLS (k = 3) the reflective elements came in two dimensions w and $3w$. At smaller wavelengths where the smaller elements started reflecting substantial energy the larger ones were reflecting energy specularly. If a reactive element like the Helmholtz Resonator presented above was used in the place of the $3w$ wide element then there would be a bandwidth were all the elements would display significant scattering. Furthermore, if the resonant wavelength was set to ⅔ of the width of the large element then the resonance would occur when half a wavelength would fit onto the smallest elements. So at that frequency all elements would radiate substantial energy in the non-specular reflection zone.

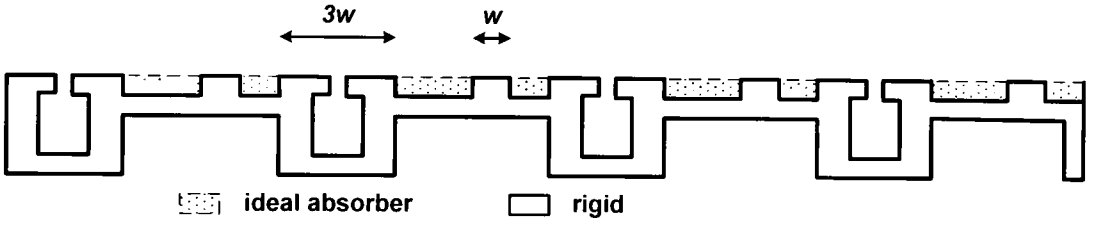

Figure 9-5. 2-D BEM geometry of an Absorption Grating Diffuser generated from 4 periods of MLS (k = 3) implemented using Helmholtz Resonators in the place of the large reflective elements.

Such a device is presented in Figure 9-5 and it is investigated using BEM. The resonant wavelength is set to $\lambda_r = 2w$ and the scattered pressure distribution is estimated. The results are displayed in Figure 9-6. While away from resonance diffusion is unaltered, at resonance the performance is improved. The use of the reactive elements has attenuated the specular lobe by 2.5dB while it has increased the side lobes at $\pm\pi/3$ by about 6dB making them comparable in reflected energy. Their contribution would be deemed even more successful if attenuation of up to 10dB was not present at $\pm\pi/8$. This is an artifact that can be traced back to the scattered field of a single resonator (Figure 9-4b) at resonance that displayed minima in the same angles.

The improvement in the uniformity of the scattered pressure distribution is small as it manages to increase the normalized diffusion coefficient at resonance from 0.06 to 0.15 but it has managed to increase the energy in the sidelobes at $\pm\pi/3$.

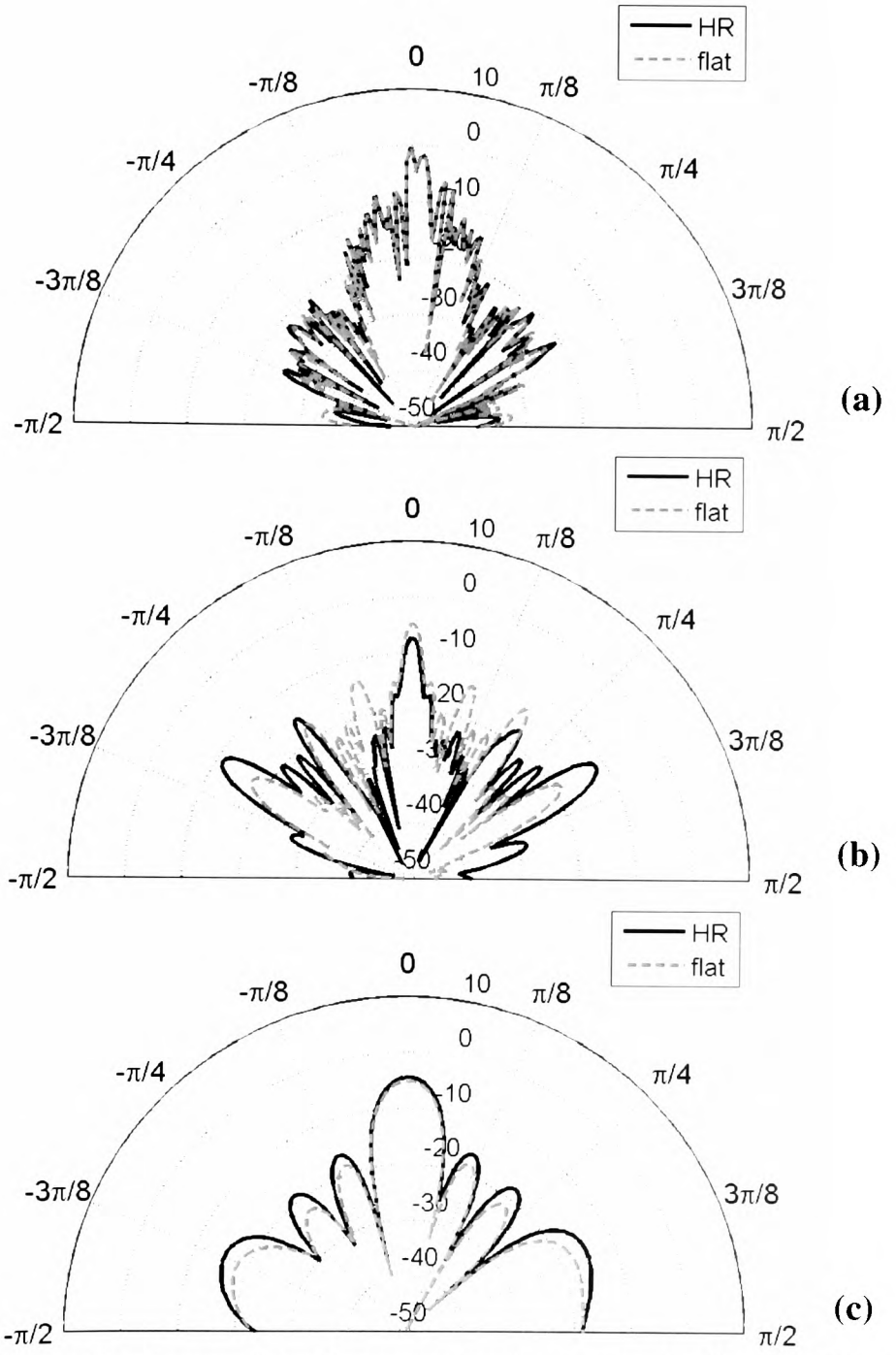

Figure 9-6. BEM predicted normal incidence scattered pressure distribution (dB) from a Absrorption Grating Diffusers implemented using Helmholtz Resonators ($\lambda_r = 2w$) compared to a flat Absorption Grating Diffuser of the same dimensions at $\lambda = w/2$ (a), $\lambda = \lambda_r = 2w$ (b) and $\lambda = 7w$ (c), where w is the width of smallest reflective element.

9.2. Imperfect absorbing elements

Standard absorption grating diffusers do not change the phase of reflections and so are unable to use destructive interference to cancel and attenuate the specular reflection lobe beyond that achieved due to absorption (see Chapter 8). The use of absorbing elements that will allow for some pressure to be reflected back but with some phase change will be studied in this Section.

The simplest way of implementing these absorbing elements is to consider wells packed with porous material. In order to use BEM in the investigation of the performance of these surfaces, the appropriate surface admittance of the absorbing elements needs to be established. Up to this point the absorbing elements discussed have been considered perfectly absorbing at all frequencies so their normalized surface admittance was set to $\beta_n = 1$. Methods of estimating the absorbing characteristics of a layer of porous material have been discussed in Section 6.2 but they have limitations for the bandwidth of application and the characteristics of the material. Furthermore, the characteristics of the material would still need to be measured or estimated. For this reason data for impedance tube measurements of the material are used.

Figure 9-7. Absorption Grating Diffuser to be measured. The black parts consist of porous absorber and the brown ones of wood.

9.2.1. Measurements Vs Boundary Element Modelling

For the implementation of the surface, black open cell foam with unknown characteristics was used. The rigid elements of the structure were constructed out of Medium Density Fibreboard (MDF). An idea of the form of the sample to be tested is presented in Figure 9-7. In black is the open cell foam while in brown the wood. The backing is made from $2.5cm$

thick MDF which was considered sufficient to act as a rigid backing while to avoid leaks from the sides a 2mm thick MDF plate was used.

The dimensions of the sample can be seen in Figure 9-8. Depth of the absorbing elements is set to $7.5cm$, the width of each element is set to $2.5cm$. The order of the elements is set using 4 periods of MLS (k = 3). The MLS used is 7 coefficients long so the overall structure is $4\times7\times2.5cm = 70cm$ in width. The measuring method as described in Section 2.3 was followed to acquire the scattered pressure distribution.

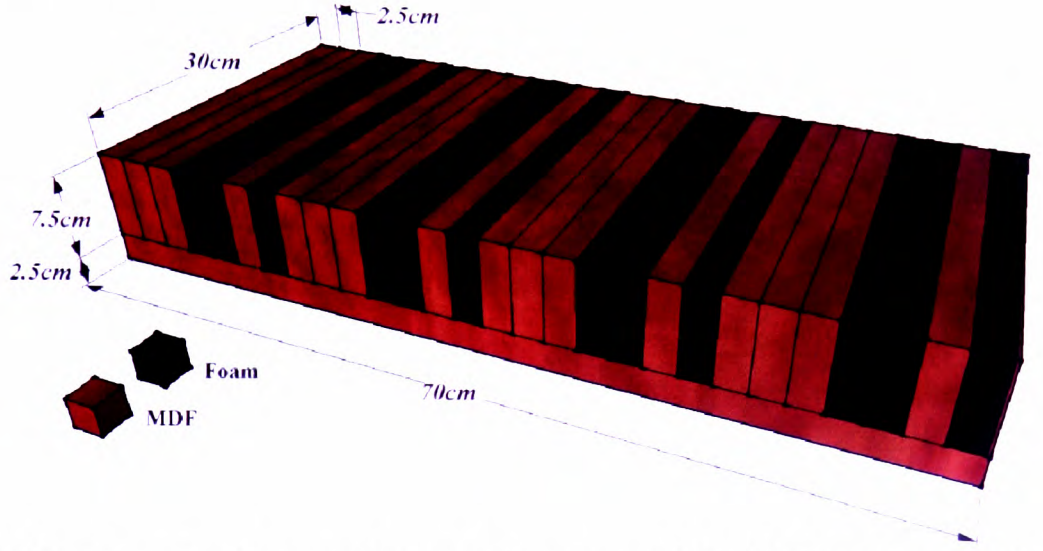

Figure 9-8. Absorption Grating Diffuser to be measured. The black parts consist of porous absorber and the brown ones of wood.

Since the sample is to be tested only in one plane the 2-D BEM is used. The normalised surface admittance to be used as an input to the simulation is estimated from impedance tube measurements.

The characteristic impedance (Figure 6-10) and wavenumber (Figure 6-11) were measured in the impedance tube with frequency range from $50Hz$ to $6.4kHz$. From that the normalised surface admittance β_n of a layer of 7.5cm of the material has been estimated (Figure 9-9). These values were used in the simulation even though they refer to plane wave propagation. Since, locally reactive surfaces are considered in BEM the plane wave assumption is valid.

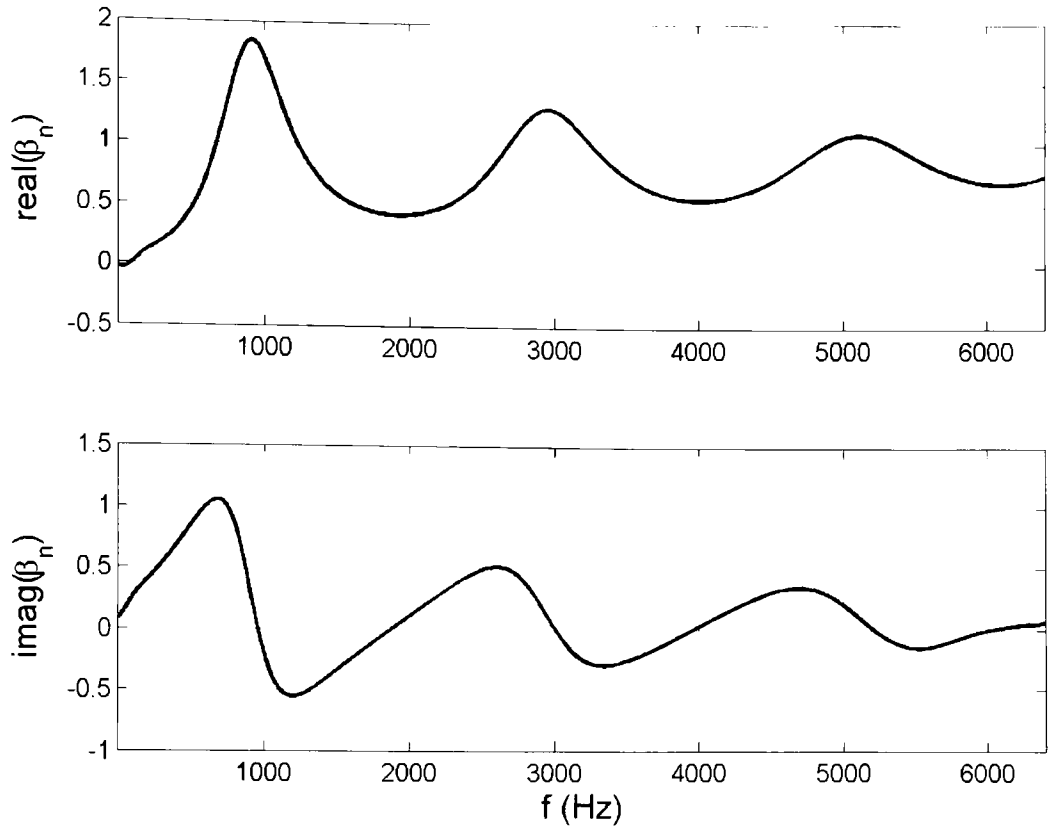

Figure 9-9. Normalised surface admittance of a 7.5*cm* deep leayer of black open cell foam estimated from its characteristic impedance and wavenumber which were measured in an impedance tube.

The comparison between the measured and predicted scattered pressure distribution from the absorption grating surface is within ±3dB for most cases while it displays disagreement at some angles that can reach 20dB (Figure 9-10). Disagreements between measured and predicted are mainly a result of human error in the positioning of the microphones as well as residues from the room's response during the measurement as discussed in Section 2.3.1. The comparison was made for other absorption gratings and the agreement was equally good. The configurations tested included modulated MLS (k = 3) with the inverse (see Section 3.4) and periodic arrangements of absorbing and reflecting elements.

The results from this investigation shows that using the surface admittance, measured in an impedance tube, as input to BEM gives good agreement with measured data. Furthermore, by establishing BEMs validity in predicting the scattered field from absorption grating surface allows for the further investigation to be carried out with this simulation technique. This results in easier testing but also in the freedom to use more receivers in the far field and so more accurately depict the scattered field.

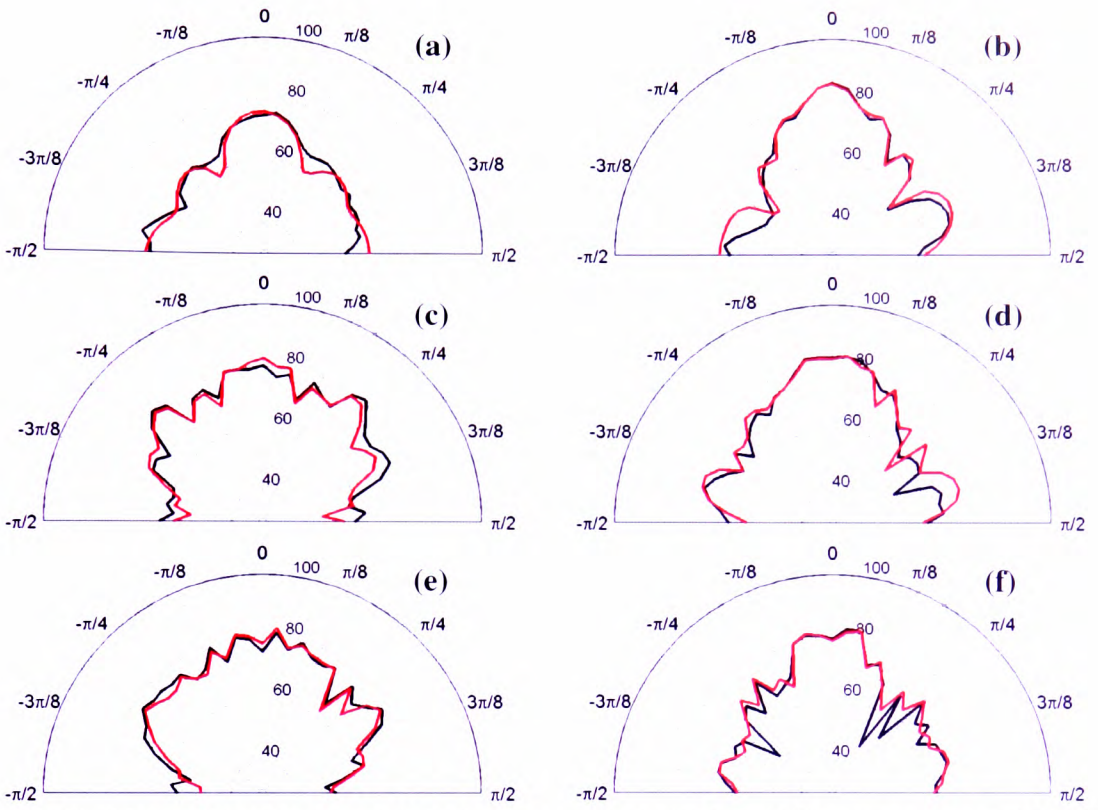

Figure 9-10. Normal incidence scattered pressure distribution (dB) measurement Vs BEM prediction from an absorption grating surface generated by 4 periods of MLS(k=3) normalized to the same sum of the reflected energy. (a) $1kHz$, (b) $2kHz$, (c) $3kHz$, (d) $4kHz$, (e) $5kHz$ and (f) $6kHz$. ——— Measured, ——— Predicted.

9.2.2. Simulations

The diffusion coefficient of the sample that was used in the previous Section can be seen in Figure 9-11. What is noteworthy from this figure is the existence of peaks showing significant diffusion at $900Hz$, $2.8kHz$ and $5kHz$. The source of this behaviour can be explained by the Fourier Model. The reflection coefficient of the foam as a function frequency can be seen in Figure 9-12. The peaks in diffusion occur when reflections from the absorbing elements have opposite phase compared to those from the reflecting surfaces; this is behaviour similar to that of PGDs. When the reflection coefficient of the porous material has phase $\varphi = \pi$, cancellation occurs when the wave reflected from the absorbing areas interacts with that from the reflective ones.

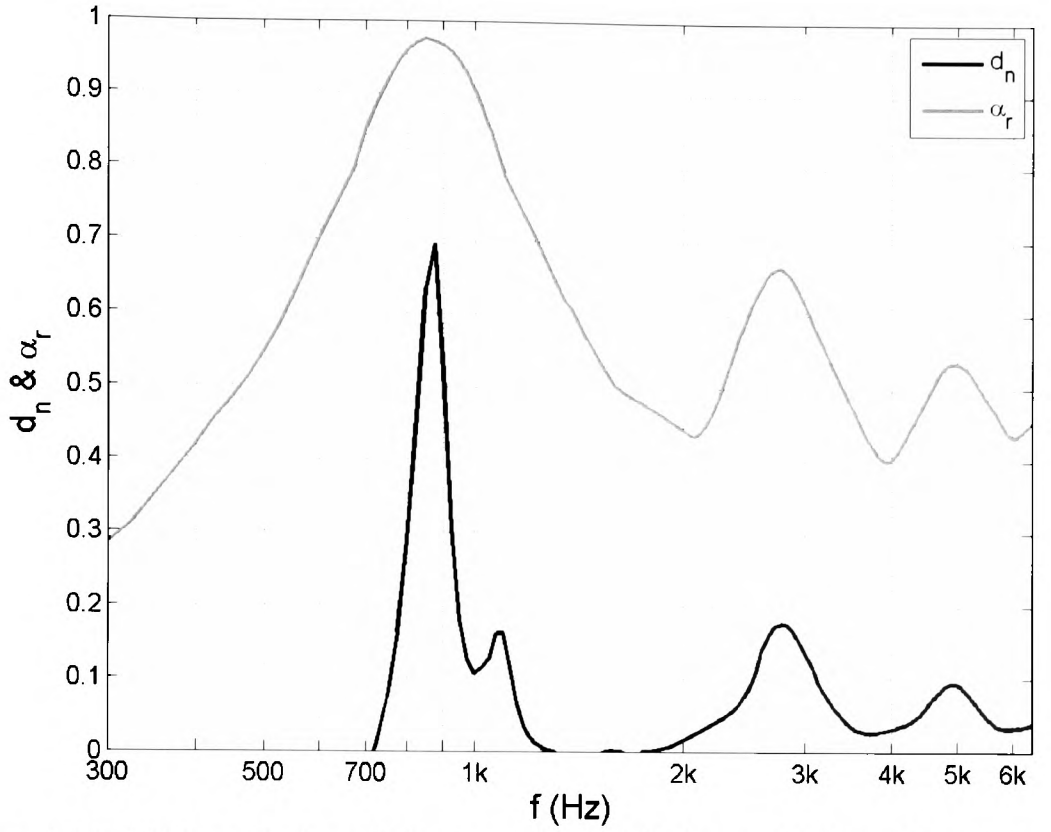

Figure 9-11. BEM prediction of the normalised diffusion coefficient (d_n) and absorption coefficient (a_r) from an Absorption Grating Diffuser arranged using 4 periods of MLS (k = 3) with the absorbing elements implemented by 7.5cm deep layer of foam.

They do not coincide exactly with the out of phase frequencies of the reflection coefficient ($950Hz$) because the pattern is affected by the periodicity of the structure as well. As discussed in the case of PGDs (see Section 4.1.2) placing diffusers of constant width in a structure results in their scattered pressure distribution to contain the interference pattern of sources spaced apart the same distance as the width of the diffuser. In this case in particular, one can see that d_n peaks between $700Hz$ and $1.2kHz$ but it displays a local minimum within the peak at $1kHz$. This is due to the periodic repetition of the diffuser which interferes with the diffusion pattern and prevents it from reaching an even higher value at $950Hz$.

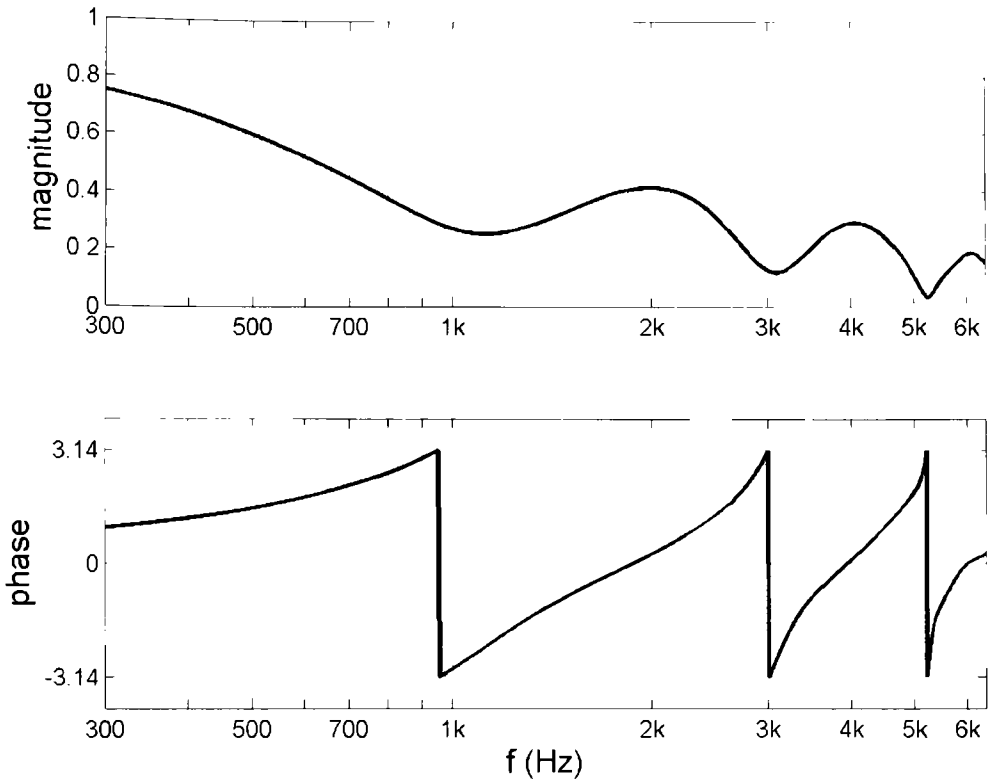

Figure 9-12. Reflection coefficient of a $7.5cm$ deep leayer of black open cell foam estimated from its characteristic impedance and wavenumber which were measured in an impedance tube.

The cancellation is evident in the polar plots of Figure 9-13. Plots (a) and (c) correspond to such frequencies and the specular lobe is attenuated by 19dB and 9dB respectively. On the other hand at $2kHz$ (Figure 9-13b) where the phase of the reflection coefficient of the foam is close to 0, there is only a 3dB attenuation of the specular lobe via absorption.

The mitigation of this lobe is the reason for the peaks in the absorption coefficient α_r of Figure 9-11. The absorption achieved at $900Hz$ is so high that the structure acts like an absorber of limited bandwidth. The peaks of diffusion at $2.8kHz$ and $5kHz$ are much lower because in their case more that a wavelength ($3\lambda/4$ and $5\lambda/4$ respectively) fits into the porous media. This results in a much lower magnitude of the reflection coefficient and hence less cancellation occurs. Even though the diffusion coefficient is lower as these frequencies more energy is scattered from the diffuser making them the most well behaving frequencies of the diffuser.

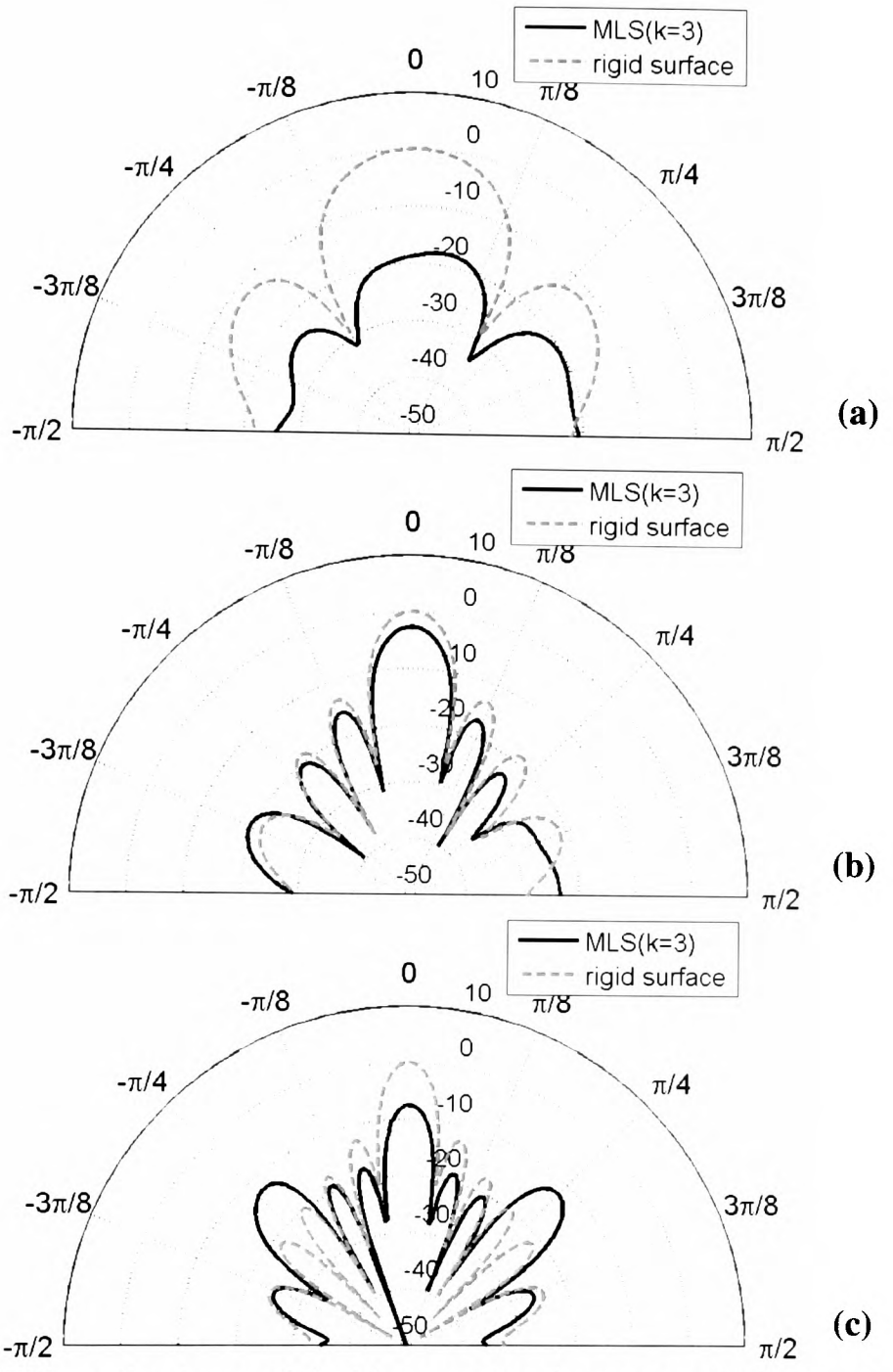

Figure 9-13. BEM predicted normal incidence scattered pressure distribution from an absorption grating surface generated by 4 periods of MLS(k=3) compared to a plane surface of the same width at $f = 900Hz$ (a), $f = 1.9kHz$ (b) and $f = 2.8kHz$ (c).

If the wells had not been occupied by the porous material the structure would be 4 periods of a Phase Grating Maximum Length Sequence Diffuser (MLSD) as presented in Section 3.1. The out of phase frequencies in the bandwidth of consideration would be its design frequency $f_0 = 1.14kHz$, where $\lambda/4$ fits into the depth of the well, and its odd multiples at 3.4 and $5.7kHz$.

The movement of these critical frequencies is a result of the lower speed of sound in the porous medium (Figure 9-14). The real part corresponds to the propagation speed of the wave in the medium while the imaginary in connected to the reactance of the material. The propagation speed in the porous medium is always smaller than 1 which is a result of the resistance of the material to the propagation of the sound wave. This means that the lower the speed of sound the higher the attenuation.

In the example discussed earlier the first peak of diffusion occurred at $950Hz$ where the speed of sound in the material is 25% lower compared to the one in air. This is the reason both for the substantial shift in the characteristic frequency and for the high absorption. Both these phenomena would not be so overwhelming if the speed of sound in the material was higher at that frequency or the frequency of interest was higher.

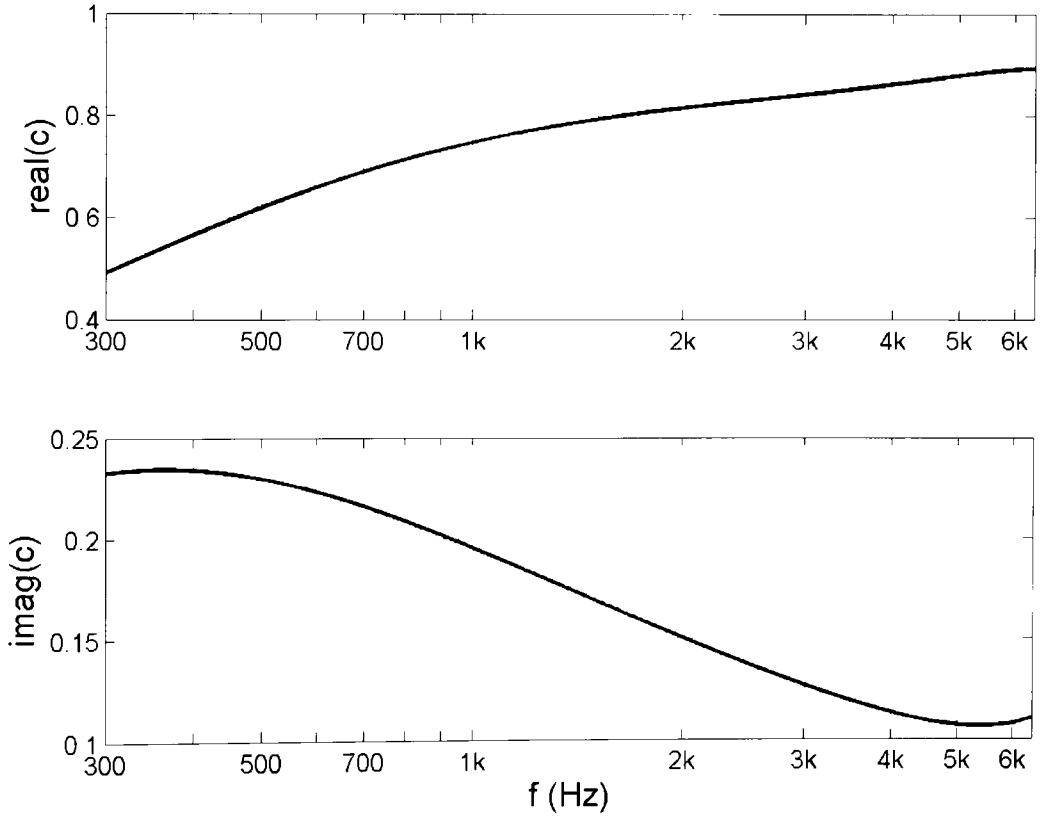

Figure 9-14. Speed of sound c_n in black open cell foam normalised to the speed of air c_0 estimated from its characteristic impedance and wavenumber which were measured in an impedance tube.

The device that is used to portray this phenomenon consists of 4*cm* wide and 2.5*cm* deep wells that are arranged by modulating a MLS (k = 3) with its inverse using the modulation sequence [1, 0, 1, 1]. If the wells were empty the Phase Grating Diffuser (PGD) would have $f_0 = 3.4kHz$. The resulting structure is 1.12*m* wide and its normalised diffusion coefficient is displayed in Figure 9-15.

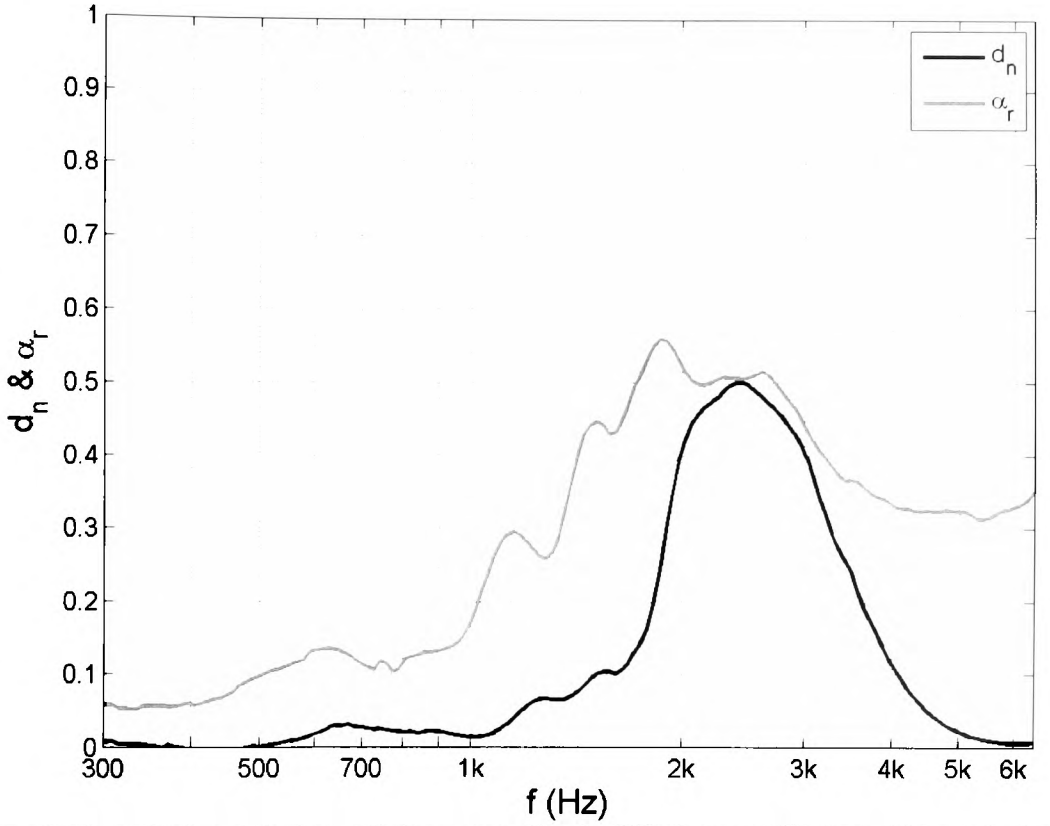

Figure 9-15. BEM prediction of the normalised diffusion coefficient (d_n) and absorption coefficient (a_r) from an Absorption Grating Diffuser arranged using 4 periods of MLS (k = 3) modulated with its inverse through the sequence [1, 0, 1, 1] with the absorbing elements implemented by 2.5*cm* deep layer of foam.

Although the frequency with the out of phase reflection coefficient for 2.5*cm* of foam is 3*kHz* the best performance is achieved at 2.5*kHz*, where both diffusion and absorption coefficient take the value of 0.5. At this frequency the diffuser has managed to attenuate the specular lobe by 15dB making is equal the level of the non-specular zone while the distribution of scattered pressure is uniform in the region of $\pm 5\pi/16$ (Figure 9-16). The performance of the diffuser is very good for a bandwidth of 1*kHz* around this frequency where the diffusion is high ($d_n > 0.4$) and the absorption is close to 50%.

This configuration results in a behaviour closer to the ones aimed for AGDs from the ideal one discussed in the previous Chapter as it manages to balance the dual performance of diffusion and absorption for a given bandwidth.

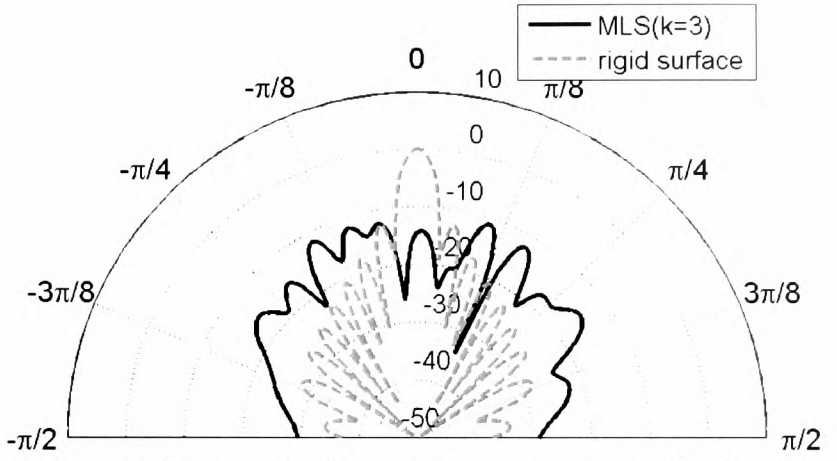

Figure 9-16. BEM predicted normal incidence scattered pressure distribution (dB) from an Absorption Grating Diffuser generated by 4 periods of MLS (k = 3) modulated with its inverse through the sequence [1, 0, 1, 1] with the absorbing elements implemented by 2.5cm deep layer of foam at f = 2.5kHz.

It is apparent that there is some advantage to using absorbing materials in PGDs since a combination of absorption and diffusion can be achieved. Furthermore, their design frequency is reduced due to the lower speed of sound in the material. Due to the nature of sound propagating in porous media it is advisable to operate in frequencies where the speed of sound in the media is not very low unless the goal is to absorb sound. This suggests that only high frequency diffusers can be implemented in this fashion. Their application could only be extended to lower frequencies if the porous material used displayed high propagation speed at low frequencies.

9.3. Absorption in wells of Phase Grating Diffusers

The phase grating behaviour of the AGD presented above forces a discussion on whether absorbing materials can be used in all PGDs to reduce their design frequency f_0. In the previous Section how the depth of a Maximum Length Sequence Diffuser (MLSD) can be reduced for the same design frequency has been shown. The extent of the reduction is dependent on two factors. The first factor is the speed of sound in the porous media at the specific frequency while the second factor is how deep the well is. MLSDs are diffusers that consist of a single well-depth which allows for the wells to be fully occupied by foam.

9.3.1. *Absorption in all the wells*

If a PRD was used instead and all its wells where filled with a porous material each well-depth would need to be rearranged so that the appropriate phase of the reflection coefficient would be achieved. Even in the case that such a structure was devised the magnitude of the reflection coefficient of each well would be different resulting in different wave interference.

An idea would be to fill all the wells with the same amount of porous material. This amount can only be as deep as the shallowest well (Figure 9-17). This would reduce the depth by only a small amount as the layer of the porous material would not be deep enough to delay the wave substantially.

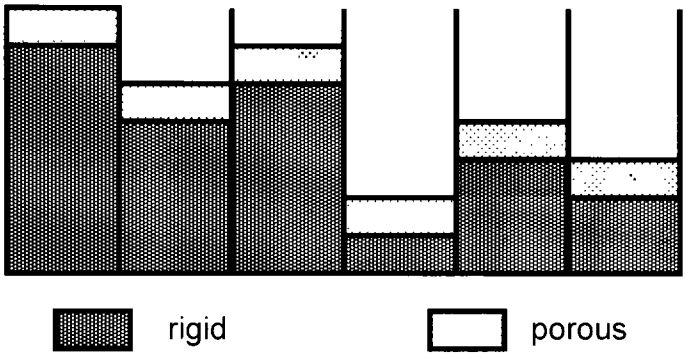

Figure 9-17. PRD (P = 7) with the same layer of porous material in all the wells.

Furthermore, MLSDs consist of about 50% wells, so when filled with foam half of the surface is still reflective. In the case of a PRD (*exp.* for P=7 [1, 3, 2, 6, 4, 5]) that consists entirely of wells there should be concern as to whether the resulting device if too absorbing. Since the layer is shallow though the absorption is not be excessive and so the diffusion properties of the PRD will not be diminished. They will be shifted to lower frequencies and the structure will display added absorption due to the existence of the porous material.

9.3.2. *Absorption in all selected wells*

Since the depth of the device is dictated by the deepest well the case of adding porous material in it can be considered (Figure 9-18). If the design frequency is set to $2kHz$ then the well depth of the deepest well will be $4.9cm$ deep for the standard QRD (P = 7). If the foam was used in a well it would need to be $4cm$ deep to achieve the required phase change. The reduction of the depth achieved is 18%.

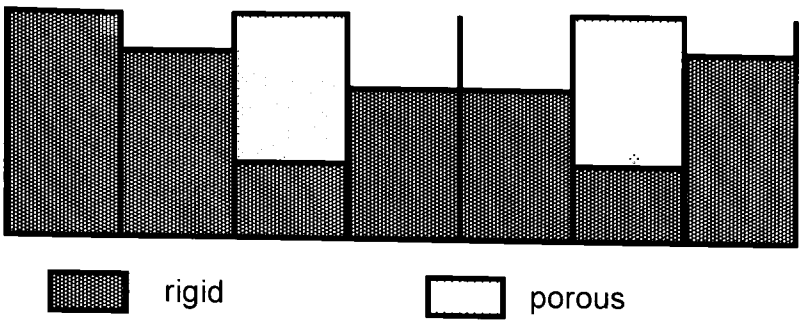

Figure 9-18. QRD (P = 7) with porous material in the deeper wells.

While being able to reduce the profile of a diffuser is very useful in diffuser design it should be pointed out that the magnitude of the reflection coefficient from the well is 0.37 rather than 1 which is required by the design of the diffuser. This will result in the diffuser not meeting the design requirements of the distribution of reflection coefficient on its surface. Furthermore, while this implementation provides the desirable phase at the design frequency f_0 it will not do so for frequencies that are multiples of f_0 where the diffuser is expected to behave ideally (see Section 3.1) due to the different speed of sound at those frequencies.

9.4. Discussion

Methods of improvement of the performance of AGDs have been presented in this Chapter. They are both aimed at making the device less passive as in the previous Chapter it has been pointed out that it fails as a diffuser.

One of the reasons for this is the inexistence of a frequency range where all the reflective elements of different width would scatter pressure uniformly. So the first approach was to incorporate reactive elements in the place of the larger reflective elements aiming at substantial dispersion at higher frequencies. Helmholtz Resonators were used, tuned to the frequency of maximum edge diffraction of the smaller elements. Even though some improvement is achieved it is only limited to the resonant frequency of the Helmholtz Resonator. Be that as it may, it points to a new method of implementation that considers the surface to consist of a series of reactive elements tuned to operate at specific frequencies.

The introduction of cancellation to AGDs has been attempted in the past by Cox[47] with ternary and quadriphase sequence diffuser where he included wells in the grid. The existence of such wells allows for out of phase pressure to be reflected from the well to interfere with the reflections from other parts of the surface.

Following the same concept of adding cancellation to AGDs a new approach is attempted. The AGD is implemented with non-perfectly absorbing elements. These elements were realised by filling wells with porous absorber. This configuration allowed for part of the energy to get reflected from the absorber with a phase difference that is dictated by the depth of the well and the speed of sound in the material. The resulting device performed as a PGD with its diffusion characteristics shifted to lower frequencies, an effect enforced by the lower speed of sound in the material. The existence of the absorber in the well provides absorption that combined with cancellation result in a very absorbing surface. If the diffuser is designed to diffuse at higher frequencies were the resistance of the material is lower the resulting device combines good diffusion with moderate absorption for a given bandwidth (in case presented here $1kHz$).

The result of the investigation in the second part of the thesis can be summarised by two points:

"Ideal Absorption Grating Diffusers in their original concept do not perform as diffusers; they behave like moderate absorbers but their performance could be improved with the addition of reactive elements."

"Absorption Grating Diffusers implemented with wells of absorption can provide 50% absorption combined with good diffusion for a given bandwidth; which was the goal of the ideal Absorption Grating Diffusers."

CONCLUSIONS AND FURTHER WORK

This thesis has been centred on diffusers generated using pseudorandom sequences. The focus was to investigate their drawbacks and to inquire as to how these limitations can be dealt with.

Part 1

The first part of this thesis investigated Phase Grating Diffusers, otherwise known as Schroeder Diffusers. These structures consist of wells of different depths which are set by a pseudorandom sequence for the design frequency f_0 of the diffuser. The generator P of the sequence gives the number of possible depths by splitting a quarter of the design wavelength into P increments. The coefficients of the sequence dictate the depth of each well. Diffusion is achieved by the interference of the waves reflected out of the wells which display different phases.

In order to create a 2-D diffuser one needs to create a 2-D sequence. The Chinese Remainder Theorem has been used to generate a 2-D diffuser from a 1-D sequence. In this thesis a novel approach has been presented that can generate a number of 2-D diffusers with the same autocorrelation properties from any 1-D sequence by altering the folding steps in the Chinese Remainder Theorem. This allows for both the investigation of a number of 2-D diffusers with the same properties and the more choices in diffuser design.

All Phase Grating Diffuser have been shown to exhibit frequencies at which they fail to diffuse sound and act like a flat plate. This occurs when the wavelength fits into the increment of the well-depths as specified by the sequence generator. This phenomenon first occurs at Pf_0 and is referred to as the first flat plate frequency of the diffuser. Known types of diffusers such as Quadratic Residue Diffusers (QRD) and Primitive Root Diffusers (PRD), have generators that are similar to the length N of the sequence. As most applications use short diffusers (typically $N = 7$ for QRDs), these flat plate frequencies occur within the audible bandwidth.

In order to treat the flat plate effect a number of solutions have been presented. Two new classes of diffusers, Power Residue Sequence Diffusers (PWRD) and Lüke Sequence Diffusers (LSD), have been presented. They both have much higher sequence generators than

their length and allow a small diffuser to have a flat plate frequency well outside the audible range. Their performance was investigated using 2-D Boundary Element Modelling.

LSDs are the superposition of a PRD and a steady step. Because the PRD has a different length than a generator ($N = P$-1) the LSD has a generator of $P(P$-1). At the flat plate frequency of the PRD, redirection rather than diffusion is achieved. Since LSD is a combination of two structures, when the PRD acts as a flat plate the LSD acts like a steady step. By using modulation, an aperiodic arrangement of the diffusers, this defect has been reduced. However, with the exception of the flat plate frequency, LSDs fail to achieve the same level of diffusion as more standard designs.

PWRDs are generated by undersampling a PRD, creating a shorter sequence based on a large generator. PWRDs can have the first flat plate frequency outside the audible bandwidth. Specifically the case of the PWRDs of length $N = 9$ generated by sampling the PRD of generator $P = 73$ every $M = 8$ wells has been shown to achieve better diffusion than standard number theoretic diffusers across the design bandwidth.

In addition to these new classes of diffusers two simple configurations have been introduced that allow for the construction of 1-D QRDs and PRDs using smaller components. This is done by taking advantage of their inner symmetries and constructing them using an element that is half the width of the diffuser. The QRDs are symmetrical with respect to the axis going through their centre so the diffuser can be formed by positioning the same component with two different orientations. Similarly, in PRDs' the second half is the inverse of the first half so the diffuser can be created by using a single structure. In this way the ratio of generator-to-width is doubled for standard Phase Grating Diffusers. Given that the flat plate frequency is closely linked to the number of their wells this allows for the doubling of the problematic frequency for a diffuser that is created for components of the same width.

Further Work

PWRDs have been shown to perform better than the commonly used number theoretic diffusers, which shows that the search for new pseudorandom sequences must continue.

Since both PWRDs and LSDs are generated from manipulating PRDs further investigation must be carried out to see how sequences can be manipulated without altering their autocorrelation properties.

For instance LSDs are created based on the fact that a linear ramp can be added to a pseudorandom sequence without affecting its autocorrelation function. It is applied to PRDs because their length is different that their generator. This is a characteristic that exists with other sequences like PWRDs. If this technique is applied to PWRDs it will not affect the magnitude of its autocorrelation function. The resulting diffuser will have a high number generator as it will be the product of the generators of the two structures. Given that PWRDs have large generators to begin with this factor is not that important. The important factor is that through this method a new class of diffuser is created that has the potential to display good diffusion properties and should be investigated. The discovery of new sequences will increase the arsenal of the designer in order to created better diffusing structures.

The relationship between PWRDs and the PRD they were created from can been further exploited. The fact that PWRDs are created from undersampling a PRD can be exploited by folding a PRD of generator $P = 73$ and length $N = 72$ into 8×9 diffuser. As presented in Section 4.4.2 2-D diffuser will consist of parallel PWRDs in one dimension. This device in principle should in addition to scattering pressure in a hemi-sphere perform ideally in this dimension. The performance of this diffuser should be further investigated.

Part 2

The second part of the thesis researched Absorption Grating Diffusers. Since their design requires the existence of ideally absorbing and ideally reflecting element to be pseudorandomly distributed on the surface, the first step was to establish a surface that could approximate the required reflection coefficient distribution.

The first configuration used densely packed layered mineral wool behind a pseudorandomly perforated mask. A similar configuration had been suggested in the past with the use of a typical porous material that resulted in the structure behaving as resonant absorbers. The use of the densely packed mineral wool resulted in the structure behaving as a damped resonator. The absorption as measured in an impedance tube displayed constant absorption in the range of $300Hz$ to $3kHz$. The sample behaves like one that consists of nearly ideal absorption in the hole-area and ideal reflection in rest of the surface. Furthermore, using impedance tube measurements it was shown that the equivalent concentrated absorption can be considered independent of the perforation pattern. In this way it has been shown that a structure with the required distribution can be constructed.

Having established a realistic implementation, the performance of the ideal surface was investigated using 2-D Boundary Element Modelling (BEM). The validity of using measured data as input to 2-D BEM was proven by comparing it to scattered pressure distribution measurements.

The research proved that the diffusers fail to provide substantial and evenly distributed scattered pressure regardless of the distribution of the reflective and absorbing elements. While some uniformity of the scattered response in the non-specular reflection zone is achieved, this is low in energy compared to the specular reflection which is insufficiently suppressed. The specular lobe is diminished only by the existence of absorption on the surface.

Both absorbing and reflecting elements have been shown to deviate from the required behaviour. The reflective elements must perform like omni-directional scatterers which they achieve for wavelengths larger that the width of the element. But at higher frequencies the reflection is more specular. Furthermore, at low frequency little sound energy is reflected. Over a narrow bandwidth, when ($w \leq \lambda \leq 3w$), substantial reflected energy and uniform scattering from a flat rigid element is achieved. For a surface with a variety of different element widths it is impossible to have a bandwidth were all the reflective elements display substantial dispersion.

At low frequencies the surface acts as an absorber as all the rigid parts are too small to reflect significant energy. At mid-frequency, the larger elements will reflect substantial energy uniformly but the device is still too absorbing as the smallest elements do not contribute to the scattered field. At higher frequencies when the smaller elements start scattering energy the larger ones reflect energy specularly.

In order to extend the non-specular behaviour of the reflective elements to higher frequencies the idea of using reactive elements has been suggested. In particular the use of a non-absorbing Helmholtz Resonator with a resonant wavelength ⅔ of the width of the reflective element has been incorporated into the surface. This was shown to extend the high frequency limit of the non-specular response of the reflective element was been moved from $\lambda_{min} = 0.83w$ to $\lambda_{min} = 0.58w$.

This configuration was used for diffusers generated from 4 periods of MLS ($k = 3$) which consists of reflective elements of width w and $3w$. The larger elements were replaced with

Helmholtz Resonator with resonance at the frequency where the edge diffraction of the smaller elements is a maximum ($\lambda = 2w$). The initial investigation conducted showed an improvement of the scattered pressure distribution only at resonance leaving the other frequency responses unaltered. This results points to the possible use of other reactive elements for these diffusers.

Diffusers where the absorbing elements are only partly absorbing were investigated. By implementing the diffuser in this fashion some cancellation was achieved between waves reflected from the solid and absorbing parts of the surface resulting in behaviour similar to a two level phase grating diffuser. The frequencies of ideal diffusion have been moved to lower frequencies due to the lower propagation speed of sound in the porous media. This has lead to the conclusion that porous materials can be used to make Phase Grating Diffusers shallower, if some absorption is desirable.

Attenuation is higher for low frequencies since then the porous material is more resistive. For a device designed for higher frequencies (e.g. $3kHz$) the diffuser manages to absorb 50% of the energy while the rest is evenly distributed for over an octave. It displays the 'ideal' performance but over a limited bandwidth.

Finally, the idea of using absorption in the wells of PRDs and QRDs has been discussed pointing towards a case that could be used to combine diffusion and absorption without altering the concept of the diffuser's design. The case of a PRD that has a layer of porous material with the same depth as the shallowest well is a device that could display interesting properties.

Further Work

The research presented in this thesis showed that common Absorption Grating Diffusers do not achieve substantial diffusion regardless of the distribution of elements on the surface. Can the design concept be rescued or should it be scraped with future research focussing on phase grating diffusers with absorption?

The scattering response of the reflective elements must be improved. In this thesis the use of Helmholtz Resonators has been used to improve this feature with small improvement only at the resonant frequency. Another approach would be to try and increase the edge diffraction of the elements. In order to do this the reflective elements must not be flat. Element such as

semicircles or other extruding geometries must be studied to investigate whether they can provide better dispersion.

Following the same reasoning the whole diffuser can be curved. Given that the absorption grating will provide 50% absorption the overall geometry of the structure will provide added diffusion. This is a concept that has been suggested before[70], but for a configuration that is now know to be overly absorbing.

On the other hand the concept of using non-perfectly absorbing element could be further exploited. In order to do so investigation into different absorbing materials must be conducted. If high absorption is required then a very resistive material must be used but if the aim is to scatter a substantial amount of energy then the material needs be less resistive. Most porous material display high resistivity at low frequencies which means that low frequency diffusers cannot be created in this way. So it is important to investigate materials that display low resistivity at low frequencies.

REFERENCES

1. Barron, M., *Auditorium Acoustics and Arquitectural Design*. 1998: E&F SPON.

2. Sabine, W.C., *Collected Papers on Acoustics*. 1993: Acoustical Society of America.

3. ISO:3382, *Acoustics Measurements of the reverberation time of rooms with reference to other acoustical parameters*. 1997.

4. D'Antonio, P. and T.J. Cox, *Diffusor application in rooms*. Applied Acoustics, 2000. **60**: p. 113-142.

5. D'Antonio, P. and T.J. Cox, *Two decades of sound diffusor design and development. Part 1 applications and design*. J. Acoust. Soc. Am., 1998. **46**(November): p. 955-976.

6. Schroeder, M.R., *Diffuse sound reflection by maximum-length sequences*. J. Acoust. Soc. Am., 1975. **57**(January): p. 149-150.

7. Angus, J.A.S., *Sound diffusers using reactive absorption grating*, in *98th Convention of the Audio Engineering Society*. 1995: Paris.

8. Schroeder, M.R., *Number theory in science and communication : with applications in cryptography, physics, biology, digital information, and computing* 5th ed. Springer series in information sciences. Vol. 7. 1984: Springer-Verlag.

9. Schroeder, M.R., D. Gottlob, and K.F. Siebrasse, *Comparative study of European concert halls correlation of subjective preference with geometric and acoustic parameters*. J. Acoust. Soc. Am., 1974. **56**(October): p. 1195-1201.

10. Schroeder, M.R., *Chaos, power laws: minutes from an infinite paradise*. 1991: W. H. Freeman & Co.

11. Cox, T.J. and P. D'Antonio, *Acoustic Absorbers and Diffusers: Theory, Design and Application*. 2nd ed. 2009, London & New York: Taylor & Francis Group.

12. D'Antonio, P. and T.J. Cox, *Two decades of sound diffusor design and development. Part 2 Prediction, measurement, and characterization*. J. Acoust. Soc. Am., 1998. **46**(December): p. 1075-1091.

13. D'Antonio, P. and J.H. Konnert, *The reflection phase grating diffusor.* J. Acoust. Soc. Am., 1984. **32**(April): p. 228-238.

14. D'Antonio, P. and J.H. Konnert, *The QRD diffractal: a new one- or two-dimensional fractal sound diffusor.* J. Acoust. Soc. Am, 1992. **40**(3): p. 113-29.

15. Angus, J.A.S., *Large area diffusors using modulated phase reflection grating*, in *98th AES Convention*. 1995.

16. Angus, J.A.S. and C.I. McManmon, *Orthogonal sequence modulated phase reflection grating for wideband diffusion.* J. Audio Eng. Soc., 1998. **46**: p. 1109-1118.

17. Cox, T.J., *The optimization of profiled diffusers.* J. Acoust. Soc. Am., 1995. **97**(May): p. 2928-2936.

18. Hargreaves, T.J., T.J. Cox, Y.W. Lam, and P. D'Antonio, *Surface diffusion coefficients for room acoustics: Free-field measures.* J. Acoust. Soc. Am., 2000. **108**(October): p. 1710-1720.

19. Mommertz, E., *Determination of scattering coefficients from the reflection directivity of architectural surfaces.* Applied Acoustics, 2000. **60**: p. 201-203.

20. Vorländer, M. and E. Mommertz, *Definition and measurement of random-incidence scattering coefficients.* Applied Acoustics, 2000. **60**: p. 187199.

21. ISO:17497-1, *Acoustics Sound-scattering properties of surfaces Part 1: Measurement of the random-incidence scattering coefficient in a reverberation room.* 2004.

22. AES-4id-2001, *AES information document for room acoustics and sound reinforcement systems Characterization and measurement of surface scattering uniformity.* 2001.

23. ISO:17497-2, *Acoustics Sound-scattering properties of surfaces Part 2: Measurement of the directional diffusion coefficient in a free field.* 2009.

24. Zeng, X., C.L. Christensen, and J.H. Rindel, *Practical method to define scattering coefficients in a room acoustics computer model.* Applied Acoustics, 2006(67): p. 771-786.

25. Fan, P. and M. Darnell, *Sequence Design for Communications Applications.* 1996: John Wiley & Sons Inc.

26. Schroeder, M.R., *Binaural dissimilarity and optimum ceiling for concert halls: more later sound diffusion.* J. Acoust. Soc. Am., 1979. **65**: p. 958-963.

27. Angus, J.A.S. and P. D'Antonio. *Two dimensional binary amplitude diffusers.* in *107th AES Convention.* 1999. New York.

28. Cormen, T.H., C.E. Leiserson, and R.L. Rivest, *Introduction to Algorithms.* The MIT electrical engineering and computer science series. 1989, Cambridge, Massachusetts London, England: The MIT Press. 823-826.

29. Burton, A.J., *The Solution of Helmholtz Equation in Exterior Domains Using Integral Equations.* National Physical Laboratory Report 1973.

30. *The author would like to acknowledge professor T.J.Cox, for supplying the 2-D direct Boundary Element Modelling software.*

31. Terai, T., *On calculation of sound fields around three dimensional objects by integral equation methods.* Journal of Sound and Vibration, 1980. **69**: p. 71-100.

32. Cox, T.J. and Y.W. Lam, *Evaluation of methods for predicting the scattering from simple rigid panels.* Applied Acoustics, 1993. **40**: p. 123-140.

33. Cox, T.J., *Objective and subjective evaluation of reflection and diffusing surfacesin auditoria.* 1992, University of Salford.

34. *The author would like to acknowledge professor T.J.Cox, for supplying the thin-panel indirect Boundary Element Modelling software.*

35. Kinsler, L.E., A.R. Frey, A.B. Coppens, and J.V Sanders, *Fundamentals of Acoustics.* 4th ed. 2000: John Wiley & Sons.

36. NetdB-PRO121. *http://www.01db-metravib.com/nvh-products.11/nvh-instruments.477/pro-121-real-time-analyser-12-channels-netdb-daq-solution.698/?L=1.*

37. NetdB-PRO132. *http://www.01db-metravib.com/nvh-products.11/nvh-instruments.477/pro-132-real-time-analyser-netdb-daq32-solution.594/?L=1.*

38. Visaton-SC4ND. *http://www.visaton.de/en/chassis_zubehoer/archiv/sc4nd_4.html.*

39. Angus, J.A.S., *Using grating modulation to achieve wideband large area diffusers.* Applied Acoustics, 1999. **60**(2): p. 143-165.

40. Dadiotis, K., J.A.S. Angus, and T.J. Cox. *Diffusers with extended frequency range.* in *123rd AES Convention.* 2007. New York.

41. Dadiotis, K., J.A.S. Angus, and T.J. Cox, *Lüke and power residue sequence diffusers.* J. Acoust. Soc. Am., 2008(April).

42. Cox, T.J. and P. D'Antonio, *Acoustic phase gratings for reduced specular reflection.* Applied Acoustics, 2000. **60**: p. 167-186.

43. Feldman, E., *A reflection grating that nullifies the specular reflection: A cone of silence.* J. Acoust. Soc. Am, 1995. **98**(1): p. 623–34.

44. *Visaton SC4ND.* Available from: http://www.visaton.de/en/chassis_zubehoer/archiv/sc4nd_4.html.

45. Lüke, H.D., *Families of polyphase sequences with near-optimal two valued auto- and cross-correlation functions.* Electronics Letters, 1992. **28**(January).

46. Payne-Johnson, E.C., G.A. Gehring, and J.A.S. Angus. *Improvements to binary amplitude diffusers.* in *122nd AES Convention.* 2007. Austria.

47. Cox, T.J., J.A.S. Angus, and P. D'Antonio, *Ternary and quadriphase sequence diffusers.* J. Acoust. Soc. Am., 2006. **119**(January): p. 310-319.

48. *RPG BAD panel.* Available from: http://www.rpginc.com/products/badpanel/index.htm

49. Dadiotis, K., J.A.S. Angus, and T.J. Cox, *Pseudorandom Sequences for Binary Amplitude Diffusers*, in *156th ASA Meeting.* 2008: Miami USA.

50. Cox, T.J. and P. D'Antonio, *Acoustic Absorbers and Diffusers: Theory, Design and Application.* 2004, London & New York: Spon Press.

51. Kuttruff, H., *Acoustics an Introduction.* 2007, London & New York: Taylor & Francis Group.

52. Allard, J.F., *Propagation of Sound in Porous Media: Modelling Sound Absorption Materials*. 1993, London: Chapman & Hall.

53. Delany, M.E. and E.N. Bazley, *Acoustical properties of fibrous absorbent materials.* Applied Acoustics, 1970. **3**(105-116): p. 105.

54. ISO:10534-2, *Acoustics Determination of sound absorption coefficient and impedance in impedance tubes, Part 2: Transfer-function method.* 1998.

55. *Brüel & Kjær PULSE 3560B*. Available from: http://www.bksv.com/Products/PULSEAnalyzerPlatform/PULSEHardware/PortablePULSE3560B.aspx.

56. Farina, A., *Simultaneous measurement of impulse response and distortion with a swept-sine technique*, in *108th Convention Audio Engineering Society*. 2000: Paris. p. 18–22

57. Smith, C.D. and T.L. Parrott, *Comparison of three methods for measuring acoustic properties of bulk materials*. J. Acoust. Soc. Am, 1983(74): p. 1577–82.

58. Song, B.H. and J.S. Bolton, *A transfer-matrix approach for estimating the characteristic impedance and wave numbers of limp and rigid porous materials.* J. Acoust. Soc. Am, 2000. **107**(3): p. 1131-1152.

59. *Brüel & Kjær 4206T*. Available from: http://www.bksv.com/doc/Bp1039.pdf

60. Helmholtz, H.V., *On the Sensations of Tone as a Physiological Basis for the Theory of Music*. 1885: Longmans, Green, and Co.

61. Rayleigh, J.W.S., *The Theory of Sound*. Vol. 2. 1942, New York: Dover Publications.

62. Elson, A., *Architectural Acoustics*. 1921: Oxford University Press.

63. Fuchs, H.V. and X. Zha, *Micro-perforated structures as sound absorbers A review and outlook.* ACTA Acustica United with Acustica, 2006. **92**: p. 139-146.

64. Cremer, L. and H.A. Müller, *Principles and Applications of Room Acoustics: Volume 2*. 1982, London and New York: Applied Science Publishers.

65. Mechel, F.P., *Formulas of Acoustics*. 2002, Section G: Springer.

66. Ingard, U., *On the theory and design of acoustic resonators.* J. Acoust. Soc. Am., 1953. **25**(November): p. 1037-1061.

67. Wu, T., T.J. Cox, and Y.W. Lam, *From a profiled diffuser to an optimized absorber.* J. Acoust. Soc. Am, 2000. **108**(2).

68. *The author would like to acknoledge professor T.J.Cox, for supplying the 3-D direct Boundary Element Modelling software.*

69. Fahy, F.j., *Foundations of Engineering Acoustics.* 2001, London: Academic Press.

70. *RPG BAD Arc.* Available from: http://www.rpginc.com/products/badarc/index.htm.